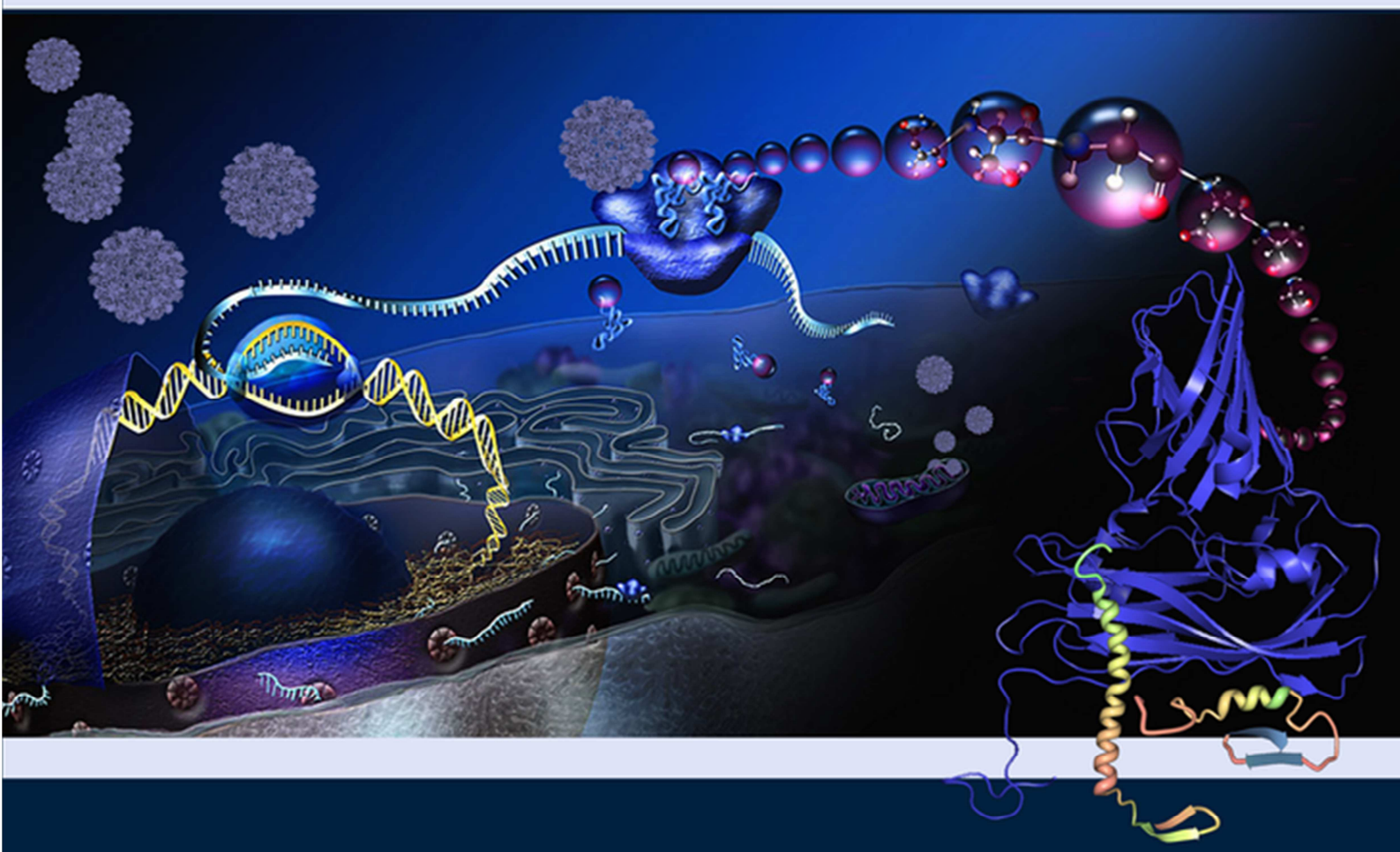

RELACIÓN ESTRUCTURA-FUNCIÓN DE LAS PROTEÍNAS VIRALES IMPLICADAS EN EL MOVIMIENTO DE LOS CARMOVIRUS Y SU INTERACCIÓN CON FACTORES CELULARES

Marta Serra Soriano

Directores
Pf. Vicente Pallás Benet
Dr. José Antonio Navarro Bohigues

Enero 2016

Esta Tesis Doctoral se ha realizado con la financiación del proyecto: "INTERACCIONES PATOGENO-HUESPED EN EL TRANSPORTE CELULAR Y VASCULAR DE VIRUS DE INTERES AGRONÓMICO" del Ministerio de Ciencia e innovación- Programa Biotecnología (BIO2008-03528) y con la Beca del Programa FPI (BES-2009-021943) del Ministerio de Ciencia e Innovación.

Relación estructura-función de las proteínas virales implicadas en el movimiento de los carmovirus y su interacción con factores celulares

Memoria presentada por

MARTA SERRA SORIANO

para optar al grado de

DOCTOR EN BIOTECNOLOGíA

Directores

Profesor VICENTE PALLÁS BENET

Doctor JOSÉ ANTONIO NAVARRO BOHIGUES

Enero 2016

A Júlia i Santi

UNIVERSIDAD
POLITECNICA
DE VALENCIA

Don Vicente Pallás Benet, Doctor en Ciencias Biológicas, Profesor de Investigación del Consejo Superior de Investigaciones Científicas en el Instituto de Biología Molecular y Celular de Plantas (Universidad Politécnica de Valencia- Consejo Superior de Investigaciones Científicas)de Valencia.

Don José Antonio Navarro Bohigues, Doctor en Ciencias Biológicas, Investigador Postdoctoral en el Instituto de Biología Molecular y Celular de Plantas (Universidad Politécnica de Valencia- Consejo Superior de Investigaciones Científicas)de Valencia

CERTIFICA:

Que doña Marta Serra Soriano, Licenciada en Bioquímica y Biología por la Universidad de Valencia, ha realizado bajo su dirección el trabajo que con título "Relación estructura-función de las proteínas virales implicadas en el movimiento de los carmovirus y su interacción con factores celulares" presenta para optar al grado de Doctor en Biotecnología por la Universidad Politécnica de Valencia.

Y que así conste a los efectos oportunos, firman el presente certificado en Valencia a _____ de _____ 2015.

Firmado:José Antonio Navarro Bohigues **Firmado: Vicente Pallás Benet**

“Uno nunca se da cuenta de lo que se ha hecho,

sólo puede ver lo que queda por hacer”

Marie Curie

ÍNDICE DE CONTENIDOS

ABREVIATURAS

AIF	Apoptosis-inducing factor
AG	Aparato de Golgi
BiFC	Bimolecular fluorescence complementation
COP	Coatomer proteins
CP	Coat protein
DGB	Double gene block
DGBp	Double gene block protein
dsRNA	Double strand RNA
ERES	Endoplasmic reticulum export sites
ERGIC	ER-Golgi intermediate compartment
EMSA	Electroforetic mobility shift assay
NPC	Nucleoprotein complexes
MP	Movement protein
MT	Microtubule
MF	Microfilament
NCAP	Non cell autonomous proteins
ORF	Open reading frame
RdRp	RNA dependent RNA polymerase
RE	Retículo endoplasmático
PABP	Poly(A)binding protein
PD	Plasmodesmata
PDLP	Plasmodesmata located proteins
PPU	Pore plasmodesmal unit
PTGS	Post-transcriptional gene silencing

SEL	Size exclusion limit
siRNA	Small interfering RNA
ssRNA	Single strand RNA
TGB	Triple gene block
TGBp	Triple gene block protein
TMD	Transmembrane domain
vRNP	Viral ribonucleoprotein complex
Y2H	Yeast two hybrid

RESUMEN

El género *Carmovirus* (familia *Tombusviridae*) representa al menos 19 especies de virus de plantas que afectan a numerosas especies cultivadas, en muchos casos con una gran repercusión económica. El genoma del MNSV (gRNA) está compuesto por una molécula de RNA monocatenario de polaridad positiva de 4,3 kb, con un extremo 5' sin estructura "cap" (m^7G^5pppNp) y un extremo 3' no poliadenilado. El genoma del MNSV codifica cinco proteínas funcionales flanqueadas por dos regiones no traducibles de 95 nt (en el extremo 5') y 280 nt (en el extremo 3'). La ORF más próxima al extremo 5' es una proteína de 29 kDa (p29) que finaliza con un codón ámbar y codifica la RNA polimerasa dependiente de RNA (RdRp). Continuando con la lectura a través de dicho codón se obtiene una proteína de 89 kDa (p89), también implicada en la replicación del virus. Las dos ORFs situadas en la parte central del genoma, codifican dos pequeñas MPs, denominadas generalmente DGBp1 y DGBp2 (*double gene block of proteins*, DGBps). DGBp1 es una proteína que une RNA necesaria para el transporte intercelular del genoma viral, mientras que DGBp2 es una proteína asociada a membrana cuya localización en el PD es imprescindible para el movimiento célula a célula del virus. Por último, la ORF del extremo 3' representa la proteína de cubierta (CP). En el caso del MNSV el virión está formado por partículas isométricas de unos 30 nm de diámetro, constituidas aproximadamente por 180 subunidades de la proteína de cubierta.

Resultados previos obtenidos en el grupo de investigación donde se ha realizado la presente Tesis habían puesto de manifiesto que el MNSV utiliza la ruta de secreción celular, a través de su proteína de membrana DGBp2 (p7B), para alcanzar la periferia celular. Hasta el momento de realizar la presente Tesis los conocimientos sobre las señales/motivos de las proteínas de membrana que facilitan o permiten dicho transporte eran más bien escasos. En este trabajo hemos determinado los residuos implicados en la salida de una proteína transmembrana viral en la ruta de secreción temprana (DGBp2, p7B MNSV). Los residuos implicados se encuentran tanto en la región Nt (citosólica) como en la Ct (luminal) siendo éste uno de los primeros ejemplos descritos en plantas de señal luminal de salida de RE. Con todos estos datos se ha propuesto un modelo en el que después de la inserción y correcto plegamiento de la

proteína en la membrana del RE, el Ct luminal de p7B interacciona a través del residuo K_{49} con un adaptador transmembrana asociado al citoesqueleto de actina para su movimiento y concentración en el RE cortical. El motivo Nt citoplasmático sería necesario para el ensamblaje de la vesícula COPII.

Por otra parte se ha profundizado en el estudio del interactoma de las MPs de los carmovirus y se han identificado, mediante un ensayo de doble híbrido (Y2H), tres proteínas celulares capaces de interaccionar con tres DGBp1 procedentes de tres carmovirus diferentes (MNSV, TCV y CarMV). Estos factores celulares son la proteína P3 del ribosoma 60S (RPP3A), la subunidad g del factor de iniciación de la traducción 3 (eIF3g) y el factor de transcripción WRKY36. Estas interacciones fueron confirmadas por BiFC. Además, mediante ensayos de mutagénesis se demostró que el dominio de unión de estas DGBp1 es un dominio Ct (FNF) conservado. El hecho de que estas tres proteínas interaccionen con los mismos factores sugiere un posible mecanismo común para todos o la mayor parte de los carmovirus.

Las CPs virales constituyen el paradigma de la multifuncionalidad proteica y, además de su obvio papel estructural, intervienen en un gran número de procesos del ciclo viral, incluyendo el transporte del RNA viral. La región Nt desestructurada de la CP del MNSV, al igual que para otros virus de RNA, generalmente es la encargada de unir el RNA viral por lo que se le suele llamar dominio R. Mediante mutantes de deleción y sustitución se ha demostrado que este dominio R (que en el MNSV comprende los primeros 94 residuos) no interviene solo en la encapsidación y unión del genoma viral, sino que es la responsable de la multifuncionalidad de la CP. Mediante EMSAs con mutantes de deleción se pudo determinar que la región R es esencial para la unión del RNA. Además se observó que dentro del dominio R se encuentra una región conservada entre los aa 60 al 91, que parece desempeñar un papel tanto en la unión de RNA genómico in vitro como en la encapsidación de RNAs subgenómicos. Sin embargo, en ensayos de encapsidación se observó que todo el dominio R es esencial para la encapsidación del genoma completo y que la región comprendida entre el residuo 31 y el 91 es necesaria para el movimiento tanto célula a célula como sistémico. Finalmente, utilizando PVX como vector de expresión, se demostró que la

CP del MNSV puede actuar como un supresor del silenciamiento mediante la unión a los sRNAs.

Con muy contadas excepciones, los virus de plantas utilizan el floema para trasladarse hacia las partes distales de la planta desde los sitios de infección. Con objeto de conocer el proteoma del floema de plantas infectadas y poder en el futuro identificar posibles proteínas del huésped que faciliten o dificulten el transporte sistémico de los virus, en el último capítulo se llevó a cabo un análisis proteómico comparativo, mediante 2D-DIGE, entre floemas de plantas de melón infectadas con MNSV y plantas sanas. Se detectaron 1046 spots de los cuales 25 poseían cambios significativos entre las dos condiciones. Después de someter las proteínas a un análisis de espectrometría de masas, se identificaron 19 proteínas que correspondían a 22 spots (13 de los cuales estaban sobrerrepresentados y en 9 había disminuido su expresión). Muchas de las proteínas identificadas están involucradas en muerte celular y el control de la homeostasis redox. Dos de estas 19 proteínas no habían sido descritas previamente en ensayos proteómicos: una carboxilesterasa con homología a la hsr203J de tabaco y la fumarilacetoacetato hidrolasa 1, ambas consideradas como reguladores negativos de la muerte celular. Los resultados obtenidos apuntan a que la respuesta de defensa debida a la infección viral puede ser transferida al floema como variaciones en los niveles de proteínas que se encuentran en el mismo para actuar como reguladores clave de esta defensa frente a patógenos manteniendo la señalización sistémica.

RESUM

El gènere *Carmovirus* (família *Tombusviridae*) representa almenys 19 espècies de virus de plantes que afecten nombroses espècies conreades, en molts casos amb una gran repercussió econòmica. El genoma del MNSV (gRNA) està compost per una molècula de RNA monocatenari de polaritat positiva de 4,3 kb, amb un extrem 5' sense estructura "cap" (m7G5pppNp) i un extrem 3' no poliadenilat. El genoma del MNSV codifica 5 proteïnes funcionals flanquejades per dues regions no traduïbles de 95 nt (a l'extrem 5') i 280 nt (a l'extrem 3'). La ORF més propera a l'extrem 5' és una proteïna

de 29 kDa (p29) que finalitza amb un codó ambre i codifica la RNA polimerasa RNA depenent (RdRp). Continuant amb la lectura a través d'aquest codó s'obté una proteïna de 89 kDa (p89), també implicada en la replicació del virus. Les dues ORFs situades a la part central del genoma, codifiquen dues petites MPs, denominades generalment DGBp1 i DGBp2 (*double gene block of proteins*, DGBps). DGBp1 és una proteïna que uneix RNA necessària per al transport intercel·lular del genoma viral, mentre que DGBp2 és una proteïna associada a membrana amb una localització en el PD que és imprescindible per al moviment cèl·lula a cèl·lula del virus. Finalment, l'ORF de l'extrem 3' representa la proteïna de coberta (CP). En el cas del MNSV el virió està format per partícules isomètriques d'uns 30 nm de diàmetre, constituïdes aproximadament per 180 subunitats d'aquesta proteïna.

Resultats previs obtinguts en el grup de recerca on s'ha realitzat la present Tesi havien posat de manifest que el MNSV utilitza la ruta de secreció cel·lular, a través de la seva proteïna de membrana DGBp2 (p7B), per arribar-hi a la perifèria cel·lular. Fins al moment de realitzar la present Tesi els coneixements sobre els senyals/motius de les proteïnes de membrana que faciliten o permeten aquest transport eren més aviat escassos. En aquest treball hem determinat els residus implicats en el transport d'una proteïna transmembrana viral a través de la ruta de secreció primerenca (DGBp2, p7B MNSV). Els residus implicats es troben tant a la regió Nt (citosòlica) com en la Ct (luminal) sent aquest un dels primers exemples descrits en plantes de senyal luminal de sortida de RE. Amb totes aquestes dades s'ha proposat un model en el qual després de la inserció i correcte plegament de la proteïna en la membrana del RE, el Ct luminal de p7B interacciona a través del residu K_{49} amb un adaptador transmembrana associat al citoesquelet d'actina per al seu moviment i concentració en el RE cortical. El motiu Nt citoplasmàtic caldria per a l'acoblament de la vesícula COPII.

D'altra banda s'ha aprofundit en l'estudi del interactoma de les MPs dels carmovirus i s'han identificat, mitjançant un assaig de doble híbrid (Y2H), tres proteïnes cel·lulars capaces d'interaccionar amb tres DGBp1 procedents de tres Carmovirus diferents (MNSV, TCV i CarMV). Aquests factors cel·lulars són la proteïna P3 del ribosoma 60S (RPP3A), la subunitat g del factor d'iniciació de la traducció 3 (eIF3g) i el factor de transcripció WRKY36. Aquestes interaccions van ser confirmades per BiFC. A més,

mitjançant assajos de mutagènesi es va demostrar que el domini d'unió d'aquestes DGBp1 és un domini Ct (FNF) conservat. El fet que aquestes tres proteïnes interaccionen amb els mateixos factors suggereix un possible mecanisme comú per a tots o la major part dels carmovirus.

Les CPs virals constitueixen el paradigma de la multifuncionalitat proteica i, a més del seu obvi paper estructural, intervenen en un gran nombre de processos del cicle viral, incloent el transport de l'RNA viral. La regió Nt desestructurada de la CP del MNSV, igual que per altres virus de RNA, generalment és l'encarregada d'unir l'RNA viral pel que se li sol cridar domini R. Mitjançant mutants de deleció i substitució s'ha demostrat que aquest domini R (que en el MNSV comprèn els primers 94 residus) no intervé només a la encapsidación i unió del genoma viral, sinó que és la responsable de la multifuncionalitat de la CP. Mitjançant EMSAs amb mutants de deleció es va poder determinar que el domini R essencial per a la unió de l'RNA. A més es va observar que dins del domini R es troba una regió conservada entre els aa 60 al 91, que sembla tenir un paper tant en la unió de RNA genòmic in vitro com en l'encapsidació de RNAs subgenómicos. No obstant això, en assajos d'encapsidació es va observar que tot el domini R és essencial per a l'encapsidació del genoma complet i que la regió compresa entre el residu 31 i el 91 és essencial per al moviment tant cèl·lula a cèl·lula com sistèmic. Finalment, utilitzant PVX com a vector d'expressió, es va demostrar que la CP del MNSV pot actuar com un supressor de silenciament mitjançant la unió als sRNAs.

Amb molt comptades excepcions, els virus de plantes utilitzen el floema per traslladar-se cap a les parts distals de la planta des dels llocs d'infecció. Amb l'objecte de conèixer el proteoma del floema de plantes infectades i poder en el futur identificar possibles proteïnes de l'hoste que facilitin o dificultin el transport sistèmic dels virus, en l'últim capítol es va dur a terme una anàlisi proteòmic comparatiu, mitjançant 2D-DIGE, entre floemas de plantes de meló infectades amb MNSV i plantes sanes. Es van detectar 1046 espots dels quals 25 tenien canvis significatius entre les dues condicions. Després de sotmetre les proteïnes a una anàlisi d'espectrometria de masses, es van identificar 19 proteïnes que corresponien a 22 espots (13 dels quals estaven sobrerepresentats i en 9 havia disminuït la seva expressió). Moltes de les proteïnes identificades estan involucrades en mort cel·lular i el control de l'homeòstasi redox. Dues d'aquestes 19

proteïnes no havien estat descrites prèviament en assajos proteòmics: una carboxilesterasa amb homologia amb la hsr203J de tabac i la fumarilacetoacetat hidrolasa 1, ambdues considerades com a reguladors negatius de la mort cel·lular. Els resultats obtinguts apunten que la resposta de defensa a causa de la infecció viral pot ser transferida al del floema mitjançant una variació dels nivells de les proteïnes que es troben en ell per a actuar com a reguladors clau d'aquesta defensa enfront de patògens mantenint la senyalització sistèmica.

SUMMARY

Genus *Carmovirus* (family *Tombusviridae*) represents at least 19 species of plant viruses that affect numerous cultivated species, in many cases with a major economic impact. MNSV genome (gRNA) is composed of a 4.3 kb single strand RNA molecule of positive polarity, without 5' end cap structure (m7G5pppNp) and an unpolyadenylated 3’ end. MNSV genome encodes five functional proteins flanked by two untranslatable regions of 95 nt (in the 5 'end) and 280 nt (at the 3' end). The ORF closest to the 5' end is a 29 kDa protein (p29) that ends with an amber codon and code for the RNA dependent RNA polymerase (RdRp). Stop codon readthrough results in an 89 kDa protein (p89), also involved in virus replication. The two ORFs located in the central part of the genome, code for two small MPs, generally referred DGBp1 and DGBp2 (*double gene block of proteins*, DGBps). DGBp1 is an RNA binding protein required for the intercellular transport of the viral genome, while DGBp2 is a membrane-associated PD whose location in the PD is essential for cell to cell movement of the virus. Finally, ORF at the 3' end represents the coat protein (CP). In the case of MNSV, virions consist of isometric particles of approximately 30 nm in diameter, made with about 180 subunits of the coat protein.

Previous results obtained in the research group where this thesis has been performed shown that the MNSV uses the cellular secretory pathway, through its membrane protein DGBp2 (p7B) to reach the cell periphery. Knowledge about signals/motifs of membrane proteins that facilitate or permit such transport was then rather scarce. In this work we determined the residues involved in the transport of a viral

transmembrane protein through the early secretory pathway (DGBp2, MNSV p7B). The residues involved are located in both the Nt (cytosolic) and Ct region (luminal) being one of the first examples in plants of a luminal ER export signal. With this information we have proposed a model in which after insertion and correct folding of the protein in the ER membrane, the luminal Ct of p7B interacts through the K_{49} residue with a transmembrane adapter associated with the actin cytoskeleton for movement and concentration in the RE-cortical. Nt cytoplasmic seems to be necessary to associate with the COPII vesicle components.

Moreover, we have deepened in the study of the interactome of the carmovirus MPs and we have identified through a two-hybrid assay (Y2H), three cellular proteins capable of interacting with three DGBp1 from three different carmovirus (MNSV, TCV and CarMV). These cellular factors are the 60S ribosomal protein P3 (RPP3A), the g subunit of the translation initiation factor 3 (eIF3g) and the transcription factor WRKY36. These interactions were confirmed by BiFC. Furthermore, mutagenesis assays showed that binding domain of these DGBp1 is a FNF conserved domain at the very Ct end. The fact that these three proteins interact with the same host factors suggest a possible mechanism common to most if not all carmoviruses.

Viral CPs are the paradigm of protein multifunctionality. In addition to its obvious structural role, they are involved in many processes of the viral cycle, including transport of viral RNA. The unstructured Nt region of MNSV CP, as for other RNA viruses, generally is responsible for viral RNA binding so it is usually called R domain. By using substitution and deletion mutants, we have shown that this R domain (which in MNSV comprising the first 94 residues) is not involved only in the packaging and binding of the viral genome, but is also responsible of CP multifunctionality. By EMSA assays with deletion mutants we could determine that the R domain was essential for binding of RNA. It was further noted that within the R domain there was a conserved region between aa 60 to 91 region, which appears to play a role in both the genomic RNA binding and in vitro encapsidation of subgenomic RNAs. However, in packaging assays, it was observed that the R domain is essential for full genome encapsidation and that the region between residue 31 and 91 is required for both cell to cell and

systemic movement. Finally, using PVX as an expression vector, we showed that MNSV CP can act as a suppressor of silencing most likely by sequestering sRNAs.

With very few exceptions, plant viruses use the phloem to move from infection sites to distal parts of the plant. In order to know the phloem proteome of infected plants and to identify in the future potential host proteins that facilitate or hinder the systemic transport of viruses, in the last chapter we conducted a comparative proteomic analysis by 2D-DIGE between phloem of MNSV-infected and healthy melon plants. From a total of 1046 spots, 25 were detected having significant abundance changes between the two conditions. After mass spectrometric analysis, 22 spots corresponding to 19 protein, were identified (13 of which were overrepresented and 9 had decreased abundance). Many of the identified proteins were involved in cell death and control of redox homeostasis. Two of these 19 proteins were never described in phloem proteomic assays: a carboxylesterase with homology with the *N. tabacum* hsr203J and the fumarylacetoacetate hydrolase 1, both considered as negative regulators of cell death. The results suggest that defense response due to viral infection can be transferred to the phloem as a variation in level of phloem proteins that act as key regulators to maintain systemic signaling in defense against pathogens.

INTRODUCCIÓN GENERAL

1.1 INFECCIONES VIRALES EN PLANTAS: UNA VISIÓN GENERAL

Las plantas son huéspedes de multitud de patógenos tales como bacterias, hongos, nematodos, insectos y virus. Los virus son importantes patógenos de plantas que pueden llegar a constituir el 47% de los eventos epidémicos en plantas cultivadas, un porcentaje que puede verse sensiblemente aumentado debido al incremento de la gama y distribución de insectos vectores causado por el cambio climático y la disminución en la eficacia y/o el uso de insecticidas químicos. Los virus de plantas están compuestos básicamente por ácidos nucleicos y proteínas aunque en algunas especies pueden presentar lípidos en su estructura. El material genético que porta la información hereditaria puede ser de diferente composición (DNA o RNA de doble o simple cadena, de polaridad positiva o negativa dependiendo de si puede ser usado cómo molde en la traducción o no, respectivamente) y estructura (monopartito, multipartito, circular o lineal). El tamaño de estos genomas rara vez excede las 10 kilobases (kb) y la mayoría codifican de 4 a 7 proteínas algunas de las cuales pueden ser multifuncionales. Generalmente el genoma viral se encuentra protegido por una cubierta proteica externa, denominada cápsida compuesta por subunidades proteicas (CP, de *coat protein* o proteína de cubierta). Estas subunidades son químicamente idénticas y constituyen el componente mayoritario de los virus. Se suelen ensamblar siguiendo una morfología helicoidal o icosaédrica. Al conjunto de material genético y cubierta se le conoce como virión o partícula vírica. Debido a su pequeño tamaño, su simplicidad estructural y su falta de actividad metabólica, los virus poseen limitaciones al tipo de procesos que son capaces de emprender por sí mismos. De hecho la gran mayoría de virus depende de otros organismos, directa o indirectamente, para infectar y diseminarse de una planta a otra. Aun así son capaces de infectar sistémicamente las plantas debido a que han evolucionado para manipular la maquinaria celular y evadir los mecanismos de defensa de su huésped favoreciendo su replicación y, por tanto, el avance de la infección (Marsh and Helenius, 2006; Vuorinen *et al.,* 2011) (apartados 1.2.2 y 1.2.3). Hasta ahora, el Comité Internacional de Taxonomía de Virus (International Committee on Taxonomy of Viruses, ICTV) ha propuesto y aprobado más de 1000 especies de virus de plantas, agrupadas en 25 familias y 109 géneros (9th report of ICTV; http://ictvonline.org/virusTaxonomy.asp).

El estudio de los virus de plantas ha contribuido de manera decisiva al establecimiento de nuevos paradigmas en biología fundamental. Entre éstos cabría destacar la demostración de que no solo el DNA sino también el RNA era portador de la información hereditaria, la contribución a la elucidación de parte del código genético, el transporte intercelular de macromoléculas (RNAs y proteínas), el descubrimiento de nuevos mecanismos de regulación traduccional, el silenciamiento génico post-transcripcional y la metilación de DNA mediada por RNA (ver revisiones de (Mandadi and Scholthof, 2013, Pallás, 2007).

El ciclo viral de los virus de plantas es un proceso complejo y dada la enorme variabilidad de virus, los ciclos replicativos son muy diversos. Sin embargo, se puede dividir el ciclo de vida típico en una serie de etapas comunes (Figura 1). El primer paso que debe acometer un virus para completar su ciclo es el de la entrada en la célula huésped. Dado que estos patógenos no son capaces de atravesar la pared celular por sí mismos, la entrada debe estar asistida por vectores biológicos y/o a través de heridas. Una vez en el interior celular el virus se desencapsidará liberando el genoma viral y se iniciará la traducción de las proteínas virales. En aquellos virus con genomas de RNA de simple cadena y polaridad positiva (ssRNA(+)), éstos servirán directamente como RNAs mensajeros (mRNAs) mientras que, en el caso de los genomas virales de RNA de simple cadena y polaridad positiva (ssRNA(-)) o de RNA bicatenarios (dsRNA), serán utilizados como molde para la síntesis de mRNAs. Los virus con genoma de DNA deben hacer un paso previo por el núcleo para sintetizar sus mRNAs, que posteriormente serán conducidos al citoplasma para ser traducidos. En paralelo el virus irá produciendo copias de su genoma mediante un complejo proceso replicativo cuyos mecanismos dependerán del tipo de genoma que posea (RNA o DNA). Finalmente, las partículas virales se ensamblaran y se propagaran por toda la planta a través del sistema vascular, preparadas para ser transferidas a una nueva planta para iniciar otra infección.

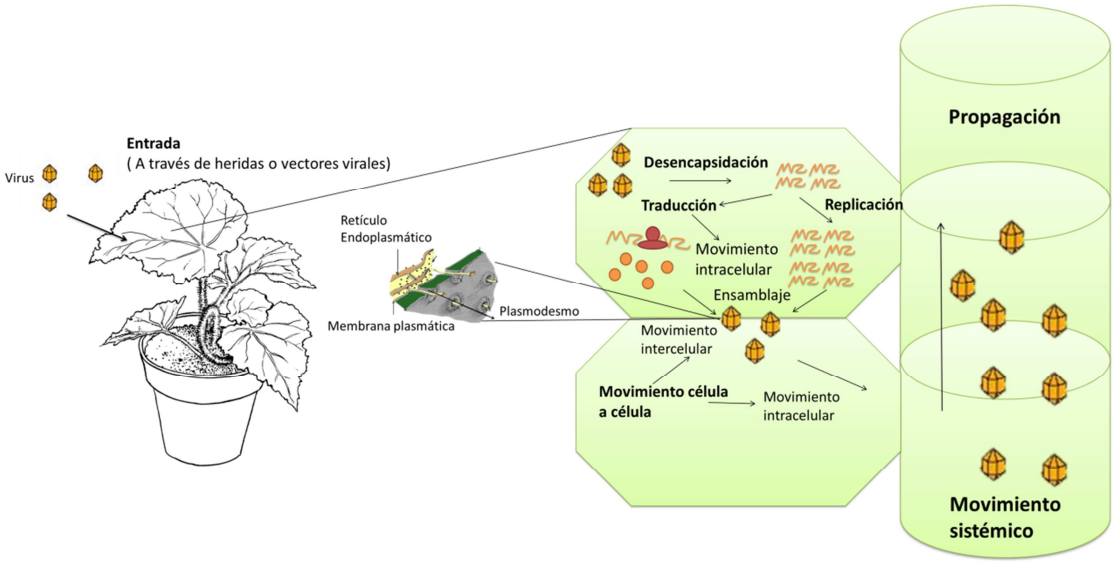

Figura 1. Representación esquemática del ciclo viral tipo de un virus de plantas donde se observa las 6 fases principales del ciclo: (1) entrada; (2) desencapsidación; (3) traducción; (4) replicación; (5) ensamblaje de viriones y (6) propagación del virus (la cual incluye el movimiento célula a célula) y sistémico.

A causa del avance de la infección y de la acumulación de proteínas virales se ven alteradas muchas rutas de señalización y procesos metabólicos, lo que provoca una gran variedad de respuestas en el huésped así como defectos en el crecimiento y desarrollo de la planta, induciendo en muchos casos la aparición de síntomas. Éstos van desde mosaicos, clorosis, lesiones necróticas, lesiones circulares, hasta retraso en el desarrollo, enanismo y marchitez entre otros. Un buen conocimiento del ciclo infeccioso del virus y los factores implicados en el mismo, pueden facilitar el desarrollo de estrategias que ayuden a combatir los daños ocasionados por estos patógenos. Dado que un capítulo importante de la presente Tesis ha tenido como objeto de estudio el movimiento intra e intercelular de los virus de plantas, a continuación se describen los principales mecanismos que los virus utilizan para trascolarse así como las características estructurales y funcionales de las proteínas virales que facilitan dicho transporte. Para otros aspectos importantes del ciclo viral, tales como la replicación y la traducción se recomienda la lectura de revisiones recientes del tema (Ahlquist, 2006, Barajas *et al.,* 2014, Miller and Krijnse-Locker, 2008).

1.2 EL MOVIMIENTO DE LOS VIRUS DE PLANTAS

Como se ha mencionado anteriormente, el ciclo de infección de un virus de plantas se inicia con la entrada del mismo a la célula vegetal (Figura 1). Ya en el interior, el virus se desencapsida y, entonces, su genoma debe moverse hasta su sitio de replicación. Una vez que el virus ha infectado la primera célula, puede colonizar las adyacentes a través de los plasmodesmos (PDs), canales que ofrecen conexiones citoplasmáticas entre células contiguas, en un proceso conocido como movimiento local o célula a célula (Fernández-Calvino *et al.,* 2011) (Figura 1). Con anterioridad, el virus tiene que desplazarse desde su punto de replicación hasta los PDs en un movimiento generalmente denominado intracelular. El movimiento a larga distancia o sistémico de los virus ocurre a través del sistema vascular, generalmente utilizando el floema (Pallás *et al*., 2011, Vuorinen *et al*., 2011), por el que se desplaza hacia los tejidos y órganos alejados del sitio inicial de la infección. Este transporte conlleva la descarga del virus al floema, bien en forma de complejo ribonucleoproteico o como virión, que siguiendo la ruta de fotoasimilados alcanza otros órganos de la planta hasta invadirla por completo. Para llevar a cabo estos procesos los virus requieren tanto de factores propios como de la célula huésped.

1.2.1 Las proteínas de movimiento

1.2.1.1 Características funcionales y estructurales

Los virus de plantas codifican una serie de factores propios conocidos como proteínas de movimiento (MP, de *movement protein*) que facilitan los diferentes pasos del movimiento viral intra e intercelular. Las MPs se han identificado prácticamente en todos los virus, pero el número, la estructura y la interacción con factores de la célula huésped, así como el modo de acción, varía dependiendo de la especie. A pesar de la falta de similitud observada entre las MPs, la mayoría de ellas presenta una serie de características y/o funciones comunes, entre las que destacan: i) la capacidad de unión de RNA, que generalmente se realiza de forma cooperativa y sin especificidad de secuencia y que normalmente se produce a través de un dominio helicoidal rico en aminoácidos con carga neta positiva (Berna *et al.,* 1991, Herranz and Pallás, 2004, Herranz *et al.,* 2005, Marcos *et al.,* 1999c, Navarro *et al.,* 2006, Vilar *et al.,* 2001, Vilar

et al., 2005); ii) la interacción con el sistema de membranas de la célula y con el citoesqueleto (Waigmann *et al.,* 2004) y iii) la localización en los PDs e interacción con sus componentes (Wolf *et al.*, 1989; Oparka *et al.*, 1997; Liu and Nelson, 2013). La convergencia en la funcionalidad de estas proteínas de movimiento explica que estas proteínas sean funcionalmente intercambiables (Deom *et al.,* 1994; Sánchez-Navarro *et al.,* 2006; Fajardo *et al.,* 2013) incluso en virus con genomas de distinta naturaleza (Sánchez-Navarro *et al.,* 2010).

Si bien todas estas funciones son necesarias para llevar a cabo con éxito la infección, el tipo de estructuras requeridas y los factores necesarios variarán en función del virus y su modo de acción, muchas veces condicionado por el tipo de proteínas de movimiento. Así, las funciones anteriormente descritas pueden recaer en una única proteína o bien estar distribuidas en diferentes polipéptidos, normalmente de menor tamaño y agrupados en bloques génicos. A continuación se describen las principales características de las MPs clasificadas en función del número de proteínas implicadas en el transporte viral y/o su tamaño.

1.2.1.2 Clasificación de las proteínas de movimiento virales

La superfamilia 30K.

Este grupo es el mayoritario e incluye las MPs de hasta 18 géneros diferentes de virus de plantas entre los que destacan los géneros *Ilarvirus*, *Alfamovirus*, *Tobamovirus* o *Bromovirus*. Todos ellos presentan una única MP cuya proteína de referencia es la proteína 30K del virus del mosaico del tabaco (*Tobacco mosaic virus*, TMV) (Figura 2). Las MPs de la superfamilia 30K muestran una baja similitud en su secuencia, con pocos dominios conservados: un motivo $LXDL_{50\text{-}70}G$ y una región hidrofóbica junto el extremo amino terminal (Nt) del motivo anterior. Sin embargo, presentan una conformación tridimensional común. En la región central presentan un patrón de elementos de estructura secundaria conservados, formado por cuatro α-hélices (α1-4) y siete β-hojas (β1-7), mientras que los dominios Nt y carboxilo terminal (Ct) son más variables (Melcher, 1990, 2000). A pesar de esta baja similitud se ha demostrado que muchas de las proteínas de la superfamilia 30K son funcionalmente intercambiables lo que pone de manifiesto su alto grado de conservación funcional (Stavolone *et al.,* 2005; Sánchez-

Navarro *et al.,* 2010). La proteína más estudiada de esta gran familia de MPs virales es la proteína de movimiento del TMV (revisado en Waigman *et al.,* 2007). Para la MP del TMV se demostró inicialmente su capacidad de unir RNA (Citovsky *et al.,* 1992), modificar el tamaño de exclusión de los PDs (Wolf *et al.,* 1989), su asociación al citoesqueleto (Heinlein *et al.,* 1995, 1998) y más recientemente su asociación al RE (Kawakami *et al.,* 2004). Aunque se propuso que esta proteína se integraba en las membranas del RE a través de dos fragmentos transmembrana, resultados recientes obtenidos por nuestro grupo pusieron de manifiesto que la MP del TMV (Peiró *et al.,* 2014) y la del virus de los anillos necróticos de los prunus (*Prunus necrotic ringspot virus*, PNRSV) (Martínez-Gil *et al.,* 2009) se asociaban periféricamente al RE sin constituir verdaderas proteínas integrales de membrana (Figura 2). Aunque se requieren más estudios, estos resultados podrían generalizarse a las MPs de la superfamilia 30K con las consiguientes implicaciones que dicha topología tendría para la translocación intracelular de la proteína y para sus funciones como diana de factores de avirulencia en las interacciones incompatibles.

El bloque de los dos genes (double gene block, DGB).

Los carmovirus presentan, en la región central de su genoma, dos pequeñas ORFs adyacentes o muy poco solapadas que se conocen como el bloque de los dos genes (*double gene block*, DGB). La implicación de estas proteínas en el movimiento local ha sido demostrada únicamente en el caso del virus de las manchas necróticas del melón (*Melon necrotic spot virus*, MNSV), del virus del arrugamiento del nabo, (*Turnip crinckle virus*, TCV) y del virus de la rotura de la flor del pelargonio (*Pelargonium flower break virus*, PFBV) (Hacker *et al.,* 1992; Li *et al.,* 1998; Cohen *et al.,* 2000; Genovés *et al.,* 2006; Martínez-Turiño and Hernández, 2011). Sin embargo, las DGBps correspondientes al virus del moteado del clavel (*Carnation mottle virus*, CarMV), especie tipo del género, y del MNSV son las mejor caracterizadas funcional y estructuralmente (Wobbe *et al.,* 1998; Marcos *et al.,* 1999; Cañizares *et al.,* 2001; Vilar *et al.,* 2001, 2005; Genovés *et al.,* 2006, 2009, 2010, 2011; Navarro *et al.,* 2006; Martínez-Gil *et al.,* 2007). El CarMV codifica dos pequeñas proteínas de movimiento, p7 (DGBp1) y p9 (DGBp2) (Figura 2) que en el caso del MNSV se denominan p7A y p7B,

respectivamente. A pesar de que estas MPs no comparten motivos de secuencia con los miembros de la superfamilia 30K, poseen dominios funcionalmente similares.

Según datos experimentales de dicroísmo circular y de predicción *in silico* de estructura, la DGBp1 presenta tres dominios: el Nt, variable y desestructurado, el Ct, plegado en una conformación β-hoja plegada y el dominio central, con una estructura secundaria en α-hélice que es la responsable de la unión a RNA tanto a nivel de estructura primaria (aminoácidos cargados positivamente) como secundaria (Marcos *et al.,* 1999; Vilar *et al.,* 2001, 2005; Navarro *et al.,* 2006).

La segunda proteína implicada en el movimiento de los carmovirus (DGBp2) contiene, en la mayoría de los casos, dos dominios hidrofóbicos estructurados en α-hélice característicos de fragmentos transmembranas. En el caso de la DGBp2 del PFBV (p12) además de poseer dos fragmentos transmembrana se ha demostrado que presenta propiedades de unión a RNA (Martínez-Turiño and Hernández, 2011). Sin embargo, tres especies de carmovirus entre las que se encuentra el MNSV, solo presentan uno de estos dominios (Figura 2) (Navarro *et al.,* 2006). Se ha demostrado que la p9 del CarMV es capaz de insertarse *in vitro* en microsomas derivados de la membrana de retículo endoplasmático (RE) adquiriendo una topología en forma de U y exponiendo los extremos Nt y Ct hacia el lado citoplasmático (Vilar *et al.,* 2002). En el caso de la p7B del MNSV se ha demostrado tanto *in vitro* como en células vegetales que esta proteína adquiere una topología de tipo II en la que su extremo Nt se orienta hacia el citosol (Martínez-Gil *et al.,* 2007; Genovés *et al.,* 2011). Independientemente del número de dominios hidrofóbicos, la inserción de la DGBp2 en la membrana sigue un proceso cotraduccional asistido por la maquinaria de translocación celular (Vilar *et al.,* 2002, Saurí *et al.,* 2005, Martínez-Gil *et al.,* 2007). Además de estos dominios hidrofóbicos, la DGBp2 presenta un extremo Ct con un potencial plegamiento en β-hoja plegada cuya función se desconoce (Navarro *et al.,* 2006).

El bloque de los tres genes (triple gene block, TGB).

Este grupo de virus presenta hasta tres ORFs esenciales en el movimiento célula a célula que se organizan de manera contigua (Figura 2), aunque un poco solapada, en su genoma constituyendo el característico bloque de tres genes (TGB) (Morozov and

Solovyev, 2003). El factor proteico correspondiente a cada gen se denomina TGBp1, TGBp2 y TGBp3, en sentido 5'-3'. Los virus que presentan este sistema de proteínas de movimiento pueden dividirse en dos clases. La primera clase incluye los géneros *Hordeivirus, Peculovirus, Pomovirus y Benyvirus* que son virus que presentan una morfología de varilla. En la segunda clase se encuentran virus de morfología filamentosa pertenecientes a los géneros *Potexvirus, Carlavirus, Foveavirus y Allexivirus*, que además de las TGBps requieren la proteína de cubierta para su movimiento célula a célula. Las TGBp1 presentan un dominio NTPasa/helicasa con varias regiones ricas en Arg y Lys implicadas en la unión de RNA. Por otro lado, las TGBp2 y TGBp3 contienen dominios hidrofóbicos capaces de insertarse en la membrana. La TGBp2 presenta dos secuencias hidrofóbicas internas y separadas por una región central muy conservada. Las TGBp3 de la clase 1 poseen dos posibles fragmentos transmembrana mientras que las correspondientes a los virus de la clase 2 presentan un único dominio hidrofóbico (Morozov and Solovyev, 2003).

Otras proteínas de movimiento.

Dentro de este grupo menos estudiado se encuentran los virus pertenecientes al género *Tymovirus*. Éstos codifican en su genoma una única MP, la cual presenta un tamaño molecular de entre 69 y 85 kDa (Figura 2). Al igual que la MP del TMV las proteínas de movimiento de los virus de este género son capaces de unir RNA, aumentar el límite de exclusión molecular del plasmodesmo (SEL, de *size exclusion limit*) y transportar el RNA viral (vRNA) a través del mismo (Drugeon and Jupin, 2002). En el otro extremo encontramos a los closterovirus que necesitan hasta cinco proteínas, tres implicadas directamente en el movimiento (p6, p64, y HSP70h) y dos estructurales (proteína de cubierta mayor y menor), para su movimiento célula a célula (Prokhnevsky *et al.,* 2002; Peremyslov *et al.,* 2004). El último mecanismo se encuentra representado por los virus de DNA conocidos como geminivirus que se replican en el núcleo. El movimiento de estos virus necesita dos proteínas; la denominada NSP (de *nuclear shuttle protein*) que es la encargada de transportar el genoma viral desde el núcleo al citosol y una segunda que se une a los complejos NSP-genoma viral para transportarlos a la célula adyacente (Noueiry *et al.,* 1994).

Como se ha comentado anteriormente, para el movimiento viral son necesarias las diferentes MPs y en muchos casos no son los únicos factores implicados. Algunos virus requieren de otras proteínas virales como la CP, replicasas, factores de transporte virales o chaperonas virales (Dolja *et al.,* 2006, Verchot-Lubicz *et al.,* 2010). Además, tal y como se ha puesto de manifiesto en el apartado anterior algunos virus requieren de otras proteínas del huésped para llevar a cabo su desplazamiento y/o replicación. En general podemos clasificar los factores celulares que intervienen en seis categorías: 1) elementos de los plasmodesmos y de la periferia celular, como pueden ser la calreticulina (Chen *et al.,* 2005) o proteínas de síntesis de polisacáridos (Selth *et al.,* 2006); 2) componentes del citoesqueleto, como los filamentos de actina, tubulina o miosinas (Navarro *et al.,* 2006; Sambade *et al.,* 2008, Genovés *et al.,* 2010; Su *et al*., 2010; Amari *et al.,* 2011); 3) proteínas relacionadas con el tráfico de vesículas (Huang *et al.,* 2001); 4) chaperonas (Shimizu *et al.,* 2009, Krenz *et al.,* 2010); 5) proteínas nucleares (Matsushita *et al.,* 2002, Kim *et al.,* 2007); 6) otras proteínas de diversa naturaleza y función tales como kinasas (Yoshioka *et al.,* 2004, Modena *et al.,* 2008), factores de traducción (Robaglia and Caranta, 2006) o componentes de fotosistemas (Jiménez *et al.,* 2006) entre otros. Además de estos factores suelen estar directamente implicados el citoesqueleto y el sistema de endomembranas interviniendo en diferentes procesos y etapas a lo largo del ciclo viral.

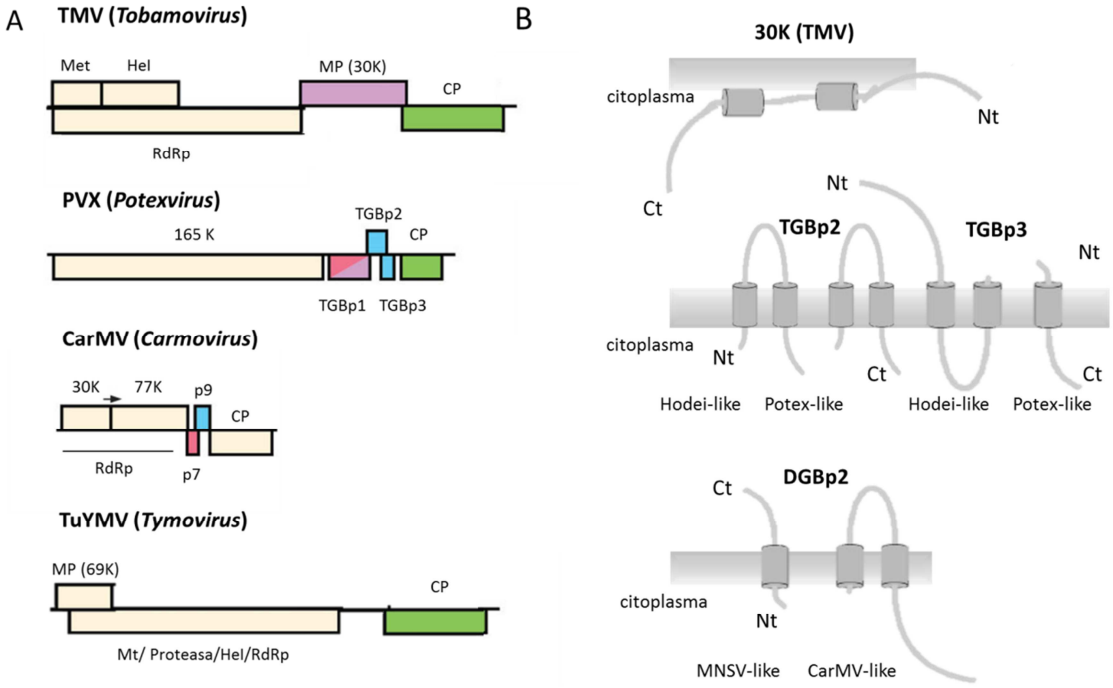

Figura 2. A) Esquema de la organización genómica del virus del mosaico del tabaco (*Tobacco mosaic virus*, TMV), del virus X de la patata (*Potato virus X*, PVX), del virus del moteado del clavel, *Carnation mottle virus*, CarMV) y del virus del mosaico amarillo del nabo (*Turnip yellow mosaic virus*, TuYMV). B) Topología de membrana predicha para las MPs de TMV (Peiró *et al.,* 2014), las TGBp2 y TGBp3 (Morozov *et al.,* 2003) y la DGBp2 (Navarro *et al.,* 2006).

1.2.2 Movimiento célula a célula

Como hemos visto el desplazamiento del virus por el citoplasma de la célula infectada (movimiento intracelular) hasta la periferia está estrechamente regulado y coordinado por factores celulares. Una vez en la periferia el virus se desplazará desde la célula inicialmente infectada a sus células vecinas (movimiento intercelular). Estos dos movimientos intra e intercelular son los que comprende el movimiento célula a célula y en muchos de los casos el segundo está altamente condicionado por el primero. Existen diversas estrategias de desplazamiento y translocación célula a célula aunque todas ellas comparten una etapa, el paso a través del PD. Los PDs son canales estrechos recubiertos por la membrana plasmática y atravesados por una prolongación del RE conocida como desmotúbulo (ver Figura 1 y3). Por tanto, los PDs proporcionan continuidad de membrana y citosólica entre células adyacentes. El control del flujo de macromoléculas a través del PD se encuentra muy controlado. Uno de los mecanismos propuestos para ejercer este control se basa en la dilatación/constricción de un anillo localizado en la entrada/salida del PD y cuyo componente fundamental sería la calosa

(Maule, 2008; Thomas *et al.,* 2008). Para atravesar con éxito los PDs los virus utilizan diferentes estrategias. Los dos principales mecanismos utilizados por los virus para translocarse de una célula a otra son el movimiento guiado por túbulos y el movimiento basado en complejos ribonucleoproteicos.

1.2.2.1 Movimiento mediado por túbulos

Este modelo se basa en la asociación de las MPs en forma de unas estructuras tubulares que desorganizan completamente el desmotúbulo del PD para su translocación (Figura 3). En este caso la MP es capaz de modificar el plasmodesmo bioquímica y estructuralmente para permitir el paso de viriones completos. El ensamblaje de las MPs al formar los túbulos capturaría en su interior las partículas virales a transportar que posteriormente serían liberadas en la célula adyacente tras la desestructuración de los túbulos. Esta es una capacidad intrínseca de algunas proteínas de la superfamília 30K siendo en el virus del mosaico del chícharo (*Cowpea mosaic virus*, CPMV) donde se observó por primera vez (Scheer and Groenewegen, 1971). Tal y como se ha descrito anteriormente esta familia de MPs comprende una gran variedad de géneros que incluyen virus con genomas de RNA de simple cadena negativa o positiva y virus de DNA de simple (Begomovirus) y doble cadena (Badnavirus y Caulimovirus). Las MPs de los virus formadores de túbulos podrían alcanzar los PDs de dos maneras: (1) difundiendo desde su lugar de síntesis a la membrana plasmática y más tarde a los plasmodesmos. Esta idea se basa en que tratamientos con orizalina y latrunculina (sustancias capaces de desestabilizar los microtúbulos y filamentos de actina respectivamente) no afectan a la localización de la MP del CPMV en los PDs; o (2) las MPs o incluso los viriones serían transportados hacia los plasmodesmos mediante su asociación con vesículas de la ruta de secreción derivadas del aparato de Golgi (AG) como en el caso del virus del entrenudo corto de la vid (*Grapevine fanleaf virus,* GFLV) (Pouwels *et al.,* 2002; Laporte *et al., ,*2003; Ritzenthaler and Hofmann, 2007).

Dentro de los componentes de los PDs, recientemente se han identificado una familia de proteínas integrales de membrana que son capaces de interaccionar con los MPs formadoras de túbulos y facilitar su movimiento (Amari *et al.,* 2010). Estas

proteínas localizadas en el PD, denominadas PDLPs (de *plasmodesmata located protein*) se transportan a través de la ruta de secreción para alcanzar el PD, concretamente la membrana plasmática que atraviesa el plasmodesmo (Thomas *et al.,* 2008). La MP del GFLV, clasificada como formadora de túbulos, interacciona con PDLP1 actuando probablemente como los receptores tanto para el ensamblaje de las estructuras tubulares como para el movimiento del virus (Amari *et al.,* 2010). Además la inactivación de la miosina XI ha puesto de manifiesto su implicación en el transporte intracelular y en el direccionamiento de los receptores PDLPs a los PDs y consecuentemente en el movimiento célula a célula del GFLV (Amari *et al.,* 2011).

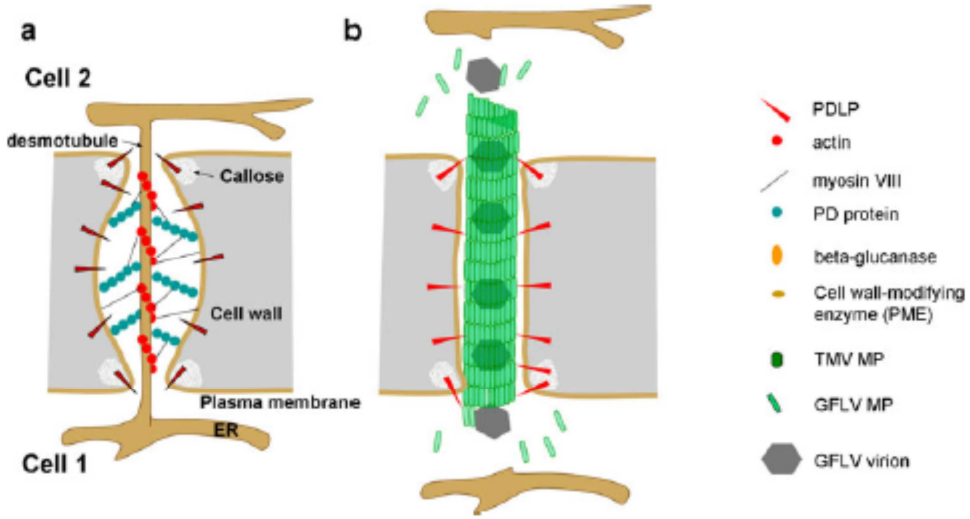

Figura 3. Modelo de modificación del PD por la formación de túbulos. A) PD sin modificar. B) Modificación del PD por la MP del GFLV. El ensamblaje de la MP formando túbulos tiene lugar a través de la interacción de la MP con PDLP. El túbulo reemplaza el desmotúbulo del interior del plasmodesmo. Los viriones son transportados entre las células gracias a la polaridad generada por el ensamblaje-desensamblaje del túbulo (adaptado de Niehl and Heilein, 2011).

1.2.2.2 Movimiento basado en complejos ribonucleoproteicos (RNP)

En general este modelo está basado en la formación de un complejo entre la MP y el genoma del virus que facilita el paso a través de los PDs. A diferencia del modelo anterior no se modifica irreversiblemente la estructura interior del PD, aunque se requiere un incremento en el tamaño del poro (Atkins *et al.,* 1991; Ding *et al.,* 1992; Seemanpillai *et al.,* 2006; Waigmann *et al.,* 2007). Estos complejos ribonucleoproteicos, son transportados hacia los plasmodesmos utilizando diferentes vías. Estas rutas dependerán principalmente del tipo y del número de proteínas de movimiento que

codifique el genoma de los diferentes virus. Así pues podemos encontrar 5 tipos de mecanismos, el basado en una MP, en dos MPs, en tres MPs (con dos subtipos *Hordeivirus* y *Potexvirus)* y finalmente aquel que requiere múltiples MPs (Figuras 2 y 3) (ver apartado siguiente)

1.2.2.3 Mecanismos de transporte intracelular de los virus de plantas

Virus que codifican una MP: superfamilia 30K

El modelo propuesto se basa en el TMV (género *Tobamovirus*). Fue el primer virus descubierto y su proteína de 30 kDa (P30) fue el primer factor viral identificado como MP (Meshi *et al.,* 1989). Tal y como se ha descrito anteriormente la MP del TMV une ssRNAs (Citovsky *et al*., 1990), se localiza en el PD (Tomenius *et al*., 1987; Atkins *et al*., 1991) e incrementa el SEL, interacciona con los microtúbulos (MT) y con diferentes factores celulares (Niehl and Heilein, 2011). A pesar de todas estas propiedades, la MP del TMV es necesaria pero no suficiente para el movimiento célula a célula (Heinlein and Epel, 2004). De hecho parece ser que la replicasa del TMV también está involucrada en el proceso (Hirashima and Watanabe, 2001, 2003; Guenoune-Gelbart *et al.,* 2008).

El proceso general empieza con el desensamblaje de la cápsida del TMV, el RNA viral se adhiere a unos sitios específicos del RE mediante su estructura cap (5' metilguanosina) generando estructuras granulares características (Christensen *et al.,* 2009). La MP se asociaría entonces con las membranas del ER y se uniría a las copias del RNA viral que se estarían generando conformando el complejo de replicación viral (VRC). Este VCR incluiría también otros componentes necesarios para la replicación y se desplazaría hasta alcanzar los plasmodesmos constituyendo probablemente el complejo maduro de movimiento (*viral movement complex*, VMC) (Figura 4A) (Asurmendi *et al.,* 2004; Kawakami *et al.,* 2004; Sánchez-Navarro *et al.,* 2006; Aparicio *et al.,* 2010; Tilsner *et al*.,, 2012). Además, se ha propuesto que la CP induce un cambio conformacional en la MP que provocaría un incremento de la afinidad por el RNA viral (Andreev *et al,.* 2004). Inicialmente, los VRCs estarían anclados a puntos de intersección entre el RE cortical y los MTs denominados C-MERs (*cortical MT-associated ER sites*) (Figura 4A, punto 1). Algunos VRCs podrían liberarse por la

polimerización de los MT y ser impulsados por el RE mediante los microfilamentos de actina (MF) (Figura 4A, punto 2) o directamente por la propia polimerización de los MTs (Figura 4A, punto 3). Una vez aumentada la apertura del PD, los VRCs o VMCs se desplazarían a las células adyacentes (Figura 4A, punto 4). En estadios medios de la infección, la MP podría acumularse en los VCRs y MTs antes de degradarse (Figura 4A, punto 5).

Virus que codifican el bloque de los dos genes (double gene block, DGB)

El movimiento intracelular de este grupo de virus se basa en la acción conjunta y coordinada de dos MPs. Este par de proteínas, inicialmente denominadas proteínas del bloque de los dos genes (DGB) (Hull, 2002), están presentes entre los miembros de los géneros *Carmovirus*, *Alphanecrovirus*, *Betanecrovirus*, *Gallantivirus* and *Panicovirus* (Navarro *et al.,* 2006). Actualmente no se conoce con exactitud los componentes del VMC y el mecanismo de transporte de estos virus. Sin embargo, estudios realizados con el TCV y el MNSV sugieren que la encapsidación no es necesaria para el movimiento célula a célula aunque la CP es requerida, en mayor o menor medida dependiendo del huésped, por su capacidad de actuar como supresor del silenciamiento de RNA (Hacker *et al.,* 1992; Cohen *et al.,* 2000; Genovés *et al.,* 2006).

La primera de las MPs, la DGBp1, presenta propiedades de unión a RNA (Marcos *et al.,* 1999; Vilar *et al.,* 2001, 2005; Navarro *et al.,* 2006) y es capaz de interaccionar consigo misma (Genovés *et al.,* 2009). También se ha podido determinar que se acumula autónomamente en la periferia celular y que su movimiento es dependiente de los MFs (Genovés *et al.,* 2009). Esto sugiere que podría ser la encargada de unir el vRNA e iniciar el movimiento intracelular hacia los PDs (Figura 4B, punto 1).

La segunda de las MPs implicada en el movimiento de estos virus ha sido clasificada en dos categorías, dependiendo de si tiene uno o dos dominios transmembrana (TMDs) como la p7B del MNSV o la p9 del CarMV, respectivamente (Navarro *et al.,* 2006). Al parecer en ambos casos la MP sería insertada en la membrana del RE de manera cotraduccional para iniciar su transporte al PD (Figura 4B, punto 2). Sin embargo sólo en el caso de la DGBp2 del MNSV se ha podido demostrar un transporte a través de la ruta de secreción celular dependiente de las vesículas

COPII (Figura 4B, punto 3) y mediada por el aparato de Golgi (AG) (Figura 4B, punto 4)(Genovés *et al.,* 2010), aunque no se descarta la salida desde el RE a otras membranas celulares (Martínez-Turiño and Hernández, 2011). El papel concreto de la DGBp2 en el transporte viral todavía se desconoce pero su presencia en el PD es esencial para el mismo. Inicialmente, se propuso un modelo simple según el cual la DGBp2 interaccionaría con DGBp1 que a su vez estaría unida al vRNA. Este complejo ternario sería transportado hasta el PD guiado por DGBp2 a través del sistema de endomembranas (Marcos *et al.,* 1999; Vilar *et al.,* 2002; Navarro *et al.,* 2006). Sin embargo, el hecho de que DGBp1 y DGBp2 puedan seguir rutas separadas para llegar al PD cuestiona este primer modelo.

Virus que codifican el bloque de los tres genes (triple gene block, TGB)

Muchos virus de ssRNA poseen un módulo de tres genes solapados conocido como bloque de los tres genes o TGB (de *triple gene block*). Las proteínas codificadas en estos genes (TGBp1, TGBp2 y TGBp3) son imprescindibles para el movimiento viral y trabajan de forma coordinada para transportar el vRNA hasta los PDs (Morozov and Solovyev, 2003; Solovyev *et al.,* 2012; Verchot-Lubicz *et al.,* 2010). Inicialmente se clasificaron en dos grupos atendiendo a las diferencias estructurales de las proteínas: las presentes en potexvirus (Figura 4C) y en hordeivirus (Figura 4D) así como en otros virus relacionados (Morozov and Solovyev, 2003; Verchot-Lubicz *et al.,* 2007).

Los potexvirus necesitan la CP para el movimiento célula a célula (Scholthof, 2005) y codifican una TGBp1 que actúa como supresor del silenciamiento, a nivel de la RNA polimerasa 6 dependiente de RNA (RDR6). Es el caso del virus del mosaico del bambú (*Bamboo mosaic virus*, BaMV) cuyo movimiento se basa en la interacción de TGBp3 con TGBp2 en el RE para ser dirigidas a la periferia celular, donde se acumulan en estructuras específicas (Harries *et al.,* 2009). Recientemente se ha observado que el complejo TGBp2/3 recluta a los viriones a través de la interacción CP-TGBp2 en las factorías virales (Figura 4C, punto 1). Posteriormente, la TGBp1 que se va sintetizando en las factorías virales (Figura 4C, punto 2) o en el citoplasma (Figura 4C, punto 3) se va incorporando mediante la interacción con TGBp2 y/o la CP del virión a este complejo TGBp2/3-virión. Todo este complejo se dirige al PD dirigido por una señal de

transporte hacia dominios altamente curvados del RE, como el desmotúbulo del PD, que se encuentra en TGBp3 (Figura 4C, punto 4) (Chou *et al.,* 2013).

Por otra parte, los hordeivirus no necesitan la CP para moverse célula a célula (Scholthof, 2005; Jackson *et al.,* 2009) y poseen otro supresor del silenciamiento diferente de TGBp1. En estos casos, como en el del virus del enanismo del tallo de la patata (*Potato mop-top virus*, PMTV) la TGBp3 forma vesículas móviles derivadas del RE e interacciona directamente con TGBp2 (Figura 4D, punto 1). Posteriormente, el complejo TGBp1/vRNA (la TGBp1 actuaría como una especie de proteína de cubierta) sería incorporado a las vesículas mediante la interacción de TGBp2 con el vRNA (Figura 4D, punto 2). Estas vesículas se moverían por la red que forma el RE y los MFs hasta el PD transportando el complejo TGBp1/2/3/vRNA (Figura 4D, punto 3). Una vez en los PDs TGBp2/3 colaboran dilatando el poro del PD para facilitar el paso del vRNA a través del mismo (Tamai and Meshi, 2001) (Figura 4D, punto 4). Sin embargo, estas MPs no se mueven célula a célula sino que son "recicladas" a través de la formación de vesículas endocíticas para posteriores ciclos de transporte intracelular (Figura 4D, punto 5) (Haupt *et al.,* 2005).

Virus que codifican múltiples proteínas de movimiento

Es el caso de los closterovirus como el virus del amarilleo de la remolacha (*Beet yellows virus*, BYV), que necesariamente requieren el ensamblaje del virión para el movimiento célula a célula. Esos virus poseen viriones filamentosos compuestos por dos partes diferentes: un cuerpo largo formado por la CP mayor y una región corta formada por la CP menor (CPm) (Dolja, 2003). En el movimiento célula a célula del BYV intervienen cinco proteínas, 4 de las cuales forman parte del virión: HSP70h (homóloga a la HSP70 celular); una proteína de 64 kDa, la CP y la CPm. La quinta proteína es una MP de 6 kDa que se inserta en las membranas del RE rugoso. No se conoce cuál es su papel específico y aunque no interviene en el ensamblaje del virión es esencial para el movimiento viral (Peremyslov *et al.,* 2004; Zamyatnin *et al.,* 2006). HSP70h presenta actividad ATPasa, se localiza en el PD (Medina *et al.,* 1999) y presenta un transporte autónomo a los PDs mediado por los MFs y las miosinas de clase VII (Avisar *et al.,* 2008; Prokhnevsky *et al.,* 2005). HSP70h interacciona fuertemente con el extremo de

los viriones filamentosos constituido por subunidades de CPm, por lo que esta región podría representar un mecanismo para el transporte impulsado por la energía procedente de la actividad ATPasa de HSP70h (Dolja 2003).

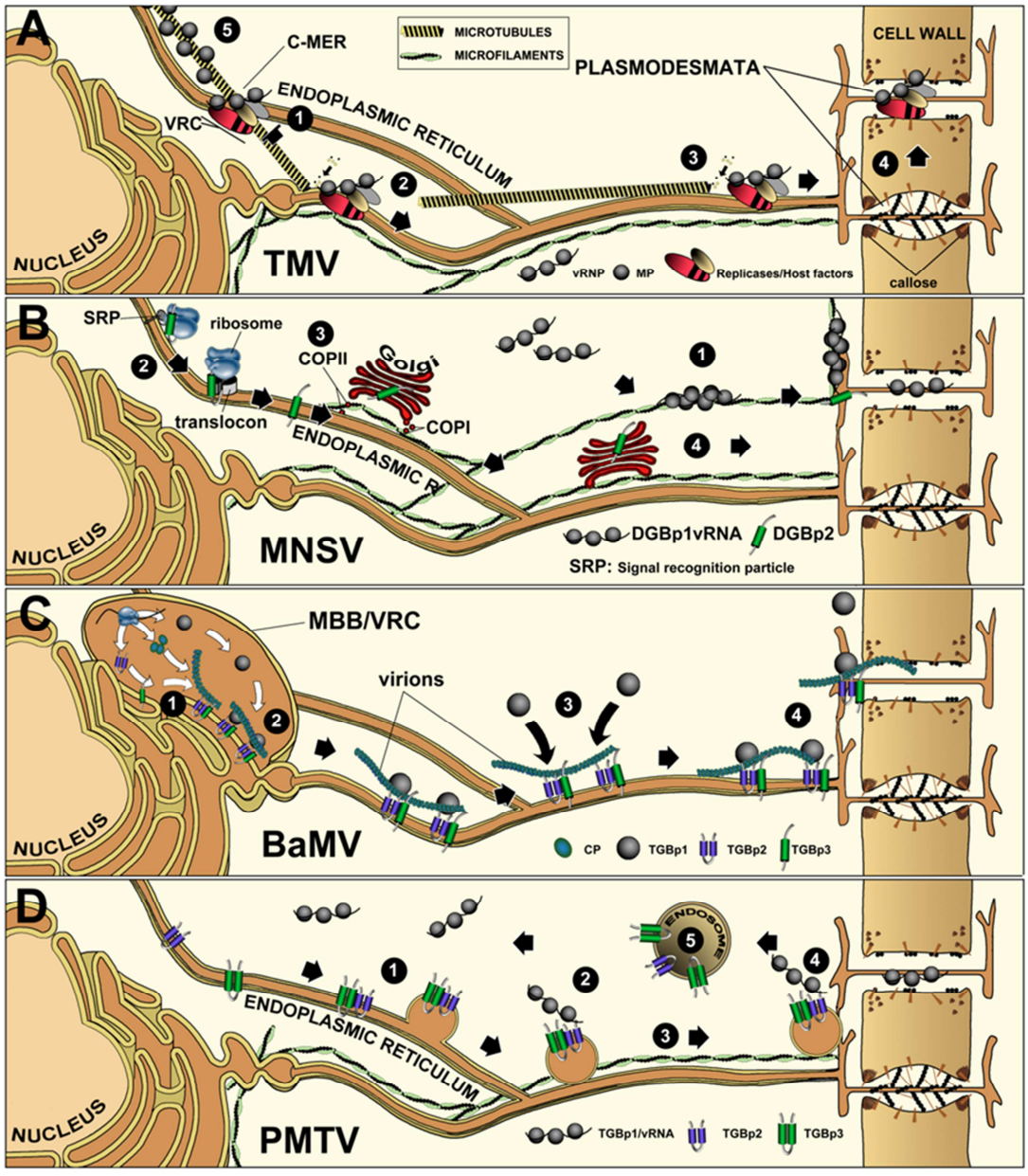

Figura 4. Cuatro modelos diferentes de transporte intracelular de los virus de plantas. A) virus del mosaico del tabaco (*Tobacco mosaic virus*, TMV). B) Virus de las manchas necróticas del melón (*Melon necrotic spot virus*, MNSV) C) Virus del mosaico del bambú (*Bamboo mosaic virus*, BMV). D) Virus del enanismo del tallo de la patata (*Potato mop-top virus*, PMTV). Ver texto para detalles. Modificado de Pallas *et al*. 2015.

1.2.3 Movimiento sistémico

Después de la replicación en las células infectadas los virus se mueven célula a célula a través de los PDs e inician una nueva ronda de replicación en la célula recién colonizada. Este proceso se repite hasta que los virus alcanzan los tejidos vasculares donde utilizan rutas de transporte preexistentes para propagar su infección a toda la planta (Wan *et al.,* 2015). En general este proceso puede dividirse en 4 etapas (Pallás *et al.,* 2011). (1) Entrada del virus en el parénquima vascular a través de las células de la vaina. (2) Translocación a las células acompañantes y a continuación a los elementos cribosos del parénquima vascular. (3) Transporte por los elementos cribosos hacia partes distales de la planta. (4) Entrada desde los elementos cribosos y las células acompañantes al parénquima vascular de regiones no infectadas. El movimiento sistémico y la distribución final en planta de los virus es un proceso complejo que depende entre otros muchos factores del estado del desarrollo de la planta y de las condiciones ambientales (e.g. Leisner *et al*., 1993; Mas and Pallás, 1993; Lunello *et al*., 2007). Aunque en este trabajo no se han abordado estudios directamente implicados en el movimiento vascular de los virus se describe a continuación una breve visión general del mismo. Para un mayor conocimiento se recomienda consultar extensas revisiones sobre el tema (Nelson and van Bel, 1998; Ueki and Citovsky, 2007; Vuorinen *et al*., 2011; Pallas *et al*., 2011).

La principal ruta para propagar la infección sistémicamente es a través del floema. La función de este tejido vascular es transportar y repartir por todo el cuerpo de la planta las sustancias carbonadas producidas durante la fotosíntesis (Figura 5), o aquellas movilizadas desde los lugares de almacenamiento, y otras moléculas como las hormonas. Está formado por dos tipos de células principalmente: las conductoras y las no conductoras. Las conductoras constituyen los elementos cribosos en angiospermas y las células cribosas en pteridofitas y gimnospermas. Ambas están constitudas por células vivas, aunque sin núcleo, y con la pared primaria engrosada por depósitos de calosa. Dentro de los elementos no conductores se encuentran las células parenquimáticas, siendo las más abundantes las denominadas células acompañantes (Lalonde *et al.,* 2001; Spicer, 2014).

El paso de las células del mesófilo al parénquima vascular no presenta ningún obstáculo para el virus diferente a los asociados al movimiento entre células del mesófilo, mientras que la infección de las células acompañantes sí representa un paso limitante en el transporte sistémico del virus (Moreno *et al.,* 2004; Vuorinen *et al.,* 2011). Una vez alcanzadas las células acompañantes, el PD que conecta estas células con los elementos cribosos es un PD especializado llamado PPU (de *pore plasmodesmal unit*). Estos difieren de los otros PDs en que en el lado de las células acompañantes están siempre ramificados; sin embargo en el lado del elemento criboso poseen un solo canal (Oparka and Turgeon, 1999). Por otra parte los PPUs poseen un límite de exclusión (SEL) mayor que en el caso de los PDs y se cree que la carga y descarga de los virus al floema se realiza a través de estos elementos PPU. Esto induciría a pensar que el paso a través de estos elementos se podría realizar con mayor facilidad; sin embargo ni viriones ni complejos vRNPs pueden atravesar los PPUs de forma pasiva. Debe existir algún tipo de factor y/o proceso que facilite el paso a estos elementos virales a través de los PPUs. En este sentido cabe destacar que la MP del virus del mosaico del pepino (*Cucumber mosaic virus,* CMV) interacciona de alguna forma con los PPUs aumentando el SEL y facilitando el paso del virus al sistema vascular (Blackman *et al.,* 1998).

Los virus tienen un fácil acceso a los elementos cribosos debido a que los plasmodesmos que conectan estos tipos de células presentan una estructura diferente a los que se encuentran entre células del mesófilo, y un SEL muy elevado que no restringe el paso del virus. El mecanismo y la forma (complejo ribonucleo-proteico o virión) con la que el virus alcanza estas células se desconocen. Una vez el virus se encuentra en el floema viajará siguiendo el patrón del flujo de fotoasimilados. En algunas combinaciones virus-huésped, como MNSV-melón, se ha puesto de manifiesto que el virus viaja hacia la parte aérea a través del floema interno mientras que hacia la raíz lo hace por el floema externo (Gosálvez-Bernal *et al.,* 2008). Se tienen pocos detalles del mecanismo de descarga viral del sistema floemático aunque podría producirse un proceso inverso al de carga salvando las diferencias existentes entre los tejidos de partida y de destino.

El otro elemento vascular utilizado, aunque mucho menos frecuentemente, por los virus de plantas para el movimiento sistémico es el xilema. Los elementos conductores del xilema son las traqueas y traqueidas. Las traqueidas son células largas o cortas que se comunican longitudinalmente, de forma que cada traqueida es una célula. Sus extremos recuerdan la punta de una aguja hipodérmica y están perforadas con punteaduras, con pared secundaria lignificada y lumen celular. La tráquea es el conjunto de todas las traqueidas comunicadas también lateralmente. Poseen como función primaria la conducción, y como función secundaria el sostén (Figura 5) (Roberts and McCann, 2000). Como ejemplo, se han detectado la CP del virus del enanismo ramificado del tomate (*Tomato bushy stunt virus*, TBSV) (Manabayeva *et al.,* 2013), del virus del moteado amarillo del arroz (*Rice yellow mottle virus*, RYMV) (Opalka *et al.,* 1998), del virus del mosaico del trigo transmitido por el suelo (*Soil-borne wheat mosaic virus*, SBWMV) (Verchot *et al.,* 2001), del virus del mosaico moteado verde del pepino (*Cucumber green mottle mosaic virus*, CGMMV) (Moreno *et al.,* 2004) y del PVX (Betti *et al.,* 2012) en los vasos del xilema.

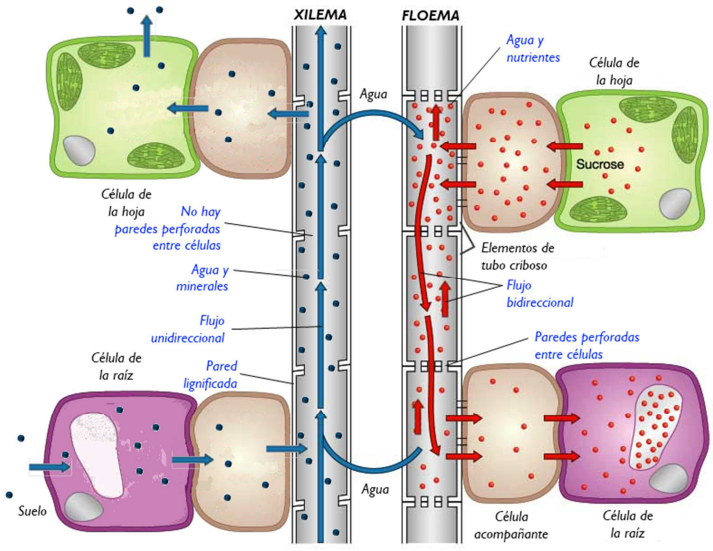

Figura 5. Esquema de los principales elementos del xilema y del floema que constituyen el sistema vascular en plantas.

1.3 TRANSPORTE DE MACROMOLÉCULAS ENTRE EL RETÍCULO ENDOPLASMÁTICO Y EL APARATO DE GOLGI

La asociación de los virus de plantas con las membranas celulares es un proceso que ocurre en alguna etapa del ciclo vital de estos patógenos. La replicación de los virus de RNA es citoplásmica pero sus replicasas son dirigidas hacia las membranas del RE y de otros orgánulos, como los peroxisomas, mitocondrias y cloroplastos, donde generan los verdaderos complejos replicativos. Además, como se ha descrito anteriormente, muchas de las MPs son proteínas integrales de membrana que se insertan en las membranas del RE. El sistema de membranas desempeña un papel esencial en el movimiento intracelular de los virus, y especialmente en el transporte de la p7B del MNSV, por lo que consideramos oportuno incluir en esta memoria una breve descripción de cómo se realiza el transporte de macromoléculas a través del sistema de endomembranas celular.

Las células eucariotas superiores han desarrollado un sistema de membranas endógeno que les permite tanto captar las macromoléculas del exterior como liberarlas desde el interior celular, así como incorporar las proteínas a membranas o desplazarlas a otros orgánulos. Este tráfico de macromoléculas está muy organizado en ambos sentidos constituyendo: (i) la vía secretora que va hacia el exterior, básicamente, desde el retículo endoplásmico (RE) pasando por el aparato de Golgi (AG) a la superficie celular, con una ruta lateral que va a los lisosomas/vacuolas y otros orgánulos como los cloroplastos (revisado en Hanton *et al.,* 2005; Matheson *et al.,* 2006) y (ii) la vía endocítica que va hacia el interior, desde la membrana plasmática a los endosomas y lisosomas/vacuolas (revisado en Aniento and Robinson, 2005; Robinson *et al.,* 2007). Ambas rutas no son totalmente independientes puesto que llegan a interconectarse a diferentes niveles (Figura 6).

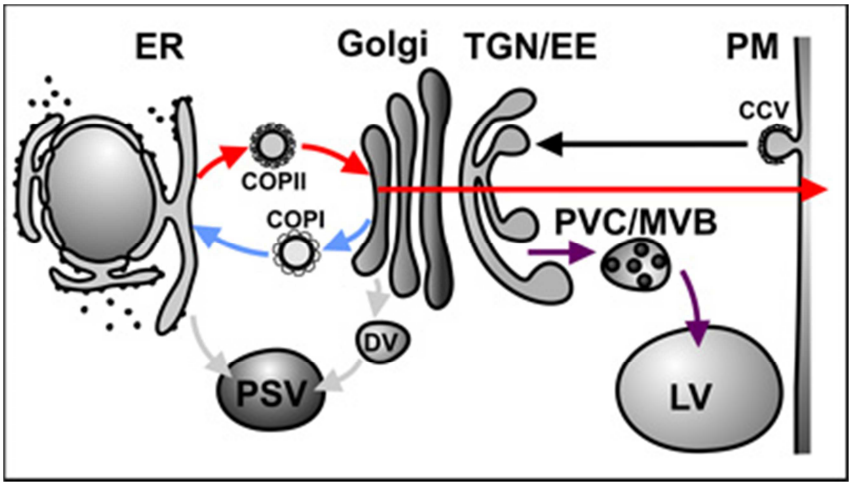

Figura 6. La ruta de secreción en plantas. En rojo se indica el transporte a la membrana plasmática (plasma membrane, PM) desde el retículo endoplasmático (endoplasmic reticulum, ER) via el aparato de Golgi (Golgi) siguiendo la red post-Golgi (*trans*-Golgi network, TGN). En azul, el transporte retrogrado desde la cara cis del Golgi hasta el ER. En negro, la endocitosis desde la PM vía el TGN hasta el endosoma temprano (early endosome, EE). En morado, el transporte a la vacuola lítica (lytic vacuole, LV) a través del compartimento prevacuolar (prevacuolar compartment, PVC). En gris, el transporte a la vacuola de almacén (protein storage vacuole, PSV) puede ocurrir desde el ER o vía vesículas densas desde el GA (dense-vesicles, DV).

Funcionalmente, el sistema de endomembranas de plantas es similar al de levaduras o animales e incluye la síntesis y transporte de moléculas de la ruta secretora a sus destinos finales. Sin embargo, estructuralmente, el de plantas presenta una serie de peculiaridades que necesitan ser descritas: (i) no existe un compartimiento intermedio entre el RE y el AG (Neumann *et al.,* 2003), conocido en mamíferos como ERGIC (*endoplasmic reticulum-golgi intermediate compartment*); (ii) el AG forma numerosas vesículas dispuestas por el citosol capaces de moverse a gran velocidad a través de la red de los microfilamentos de actina-miosina (Boevink *et al.,* 1998; Nebenführ *et al.,* 1999; Brandizzi *et al.,* 2002); (iii) estas vesículas podrían interaccionar directamente con el retículo endoplásmico para el intercambio de moléculas cargo en los dominios denominados ERES (*endoplasmic reticulum export sites*) que forman unidades móviles junto con el AG (Yang *et al.,* 2005) y (iv) las plantas presentan uno o más compartimentos, de gran tamaño y con diferentes funciones, llamados vacuolas, destacando su función en la degradación de proteínas acometida por la vacuola lítica y almacenamiento (Hanton *et al.,* 2006). Por su parte, en mamíferos, no existen las vacuolas y la degradación proteica se desarrolla en los lisosomas, no existentes en plantas, que aparecen en forma de pequeñas y numerosas vesículas distribuidas por toda la célula.

Las proteínas sintetizadas *de novo* entran en la ruta biosintética-secretora cuando atraviesan la membrana del RE posttraduccional o, en la mayoría de casos, cotraduccionalmente. Tanto las proteínas integrales de membrana como aquellas solubles emplean la misma maquinaria celular, conocida como translocón, para su inserción o translocación en el RE. Las proteínas que han de ser dirigidas hacia el translocón presentan en su extremo Nt una secuencia señal (SS) que consiste en uno o más residuos cargados seguidos de entre 12 y 20 aminoácidos hidrofóbicos. Algunas proteínas de membrana carecen de SS. En estos casos, el primer fragmento transmembrana actúa como una señal de direccionamiento anclando la proteína a la membrana puesto que, a diferencia de la SS, no es eliminado posteriormente.

El AG actúa como la mayor estación de intercambio de macromoléculas en células vegetales (Jurgens, 2004), estando involucrado en el tráfico desde el RE a los diferentes tipos de vacuolas o a la membrana plasmática (Figura 6). Además, el AG presenta una estructura polarizada donde las proteínas entran por la cara *cis* en vesículas recubiertas de proteínas de revestimiento (COPII) que provienen del RE (Hanton *et al.,* 2005, 2006; Matheson *et al.,* 2006) y salen en vesículas diferentes por la cara *trans* hacía la superficie u otros orgánulos (Hanton *et al.,* 2007). Estas dos redes son importantes en la clasificación de las proteínas: las que llegan a la cara *cis* pueden seguir a través del AG o volver al RE (transporte anterógrado o retrógrado, respectivamente); las que salen por la cara *trans* a la red post-Golgi son clasificadas según su destino sea los lisosomas/vacuolas, las vesículas de secreción o la superficie celular (Hawes and Satiat-Jeunemaitre, 2005; Hanton *et al.,* 2007). Más aún, durante el paso a través del AG, las moléculas transportadas pueden sufrir modificaciones covalentes ordenadas, como la glucosilación (Scheiffele and Fullekrug, 2000).

Las vesículas COPII destinadas al AG emergen desde las regiones especializadas del RE llamadas ERES (revisado en Hanton *et al.,* 2005; Matheson *et al.,* 2006). En principio, estas vesículas no son selectivas y transportan cualquier proteína que esté correctamente plegada siempre que su destino final sea la secreción al espacio extracelular (Phillipson *et al.,* 2001). Sin embargo, pueden existir señales en su secuencia que favorecen el transporte específico de las proteínas solubles hacia determinados compartimientos de la célula. En este caso, las proteínas solubles que se

incorporan en el interior de las vesículas parecen ser reconocidas por receptores transmembrana, los cuales interaccionarían mediante su dominio citosólico con la cubierta COPII.

Por otro lado, se asume que las proteínas con un único fragmento transmembrana son exportadas del RE por un mecanismo similar al de las proteínas solubles siguiendo un flujo pasivo. En este caso, su destino viene dictado por la longitud de su dominio hidrofóbico y el aumento en el espesor de las membranas que constituyen el RE, el AG y la membrana plasmática (Andreeva *et al.,* 2000; Phillipson *et al.,* 2001; Brandizzi *et al.,* 2002; daSilva *et al.,* 2004). Sin embargo, pueden existir determinadas señales en el domino citosólico de estas proteínas transmembrana que modifiquen el destino dictado por el fragmento hidrofóbico (Hanton *et al.,* 2005). El dominio citosólico de las proteínas transmembrana que van a ser transportadas hacia el aparato de Golgi interactúa con las proteínas que formaran las denominadas vesículas COPII y son ancladas y concentradas en el compartimento de exportación naciente. Por tanto las proteínas COPII serían necesarias para seleccionar las moléculas transmembrana que van a ser transportadas, además de para formar el compartimento de exportación.

1.3.1 El transporte anterógrado

El transporte anterógrado depende del ensamblaje de un complejo proteico denominado COPII (*coat protein*, COP) en los ERES (Figura 7). El complejo COPII incluye tres componentes citosólicos: una pequeña GTPasa (Sar1) y dos pequeños heterodímeros estructurales tipo Rab1, Sec23/24 y Sec 13/31. El ensamblaje se inicia con la activación de la proteína sec12, localizada y distribuida por la membrana del RE, que actúa como un factor de intercambio de nucléotidos de guanina (GEF) para la GTPasa Sar1. Cuando Sar1 une GTP expone una α-hélice anfipática que le facilita la asociación con la membrana del RE. Una vez asociada a la membrana recluta al heterodímero formado por las proteínas Sec23/24 mediante su interacción con Sec23. En ausencia de una proteína susceptible de ser transportada o “cargo”, Sec23 aumenta la capacidad GTPasa de Sar1 y este complejo incipiente se desensambla. Sin embargo, en presencia de una molécula “cargo” que interaccione generalmente con sec24, el complejo formado por Sar1-Sec23/24 y la molécula cargo se estabiliza reclutando al

heterotetrámero formado por Sec13/31 encargado de formar el revestimiento de la vesícula, facilitar la deformación de la membrana del retículo y permitir la salida de la vesícula ensamblada.

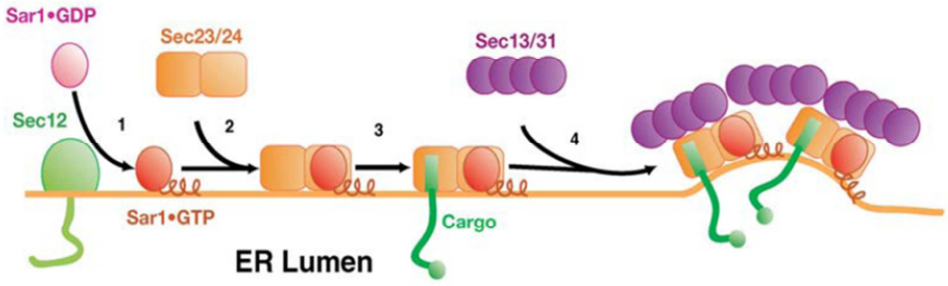

Figura 7. Ensamblaje secuencial del complejo COPII. Se inicia con la activación de la GTPasa Sar1. En presencia de una molécula cargo, Sar1 se une a Sec12 y se activa mediante el intercambio de GDP por GTP. Una vez activada, Sar1 recluta a Sec23/24 que proporciona el soporte de unión a la proteína cargo, formando el complejo previo a la formación de la vesícula. Por último se une Sec 13/31, que formará el revestimiento final (Lee *et al.*, 2004).

1.3.2 El transporte retrógrado

En el transporte retrógrado, las proteínas se mueven desde el AG al RE y está mediado por vesículas recubiertas del complejo proteico COPI compuesto de una pequeña GTPasa (ARF1) y un complejo heptamérico de proteínas de cubierta (Matheson *et al.,* 2006). El mecanismo de ensamblaje es muy similar al de las COPII, salvo por que la proteína que intercambia nucleótidos se denomina Gea1 y la pequeña GTPasa en este caso se trata de Arf1. Una vez está unida a la membrana del AG, Arf1 recluta un complejo heptamérico preensamblado que formará el revestimiento de la vesícula y mediará la deformación de la membrana, facilitando la liberación de la vesícula formada (Figura 8).

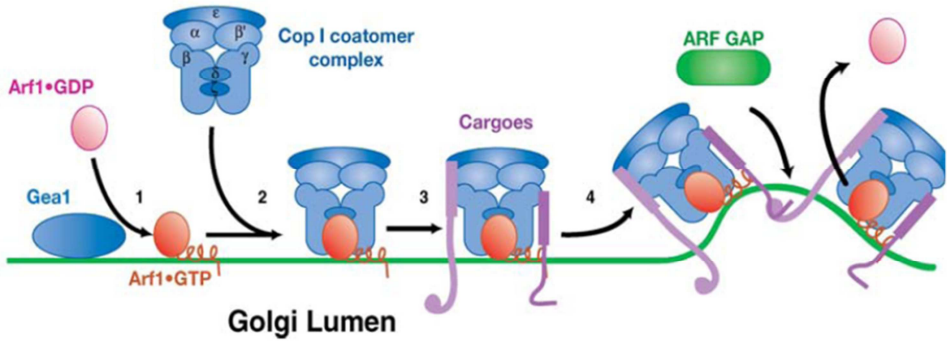

Figura 8. Ensamblaje secuencial del complejo COPI. Se inicia con la activación de la GTPasa Arf1. En presencia de una molécula cargo, Arf1 se une a Gea1 y se activa mediante el intercambio de GDP por GTP. Una vez activada, Arf1 recluta el complejo del coatómero peensamblado que proporciona el soporte de unión a la proteína cargo, formando el revestimiento de la vesícula. Por último se facilita la gemación de la membrana reclutando ARF-GAP, que permite el reclutamiento de una Arf-GTPasa. Esta hidrolizará el GTP de Arf permitiendo su liberación de la membrana (Lee *et al.*, 2004).

1.4 MULTIFUNCIONALIDAD DE LAS PROTEÍNAS DE CUBIERTA VIRALES

La proteína de cubierta viral (CP) es una proteína estructural que acompaña al genoma viral dentro y fuera de las células. Normalmente estas proteínas, que suelen ser el componente proteico mayoritario de los virus, se agrupan y unen fuertemente formando el virión que envolverá y protegerá al genoma. En general los viriones suelen adoptar básicamente dos conformaciones, bastón o esfera. En el primer caso las CPs se ensamblan siguiendo una simetría helicoidal adquiriendo una apariencia de varilla rígida o filamento flexible. En el segundo caso las CPs se ensamblan siguiendo una simetría icosaédrica, con lo que se consiguen cubiertas de formas esféricas y de grandes dimensiones internas.

Además de esta función de protección y envoltura, las proteínas de cubierta intervienen en prácticamente todas las etapas de del ciclo de infección viral desde la multiplicación hasta la diseminación, incluida la asistencia en la replicación, el movimiento entre células y órganos y en la transmisión entre plantas a través de un vector biológico. Las CPs virales pueden considerarse por tanto los prototipos de proteínas multifuncionales. A continuación se repasan de manera muy breve las principales funciones que dichas proteínas tienen al margen de su obvio papel estructural.

1.4.1 Funciones de las proteínas de cubierta virales

1.4.1.1 Traducción del RNA viral (vRNA)

Una vez dentro de la célula, el virus se desencapsida y en el caso de los virus de RNA de cadena positiva, deben competir con los RNAs celulares para transcribirse y traducirse. Los vRNAs sin estructura CAP y sin cola poli(A) han desarrollado estrategias alternativas para simular estas estructuras. En general la CP puede actuar de dos formas para regular la traducción, bien uniéndose al vRNA o bien mediante la interacción con proteínas del huésped (Kapp and Lorsch, 2004). El primer mecanismo estaría representado por las CPs de los ilarvirus y del virus del mosaico de la alfalfa (*Alfalfa mosaic virus*, AMV) (Bol, 1999; Pallás *et al.,* 2014). Dichas CPs se unen a la región 3'UTR de los vRNAs induciendo un cambio conformacional que activaría su síntesis (Baer *et al.,* 1994; Aparicio *et al.,* 2003). Diversos estudios han demostrado que el RNA genómico de los ilarvirus y del AMV no es infeccioso a no ser que en el inóculo esté presente la CP o el transcrito correspondiente al subgenómico de la CP (Jaspers, 1985; Callaway *et al.,* 2001). Este fenómeno es conocido con el nombre de activación genómica. Neeleman *et al* (2001) pusieron de manifiesto que la CP del AMV mimetiza las funciones de la proteína de unión a regiones poli(A) (PABP) activando la traducción de los RNAs virales. Por otra parte la CP del virus del mosaico del bromo (*Brome mosaic virus*, BMV) regula la traducción de su genoma tripartito mediante un mecanismo que es dependiente de la concentración de CP (Yi *et al.,* 2009). En presencia de cantidades elevadas de CP, ésta se une un elemento denominado B-box de su vRNA, situado dentro de la región 5'UTR, para disminuir la traducción.

La modulación de la traducción del RNA viral de forma indirecta se realiza a través de la unión/reclutamiento de factores de inicio de la traducción celulares. Así, la CP de AMV también es capaz de interaccionar con el factor eIF4G y eIFiso4G (Krab *et al.,* 2005) que son factores que se unen a la estructura 5' CAP de los mRNAs.

1.4.1.2 Replicación

La CP también desempeña un papel importante en la replicación de los virus con genomas de ssRNA(-) y dsRNA. Es el caso del virus de bronceado del tomate (*Tomato spotted wilt virus*, TSWV), en el que la asociación de la CP con los RNAs y la RNA

polimerasa dependiente de RNA (RdRp) es necesaria para la formación de complejos de replicación activos y funcionales (Kormelink *et al*.,, 2011). La CP del AMV y de los ilarvirus también interviene en la unión al complejo del replicación con el fin de regular la síntesis de su vRNA (Aparicio *et al.,* 2003; Reichert *et al.,* 2007) y su localización nucleo-citoplasmica es esencial para el ciclo infectivo del virus (Herranz *et al.,* 2012). La CP del BMV también ha sido implicada en la replicación del RNA viral a través del reconocimiento de la región promotora para la síntesis del RNA de cadena negativa cuando está presente en bajas concentraciones. Un único cambio nucleotídico en dicha región que reduce la capacidad de unión a la CP, también reduce de manera significativa la replicación viral (Ni and Kao, 2013).

1.4.1.3 Movimiento

Son muchos los casos descritos en los que la CP viral desempeña un papel esencial en el movimiento viral ya sea célula a célula, sistémico o ambos. En el primer caso podemos subdividir este tipo de movimiento, entre otras formas de hacerlo (ver apartado 1.2.2), como independiente (tobamovirus, dianthovirus, carmovirus, hordeivirus y umbraviruses) o dependiente (la mayor parte de los bromovirus, nepovirus, potexvirus y cucumovirus) de la CP. En este último caso, el movimiento de los virus podría subdividirse en dos subgrupos más: aquellos que requieren la CP porque se mueven como viriones y aquellos en los que la CP formaría parte de un complejo ternario con la correspondiente MP y el genoma viral (Waigmann *et al.,* 2004; Scholthof, 2005). Por ejemplo, el CMV usa su CP para fortalecer sus débiles complejos MP-vRNA y hacerlos resistentes a las RNasas y funcionales para el transporte célula a célula (Andreev *et al.,* 2004; Kim *et al.,* 2004). La CP del PVX reconoce y se une al extremo 5’ proximal del vRNA y a la correspondiente MP. Dado que PVX no requiere la formación del virión para su movimiento célula a célula, este virus parece moverse en forma de un complejo TGBp1-vRNA mediado por la CP (Lough *et al.,* 2000). La infección de otro potexvirus, el BaMV, requiere la interacción de la CP con la replicasa viral (Lee *et al.,* 2011). Mutantes que debilitan esta interacción son defectivos en el movimiento célula a célula. La capacidad de dimerización de la CP del AMV mediada por regiones ricas en residuos de lisina del extremo amino terminal es

esencial para el movimiento célula a célula, el movimiento sistémico y la forDI CARmación de viriones (Herranz *et al.,* 2012).

A nivel de movimiento sistémico son muchos los virus que requieren la CP para el transporte por el floema (Waigman *et al.,* 2004; Brizard *et al.,* 2006; Casado-Vela *et al.,* 2006; Elvira *et al.,* 2008; Di Carli *et al.,* 2010; Pineda *et al.,* 2010; Diaz-Vivancos *et al.,* 2008; Giribaldi *et al.,* 2011,), ya sea en forma de viriones o como complejos RNA-proteina (VNP). Sin embargo, se ha observado que en algunos casos la necesidad de la CP es dependiente del tipo de huésped, como en algunos tombusvirus, hordeivirus y tobravirus. También para el TMV, se ha determinado que generalmente necesita la CP para el movimiento sistémico (Takamatsu *et al.,* 1987; Bransom *et al.,* 1995), aunque mutantes de deleción de la CP son capaces de moverse sistémicamente en *N. benthamiana* (Bol, 2008).

1.4.1.4 Transmisión por el vector

Los virus se transmiten de una planta a otra bien mecánicamente bien a través de vectores biológicos tales como áfidos, artrópodos, nematodos y zoosporas de hongos. Generalmente la transmisión por vector necesita la formación del virión y la CP es el mayor determinante de especificidad de la interacción virus-vector (Ng and Perry, 2004). Este es el caso del MNSV y de los tombusvirus relacionados TBSV y el virus de la necrosis del pepino (*Cucumber necrosis virus*, CNV), todos son transmitidos por el hongo del suelo *Olpidium bornovanus* mediante la interacción de determinadas regiones de la CP (Kakani *et al.,* 2001) y las glicoproteínas de la membrana de las zoosporas (Kakani *et al.,* 2004, Bol, 2008). La CP del CMV también es el único factor viral implicado en su transmisión. Esta CP posee diferentes motivos responsables de la transmisión del CMV por diferentes especies de áfidos. Los aminoácidos en las posiciones 25, 129, 162, 168 y 214 son esenciales para la transmisión por *Myzus persicae*, mientras que los situados en las posiciones 129, 162 y 168 se requieren para la transmisión por *Aphis gossypii.* La CP de los potyvirus también presenta en su región amino terminal un motivo extremadamente conservado en aislados transmisibles por pulgón. Consta de tres residuos aspártico-alanina-glicina (DAG) y la alteración o eliminación de estos aminoácidos o aquellos situados cerca de este motivo provoca la

pérdida total o parcial de la transmisibilidad por pulgones de varios potyvirus. Además, la región amino terminal de la CP de los potyvirus interacciona con el dominio denominado PTK de una proteína auxiliar (HC-Pro). La pérdida de esta interacción en variantes mutadas de la CP con alteraciones en el dominio DAG se correlaciona con la pérdida de transmisión del virus. En los closterovirus, el virión consta principalmente una CP mayoritaria que constituye prácticamente toda la estructura filamentosa de la partícula. Sin embargo, existe una segunda CP minoritaria (CPm) que forma una estructura corta en un extremo del virión. Mutaciones en esta CPm del virus del amarilleamiento infeccioso de la lechuga (*Lettuce infectious yellows virus*, LIYV) impidieron su transmisión por mosca blanca indicando que la CPm constituye un determinante de transmisibilidad. En el caso de los luteovirus y polerovirus, un polipéptido minoritario (proteína RT, de *readthrough*) que forma parte del virión y que está constituido por la CP y un dominio resultado de una lectura a través del codón de parada de la CP (dominio RTD) desempeña un papel esencial en la transmisión. El dominio RT queda expuesto en la superficie del virión y su naturaleza determina la especificidad de vector (ampliado en Andret-Link and Fuchs, 2005).

1.4.1.5 Sintomatología

La infección viral requiere numerosas interacciones entre factores del virus y la planta huésped (Niehl and Heinlein, 2011; Pallás and García, 2011). La gravedad de los síntomas causados por una infección viral suele depender de las características del huésped, del virus y del ambiente en el momento de la infección. Existen numerosos estudios en los que se relaciona que mutaciones en la CP pueden alterar la gama de huéspedes y la aparición de síntomas (van Loon, 1987; Matthews, 1991; García and Pallás, 2015 para revisiones sobre el tema). En el TCV se ha observado que varios mutantes en la zona que conecta los dominios S y P de su CP causan síntomas más graves que la infección con la cepa silvestre (Lin and Heaton, 1999). También se ha demostrado que la CP de otros virus incluyendo tobamovirus (Dawson, 1992; Novikov *et al.,* 2000), luteovirus (Bencharki *et al.,* 2000) y cucumovirus (Zhang *et al.,* 1994; Sugiyama *et al.,* 2000) están relacionadas con la modulación de los síntomas. Recientemente se ha demostrado que la región N-terminal de la CP del PepMV es un determinante de patogenicidad (Duff-Farrier *et al.,* 2015). Por otra parte, está bien

documentado que las CPs virales pueden actuar como elicitores de la respuesta hipersensible (HR) mediada por genes de resistencia R tal y como se ha descrito para las CPs del TMV, TCV, CMV, PVX y PMMoV (ver Moffet, 2009 para una revisión). Por otra parte las CPs de determinados virus pueden interaccionar, por un lado, con proteínas cloroplásticas afectando la estabilidad y funcionalidad de los mismos y ocasionando los típicos síntomas de clorosis y, por otro, con factores implicados en las rutas de señalización hormonal interfiriendo y/o modulandolas. Esta desregulación ocasiona finalmente síntomas tales como enanismo y/o arrugamientos (ver García and Pallás, 2015 para una revisión).

1.4.1.6 Defensa/Silenciamiento

Los principales mecanismos de defensa de la planta están mediados por genes de resistencia (genes R) y el mecanismo de RNA de interferencia (RNAi). El primero de los mecanismos se basa en la "hipótesis guarda" (Thomma *et al.,* 2011). Esta hipótesis se basa en que un efector del virus posee como diana un componente clave (*guardee*) del sistema de defensa de la planta para tratar de anularlo y poder así invadirla de forma efectiva. El cambio que induce el efector viral en la proteína "guardee" es reconocido por una proteína R (*guard*), que como consecuencia desencadena el mecanismo de defensa (Belkhadir *et al.,* 2004) y produce una respuesta hipersensible (HR) en la planta para confinar al virus. En un huésped susceptible no existe ese gen R (Soosaar *et al.,* 2005). Estudios de doble híbrido han demostrado que la CP del TCV interacciona con un factor de transcripción (TIP, el *guardee*) de ecotipos de *Arabidopsis thaliana* con el gen de resistencia HRT (*guard*). La interacción entre el TIP y la CP es necesaria para desencadenar la respuesta de defensa mediada por HRT (Ren *et al.,* 2005). La CP de CMV también está relacionada con la defensa mediada por el gen de resistencia RCY de *A. thaliana* (Soosaar *et al.,* 2005). En el caso del TMV se ha descrito que el mantenimiento de la estructura D de la CP es esencial para desarrolla una respuesta hipersensible en *Nicotiana sylvestris* (Culver, 2002).

La defensa mediada por RNAi se desencadena principalmente por el dsRNA derivado de intermediarios de la replicación viral. Para tratar de evadir este mecanismo de defensa los virus han evolucionado para contrarrestar esta ruta de

silenciamiento de RNA a diferentes niveles (ver apartado 1.5). Las CP de varios virus, entre ellos varios carmovirus, han sido identificadas como supresores del silenciamiento (*viral suppressor of RNA silencing, VSR*) (Qu *et al.,* 2003; Qiu and Scholthof, 2004; Roth *et al.,* 2004; Soosaar *et al.,* 2005; Meng *et al.,* 2006; Pérez-Cañamás and Hernández, 2014). La CP del TCV es capaz de inhibir el silenciamiento mediado por RNA interfiriendo con AGO1, y esta función no está relacionada con el papel que desempeña en la resistencia mediada por HRT. La CP del virus de la tristeza de los cítricos (*Citrus tristeza virus*, CTV) interfiere en el silenciamiento intercelular. Otro ejemplo es la subunidad pequeña de la CP del virus del mosaico del chícharo (*Cowpea mosaic virus*, CPMV) que se ha descrito como un supresor débil del silenciamiento. La CP del PFBV (p37) actúa como VSR principalmente mediante la unión a sRNAs, aunque su localización nucleolar y la unión a factores celulares relacionados con el silenciamiento (AGO1 y 4) podrían estar también implicados. Y la CP del satélite del virus del mosaico del panicum de la familia *Tombusviridae* (*Panicum mosaic satellite virus*, SPMV) actúa como un factor de patogenicidad. Esta CP no inhibe el silenciamiento de RNA pero interfiere con la actividad supresora de la proteína p25 del PVX.

1.5 EL SILENCIAMIENTO GÉNICO EN PLANTAS

Uno de los avances más importantes en la biología de las últimas décadas ha sido el descubrimiento de que cierto tipo de moléculas de RNA pueden regular la expresión de determinados genes (ver Pallás, 2013 para revisión histórica). Este fenómeno conocido como interferencia de RNA (RNAi) es un mecanismo, evolutivamente conservado en muchos eucariotas, utilizado para suprimir o "silenciar" la expresión de determinados genes. El silenciamiento génico desempeña un papel muy importante en diversos procesos biológicos como el desarrollo, el mantenimiento de la estabilidad genómica y la defensa contra patógenos. Actúa de manera específica de secuencia por medio de pequeños RNAs de 20 a 40 nucleótidos (nt) de longitud (short interfering RNAs, siRNAs) que pueden operar a varios niveles, bien por represión transcripcional asociada con la metilación de regiones promotoras (*transcriptional gene silencing*, TGS), bien por regulación post-transcripcional asociada con la inactivación o degradación de transcritos (*post-transcriptional gene silencing*, PTGS) o bien por

represión traduccional (Kim, 2003; Adenot *et al.,* 2006; Sen and Blau, 2006; Minois *et al.,* 2010).

Existen distintas rutas de silenciamiento génico en plantas y todas constan de una serie de pasos evolutivamente conservados (Figura 9). En todos los casos el silenciamiento se desencadena por la presencia de RNAs de doble cadena (dsRNAs) de diverso origen o de RNAs monocatenarios (ssRNAs) con una alta estructura secundaria (estructuras en horquilla o *hairpin*). Estos últimos pueden derivar directamente de la replicación viral, de repeticiones invertidas, de la transcripción convergente de transgenes y transposones o de loci endógenos. De forma alternativa, los dsRNAs pueden sintetizarse por la acción de alguna de las RNA polimerasas celulares (RDR1-6 en *A. thaliana*) a partir de RNAs mensajeros (mRNAs) aberrantes o procedentes del corte endonucleotídico mediado por un tipo determinado de siRNAs conocido como microRNAs (miRNAs), así como de transcritos producidos por la RNA pol IV (Figura 9). Estos RNAs son procesados por RNasas de tipo III, denominadas Dicer (del inglés *to dice* que significa cortar en dados) o Dicer-like (DCL) en plantas, dando lugar a siRNAs de doble cadena de 18 a 25 nt. En plantas, insectos, protozoos y hongos como *Neurospora crassa* o *Magnaporthe oryzae*, las DCLs conforman pequeñas familias génicas compuestas por 2, 4 o 5 miembros que dan lugar a distintas clases de siRNAs. Por ejemplo, en *A. thaliana* se han descrito cuatro proteínas DCL (DCL1-4). DCL1 genera siRNAs de entre 18 y 21 nt, DCL2 de 22 nt, DCL3 de 24 nt y DCL4 de 21 nt. Cada tipo de siRNA participa específicamente en una o varias rutas de silenciamiento.

Las DCL son asistidas por proteínas de unión al dsRNA (HYL1, DRB2-5) en el reconocimiento y rotura del mismo. A continuación, los siRNAs son estabilizados por la metilación en el extremo 3´ mediada por la metiltransferasa HEN1 previniendo de esta manera su degradación. Estos siRNAs bicatenarios estabilizados pueden tener principalmente dos destinos: 1) ser retenidos en el núcleo para actuar sobre la cromatina (TGS) o 2) ser exportados al citoplasma por un homólogo de la exportina-5, HASTY (HST) para iniciar el silenciamiento génico posttranscripcional (*post-transcriptional gene silencing*, PTGS). Una de sus dos hebras es reclutada por las proteínas Argonauta (AGO1-10 en *A. thaliana*) a un complejo multiproteico de silenciamiento inducido por RNA o RISC (RNA-induced silencing complex) y son

utilizados como guía para reconocer los RNA mensajeros de secuencia complementaria sobre los que ejecutará su función. Ésta podría ser: 1) el corte endonucleolítico en el centro del híbrido siRNA-diana, 2) la represión de la traducción mediante mecanismos todavía desconocidos o 3) la metilación del residuo citosina del DNA o de las histonas con la ayuda de la subunidad b de la Pol IV (NRPD1b).

Según la procedencia de la cadena de dsRNA será procesada por una DCL determinada dando lugar a un tipo de siRNA que será reclutado por una AGO especifica. Por ejemplo, los miRNAs (19-25 nt) proceden de la transcripción de genes endógenos no codificantes, son procesados por DCL1, reclutados por AGO1 y desempeñan una función reguladora en *trans* sobre la expresión de mensajeros con secuencia complementaria. Los trans-acting siRNAs (ta-siRNA, 21 nt) provienen de transcritos no codificantes de genes denominados TAS, son procesados por DCL4 y posteriormente reclutados por AGO1 o AGO 7. Otros tipos de siRNAs provienen de la replicación viral o de transgenes y son producidos por la escisión mediada por DCL2 o DCL4 e interaccionan con AGO1. Los siRNAs heterocromáticos (hc-siRNAs, 23-25 nt) son sintetizados a partir de secuencias genómicas repetitivas tales como transposones, retroelementos, DNA ribosomal (rDNA), repeticiones centroméricas y regiones metiladas. Son procesados por DCL3 y se unen a AGO4 o AGO6 induciendo el silenciamiento de la cromatina (Figura 9). Finalmente, los siRNAs asociados a transcritos naturales antisentido (nat-siRNAs) provienen de los transcritos naturales antisentido (NATs) los cuales se originan a su vez de genes endógenos de la planta, codificantes o no, que comparten una complementariedad de secuencia con otros RNAs. Los nat-siRNAs son procesados por DCL1 o DCL2 (las diferentes rutas de silenciamiento génico en plantas y los tipos de siRNAs han sido ampliamente revisados en Baulcombe, 2004; Herr and Baulcombe, 2004; Vaucheret, 2006; Chapman and Carrington, 2007; Brodersen and Voinnet, 2006; Xie y Qi, 2008; Jamalkandi and Masoudi-Nejad, 2009; Ruiz-Ferrer and Voinnet, 2009; Vázquez *et al*, 2010).

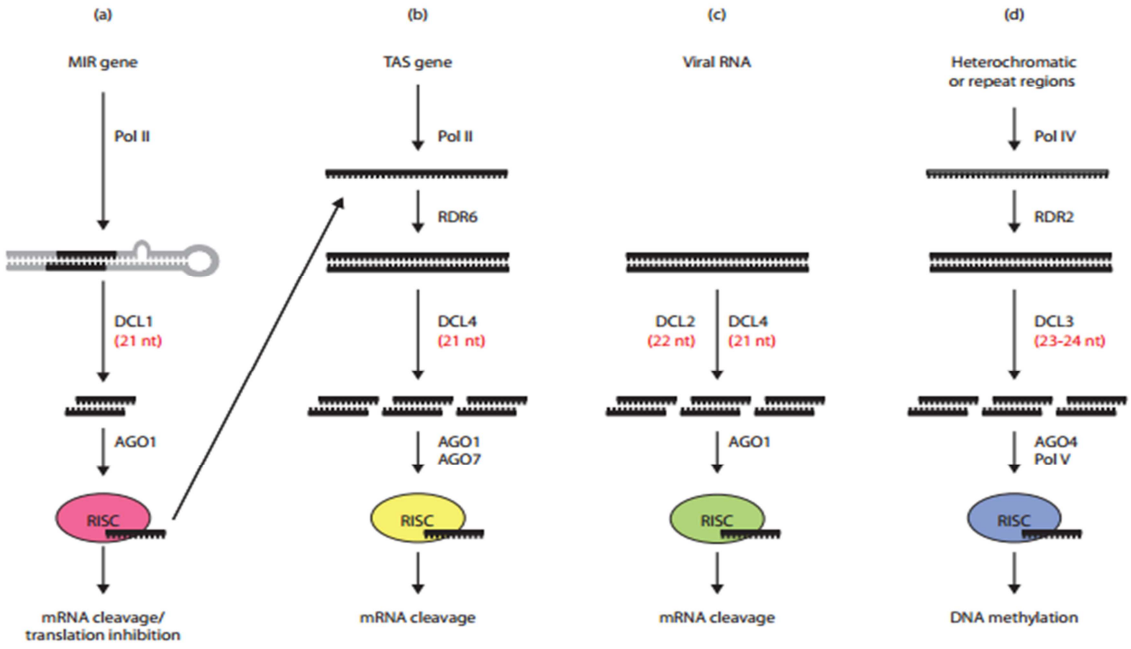

Figura 9: Representación esquemática de las diferentes rutas de silenciamiento de RNA en plantas. Los diferentes siRNAs formados a partir del corte de un dsRNA por las enzimas DCL son a) microRNAs (DCL1), b) trans-acting siRNAs (DCL4), c) siRNAs virales (DCL 2 y 4) y d) siRNAs heterocromáticos (DCL3). Estos son reconocidos por una proteína AGO específica dependiendo del tipo de siRNA e incorporados al complejo RISC, el cual está formado por AGO, el siRNA y otros factores proteicos que varían según la ruta considerada (los diferentes colores de RISC indican diferentes componentes) (Molnar *et al.,* 2010).

Los fragmentos resultantes del corte endonucleotídico de los RNAs mensajeros pueden ser degradados por la 5'-3' exoribonucleasa 4 (XRN-4) en el citoplasma o ser utilizados para amplificar la señal de silenciamiento por medio de las RNA polimerasas dependientes de RNA (RDR1-6 en *A. thaliana*). Estas proteínas utilizan los siRNAs y el RNA mensajero de secuencia complementaria para dar lugar a nuevos dsRNAs, que son procesados de nuevo por las DCLs incrementando la señal de silenciamiento. Por ejemplo, la amplificación del PTGS inducido por transgenes y virus por RDR6 requiere de la actividad de DCL4 y AGO1 mientras que el TGS de transposones y repeticiones en el núcleo por RDR2 necesita de la actividad de DCL3 y AGO4. Además las RDR son auxiliadas por SDE3, una proteína con actividad helicasa, SDE5 para asistir el proceso de amplificación y SGS3 que se une y estabiliza el RNA molde para iniciar la síntesis del dsRNA (Willman *et al*, 2011).

1.5.1 Estrategias virales contra el silenciamiento de RNA en plantas: supresores virales del silenciamiento de RNA (viral supressors of RNA silencing, VSRs)

Como respuesta al silenciamiento de RNA en plantas, los virus han desarrollado estrategias específicas basadas en la utilización de factores propios o VSRs con capacidad de suprimir el silenciamiento. Los VSRs pueden actuar en diferentes pasos de la ruta de silenciamiento inhibiendo de manera eficiente la respuesta antiviral del huésped por medio de la interacción con factores clave de la maquinaria de silenciamiento implicados en el reconocimiento de RNA viral, el procesamiento de dsRNAs, el ensamblaje del complejo RISC y la amplificación de señal. De hecho un virus puede presentar varios VSRs de forma que cada uno puede afectar a etapas diferentes de la ruta de silenciamiento (Figura 10) (Csorba *et al.,* 2015). La mayoría de los VSRs identificados son multifuncionales ya que además actúan como proteínas de cubierta, replicasas, proteínas de movimiento, factores implicados en la transmisión, proteasas o reguladores transcripcionales (Roth *et al.,* 2004; Burgyán and Havelda, 2011; Wang *et al.,* 2012). En otras ocasiones los VSRs se caracterizaron inicialmente como determinantes de patogenicidad y virulencia al estar relacionados con la aparición de síntomas durante la infección viral (García and Pallás, 2015). Actualmente también se sugiere que los VSRs podrían dar lugar a alteraciones en la expresión de siRNAs endógenos desregulando la expresión de genes celulares (Bazzini *et al.,* 2007; Shimura and Pantaleo, 2011).

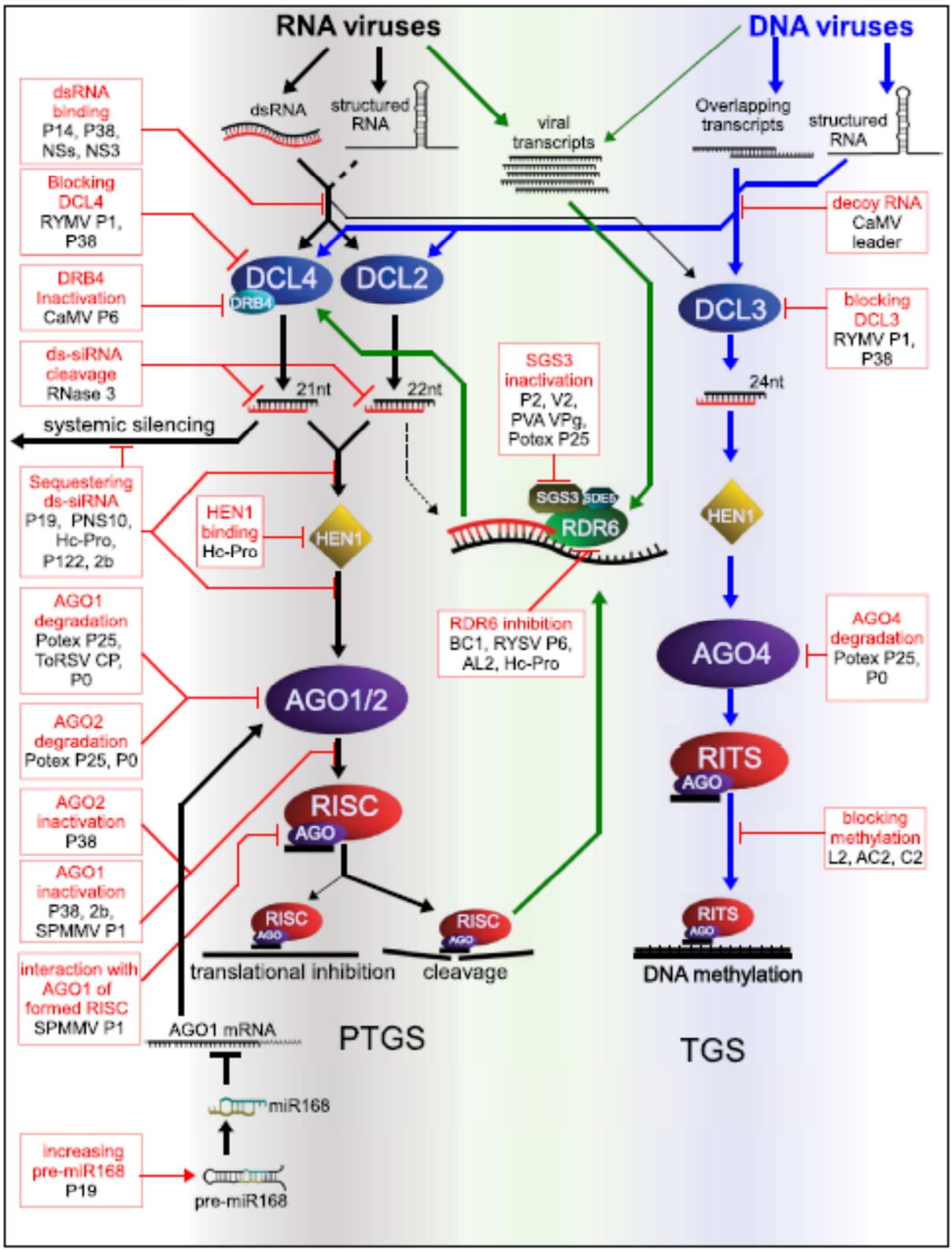

Figura 10. Esquema de los principales supresores del silenciamiento virales identificados y punto de la ruta de silenciamiento donde actúan (Csorba *et al.,* 2015).

1.6 INFECCIONES VIRALES EN PLANTAS: UNA VISIÓN GENERAL SOBRE LAS ALTERACIONES PROTEÓMICAS

Con la incorporación de las micromatrices de DNA en las dos últimas décadas han proliferado estudios acerca de la respuesta del huésped a nivel transcriptómico frente a infecciones virales (ver revisión en Whitham *et al.,* 2006; Rodrigo *et al.,* 2012). Sin embargo, los estudios a nivel de las alteraciones proteómicas que la infección viral ocasiona han tenido que esperar algunos años debido esencialmente a la sofisticación de las técnicas empleadas para la purificación y caracterización de la población proteica. En principio estos estudios proteómicos se utilizaron para "cartografíar" los perfiles proteómicos de los diferentes órganos, tejidos o tipos celulares (ver revisión de Di Carli *et al.,* 2012). Las recientes aplicaciones de las técnicas cuantitativas de "segunda generación" tal como la electroforesis en gel diferencial (DIGE) ha permitido abordar estudios comparativos sobre la expresión del proteoma en diferentes condiciones de estrés o de desarrollo. A pesar de este progreso tecnológico los estudios del proteoma diferencial en las infecciones virales están prácticamente en sus inicios.

1.6.1 Metodologías utilizadas en los estudios proteómicos

La mayoría de muestras biológicas son mezclas de proteínas, las cuales no pueden ser analizadas directamente por espectrometría de masas (MS) dada su complejidad, por lo que es necesario un paso previo de fraccionamiento que permita identificar un mayor número de proteínas. Actualmente las aproximaciones proteómicas combinan varias técnicas de separación previas al análisis de MS, lo que permite ganar resolución en la identificación del proteoma. Los dos tipos de métodos más utilizados para el fraccionamiento de proteínas son la electroforesis bidimensional en gel (2-DE) y la cromatografía líquida multidimensional (MDLC).

1.6.1.1 Electroforesis bidimensional en gel (2-DE)

Esta técnica, desarrollada por Kenrick y Margolis (1970) y por O'Farrell (1975), se caracteriza por la separación de mezclas complejas de proteínas en gel. En primer lugar se realiza un isoelectroenfoque (IEF) donde las proteínas se separan según su punto

isoeléctrico (pI). A continuación se separan por peso molecular en geles de poliacrilamida en presencia de SDS (SDS-PAGE). Actualmente se ha podido mejorar notablemente la capacidad de la 2-DE para realizar análisis comparativos con el desarrollo de la electroforesis bidimensional diferencial (2D-DIGE). Se trata de una técnica basada en el marcaje fluorescente de las proteínas previo a su separación, otorgándole una gran precisión en la cuantificación, que le permite separar varias muestras proteicas en un mismo gel. Además de poseer un estándar interno que incrementa la reproducibilidad y la fiabilidad del análisis diferencial entre muestras. (Marouga *et al.,* 2005).

1.6.1.2 Cromatografía líquida (LC)

Es una técnica de fraccionamiento que puede utilizarse para separar proteínas o péptidos según sus propiedades físicas y/o químicas. Puede usarse como un paso previo o posterior a la 2-DE o como alternativa a la misma. La cromatografía multidimensional se lleva a cabo mediante la aplicación de sucesivos fraccionamientos, utilizando diferentes tipos de columnas tales como: las de fase reversa, las de exclusión molecular, las de intercambio iónico y las de afinidad.

Las técnicas de cromatografía conectadas a equipos de espectrometría de masas en tándem más utilizadas en los estudios proteómicos son cuatro: MudPIT (*multidimensional protein identification technology*), ICAT (isotope-coded afinity tag), iTRAQ (isobaric tag for relative and absolute quantitation) y ProteomeLAB PF2D (protein fractionation 2-dimensions). Presentan una serie de ventajas frente a las 2-DE como la posibilidad de analizar proteínas con pI extremos (ácidos y básicos), las proteínas poco abundantes y las proteínas con marcado perfil hidrofóbico, ya que dada su composición y baja solubilidad están poco representadas en los mapas 2-DE. Tanto la técnica de MudPIT como la ICAT, se centran la separación de la muestra por cromatografía líquida seguido por el análisis en MS. En el caso del MudPIT la principal desventaja es el análisis posterior de los datos y la elevada variación experimental (Washburn *et al.,* 2001). Para tratar de paliar esto se pueden marcar los elementos C o N con isótopos pesados y ligeros como en el caso de la ICAT, donde se marcan las cisteínas (Jorrín *et al.,* 2007). Una evolución de esta técnica es la iTRAQ, en esta técnica

se marcan los grupos amino con isótopos isobáricos estables. Esto permite incrementar la eficiencia del marcado de los péptidos, así como la precisión y sensibilidad en la detección comparado con la ICAT (Fan *et al.,* 2011; Neilson *et al.,* 2011; Yang *et al.,* 2011).

Todas estas técnicas poseen sus ventajas e inconvenientes, por lo que el éxito de un buen análisis está directamente relacionado con la selección del método a utilizar, además del tipo de muestra a analizar y del tipo de estudio que se quiera realizar. El uso de cada uno de estos métodos de fraccionamiento no imposibilita el uso de otros ya que pueden aportar resultados complementarios (Kubota *et al.,* 2003; Kim *et al.,* 2006). Lo que ha quedado patente es que gracias al uso de estas nuevas técnicas de secuenciación masiva, transcriptómica, proteómica y metabolómica que han proporcionado gran cantidad de información, se ha obtenido una visión global de la compleja interacción entre virus-huésped además de una mejor comprensión de las estrategias de infección y de los mecanismos de defensa del huésped. De hecho la tendencia actual es la de combinar toda esta información, además de profundizar con el estudio de las modificaciones post-traduccionales, que permita diseñar nuevas estrategias de protección frente a patógenos.

1.6.2 Clasificación de las alteraciones proteómicas provocadas por una infección viral

En muchos de los trabajos analizados se observa una coincidencia significativa en las proteínas o familias de proteínas expresadas diferencialmente tras una infección viral. Podría concluirse por tanto que aunque cada virus dentro de cada planta y en distintos momentos puede desencadenar respuestas de defensa distintas, las plantas tienen la capacidad de responder a la invasión de forma general con un amplio rango de respuestas inducidas de forma coordinada (Nürnberger *et al.,* 1994; Somssich and Hahlbrock, 1998; Schenk *et al.,* 2000; Mahalingam *et al.,* 2003). Estas respuestas generales incluyen la reprogramación del metabolismo celular, la acumulación de sustancias de barrera y la síntesis de compuestos (señalización y defensa). El principal reto de estos estudios es tratar de separar aquellos cambios que son producidos como mecanismo de defensa por la planta de los que desencadena el virus para su ciclo vital.

1.6.2.1 Reprogramación del metabolismo celular.

Muchas de las proteínas expresadas de manera diferencial durante una infección viral están implicadas en la producción de energía y la regulación del metabolismo, tanto primario como secundario. Se han encontrado proteínas relacionadas con la fotosíntesis, producción de energía, azúcares, fijación de carbono, los ciclos del citrato y malato, además del metabolismo de lípidos y aminoácidos (Figura 11). Una respuesta observada en la mayoría de estudios es la regulación negativa de las proteínas relacionadas con la fotosíntesis (Di Carli *et al.,* 2012), sugiriendo que la planta está redirigiendo sus recursos hacia la defensa. En cambio, tanto en el caso del metabolismo energético como el de la síntesis de proteínas están reguladas positivamente. Esto sería consistente con la anterior observación de tal manera que la planta incrementaría la producción de energía a fin de contener y eliminar la infección. Sin embargo, hay que destacar que los virus son capaces de reclutar la maquinaria de síntesis proteica para la producción de sus propias proteínas (Walz *et al.,* 2004; Giavalisco *et al.,* 2006; Aki *et al.,* 2008; Dafoe *et al.,* 2009; Lin *et al.,* 2009). Por tanto, el incremento observado podría ser debido tanto a las necesidades del virus como a las de la planta o una combinación de ambas.

1.6.2.2 Acumulación de sustancias barrera

Como se ha comentado anteriormente una de las respuestas de las plantas frente a las infecciones es la producción de sustancias “barrera”. En muchos casos esto se traduce en una acumulación de calosa alrededor de los plasmodesmos reduciendo su permeabilidad (Bucher *et al.,* 2001; Hull, 2002; Rinne *et al.,* 2005; Zavaliev *et al.,* 2011). Esto podría explicar por qué en algunos trabajos se ha encontrado alterada la expresión de proteínas relacionadas con la formación y/o degradación de la pared celular como las pectin metilesterasas, β-glucanasas y las quitinasas (Brizard *et al.,* 2006; Li *et al.,* 2011; Yang *et al.,* 2011). Estas proteínas están relacionadas con la respuesta hipersensible (HR), la cual se caracteriza por la muerte programada de las células alrededor de las células infectadas, para confinarla y evitar así la propagación al resto de la planta. Por otra parte, estas proteínas también podrías ser reguladas positivamente debido a su implicación en el movimiento célula a célula de algunos

virus (Iglesias and Meins, 2000; Li *et al.,* 2012). La sobreexpresión de β-glucanasas disminuye la concentración de calosa favoreciendo así la permeabilidad del plasmodesmo y por tanto el movimiento intercelular (Beffa and Meins, 1996; Iglesias and Meins, 2000; Guenoune-Gelbart *et al.,* 2008). El virus podría utilizar factores celulares para combatir las propias respuestas defensivas del huésped, como el mecanismo de acumulación de calosa mencionado anteriormente, mostrando así una posible co-evolución virus-huésped.

1.6.2.3 Producción de compuestos de señalización y defensa

Una vez iniciada la infección la planta pone en marcha una serie de mecanismos de defensa. Los más extendidos y universales son la producción de especies reactivas de oxígeno (ROS), la producción de proteínas asociadas a estrés (principalmente PRs y chaperonas o HSPs de *heat shock proteins*) y factores relacionados con la ruta de degradación de proteínas (proteasoma y ubiquitina principalmente). De todas ellas se ha encontrado representación en los trabajos analizados (Figura 11). Las ROS, que generalmente hacen referencia al ion superóxido y al peróxido de hidrógeno, desempeñan un papel muy importante tanto en la señalización como directamente en defensa. Se han encontrado proteínas implicadas tanto en la producción como en la detoxificación (Walz *et al.,* 2004; Giavalisco *et al.,* 2006; Aki *et al.,* 2008; Dafoe *et al.,* 2009; Lin *et al.,* 2009; Di Carli *et al.,* 2012). Por otra parte, las PRs son proteínas asociadas a estrés que ejercen un papel muy importante en resistencia y adaptación al ambiente, y se acumulan en respuesta a una infección viral. Están agrupadas en 17 familias independientes (Campo *et al.,* 2004) a las que a algunas de ellas se les ha asociado actividad antimicrobiana (van Loon and van Strien, 1998; Muthukrishnan *et al.,* 2001; Campo *et al.,* 2004). En general se les atribuyen funciones, dependiendo de la familia, de tipo glucanasa, quitinasasa, taumatina, proteinasa, peroxidasa y defensina (Edreva, 2005). Finalmente, en prácticamente todos los trabajos se han descrito proteínas sobrerrepresentadas relacionadas con la ruta de degradación ubiquitina/proteasoma (Ventelon-Debout *et al.,* 2004; Brizard *et al.,* 2006; Lee *et al.,* 2006; Giribaldi *et al.,* 2011; Yang *et al.,* 2011; Rodrigues *et al.,* 2012). La ruta ubiquitina/proteasoma 26S es un mecanismo básico relacionado con múltiples procesos celulares. En un principio se asocia este incremento de los factores

implicados en degradación a la acumulación de proteínas virales, como las MPs y la CP (Reichel and Beachy, 2000; Drugeon *et al.,* 2002). Sin embargo, evidencias recientes sugieren que las plantas utilizan esta ruta en su respuesta inmune frente a la invasión de patógenos (Citowsky *et al.,* 2009). En el caso de los virus, la respuesta está asociada a la red de proteínas R (Jones and Dangl, 2006; Martin *et al.,* 2003). Un ejemplo es el gen N de *Nicotiana tabacum* (Whitham *et al.,* 1996; Liu *et al.,* 2002). La resistencia mediada por el gen N está basada en complejos SCF. Estos complejos han sido ampliamente caracterizados en levadura y consisten en una proteína soporte (S, Cdc53 o Culina), una proteína ubiquiti-conjugada (Cdc 34) y una proteína F-box (Patton *et al.,* 1998; Deshaies, 1999; Lechner *et al.,* 2006). Las proteínas F-box, altamente diversificadas en el proteoma de *A. thaliana* (Gagne *et al.,* 2002), son las encargadas del reconocimiento del sustrato de los complejos SCF. Estos SCF permiten dirigir directamente al proteasoma reguladores negativos de la defensa celular y/o inhibidores de apoptosis desencadenando la respuesta ante patógenos o la muerte celular programada (PCD) (Liu *et al.,* 2005, Citowsky *et al.,* 2009). Por otra parte, los virus son capaces de explotar estas rutas preexistentes para facilitar la progresión de la infección. De este modo se ha observado que eliminar el exceso de MP o CP a través de la ruta ubiquitina/proteasoma 26S no solo es beneficioso para el patógeno sino que en el caso del TMV esta ruta es necesaria para la infección (Becker *et al.,* 1993). También existen evidencias de que algunos supresores del silenciamiento (como la P0 de poleovirus) actúan dentro de un complejo SCF para suprimir las defensas antivirales, marcando el motivo PAZ de AGO1 y provocando su degradación (Pazhouhandeh *et al.,* 2006).

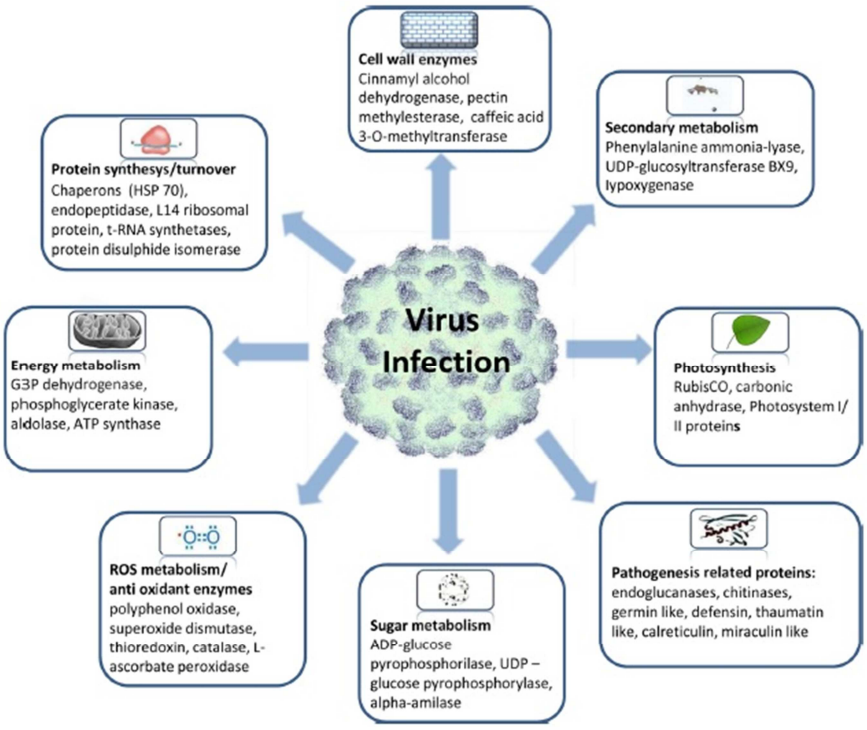

Figura 11. Esquema de las principales alteraciones proteómicas producidas tras una infección viral (Di Carli *et al.,* 2012).

1.7 EL VIRUS DE LAS MANCHAS NECRÓTICAS DEL MELÓN, MNSV

1.7.1 Sintomatología y organización genómica

El MNSV, objeto de estudio de la presente Tesis Doctoral, es el agente causal de la enfermedad del cribado del melón. Aunque los síntomas dependen de las condiciones ambientales, la sintomatología más característica se presenta en melón: la aparición en hojas jóvenes de lesiones redondas de color marrón y de 1-2 mm de diámetro, que suelen evolucionar a necrosis dando lugar a un aspecto de "cribado". En hojas adultas pueden aparecer lesiones necróticas que se extienden por los nervios. En tallos y sobre todo en el cuello de la planta aparecen estrías pardas con aspecto acorchado. Normalmente aparece una reducción en el crecimiento del fruto y en ocasiones lesiones necróticas. El síntoma más relevante, al que se le atribuye el nombre de colapso o muerte súbita del melón, es la marchitez y muerte rápida de la planta, sobre todo en condiciones de estrés hídrico y plena producción (Figura 12). A nivel celular, las alteraciones más evidentes son la acumulación de almidón en los cloroplastos, típico en situaciones de estrés, la desestructuración de las crestas mitocondriales (ver

datos no publicados en la Figura 14) y la reorganización de las mitocondrias (Gómez-Aix *et al.,* 2015).

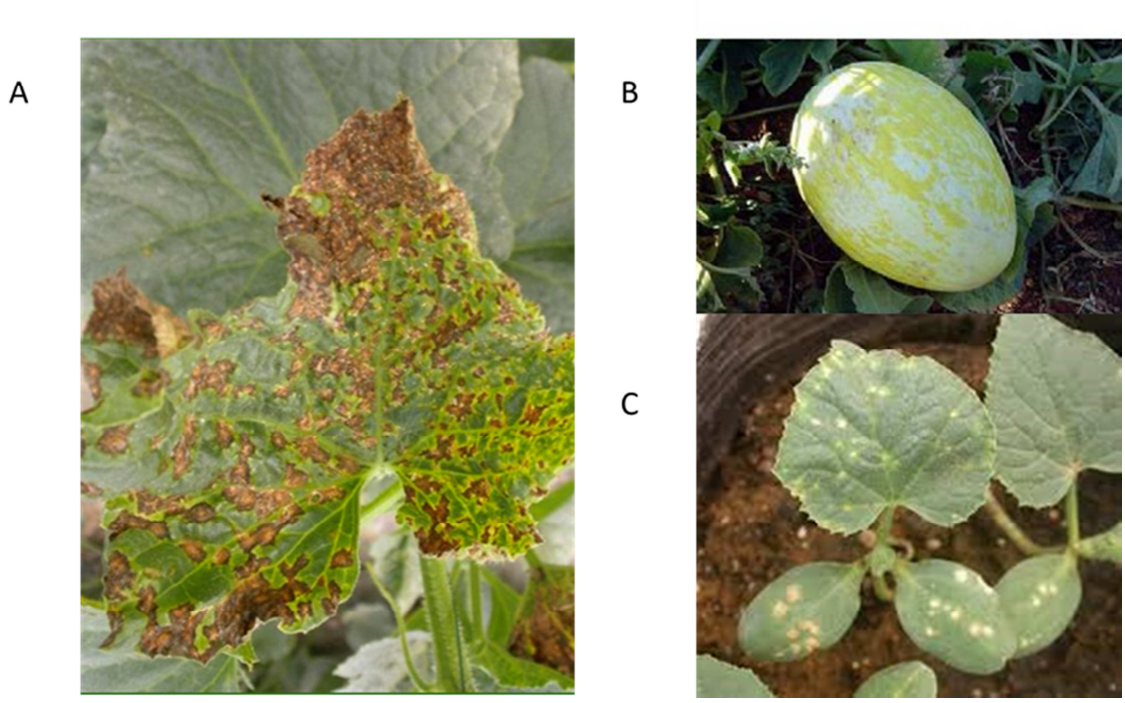

Figura 12. Síntomas de la enfermedad del cribado del melón en hojas (A), frutos de melón. (B) y plantas enteras (C).

El MNSV es un miembro del género *Carmovirus*, perteneciente a la familia *Tombusviridae*. Está formado por partículas isométricas de unos 30 nm de diámetro, constituidas aproximadamente por 180 subunidades de la proteína de cubierta (CP) (Lommel *et al.,* 2000). El genoma del MNSV (gRNA) está compuesto por una molécula de RNA monocatenario de polaridad positiva de 4,3 Kb, con un extremo 5' sin estructura "cap" (m^7G^5pppNp) y un extremo 3' no poliadenilado (gRNA). El genoma del MNSV codifica cinco proteínas funcionales flanqueadas por dos regiones no traducibles de 95 nt (en el extremo 5') y 280 nt (en el extremo 3') (Figura 13). La ORF más próxima al extremo 5' es una proteína de 29 kDa (p29) que finaliza con un codón ámbar y codifica la RNA polimerasa RNA dependiente (RdRp) (Gómez-Aix *et al.,* 2015). Continuando con la lectura de dicho codón se obtiene una proteína de 89 kDa (p89), también implicada en la replicación del virus. Las dos ORFs situadas en la parte central del genoma, son dos proteínas de 7 kDa (p7A y p7B) implicadas en el movimiento del virus (Genovés *et al.,* 2006, 2009, 2010, 2011; Navarro *et al.,* 2006). Por último, la ORF

del extremo 3' representa la proteína de cubierta (Riviere and Rochon, 1990). Esta proteína de 42 kDa es multifuncional. Aparte de su papel estructural en la encapsidación del virus interviene probablemente en el movimiento a larga distancia dentro de la planta. Además, p42 junto con p7B han sido identificadas como factores capaces de retrasar el silenciamiento génico post-transcripcional (PTGS) de la proteína de fluorescencia verde (*green fluorescent protein*, GFP). Este efecto de p42 sobre el PTGS provoca un movimiento local más eficaz del virus lo cual podría permitir un avance más rápido de la infección que el virus podría aprovechar para evadir los mecanismos de defensa que la planta desencadena a nivel local (Genovés *et al.,* 2006). La capacidad de supresión de silenciamiento para las CPs de carmovirus se ha demostrado además para el TCV (Thomas *et al.,* 2003), y el PFBV (Martínez-Turiño and Hernández, 2009). Las CPs de un virus del recientemente propuesto género *Pelarspovirus* (Scheets *et al.,* 2015), y la del virus del anillado del pelargonio (*Pelargonium line pattern virus*, PLPV) también poseen actividad VSR (Pérez-Cañamás and Hernández, 2015). Por último, p42 está implicada en la transmisión del virus por su vector, un hongo del suelo denominado *Olpidium bornovarus* (Satiyanci) Karting que pertenece a la clase de los Quitridiomicetes dentro del orden Quitridiales (Ohki *et al.,* 2010).

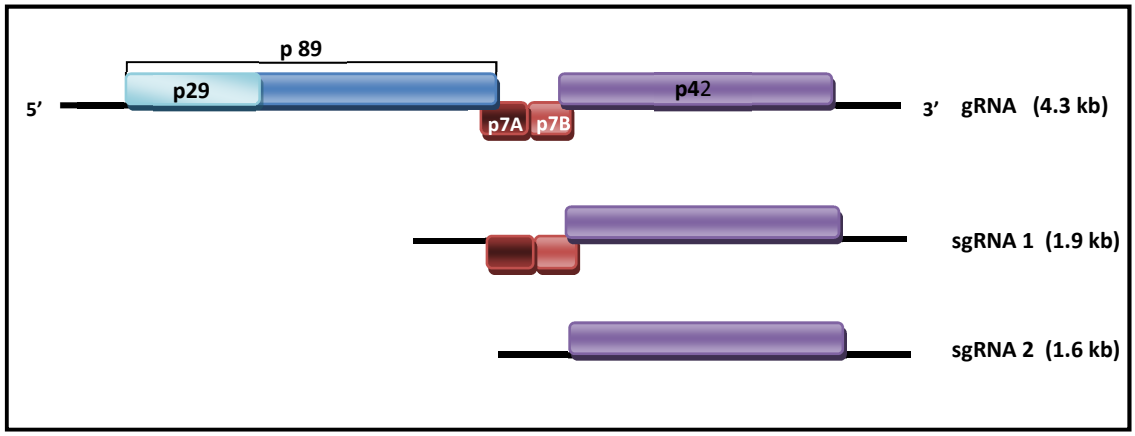

Figura 13. Organización genómica y probable estrategia de expresión de MNSV (Riviere and Rochon, 1990). Se indican las proteínas que se encuentran codificadas. El tamaño aproximado de las especies del RNA genómico y subgenómicos de MNSV se muestra a la derecha.

La detección de dos RNAs subgenómicos de 1,9 kb (sgRNA 1) y 1,6 kb (sgRNA 2) que comparten el mismo extremo 3' del gRNA sugiere una estrategia de expresión del genoma similar a la de los otros carmovirus. Básicamente consiste en que el gRNA actuaría de mensajero para la síntesis de p29 y p89. Las proteínas p7A y p7B se

producirían a partir del sgRNA 1 mientras que la proteína de cubierta se obtendría a partir del sgRNA 2 (Riviere and Rochon, 1990).

Además de su obvia importancia fitopatológica el MNSV se ha convertido en un sistema modelo para los estudios relacionados con mecanismos de rotura de la resistencia viral, regulación traduccional o movimiento viral (ej. Navarro *et al.,* 2006; Nieto *et al.,* 2006, 2011; Truniger *et al.,* 2008; Genovés *et al.,* 2006, 2009, 2010, 2011).

1.7.2 Proteínas de replicación del MNSV

Como se ha descrito anteriomente, las ORFs 1 y 2 codifican dos proteínas que participan en la replicación: un producto de 29 kDa sin dominios funcionales reconocibles y otro producto de 89 kDa (correspondiente a la RdRp viral), ambas necesarias para el proceso replicativo (Genovés *et al.,* 2006). La actividad enzimática de polimerización de p89 o de sus homólogas se ha corroborado para varios tombusvirus (Nagy and Pogany, 2000; Panavas *et al.,* 2002; Rajendran *et al.,* 2002; Panaviene *et al.,* 2004). Dada su función, RdRp es capaz de unir y reconocer el RNA viral de manera específica y una de las regiones que parece estar implicada, es un dominio rico en residuos de arginina y prolina (motivo RPR). Esta función de unión también ha sido descrita para la ORF1 de algunos tombusvirus, como el TBSV (Rajendran and Nagy, 2003) y el PFBV (Martínez-Turiño and Hernández, 2010). Se ha postulado que esta unión serviría para seleccionar y dirigir el RNA viral al complejo de replicación (Rajendran and Nagy, 2003; Martínez-Turiño and Hernández, 2010).

Sin embargo, el papel específico de la proteína de menor tamaño todavía se desconoce. Varios estudios sugieren que la ORF1 posee la información para dirigir el complejo replicativo a las membranas celulares. Entre los miembros del género *Tombusvirus* se ha observado que la ORF1 del virus del mosaico necrótico del trébol rojo (*Red clover necrotic mosaic virus*, RCNMV) y la del virus del mosaico del panicum (*Panicum mosaic virus*, PMV) se localizan en el RE (Turner *et al.,* 2004; Batten *et al.,* 2006), la ORF1 del TBSV, del virus de las manchas en anillos del cymbidium (*Cymbidium ringspot virus*, CymRSV) y del CNV se asocian a la membrana de los peroxisomas (Navarro *et al.,* 2004; McCartney *et al.,* 2005; Panavas *et al.,* 2005), mientras que las correspondientes proteínas del virus de las manchas en anillo del clavel italiano

(*Carnation Italian ringspot virus*, CIRV), PFBV y MNSV se localizan en las mitocondrias (Weber-Lotfi *et al.,* 2002; Mochizuki *et al.,* 2009; Martínez-Turiño and Hernández, 2010, 2012; Gómez-Aix *et al.,* 2015). En el caso de la p29 de MNSV, el direccionamiento hacia mitocondrias depende de un fragmento transmembrana (TMD2) y esta localización es imprescindible para la virulencia del virus puesto que desencadena la formación de manchas necróticas cuando es expresada mediante una infección con CMV en *N. benthamiana* (Mochizuki *et al.,* 2009). Se ha observado que la localización de la p29 produce cambios drásticos en la ultraestructura de las mitocondrias (ver los resultados no publicados en la Figura 14 y Gómez-Aix *et al.,* 2015). La RdRp y la ORF1 comparten el extremo Nt, donde al parecer se localizan los residuos responsables del direccionamiento de la proteína, lo que sugiere que también comparten localización subcelular. Si a esto añadimos el hecho de que se han localizado tambien la CP y el dsRNA viral en estos reordenamientos de las mitocondrias (Gómez-Aix *et al.,* 2015), es evidente que estas estructuras proporcionan un ambiente protegido para la replicación y muy probablemente constituyen los complejos replicativos del virus y/o factorías virales.

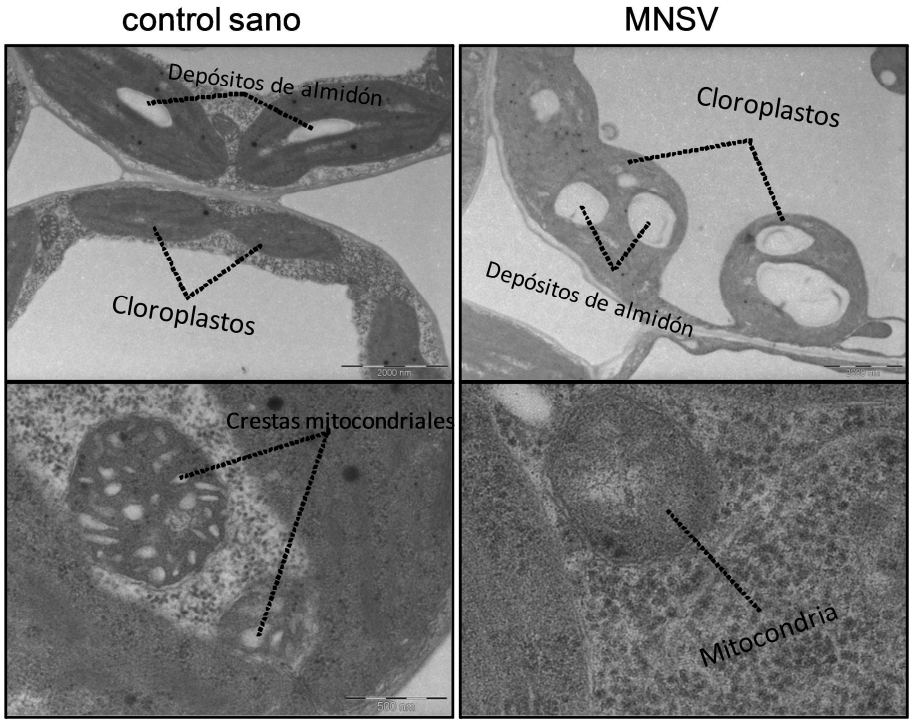

Figura 14. Imágenes de microscopía electrónica de transmisión mostrando el aspecto de los cloroplastos (arriba) y las mitocondrias (abajo) en células del mesófilo de melón sano (izquierda) o infectado con MNSV (derecha).

1.7.3 Proteínas de movimiento del MNSV

La p7A, al igual que el resto de las DGBp1 de todos los carmovirus descritos hasta el momento, presenta una cadena polipeptídica rica en aminoácidos básicos (cadenas laterales cargadas positivamente). Además, las predicciones de estructura secundaria realizadas mediante programas informáticos ponen de manifiesto la existencia de tres regiones o dominios: un extremo amino terminal sin ningún tipo de estructura secundaria aparente; un domino central con una α-hélice inducible y una región carboxilo terminal con una estructura potencial en β-hoja plegada. En el caso de la región central existen evidencias experimentales obtenidas mediante dicroísmo circular que demuestran que la predicción es correcta al menos para el CarMV y el MNSV (Vilar *et al.,* 2001, 2002, 2005; Navarro *et al.,* 2006). En general, esta región central presenta la mayor densidad de cargas positivas de la proteína encontrándose implicada en la capacidad de unión a RNA de la p7 del CarMV (Marcos *et al.,* 1999; Vilar *et al.,* 2001, 2005). Sin embargo, para la p7A del MNSV, las tres regiones estructurales parecen ser relevantes en la interacción con el RNA aunque presentan diferentes grados de implicación en el proceso. Así la región central sería la más involucrada seguida del extremo amino terminal y por último, del carboxilo terminal (Navarro *et al.,* 2006). Además, se evaluó la relación entre la capacidad a unión al RNA y en el movimiento célula a célula mediante mutagénesis dirigida de los aminoácidos básicos presentes en cada uno de los dominios estructurales. Se observó una relación directa entre la capacidad de unión a RNA *in vitro* y el movimiento célula a célula. Cuando se perdía o disminuía la afinidad en la unión a RNA *in vitro*, el movimiento célula a célula se veía impedido o reducido, respectivamente, siendo el efecto mayor cuando se alteraban los aminoácidos básicos de la región central. Además, el marcaje de esta proteína con un fluoróforo permitió determinar la localización subcelular de esta MP en plasmodesmos (PDs), otras estructuras no determinadas situadas en la periferia y asociada a los microfilamentos de actina. Finalmente, la utilización de la técnica de complementación bimolecular de la fluorescencia puso de manifiesto la capacidad de homodimerización de esta proteína que resultó ser esencial en el movimiento intercelular del virus (Genovés *et al.,* 2009)

Por otro lado, la localización subcelular de p7B obtenida mediante expresión transitoria de una fusión fluorescente (Genovés *et al.,* 2010) sugiere que esta proteína de movimiento viral utiliza la ruta de secreción celular para llegar a los PDs, puesto que inicialmente se detecta en el RE pero posteriormente es translocada al AG y a los plasmodesmos probablemente siguiendo una ruta ya descrita para otras proteínas celulares (Lee *et al.,* 2004). El hecho de que la p7B quede retenida en el RE en presencia de brefeldina A (BFA), una droga que bloquea el transporte retrógrado desde el AG al RE, o del mutante dominante Sar1 [H74L], incapaz de hidrolizar GTP, sugiere que la salida del RE de p7B es dependiente de las vesículas COPII. Además, en presencia de cualquiera de estos agentes inhibidores del transporte RE-AG, el movimiento célula a célula del MNSV se ve drásticamente afectado (Genovés *et al.,* 2010). Otra serie de evidencias experimentales que implican el transporte intracelular de p7B a los PDs a través del AG en el movimiento local del MNSV provienen de un estudio de mutagénesis dirigida sobre los determinantes de topología e inserción en el RE de esta MP (Genovés *et al.,* 2011). De los resultados obtenidos se pudo concluir que la localización subcelular de la p7B en el AG es necesaria pero no suficiente para que se dé un movimiento viral eficiente, siendo el correcto tránsito del AG a los PDs lo que realmente permite un avance normal del virus.

La p7B contiene un único fragmento transmembrana localizado en la región central hidrofóbica y estructurada en α-hélice, comprendida desde el residuo Y_{13} al L_{32}, la cual permite que la proteína se inserte en la membrana del RE co-traduccionalmente, adoptando en planta una topología de tipo II con el extremo Nt citoplásmatico y el Ct luminal (Figura 15). Un estudio reciente con mutantes de deleción de la p7B ha demostrado que el fragmento transmembrana de p7B por sí solo es capaz de dirigir la GFP a la membrana del RE, actuando como una secuencia señal al RE.

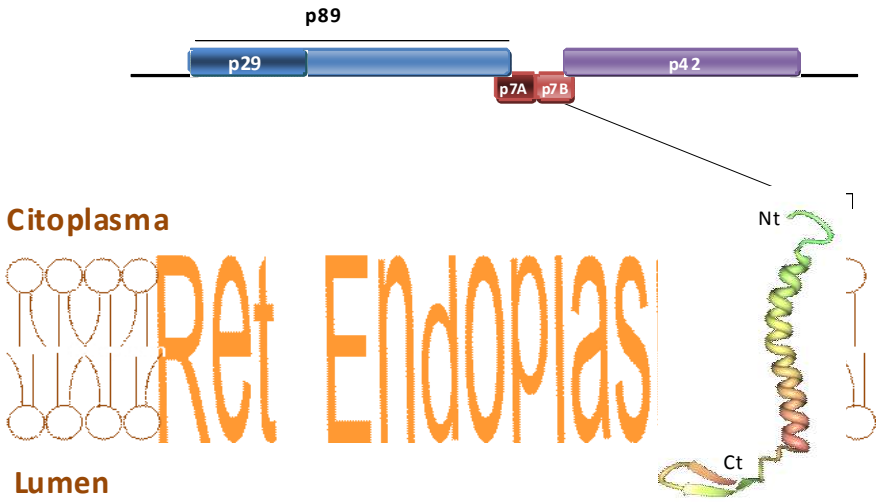

Figura 15. Representación esquemática de la estructura secundaria y topología de p7B. El fragmento transmembrana de p7B presenta una conformación en α-hélice mientras que el extremo Ct presenta cierto grado de plegamiento en hoja plegada β. La topología de tipo II hace referencia a proteínas con un solo fragmento transmembrana, sin secuencia señal y con el extremo Nt orientado hacia el citoplasma.

Los motivos estructurales que controlan el transporte de una proteína bitópica como p7B por el sistema de endomembranas celular pueden situarse tanto en el dominio hidrofóbico como en las regiones extramembranosas. Existe un incremento en el grosor de la bicapa lipídica a medida que nos acercamos a la membrana plasmática. Los fragmentos transmembrana más largos y por tanto más hidrofóbicos tienden a localizarse en un ambiente lipídico más favorable para evitar el desajuste hidrofóbico que surge cuando el fragmento transmembrana es más largo que el espesor de la bicapa lipídica (Brandizzi *et al.,* 2002). Aunque el AG ha sido descrito como posible destino por defecto para proteínas con un único dominio transmembrana de aproximadamente 19-20 aminoácidos, en ausencia de los dominios amino y carboxi terminales de p7B, la proteína fluorescente recombinante quedó retenida en el RE y no fue transportada al AG. Por tanto el dominio hidrofóbico actúa como una señal de inicio de la translocación y de retención pasiva en el RE. Estos resultados indican que el extremo amino o el carboxilo, o ambos contienen los determinantes que controlarían la salida activa de p7B del RE (Genovés *et al.,* 2011).

Se han identificado diferentes tipos de señales en los dominios citoplásmicos de las proteínas transmembrana bitópicas capaces de interaccionar con algún componente del complejo sar1, sec23/24, aunque es mayoritariamente con sec24. No existe una secuencia consenso, y en ocasiones se reducen a dos residuos cargados positiva o negativamente o dos residuos aromáticos e hidrofóbicos. Esta variedad de señales podría estar reconocida por diferentes dominios situados en diferentes isoformas de los componentes del complejo. En muchísimos menos casos, se han identificado dominios luminales implicados en el transporte dependiente de vesículas COPII en proteínas transmembrana. Sin embargo, esto nos sugiere la existencia de receptores o adaptadores proteicos transmembrana, semejantes a los que de transportan proteínas luminales, que se encargarían de transmitir la información al lado citoplásmico (Barlowe, 2003; Lee *et al.,* 2004)

1.7.4 Proteína de cubierta del MNSV

La CP del MNSV es la proteína encargada de agruparse y ensamblarse formando la partícula vírica. Una particularidad es que aunque su genoma posee una organización típica de *Carmovirus* (Figura 2) su CP es más parecida a las del genero *Tombusvirus* (Riviere *et al.,* 1989), tal y como ha confirmado la reciente publicación de la estructura 3D de la proteína con una resolución 2,8 Å (Wada *et al.,* 2008). La estructura cuaternaria sigue una simetría icosaédrica T=3 con 180 copias de 3 conformaciones cuasi equivalentes (A, B, C). Independientemente de la conformación, cada subunidad está compuesta por 3 dominios: S, P y R (Figura 16). El dominio S crea una cubierta proteica alrededor del genoma y el dominio P está involucrado en el reconocimiento de la superficie de las esporas del hongo vector, *Olpidium bornovanus*, para la propagación entre plantas (Mochizuki *et al.,* 2008; Ohki *et al.,* 2010). Finalmente, el tercer dominio R consiste en un brazo flexible formado por los 94 residuos del Nt (desde la Met 1 hasta la Gly 94), que el caso de las conformaciones A y B se proyecta hacia dentro de la partícula viral en una estructura desordenada. Se ha propuesto, dada su elevada composición en residuos de naturaleza básica, que este dominio R debe desempeñar un papel importante en la unión del RNA genómico durante la encapsidación (Rao, 2006). Por otro lado, los residuos situados entre la asparagina 60 y la glicina 94 forman un brazo ordenado en las subunidades de tipo C que se extiende

desde la cara interna del dominio S hasta el eje triaxial del icosaedro. Los brazos procedentes de tres subunidades de tipo C se encuentran en este eje generando una estructura denominada anillo β que confiere estabilidad a las partículas víricas.

Además de desempeñar un papel estructural, la CP interviene en otras etapas del ciclo de vida del virus. Está implicada en la transmisión por el vector y también se ha observado que favorece el movimiento local interfiriendo con los mecanismos de silenciamiento post-transcripcional (Genovés *et al.,* 2006).

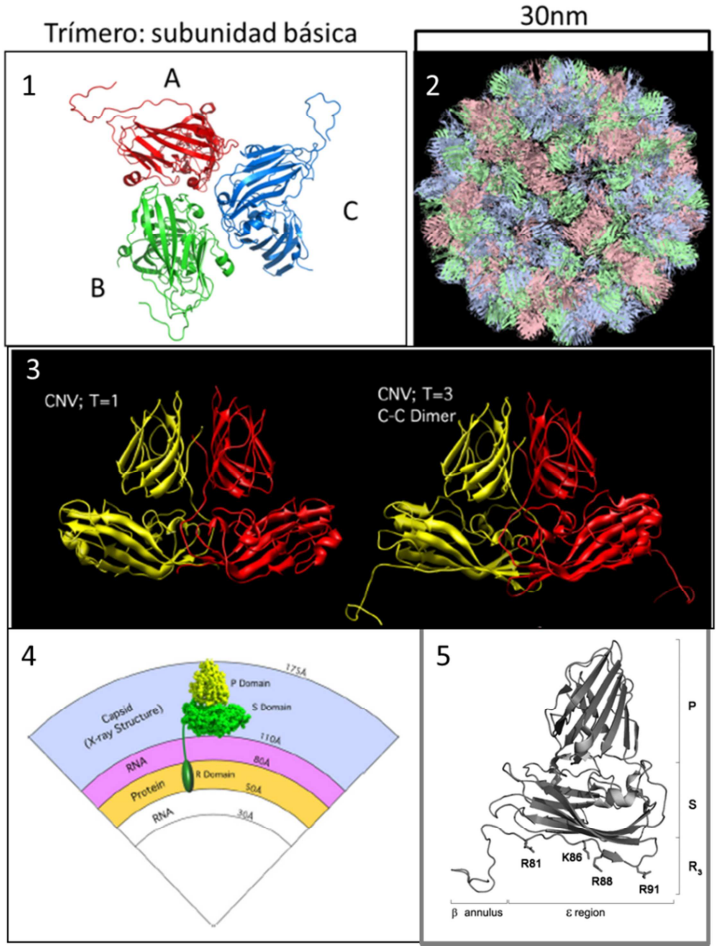

Figura 16. Comparación de las estructuras de la CP del CNV, TBSV y MNSV 1) Esquema de la estructura del virión. 2) Estructura 3D de la proteína de cubierta del MNSV. 3) Conformaciones adoptadas por las proteínas de cubierta del CNV en la conformación T=1 y T=3. 4) estructura interna adoptada por el virión de TBSV y la distribución de la proteína y el RNA. 5) Estructura de la proteína de cubierta del MNSV (adaptado de Katpally *et al.,* 2007).

JUSTIFICACIÓN Y OBJETIVOS

El ciclo vital de los virus es un proceso complejo y diverso, dada la gran variabilidad de virus existente, aunque comparten etapas comunes. Básicamente se puede dividir en la entrada a la célula, el movimiento intracelular, el movimiento intercelular, el movimiento sistémico y finalmente la dispersión hacia nuevos huéspedes mediada por vectores. Para completar estas etapas con éxito, los virus han desarrollado una gran variedad de mecanismos que dependen tanto de las proteínas virales como de factores y procesos celulares. Los virus codifican en sus genomas múltiples proteínas (MPs, CPs y VSRs, entre otras) implicadas, directa o indirectamente, en mediar el movimiento del virus por la planta y la propagación de la infección viral. La asociación de estas proteínas virales con los componentes celulares desempeña además un papel fundamental en el ciclo vital de los virus de plantas. El estudio de los factores virales y la identificación de las interacciones con los componentes celulares del huésped pueden ayudar a esclarecer los mecanismos moleculares en los que intervienen. Por esta razón el movimiento viral es una de los aspectos más estudiados en la virología de plantas. Su importancia radica en que no es trascendente sólo para el diseño de nuevas estrategias antivirales sino que también permite estudiar los procesos generales de las plantas tales como el desarrollo, las defensas naturales o el tráfico de las proteínas celulares. Sin embargo, los estudios sobre el movimiento de los carmovirus son escasos, los principales componentes de los complejos virales móviles son todavía desconocidos y apenas se conoce la participación de factores celulares.

En la presente tesis doctoral se propuso como objetivo global profundizar en los mecanismos moleculares que intervienen en el movimiento de los carmovirus, realizando una serie de estudios que incluyen: el análisis funcional y estructural de varios factores virales implicados en el movimiento viral en sus tres etapas principales (intracelular, intercelular y sistémico), la identificación de factores celulares implicados en las mismas y las alteraciones proteómicas que ocurren a nivel vascular durante la infección viral. Para la consecución de este objetivo global se plantearon los siguientes objetivos específicos:

- Estudio del mecanismo molecular que controla el trasporte intracelular de la proteína de movimiento p7B (DGBp2 del MNSV) en las etapas tempranas de su paso por la ruta de secreción celular, hacia el plasmodesmo.
- Identificación de posibles factores del huésped que interaccionen con las proteínas de movimiento DGBp1 de los carmovirus.
- Análisis funcional y estructural del domino amino terminal de la CP del MNSV y su posible implicación en las diferentes etapas y procesos del ciclo viral.
- Estudio e identificación de las alteraciones producidas en el perfil proteómico del exudado de floema de *Cucumis melo* durante una infección por MNSV.

CAPÍTULO PRIMERO

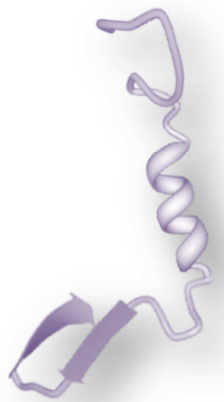

Este capítulo ha dado lugar a la siguiente publicación:

Serra-Soriano, M., Pallás, V. and Navarro, J. A. (2014). A model for transport of a viral membrane protein through the early secretory pathway: minimal sequence and endoplasmic reticulum lateral mobility requirements. *Plant J* 77:863-879.

A model for the transport of a viral membrane protein through the early secretory pathway: minimal sequence and endoplasmic reticulum lateral mobility requirements.

INTRODUCTION

Eukaryotic proteins destined for secretion, plasma membrane and other membrane compartments are transported to the Golgi apparatus through the so-called early secretory pathway. In mammalian cells, the early secretory pathway includes membrane-bounded organelles such as the endoplasmic reticulum (ER), the ER-Golgi intermediate compartment (ERGIC) and the Golgi apparatus itself, as well as coated carrier vesicles that travel in between them (Lippincott-Schwartz *et al.,* 2000).

In plants, the Golgi apparatus consists of many cisternae stacks that are distributed throughout the cytoplasm (Staehelin and Moore, 1995) but, far from being static as the perinuclear mammalian Golgi, it dynamically moves along the actin microfilaments (MF) in a myosin-dependent way (Avisar *et al.,* 2008; Avisar *et al.,* 2009). Plant Golgi is also found so intimately associated with the underlying cortical ER network that both organelles could even be physically attached to each other (daSilva *et al.,* 2004; Runions *et al.,* 2006; Sparkes *et al.,* 2009a; Sparkes *et al.,* 2009b). To adapt to such a narrow ER-Golgi interface, the plant early secretory pathway must be organized in a much different way to that of mammalian and yeast cells (Hawes *et al.,* 2008; Hawes, 2012; Brandizzi and Barlowe, 2013). No ERGIC or specific domains exist where ER-export sites (ERES) are confined, at least, as usually known (Pavelka and Robinson, 2003). Although the presence of carrier vesicles COPI and COPII remains to be unambiguously demonstrated (Hawes and Satiat-Jeunemaitre, 2005; Kang and Staehelin, 2008), plant coatomer homologs have been identified (Yang *et al.,* 2005; Hanton *et al.,* 2009; Zhang *et al.,* 2010) and COPI and COPII-dependent transport has been confirmed for soluble and transmembrane proteins (Aniento *et al.,* 2006; Hanton *et al.,* 2007b). Moreover, most plant coatomer homologs have been found in close association with Golgi stacks.

All these observations together have led to the development of the “secretory unit” concept by which Golgi, ERES and carrier vesicles move together with the ER

(daSilva *et al.,* 2004; Langhans *et al.,* 2012). An updated version of this model has been recently reported by which the bidirectional ER-Golgi transport requires the secretory unit to stop moving briefly in discrete ER regions. At this point, COPI and COPII vesicles fuse to the corresponding target membranes allowing cargo exchange (Lerich *et al.,* 2012). In any case, the mechanisms behind the regulation of cargo sorting and delivering through the early secretory pathway remain poorly characterized in plants.

Movement proteins (MPs) enable plant viruses to move from cell-to-cell by exploiting specialized channels that plant cells use to communicate with each other, the plasmodesmata (Pd) (Waigmann *et al.,* 2004; Niehl and Heinlein, 2011; Schoelz *et al.,* 2011). Consistently with their function in viral movement, many MPs initially associate with ER and cytoskeleton elements to be further targeted to Pd (Harries *et al.,* 2010; Pallás and García, 2011). It is well-established that the cellular mechanisms governing the intracellular trafficking of host proteins are sometimes recruited by viral MPs. In this sense, we have already reported that MNSV cell-to-cell movement requires the sequential transport of p7B, one of its two MPs (Navarro *et al.,* 2006), from the ER via the Golgi to Pd in a COPII-dependent pathway (Genovés *et al.,* 2010).

Unlike other MPs hijacking the secretory pathway for intracellular transport (Laporte *et al.,* 2003; Vogel *et al.,* 2007; Wei *et al.,* 2010; Yuan *et al.,* 2011; Vijayapalani *et al.,* 2012), p7B membrane topology has been extensively characterized (Navarro *et al.,* 2006; Martínez-Gil *et al.,* 2007; Genovés *et al.,* 2011). We have demonstrated that p7B behaves as a type II integral membrane protein with a cytoplasmic N-terminus and a luminal C-terminus. Moreover, transplantation of its transmembrane domain (TMD) onto a nucleo-cytoplasmic reporter redirects the protein into ER membranes but, fails to export it from there to downstream organelles (Genovés *et al.,* 2011). This observation suggests that active sorting information not only exists but is dominant over the TMD length in determining its ER-forward transport. Therefore, p7B can provide an appropriate platform for dissecting the sorting signals and trafficking strategies mediating protein migration through the endomembrane system.

Here, we examined the early trafficking steps of p7B after membrane insertion. Using deletion mutants and site-directed mutagenesis, we found that a requirement

for combinatorial motifs located at cytosolic and luminal domains could operate concomitantly to mediate ER-export and to support viral cell-to-cell movement. However, on the behavior of mutants affecting either the amino or the carboxyl terminus, different roles can be assigned to each domain. Putative explanations for these results are discussed taking into account the structural properties of p7B and the potential interactions with cellular components.

RESULTS

Both the p7B cytosolic and luminal domains are necessary for ER-export

p7B contains a short cytoplasmic N-terminal region (aa 1-12, CR), a central TMD (aa 13-32) and a luminal C-terminal region (aa 33-61, LR) (Figure 1a) (Navarro *et al.,* 2006). To examine the relative contribution of the CR and the LR to p7B trafficking, we generated two truncated GFP-tagged mutants, GFP-p7BΔNt and GFP-p7BΔCt (Figure 1b). Next, we examined their subcellular localization by transient expression and confocal laser scanning microscopy (CLSM). In a previous study, we showed that GFP-p7B trafficking within cell can be sequentially traced in time by CLSM. At approximately 24-36 hours post-infiltration (hpi), GFP-p7B fluorescence strongly labeled the ER, the nuclear envelope (NE) and some Golgi stacks (Golgi/total fluorescence ratio average of 0.19±0.09) (Figure 1c) but at 48-60 hpi, it was essentially located at Golgi (Golgi/total fluorescence ratio average of 0.82±0.11, $p<0.0001$) and Pds (Figure 1d, Figure S1) (Genovés *et al.,* 2010). Thus, to investigate mutant-specific transport deficiencies, two time-points (36 and 60 hpi) were analyzed.

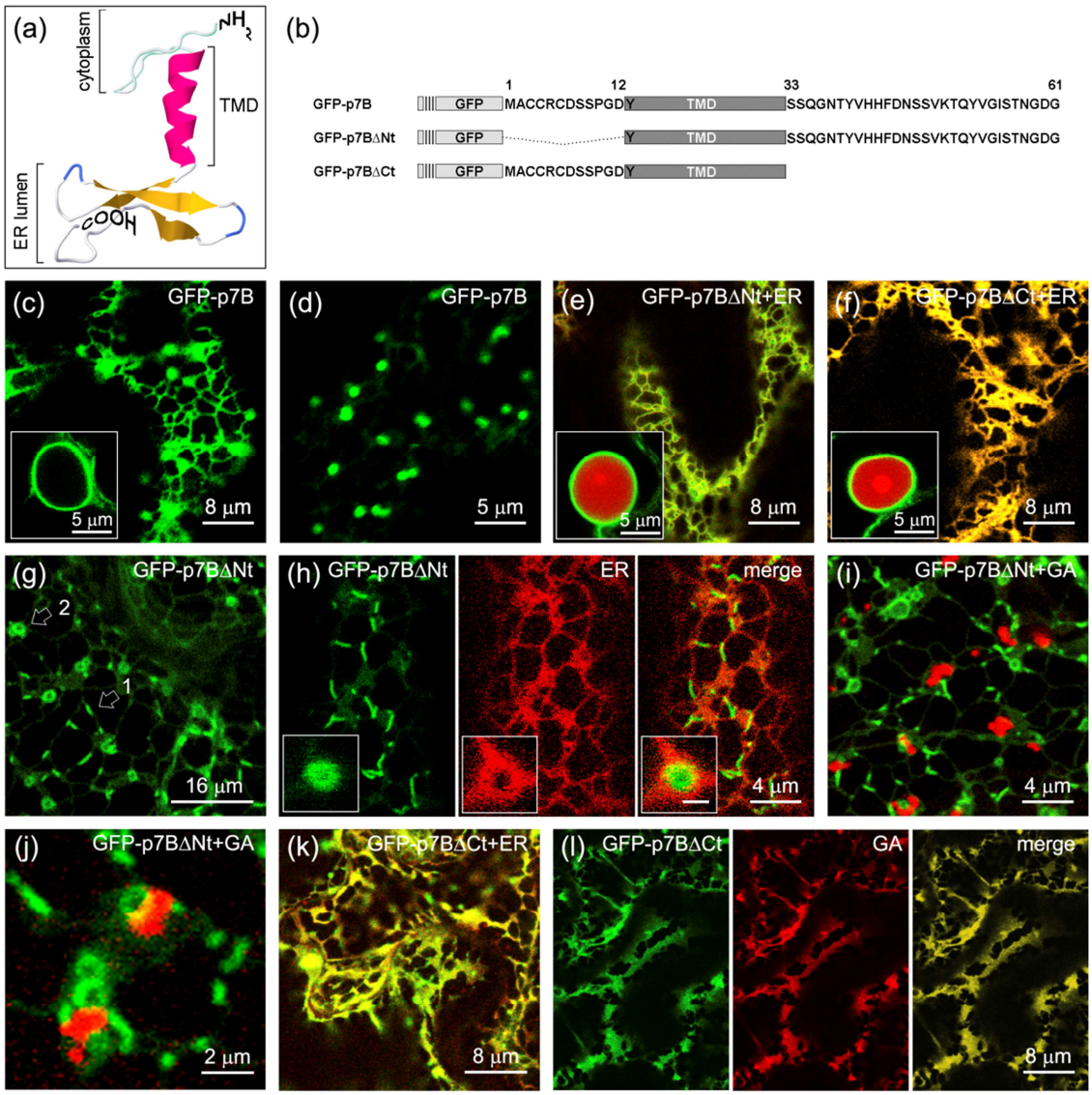

Figure 1. The lumenal and cytosolic domains of p7B are essential for ER-export. (a) 3D structure of p7B as predicted by Phyre[2] server. TMD, transmembrane domain. (b) Schematic representation of GFP-p7B, GFP-p7BΔNt and GFP-p7BΔCt fusion proteins. (c) CLSM images of *N. benthamiana* epidermal cells expressing GFP-p7B at 36 hpi. (d) Localization of GFP-p7B in Golgi bodies at 60 hpi. (e-f) Expression of GFP-p7BΔNt or GFP-p7BΔCt in combination with ER and nuclear (inlet panel) markers, ChFP-KDEL and mRFP-NLS, at 36 hpi. Yellow denotes co-localization between the GFP and ChFP or RFP signals. (g) Distribution of GFP-p7BΔNt in linear clusters (1) and ring-like structures (2) at 60 hpi. (h) Association of GFP-p7BΔNt linear clusters and ring-like structures (inlet panel) with ER marker ChFP-KDEL at 60 hpi. (i-j) Co-expresión of GFP-p7BΔNt with Golgi marker STtmd-ChFP at 60 hpi. (k) Co-expression of GFP-p7BΔCt and ER marker ChFP-KDEL at 60 hpi. (l) Co-expression of GFP-p7BΔCt and Golgi marker STtmd-ChFP at 60 hpi.

At 36 hpi, both mutants highlighted a tubular network, typical of the cortical ER morphology, and the NE. Both localizations were confirmed by co-expression with either ER-luminal (ChFP-KDEL) or nucleus (mRFP-NLS) markers (Figure 1e,f). Note that in all the figures GFP or YFP is pseudocolored in green and Cherry or RFP in red, so in merged images yellow denotes co-localization between the GFP and the Cherry/RFP

signals). This is consistent with our former finding that p7B TMD is sufficient to localize heterologous proteins into the ER (Genovés *et al.,* 2011). At 60 hpi, the early reticular pattern of GFP-p7BΔNt became bright punctate, linear (0.5-5 µm length) and ring-like (1-1.6 µm in diameter) structures that apparently moved overlying a weakly self-stained tubular network (mutant structures/total fluorescence ratio average of 0.37±0.09) (Figure 1g, Movie S1, Movie S2). When GFP-p7BΔNt was co-expressed with ER marker, the latter showed a uniform distribution throughout the ER indicating that GFP-p7BΔNt structures do not result from ER morphology alteration. Image overlapping clearly showed that GFP-p7BΔNt complexes aligned with the ER marker but partially overlapping with it (Figure 1h). This observation suggests that GFP-p7BΔNt moves over or with the ER membranes. Only occasional overlap between GFP-p7BΔNt and the Golgi marker STtmd-ChFP was observed (Figure 1i,j).

By contrast, the ER network highlighted by GFP-p7BΔCt turned into a more fenestrated form (Figure 1k). It has been reported that this situation may occur when Golgi and secretory membrane proteins accumulate in the ER after ER-Golgi transport disruption (Saint-Jore *et al.,* 2002). To evaluate this phenomenon more accurately, GFP-p7BΔCt was expressed with Golgi marker STtmd-ChFP. CLSM imaging revealed that both proteins accumulate in the ER, demonstrating that GFP-p7BΔCt interferes with the ER-to-Golgi transport (Figure 1l).

To validate the CLSM results, we further examined the distribution of the truncated proteins in sucrose gradients in relation to endomembrane markers such as the *Beet yellow virus* p6-GFP, a p7B-structurally related transmembrane protein that located into ER membranes (Peremyslov *et al.,* 2004) and the well-known Golgi marker STtmd-GFP. Microsomes from leaf tissue were loaded in the gradients and individual fractions were analyzed by immunoblotting (Figure 2a). The distribution of the truncated mutant proteins matched that of the overlapping ER and Golgi endomembrane markers peaking in fractions 11-13 (Figure 2b). Only a residual amount of both mutant proteins was recovered from the soluble fraction S1. These results reflect a broader association of the mutant viral proteins with endomembrane vesicles. According to p7B topology, we expected that ER-sorting information was present at the N-terminal region. However, cellular fractionation and CLSM localization data indicated that GFP-

p7BΔNt and GFP-p7BΔCt remain highly associated with ER membranes strongly suggesting that p7B CR and LR are both required to achieve a transport-competent state.

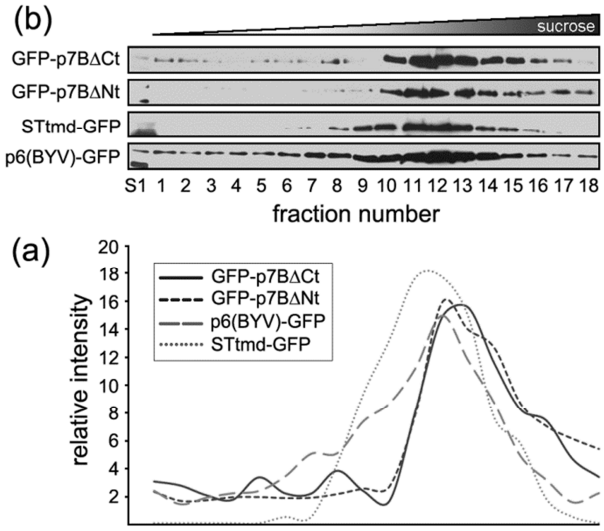

Figure 2. Localization of GFP-p7BΔNt and GFP-p7BΔCt deletion mutants by continuous sucrose gradient density. (a) Quantification, in arbitrary units, of the signals derived from the immunoblot assay of each fraction. (b) Immunoblot analyses of the gradient fractions. Equivalent volume amounts of cytosolic (S1) and microsomal (1-18) fractions were electrophoresed. Extracts were prepared at 60 hpi.

Highly conserved amino acids in the p7B cytosolic and luminal domains are critical for ER exit

To determine the sequence motifs relevant for p7B ER-exit, we generated serial alanine substitution mutants (Figure 3a). Alanine was the substitution residue of choice since its non-bulky methyl functional lateral group does not impose electrostatic or steric effects and does not alter the main-chain conformation of the protein. After expression in plants, a visual screen for mutations leading to ER retention was performed by CLSM. At 36 hpi, all mutations at CR produced a reticular network pattern suggesting ER localization (Figure S2a,b,c,d). At 60 hpi, GFP-p7B[$C_3AC_4AR_5A$] and GFP-p7B[$D_{12}AY_{13}A$] were properly targeted to the Golgi (Figure 3b,c). In contrast, no discernible difference (p=0.98) was observed between the GFP-p7B[$C_6AD_7AS_8A$] and GFP-p7B[$S_9AP_{10}AG_{11}A$] distribution (mutant structures/total fluorescence ratio average of 0.40±0.10 and 0.41±0.13) and dynamics which, in turn,

was quite similar to that observed with GFP-p7BΔNt (p=0.27 and p=0.34, respectively) (Figure 3d,e,f,g). These results strongly suggest that the N-terminal region between amino acids 6 and 11 (CDSSPG) contains a sequence motif essential for p7B ER-export.

Next, we examined the C-terminal mutants localization. At 36 hpi, all of them were properly inserted into the ER (Figure S2,e-m) but at 60 hpi, only the $K_{49}AT_{50}AQ_{51}A$ mutation caused ER-retention of the fusion protein and displayed an ER-fenestrated morphology comparable to that observed with GFP-p7BΔCt (Figure 3h,i). Hence, ER-to-Golgi targeting of Golgi marker STtmd-ChFP was also impaired indicating that GFP-p7B[$K_{49}AT_{50}AQ_{51}A$] also interferes with the anterograde transport. The other C-terminal mutant for which the ER-to-Golgi traffic was affected was the GFP-p7B[$D_{60}AG_{61}A$], which exhibited a punctate distribution that did not overlap with Golgi (Figure 3j). One possible explanation for this pattern is that GFP-p7B[$D_{60}AG_{61}A$] accumulates in a post-Golgi endosomal compartment. However, it is more likely that punctate stains would correspond to mutant-induced membrane inclusions. The remaining mutations had influence neither on Golgi marker distribution nor COPII-dependent transport including $G_{54}AI_{55}AS_{56}A$, $V_{40}AH_{41}AH_{42}A$, and $Y_{52}AV_{53}A$ mutations (Figure 3k,l,m) and $N_{37}AT_{38}AY_{39}A$, $F_{43}AD_{44}AN_{45}A$, $S_{46}AS_{47}AV_{48}A$ and $G_{54}AI_{55}AS_{56}A$ mutations (Figure S3).

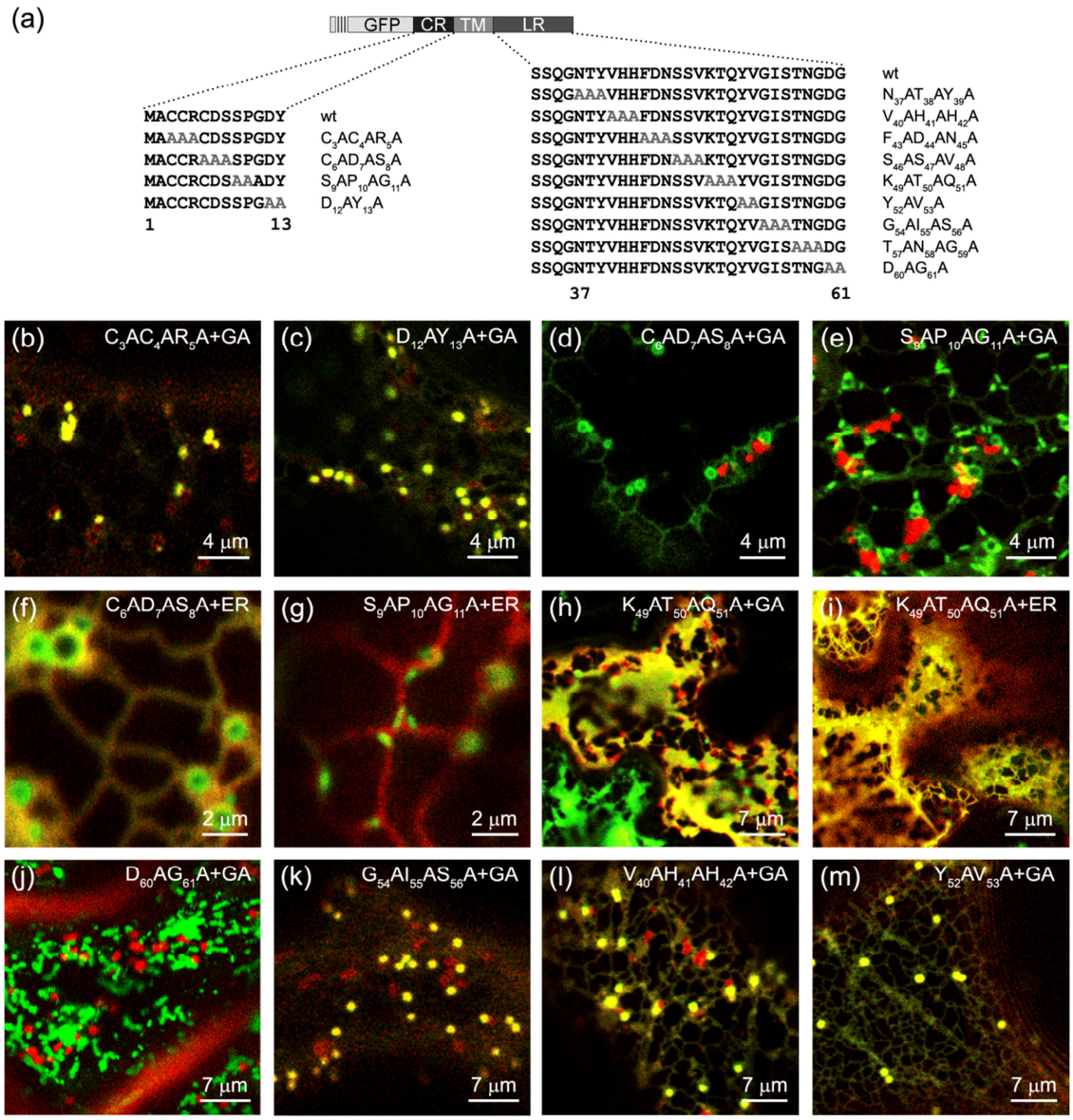

Figure 3. Identification of sequence motifs involved in p7B ER-export by mutations to alanine. (a) Schematic representation of GFP-p7B fusion protein and mutations introduced into p7B cytoplasmic (CR) and luminal (LR) domains. (b-m) CLSM images of *N. benthamiana* leaf epidermal cells expressing the indicated GFP-p7B mutants either in combination with Golgi marker ChFP-STtmdSTtmd-ChFP or ER marker ChFP-KDEL at 60 hpi.

The sequence alignment of ten MNSV-like MPs revealed that, within the CDSSPG stretch, the proline was strictly conserved and the aspartic acid at -3 position from this proline was observed in half of the sequences (Figure 4a). For all the rest, a negative charged residue was observed at -1, -2 or -4 position. We also notice that the most abundant residues found in reverse turns (D, G, P, Q and S, Rose *et al.,* 1985) were observed along this region in all MPs. In fact, DSSP motif was predicted (Kaur and Raghava, 2004) to adopt a type IV β-turn conformation bringing D7 and P10 residues

so close (6.2 Å) to allow the formation of an intra-turn hydrogen bond (Figure 4b). Similar folding was predicted for the rest of MPs. Since reverse turns have long been described to participate in molecular recognition processes (Hutchinson and Thornton, 1994; Rose *et al.,* 1985), we can hypothesize that this β-turn may be involved in host protein interactions controlling p7B transport. Consistently with this hypothesis, the GFP-p7B[$D_7AP_{10}A$] construct, which presents a significant loss of the turn potential of tetramer DSSP, reproduced the ER-retention pattern (mutant structures/total fluorescence ratio average of 0.36±0.09) and mobility observed in related GFP-p7BΔNt, GFP-p7B[$C_6AD_7AS_8A$] and GFP-p7B[$S_9AP_{10}AG_{11}A$] mutants (p=0.72, p=0.14 and p=0.20, respectively) (Figure 4c,d).

By focusing on the Ct-domain, the KTQ motif was highly conserved among MNSV-like proteins (Figure 4a) and in less structurally related carmovirus MPs (Figure S4). However, lysine was the most conserved residue in the triplet. To ascertain its contribution in ER-forward trafficking, GFP-p7B[$K_{49}A$] mutant was generated and its localization examined. GFP-p7B[$K_{49}A$] expression prevented Golgi localization of Golgi marker STtmd-ChFP showing an ER distribution similar to that observed with GFP-p7B[$K_{49}AT_{50}AQ_{51}A$] (Figure 4e). This led us to suggest that both the DSSP domain conformation and K49 residue are critical for p7B ER-exit.

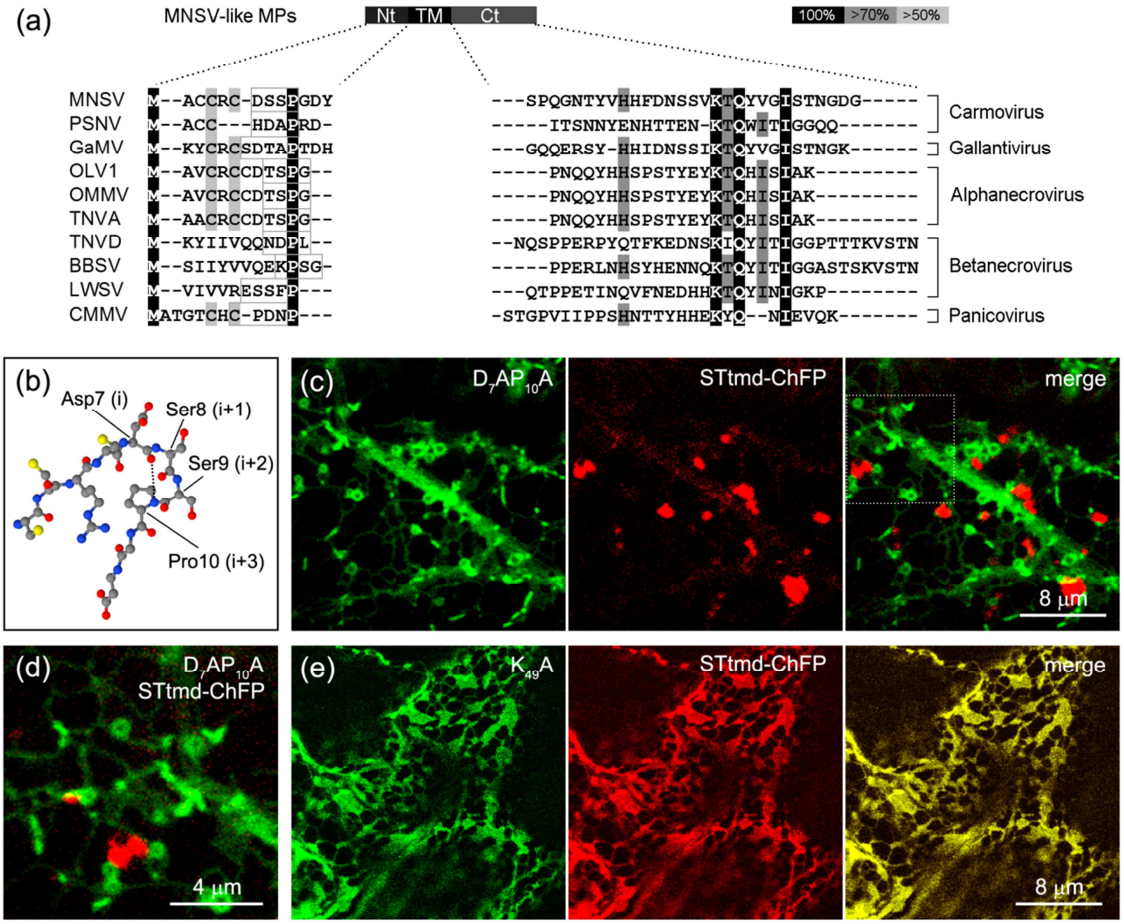

Figure 4. Minimal sequence requirement for p7B ER-export comprises highly or strictly conserved residues. (a) Sequence alignment of the extramembranous regions of p7B-related proteins from Tombusviridae family members. The abbreviated name of the viral species (left) and genus (right) are given. Full name of each virus is shown in Table S2. Black boxes with white lettering represent absolutely conserved residues, while grey boxes with black lettering represent highly conserved residues. Putative reverse turns are enclosed in white boxes. (b) Schematic view of the putative DSSP β-turn structure. The aspartic CO group is most likely hydrogen bonded to the proline NH group (pointed line). (c) CLSM images of *N. benthamiana* epidermal cells expressing GFP-p7B[D7AP10A] in combination with Golgi marker ChFP-STtmdSTtmd-ChFP at 60 hpi. (d) Magnification of the region squared in merged panel (c) to provide additional resolution. (e) CLSM images of *N. benthamiana* leaf epidermal cells showing how GFP-p7B[K49A] expression inhibits Golgi-to-ER trafficking of Golgi marker ChFP-STtmdSTtmd-ChFP at 60 hpi.

The cytosolic exposition of the structural motif DSSP is essential to trigger Sar1 recruitment to ER membranes

The initial step for COPII-mediated transport to Golgi involves selecting membrane cargoes and receptors during the assembly of the ternary complex Sar1/Sec23/Sec24 (Brandizzi and Barlowe, 2013). This prebudding complex is completed by subsequent recruitment of the heterotetramer Sec13/31. All subunits are found in the cytosol but a Sec12-mediated conformational change of the GTPase Sar1, leads to its ER-

membrane association and consequently, to the sequential recruitment of the remaining components. The factors regulating Sar1 activation remain unclear although it has been reported that the ER-membrane recruitment of some COPII subunits is upregulated by the presence of membrane cargoes in a signal-dependent fashion (Hanton *et al.,* 2009); i.e. Sar1-YFP accumulates as bright dots associated with Golgi stacks (ERES) upon Golgi proteins overexpression (daSilva *et al.,* 2004).

To test whether the wild-type p7B, $D_7AP_{10}A$ and $K_{49}A$ mutants can induce COPII assembly or not, we expressed Sar1-YFP in combination with the corresponding ChFP-tagged proteins. At 48 hpi, Sar1-YFP either alone or co-expressed with ChFP-p7B[$D_7AP_{10}A$] exhibited a cytosolic distribution except for sporadic punctate structures (Figure 5a,b,c). As expected, the Golgi marker STtmd-ChFP and ChFP-p7B induced Sar1-YFP accumulation in close association with Golgi bodies (Figure 5d,e). Additionally, the number of Sar1-YFP dots seems to increase in the presence of ChFP-p7B[$K_{49}A$] as compared to those induced by the wild-type protein (Figure 5f).

To corroborate this observation, we quantified the number of Sar1-YFP dots from 30-40 cells (Figure 5g). In those cells expressing STtmd-ChFP, there were, on average, 0.163 ERES per 100 μm^3 but, in the presence of ChFP-p7B, the number of ERES per 100 μm^3 lowered to 0.09. It is known that protein transport properties influence ERES formation (Hanton *et al.,* 2007a). Therefore structural differences related with protein-specific sorting motifs can explain the less pronounced tendency of p7B to stimulate ERES formation as compared to the Golgi marker. On the other hand, the number of Sar1-YFP dots per 100 μm^3 significantly increased to 0.155 with ChFP-p7B[$K_{49}A$] (p=0.0025). These ER-associated punctate structures probably do not represent *de novo* synthesis of active ERES as mutant protein accumulates in a non-competent state for transport. In this scenario, the inhibition of COPII-dependent transport most likely occurs through sequestration of Sar1 that is no longer available for competent cargoes. In any case, it is evident the p7B ability to recruit Sar1 to the ER membrane is lost in the $D_7AP_{10}A$ mutant suggesting that the cytosolic exposition of the structural motif DSSP is unequivocally required. It remains to be established whether a direct interaction between DSSP motif and Sar1 or some other COPII components takes place.

Movement of GFP[$D_7AP_{10}A$] complexes is dependent on the actomyosin system and accumulates in close proximity to stationary Golgi stacks after latrunculin B treatment.

We next examined the influence of ER-Golgi transport inhibition on GFP-p7B[$D_7AP_{10}A$] spatial distribution and dynamics. For this purpose, 1-cm diameter discs of *N. benthamiana* leaves expressing GFP-p7B[$D_7AP_{10}A$], alone or in combination with STtmd-ChFP, were incubated in the presence of the secretory inhibitor brefeldin A (Brandizzi *et al.,* 2002b). Within 1 hour, the Golgi marker STtmd-ChFP was redistributed into the ER that, morphologically, showed an increase in flat sheet-like regions. In contrast, the drug did not affect the GFP-p7B[$D_7AP_{10}A$] complexes that still moved in close association with tubules or along cisternal rims. Moreover, they were often enclosed within these BFA-induced cisternae (Figure 6a,b, Movie S3). A similar dynamics has been described for the Golgi stacks trafficking across the surface of calnexin-labeled ER (Runions *et al.,* 2006; Yang *et al.,* 2005) suggesting that similar mechanisms drive GFP-p7B[$D_7AP_{10}A$] complexes.

In plants, movement of organelles such as Golgi stacks is highly dependent on the actomyosin scaffold which is extensively aligned with the ER (Avisar *et al.,* 2008; Ueda *et al.,* 2010). To determine whether this same situation can apply to GFP-p7B[$D_7AP_{10}A$] mobility, we explored its potential association with the MFs. Co-expression of GFP-p7B[$D_7AP_{10}A$] with acting-binding protein DsRed-talin (used as MFs marker protein) revealed that most of GFP-p7B[$D_7AP_{10}A$] complexes arranged along ER-associated MFs (Figure 6c). Interestingly, ring-like structures were observed in close association with actin bundles converging points where cross-linking actin binding proteins usually accumulate (Huang *et al.,* 2011) (Figure 6d).

To further clarify the role of the actin cytoskeleton in mutant translocation, similar assay was performed as before, but using the MFs assembly inhibitor latrunculin B (latB). After 1-hour incubation, we found that the GFP-p7B[$D_7AP_{10}A$] complexes were severely halted showing that their intracellular movement was dependent on intact MFs (Movie S4). Moreover, the GFP-p7B[$D_7AP_{10}A$] complexes were clustered together on small islands of lamellar ER formed at the junctions of the ER tubules. This situation is highly reminiscent of that observed with Golgi bodies after actin cytoskeleton

disintegration (Boevink *et al.,* 1998). Hence, the GFP-p7B[$D_7AP_{10}A$] complexes (Figure 6e) accumulate in close association and/or in direct contact with immobilized Golgi bodies when co-expressed in the presence of latB (Figure 6f,g,h, Movie S4). The rationale for this is that MFs can provide the framework upon which the GFP-p7B[$D_7AP_{10}A$] complexes laterally move over the ER surface as Golgi stacks do.

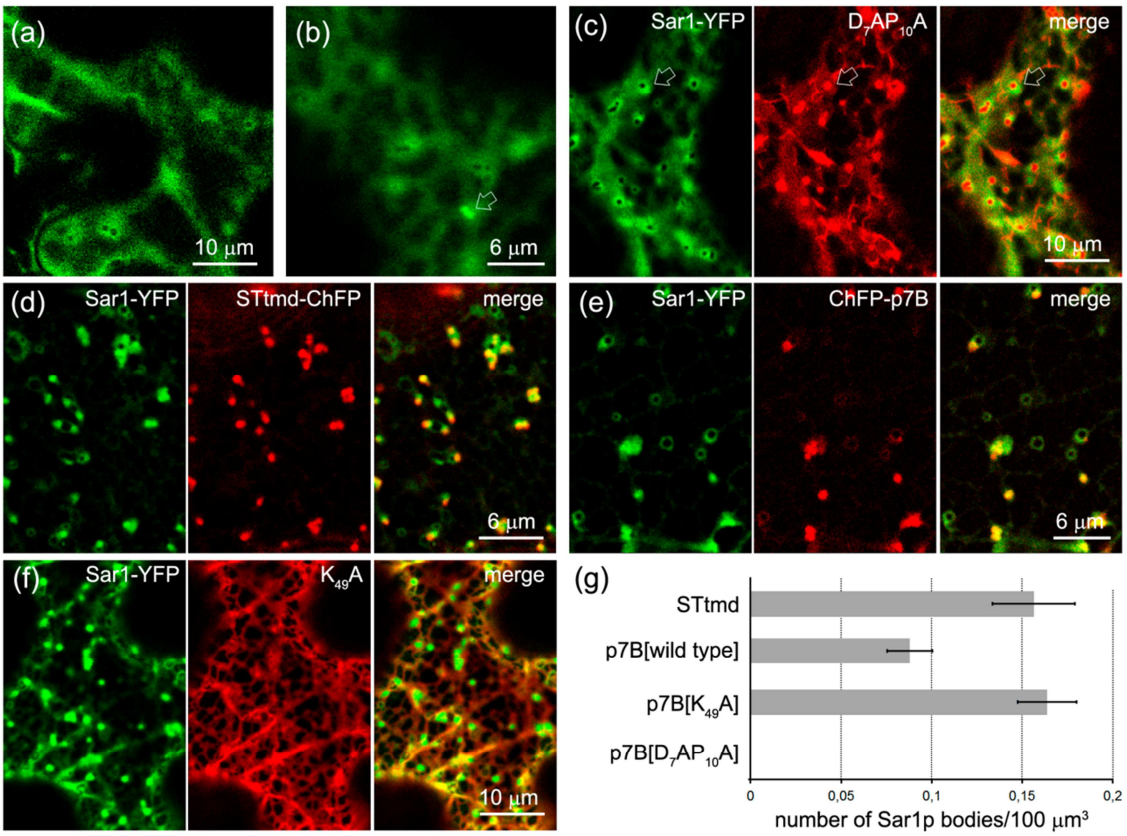

Figure 5. The ChFP-tagged D7AP10A and K49A mutants display different capacity to recruit Sar1 into ER membranes when expressed in *N. benthamiana* leaf epidermal cells. (a-b) Cytoplasmic distribution of Sar1-YFP with occasional bright spots indicated by arrow in (b). (c) Co-expression of Sar1-YFP and ChFP-p7B[D7AP10A]; Sar1-YFP maintained the cytoplasmic staining except for sporadic bright spots located in close proximity to ChFP-p7B[D7AP10A] ring-like structures (indicated by arrows). (d) Sar1-YFP recruitment upon expression of Golgi protein ChFP-STtmdSTtmd-ChFP. (e) Co-expression of ChFP-p7B and Sar1-YFP. (f) Co-expression of ChFP-p7B[K49A] and Sar1-YFP. (g) Quantification of Sar1 recruitment to punctuatepunctate structures. Sar1-YFP images are pseudocolored in green.

The Ct-luminal domain dynamically regulates acto-myosin-dependent ER lateral diffusion of GFP-p7B[$D_7AP_{10}A$]

The influence of $D_7AP_{10}A$ and $K_{49}A$ mutations on ER lateral translocation of p7B was further studied by fluorescence recovery after photobleaching (FRAP). For this purpose, we transiently expressed GFP-p7B, GFP-p7B[$D_7AP_{10}A$] or GFP-p7B[$K_{49}A$]

constructs on *N. benthamiana* leaves. To minimize the interference of GFP-p7B[$D_7AP_{10}A$] complexes with the recovery curves, fluorescence intensity values were gathered at 36 hpi, when GFP-tagged proteins were homogenously distributed through the ER, and plotted vs time (Figure 7a). To deeper examine the role of actin polymerization in the mobilization of GFP-tagged proteins, we pretreated tissue samples either with DMSO or latB. Table 1 provides the percentage of maximum fluorescence recovery (MFR), which corresponds to the mobile fraction, and the half-time of maximum recovery ($t_{1/2}$) values.

In the presence of DMSO, the MFR reached by GFP-p7B[$K_{49}A$] (39.54±2.44 %) was significantly smaller compared with GFP-p7B (75.98±2.20 %, $p<0.0001$) and GFP-p7B[$D_7AP_{10}A$] (65.72±2.50 %, $p<0.0001$). To a lesser extent, the MFR reached by GFP-p7B[$D_7AP_{10}A$] was significantly ($p=0.0048$) smaller compared with GFP-p7B. In addition, GFP-p7B[$K_{49}A$] took significantly longer to reach the $t_{1/2}$ than either GFP-p7B (5.07±0.31 s vs 3.36±0.23, $p=0.0001$) or GFP-p7B[$D_7AP_{10}A$], (5.07±0.31 s vs 3.54±0.34 s, $p=0.0019$). No significantly differences ($p=0.685$) were observed between GFP-p7B and GFP-p7B[$D_7AP_{10}A$]. The GFP-KDEL construct showed rapid (0.91±0.26 s) and near-complete (89.34±0.13 %) recovery indicating that cellular photodamage contribution to immobile fractions was minimal (Figure 7a, Table 1, Table S2). The GFP-p7B[$K_{49}A$] slow mobility suggests that p7B lateral diffusion into membranes may be regulated through the LR. Therefore, we postulate that this domain must interact with a membrane-spanning factor showing actomyosin-dependent mobility.

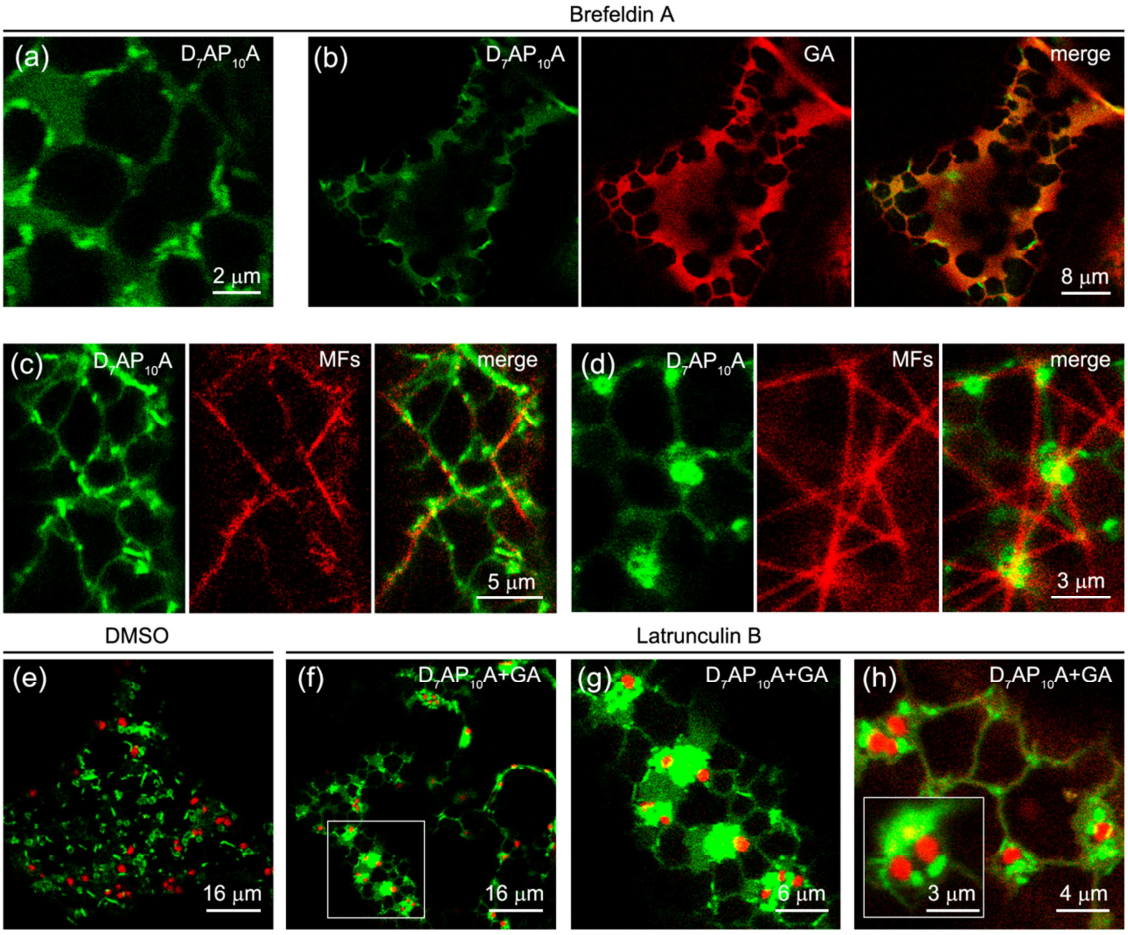

Figure 6. Effect of brefeldin A and latrunculin B on GFP-p7B[D7AP10A] mobility and distribution. (a-b) CLSM image of a *N. benthamiana* epidermal cell expressing GFP-p7B[D7AP10A], alone (a) or in combination with Golgi marker ChFP-STtmdSTtmd-ChFP (b), after brefeldin A treatment. (c-d) CLSM images of *N. benthamiana* epidermal cells showing a close spatial relationship between microfilaments (MFs), highlighted by DsRed-talin, and GFP-p7B[D7AP10A] linear clusters (c) or ring-like structures (d). (e-f) CLSM image of an epidermal cell expressing GFP-p7B[D7AP10A] in combination with Golgi marker ChFP-STtmdSTtmd-ChFP after soaking tissue disc in DMSO or latrunculin B solution, respectively. (g) Magnification of the region squared in (f). (h) Additional scans to provide better resolution.

To determine whether the $K_{49}A$ mutant reduced mobility may be due to the disruption of the interaction with the cytoskeleton, we repeated the FRAP experiments after latB treatment (Figure 7b). We found that MFs depolymerization had no effect on the GFP-p7B[$K_{49}A$] recovery kinetics but significantly decreased the GFP-p7B[$D_7AP_{10}A$] MFR at levels comparable with those of GFP-p7B[$K_{49}A$] (49.21±2.71 % vs 47.20±2.90 %) (Figure 7b, Table 1, Table S2). These findings indicate that actomyosin-dependence mobility may be associated with a functional LR. Unexpectedly, GFP-p7B recovery in the presence or absence of latB did not change. Note that mutant proteins remained arrested on the ER membranes while GFP-p7B actively trafficked from the ER to Golgi

since this transport did not require the actin cytoskeleton (Brandizzi *et al.,* 2002b). Recovery kinetic depends on different factors, and active sorting and trafficking may also contribute to increase GFP-p7B turnover in ER membranes, possibly buffering the latB effect.

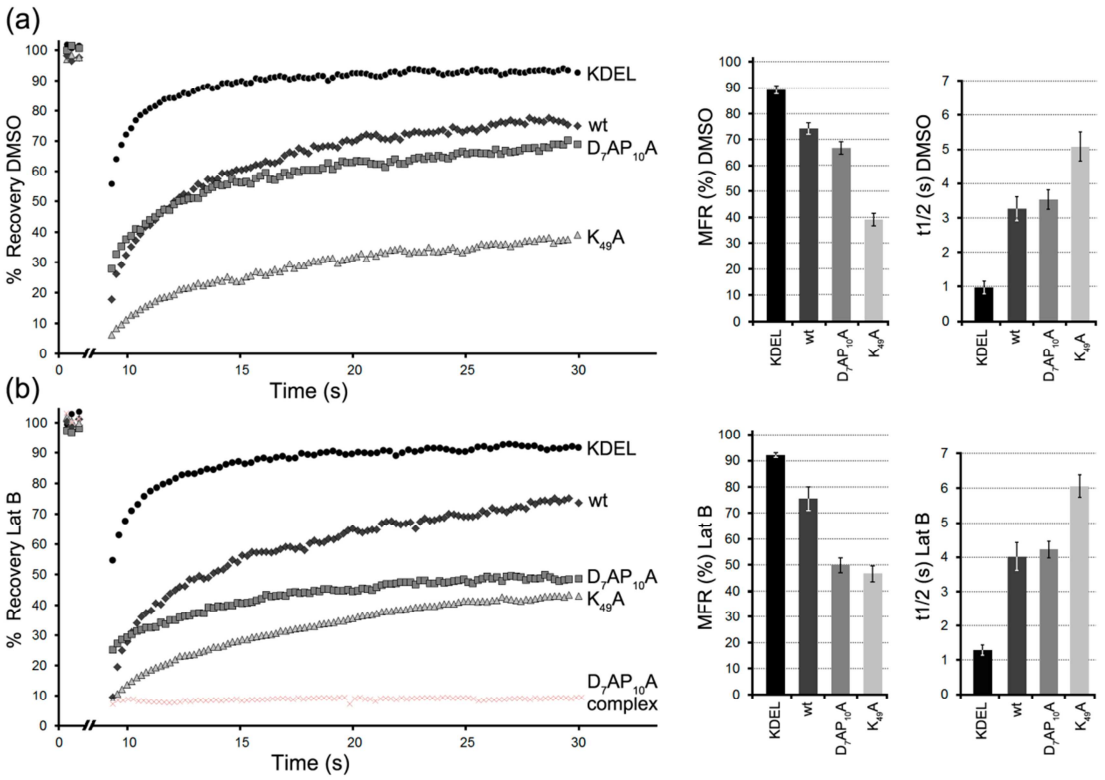

Figure 7. Fluorescence recovery after photobleaching (FRAP) of GFP-p7B (wt), GFP-p7B[D7AP10A], GFP-p7B[K49A] and GFP-KDEL proteins in ER membranes of *N. benthamiana* cells. Data points for 10 FRAP curves from different cells expressing each GFP-tagged protein were double normalized, averaged and fitted to a single exponential function. (a-b) FRAP curves, maximum fluorescence recovery (MFR) and half-time of maximum recovery (t1/2) after treatment with DMSO (a) or latrunculin B (b) for each GFP-tagged protein. ER luminal marker GFP-KDEL was used as control for the presence of cellular damage.

Table 1. ER membrane dynamics determined by fluorescence recovery after photobleaching

Treatment	GFP fusion	Halt-time of maximum recovery (s)	Maximum fluorescence recovery (%)
DMSO	wt	3.36 ± 0.23	75.98 ± 2.20
	$D_7AP_{10}A$	3.54 ± 0.34	65.72 ± 2.50
	$K_{49}A$	5.07 ± 0.31	39.54 ± 2.44
	KDEL	0.91 ± 0.26	89.34 ± 0.13
Latrunculin B	wt	3.98 ± 0.37	77.37 ± 5.45
	$D_7AP_{10}A$	4.32 ± 0.31	49.21 ± 2.71
	$K_{49}A$	5.88 ± 0.26	47.20 ± 2.90
	KDEL	1.24 ± 0.26	92.19 ± 0.16

To narrow down the GFP-p7B[$D_7AP_{10}A$] complexes identity, we also performed FRAP experiments at 60 hpi when linear and ring-like structures appeared. After latB treatment, laser beam was focused to bleach these immobilized GFP-p7B[$D_7AP_{10}A$] structures. As shown in Figure 7b ($D_7AP_{10}A$ complex recovery curve), little or no fluorescence recovery was observed into the photobleached area reflecting no exchange of fluorescent subunits from the ER pool and the extent to which GFP-p7B[$D_7AP_{10}A$] molecules were stably immobilized in a dynamic macromolecular complex. Unlike the dimerization ability of BYV p6 (Peremyslov *et al.,* 2004), no intermolecular interactions between p7B copies were observed in the bimolecular fluorescence complementation (BiFC) assays (Methods S1, Figure S5). Therefore, interacting oligomeric cellular proteins are possibly required for GFP-p7B[$D_7AP_{10}A$] complexes stabilization.

Mutational analysis of p7B estramembranous domains in MNSV cell-to-cell movement

To assess the relevance of the identified p7B sorting motifs in MNSV cell-to-cell movement, $C_6AD_7AS_8A$ and $S_9AP_{10}AG_{11}A$ mutations in the CR and $K_{49}AT_{50}AQ_{51}A$ mutation in the LR were introduced into a GFP-tagged MNSV-infectious binary vector (Figure 8a). Moreover, $C_3AC_4AR_5A$ and $D_{12}AY_{13}A$ mutations in the CR and $F_{43}AD_{44}AN_{45}A$ in the LR were used as control. Five days after agroinfiltration in melon leaves, local

spread of infection was measured by quantifying the fluorescent area. Approximately 100 of the individual infection foci were analyzed per variant.

All mutations introduced into the CR were functional in viral cell-to-cell movement, but showed pronounced differences in relation to the infected area. As expected, virus carrying $C_3AC_4AR_5A$ and $D_{12}AY_{13}A$ mutations (Figure 8c,f) behaved basically like wild-type (Figure 8b) showing an average infection foci size of 3.44±0.41 mm^2 and 3.35±1.5 mm^2, respectively (95.5 % and 92.8 % of the local movement vs the wild-type, Figure 8i). Even though $S_9AP_{10}AG_{11}A$ mutation resulted in reduced viral movement (1.51±0.50 mm^2, 41.87 %) (Figure 8e,i), the most severe effect was found for the $C_6AD_7AS_8A$ mutation, which drastically restricted viral movement to foci of a few cells (0.51±0.22 mm^2, 14.26%) (Figure 8d,i). These results are consistent with those obtained with GFP-p7B[$C_6AD_7AS_8A$] and GFP-p7B[$S_9AP_{10}AG_{11}A$] mutants suggesting that inhibition of p7B ER-export could be related with the drastic reduction in viral cell-to-cell movement. Since the two latter mutations still supported viral movement, albeit inefficiently, it suggests that mutant MPs are still reaching the cellular periphery by ER-mediated lateral translocation as occurs with *Tobaco mosaic virus* (TMV) MP (Liu and Nelson, 2013). Consistently with this hypothesis, we observed that protein complexes, like those from GFP-p7B[$D_7AP_{10}A$], accumulate at the cellular periphery when transiently expressed (Figure S6). Within the LR, in contrast to $F_{43}AD_{44}AN_{45}A$ mutation (3.15±0.38 mm^2, 87.20%, Figure 8g,i), $K_{49}AT_{50}AQ_{51}A$ mutation completely abolished virus movement ability as all the detected infection foci were unicellular (Figure 8h,i). Note that ER-export of GFP-p7B[$K_{49}AT_{50}AQ_{51}A$] was impaired and the lateral mobility of the related GFP-p7B[$K_{49}A$] mutant was limited. Consequently, these results highlight that p7B ER-export but also their ER-lateral translocation are both essential for efficient MNSV cell-to-cell movement.

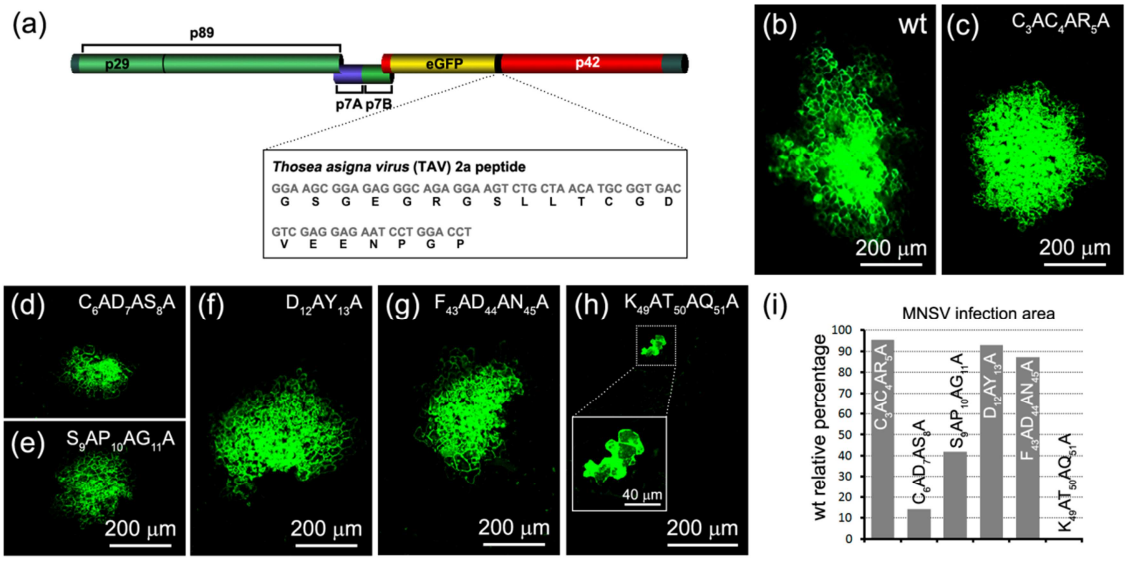

Figure 8. Influence of mutations in the cytoplasmic and luminal domains of p7B on MNSV cell-to-cell movement. (a) Schematic representation of the recombinant infectious clone pMNSV(Al)/GFP used in this assay. The GFP and coat protein were simultaneously expressed using the "self-cleaving" TAV 2a peptide (TAV 2a ORF is shown below). Viral and fluorescent protein names are indicated. (b-h) CLSM images taken at 4-5 days post-agroinfiltration of wild-type MNSV(Al)/GFP and mutant constructs in melon plant leaves. Images are representative of infection foci observed at least in three independent experiments. Mutations are indicated in the upper right side of each panel. (i) Infection spread of each mutant construct measured as fluorescent area. Results are presented as a percentage relative to wild type infection.

DISCUSSION

The default destination of type I membrane proteins appeared to be dependent on its TMD length (Brandizzi *et al.,* 2002a). However, it is now evident that not all single-spanning proteins exit the ER by bulk-flow, rather a selective process mediated through COPII-coated transport vesicles is the rule for the ER-sorting. Although much is known about the host factors involved in this transport, the signals/motifs governing the membrane proteins trafficking remain poorly understood. We previously showed that p7B TMD was sufficient to promote protein insertion into ER membranes but not to induce its ER-export (Genovés *et al.,* 2010; 2011) suggesting that active ER-export information must be included within the p7B CR or LR. Through a mutational analysis, we present here evidence that p7B ER-export relies on contributions from a putative cytosolically-exposed β-turn composed of DSSP residues and a luminal-oriented lysine (K49). The multiple sequence alignment of p7B homologs indicates that both motifs are well conserved in related MPs from other *Tombusviridae* family members, thereby supporting their functional relevance during viral biology.

Our results argue against the observation that some transmembrane secretory proteins display only cytoplasmic ER-sorting signals, usually diacidic (DXE), dihydrophobic/diaromatic (FF, YY, LL, or FY), dibasic (R/KxR/K) and Tyr-based motifs, which are actively recognized by the prebudding COPII complex (Aniento *et al.,* 2006; Robinson *et al.,* 2007). In the few cases in which the involvement of both Nt- and Ct sequence motifs has been demonstrated (e.g. Jung *et al.,* 2011) both termini had a cytoplasmic location. A common feature shared by most sorting signals, including those of p7B, is the presence of charged residues which underlies an essential role for electrostatic interactions during the recognition process (Schoberer *et al.,* 2009). Even a single proline has been characterized as an ER-export determinant located at position +2 from the cleavage peptide signal of the Golgi-localized soluble protein NUCB1 (Tsukumo *et al.,* 2009).

Three-dimensional arrangement of the different cargo-binding sites in COPII components, Sar1 and Sec24, and some other accessory proteins suggests that both chemical interactions and the proper orientation of functional groups determines cargo selection (Lee and Miller, 2007; Quintero *et al.,* 2010). The β-turn structure backbone may favor a specific conformation of the amino acid side chains within and/or nearby the turn structure suitable to interact with its receptor binding site. This assumption is further supported by the observation that a β-turn structure was essential for the apical membrane sorting of the rat ileal bile acid transporter, for the basolateral membrane targeting of mammalian polymeric immunoglobulin and transferrin receptors and for the internalization of low density lipoprotein receptor and lysosomal acid phosphatase (Bansal and Gierasch, 1991; Eberle *et al.,* 1991; Aroeti *et al.,* 1993; Dargemont *et al.,* 1993; Sun *et al.,* 2003).

As seems to occur in p7B transport, cooperation among different targeting determinants playing no redundant role in all three domains of transmembrane cargoes has been reported; i.e. in the yeast guanosine diphosphatase ER-export (Dancourt and Barlowe, 2009). Contributions to anterograde transport from the luminal domain have also been detected in a few cases such as yeast alkaline phosphatase (ALP) (Dancourt and Barlowe, 2009), Ktr3p mannosyltransferase (Bue and Barlowe, 2009) and mammalian p23 (Blum and Lepier, 2008). However, K49 of p7B

represents one of the first examples where luminal ER-export signals have been identified in plants. As ER-export depends mainly on cytoplasmic COPII vesicles, additional ER membrane-spanning factors that link such luminal transmembrane cargo domains with cytoplasmic COPII components are necessary. For instance, Cornichon family members, such as *Drosophila* Cornichon, yeast Erv14p and two mammalian Cornichon paralogs, are believed to interact with luminal sorting signals of Gurken, Axl2p and TGF proteins, respectively. Interestingly, yeast Erv26p specifically associates with the luminal region of the type II membrane proteins ALP and Krt3p (Dancourt and Barlowe, 2010). Transmembrane sorting adaptors appear highly conserved among eukaryotic species and must, consequently, occur also in plants. From previous results, putative multiple binding partners, accessory proteins or transport receptors proteins, are evidently required for p7B ER-export.

Studies about $D_7AP_{10}A$ mutant dynamics and its association with a Golgi marker upon immobilization through latB treatment strongly suggest that both employ the same mechanism and pathway to be translocated across the ER surface. $D_7AP_{10}A$ mutant complexes most likely represent a trapped state of the protein caused by its inability to interact with the COPII prebudding complex. Note that the $D_7AP_{10}A$ mutant did not induce *de novo* formation of ERES. In addition, considering that we did not observe p7B dimerization in BiFC experiments, $D_7AP_{10}A$ mutant complexes most likely result from the interaction with an unknown oligomeric cellular factor. We cannot rule out the possibility that this factor could be a transmembrane adaptor interacting with the p7B LR. Indeed, under native condition, Erv proteins have been detected as oligomers, a property shared with other protein adaptor families (Dancourt and Barlowe, 2010).

Changes in ER morphology and anterograde traffic interfering phenotype indicate a close relationship between $K_{49}A$ mutant and the plant early secretory pathway. However, FRAP analyses revealed that K49 is essential for early lateral diffusion of p7B into ER membranes. The transmembrane adaptor may also link the viral protein either directly or indirectly to actin cytoskeleton promoting its movement and concentration. In mammalian cells, local concentration of the traffic vesicle components and proteins to be transported occurs at relatively fixed ERESs close to the ERGIC, thus maximizing

the transport efficiency (Dukhovny *et al.,* 2009; Zanetti *et al.,* 2012). Access of transmembrane proteins to exit sites depends highly on lateral diffusion within ER membranes. Reduced lateral diffusion could, in turn, diminish sorting efficiency and sequestration of protein cargoes into budding vesicles resulting in ER-to-Golgi transport inhibition (Prosser *et al.,* 2008). In plants, vesicle traffic releasing has been proposed to be a fast and continuous process triggered by an upcoming motile Golgi stack that halts only to allow the fusion either of COPII-Golgi or COPI-ER membranes (Langhans *et al.,* 2012, Lerich *et al.,* 2012). Whether cargoes accumulate at some point during their transit in plants before vesicle packaging is unknown but p7B lateral diffusion appears to be essential for ER-export. Because of the dynamic nature of plant early secretory pathway, cargo proteins should be propelled through the same route by which the "secretory unit" travels to increase the chances of a productive interaction between them. This route usually consists in the cortical ER network tightly associated with the actin cytoskeleton. An interesting case has been recently reported. During the membrane envelopment process of the *Tomato spotted wilt bunyavirus*, the viral glycoprotein Gc remains arrested in the ER but in the presence of the cytosolic viral nucleoprotein N its distribution changes from reticular into punctate spots corresponding to ERESs. Gc concentration at ERES, which is required to COPII-dependent transport to the Golgi, is mediated by an interaction between its cytoplasmic tail and N (Ribeiro *et al.,* 2013).

From the results obtained herein, a model is proposed by which following ER-membrane insertion and proper folding, the p7B LR may interact through the K49 residue with an actin cytoskeleton associated transmembrane adaptor to be concentrated and propelled along the cortical ER (Figure 9). Despite the molecular mechanisms by which these receptors link cargo to coat remain poorly understood, a p7B cytoplasmic β-turn motif may also play an essential role to induce COPII vesicle assembly directly or indirectly (Figure 9). Further research into the interactions between p7B and cellular components may help to clarify the poorly understood mechanism controlling the traffic of transmembrane proteins within plant cells.

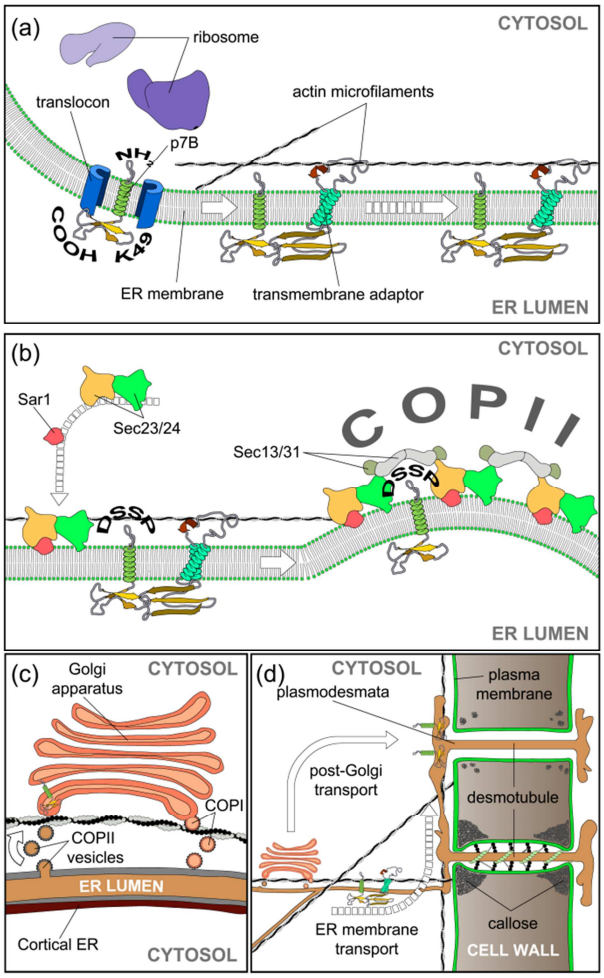

Figure 9. Model for the Golgi-dependent MNSV p7B intracellular transport. (a) After the p7B transmembrane domain (TMD) anchors the protein to the ER membrane with a type II topology (cytoplasmic N-terminus and luminal C-terminus) (Navarro *et al.,* 2006; Martínez-Gil *et al.,* 2007; Genovés *et al.,* 2011), the p7B luminal region would interact throughout lysine 49 with a transmembrane adaptor conferring actin-dependent mobility to the viral protein along the cortical ER. Because of the dynamic nature of plant early secretory pathway, ER lateral translocation may increase the chances of a productive interaction between cargo proteins and components of the "secretory unit". (b) At this point, the p7B cytosolic-exposed DSSP β-turn can trigger the recruitment of Sar1, and most likely of the rest of COPII components (Sec23/24 and Sec13/31), to ER membrane.(c) Finally, p7B would be delivered to Golgi apparatus using the COPII-dependent pathway (Genovés *et al.,* 2010) and under the influence of the TMD hydrophobic profile (Genovés *et al.,* 2011) (d) Although an inefficient transport of p7B to cellular periphery may occur by ER lateral diffusion, it is obvious that post-Golgi plasmodesmata targeting of p7B is essential for cell-to-cell movement.

EXPERIMENTAL PROCEDURES

Molecular cloning and markers

pBSGFP-p7B and pBSChFP-p7B plasmids, which contain appropriate elements for gene expression and N-terminal fusion of either green (GFP) or cherry (ChFP) fluorescence protein to p7B, respectively, were previously constructed (Genovés *et al.,* 2010). Both plasmids were used as PCR templates to obtain mutants of interest. Amino and carboxyl-truncation were constructed by inverse PCR. Mutations-to-alanine were introduced by site-directed mutagenesis using the QuickChange XLSite-Direct Mutagenesis Kit (Agilent Technologies, Santa Clara, CA, http://www.agilent.com). All the expression cassettes were inserted into pMOG800 (Knoester *et al.,* 1998). Primers are listed in Table S1.

The binary GFP-tagged full-length cDNA clone of MNSV-Al (DQ339157), pM(MNSV/Al-GFP), was obtain by modification of previously described pMNSV(Al)-Δcp-GFP plasmid (Genovés *et al.,* 2006). In brief, the encoding *Thosea asigna virus* (TaV) 2A sequence (GSGEGRGSLLTCGDVEENPGP) (Kim *et al.,* 2011) was inserted downstream GFP by inverse PCR. Next, the coat protein gene was amplified and cloned downstream from the TaV 2a sequence. The recombinant cDNA was cloned into pMOG800 between the CaMV 35S promoter and the potato proteinase inhibitor II terminator (PoPit). Mutations-to-alanine were introduced as described above.

Plasmids encoding the mouse talin actin-biding domain fused to the DsRed fluorescent protein (dsRed-talin), the rat α-2,6-sialyltransferase transmembrane domain fused to ChFP (STtmd-ChFP) and SV40 nuclear localization signal (NLS) fused to mRFP (mRFP-NLS) were provided by Prof. V. V. Dolja. ER marker was engineered by adding the calreticulin peptide signal and ER-retrieval sequence KDEL to ChFP (ChFP-KDEL). Construct encoding tobacco Sar1-YFP fusion was provided by Prof. C. Hawes.

Transient expression

Agrobacterium tumefaciens cultures harboring the relevant binary constructs were infiltrated into *N. benthamiana* leaves as described previously (Genovés *et al.,* 2011). Bacterial OD at 600 nm was adjusted to 0.025 for Sar1p-YFP and to 0.1-0.2 for

the rest of constructs. Plants were kept in growth chambers in 16h light at 25 °C and 8h dark at 22 °C.

Microsomal fractionation and immunoblotting

Microsomal fractionation was carried out as previously described (Genovés *et al.,* 2010). Briefly, the crude lysates from *N. benthamiana* leaves were filtrated and ultracentrifuged at 30,000 g to generate the cytosolic (S1) and the microsomal fraction. Latter was resuspended (20mM HEPES, pH 6.8; 150 mM potassium acetate; 250 mM mannitol and 5 mM $MgCl_2$), placed onto continuous sucrose gradient (20-60%) and further ultracentrifuged at 100,000 g during 17 hours. Eighteen fractions were collected and analyzed by immunoblotting using anti-GFP antibody.

Brefeldin A and Latrunculin B treatments

At 60 h post-infiltration, 1-cm diameter disks were cut out from *N. benthamiana* leaves expressing GFP-p7B[$D_7AP_{10}A$] alone or in combination with STtmd-ChFP. Tissue samples were immersed into brefeldin A (10 µg/ml) or latrunculin B (25 µM) for 1h. Drugs were diluted in DMSO 10 mM. Controls were performed by tissue immersion into DMSO 10 mM.

Cell-to-cell movement bioassays

Cell-to-cell movement ability of the MNSV(Al)-GFP and mutant variants were assayed on *Cucumis melo* L. subsp. melo cv. Galia. Briefly, fully expanded leaves from two-weeks-old seedlings were infiltrated with a suspension of *A. tumefaciens* carrying each binary vector. Three independent bioassays with five plants per mutant were performed. At three days post-infiltration (dpi), fluorescent infection foci images were taken with Leica MZ12 fluorescent stereo microscope and infection areas were measured using ImageJ 1.41o software. Data was analyzed with MS Excel.

Confocal laser scanning microscopy.

To study the subcellular localization of the fluorescent tagged proteins imaging was conducted with a Leica TCS SL confocal laser-scanning microscope (Leica Microsystems GmbH, Wetzlar, Germany, http://www.leica-microsystems.com). GFP

and YFP fluorescence was visualized by 488 nm excitation with a Kr/Ar laser and their emission was examined with a bandpass filter for 500-530 nm. For imaging of ChFP fluorescence, excitation at 514 nm was used whereas the emission was observed at 600-620 nm.

Subcellular fluorescence was measured using FIJI software (http://fiji.sc/Fiji). For quantification of Golgi/total fluorescence ratio, 50 images of cortical sections of different cells expressing GFP-p7B were used from at least three independent experiments. The Golgi stacks were selected on the GFP image and the mean fluorescence in these regions and total image fluorescence were measured. The ratio of these two mean fluorescences gave to the Golgi/total ratio. Values were expressed as the mean±SE.

Fluorescence recovery after photobleaching (FRAP) experiments.

FRAP experiments were performed on an inverted Zeiss LSM 780 confocal microscope (Carl Zeiss, Oberkochen, Germany, http://www.zeiss.com), using the 488 nm line of an Argon laser with a Plan-Apochromat 63x/1.40 oil objective (5x optical zoom and 256x256 pixel resolution image). Circle ROIs (region of interest) of 1.7 µm diameter were scanned three times before a bleach pulse (25% power, 100% transmission, 100 iterations) and then, a series of 97 single section images were collected at low laser power (25% power, 2% transmission) at 191 ms intervals. Raw fluorescence intensity values from bleached, background and reference ROIs were obtained using the FRAP module of the Zen 2011 software. FRAP recovery curves were double normalized (Phair *et al.,* 2004) and fitted by single exponential function with Graphpad Prism software. The standard Student's t-test was used to determine the statistical significance of results. All quantitative values represent averages ± s.d. from at least 10 ROIs from three independent experiments.

SUPPORTING INFORMATION

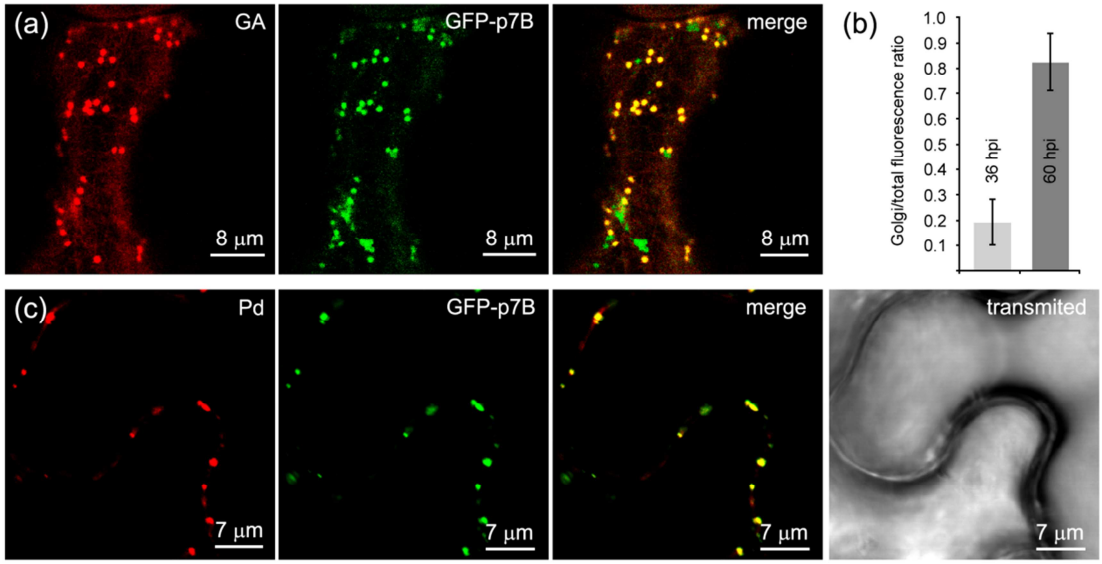

Figure S1. Co-expresion of GFP-p7B with Golgi and plasmodesmata markers at 60 hpi. Quantification of GFP-p7B fluorescence in Golgi stacks at 36 and 60 hpi.

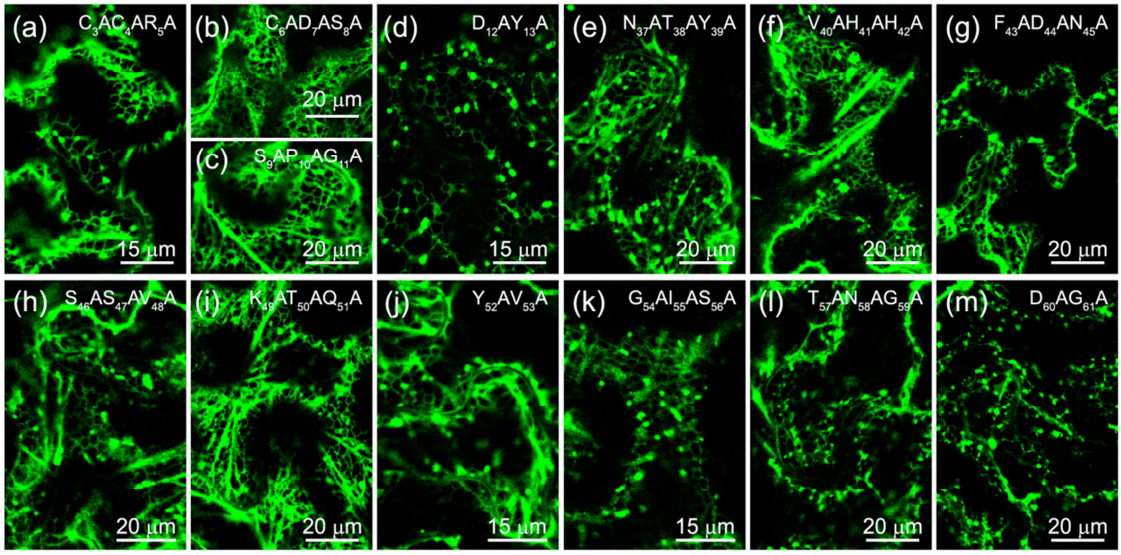

Figure S2. Endoplasmic reticulum localization of all GFP-p7B alanine substitution mutants used in this study at 36 hpi.

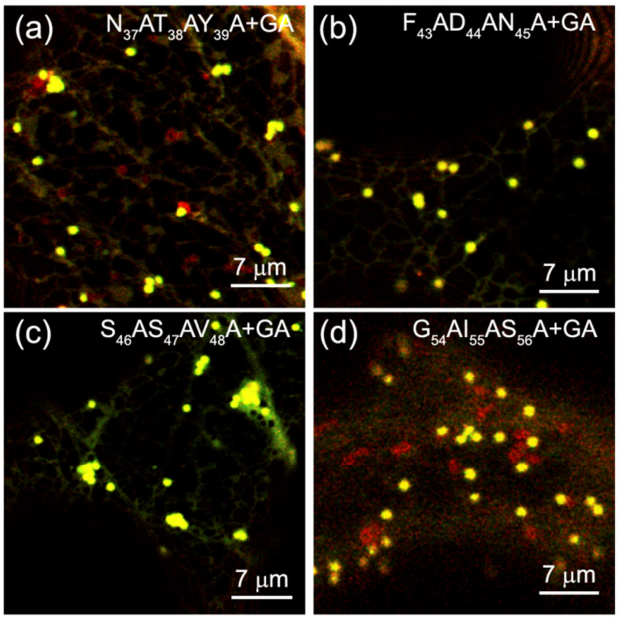

Figure S3. Golgi apparatus localization of GFP-p7B[$N_{37}AT_{38}AY_{39}A$], GFP-p7B[$F_{43}AD_{44}AN_{45}A$], GFP-p7B[$S_{46}AS_{47}AV_{48}A$] and GFP-p7B[$G_{54}AI_{55}AS_{56}A$] at 60 hpi.

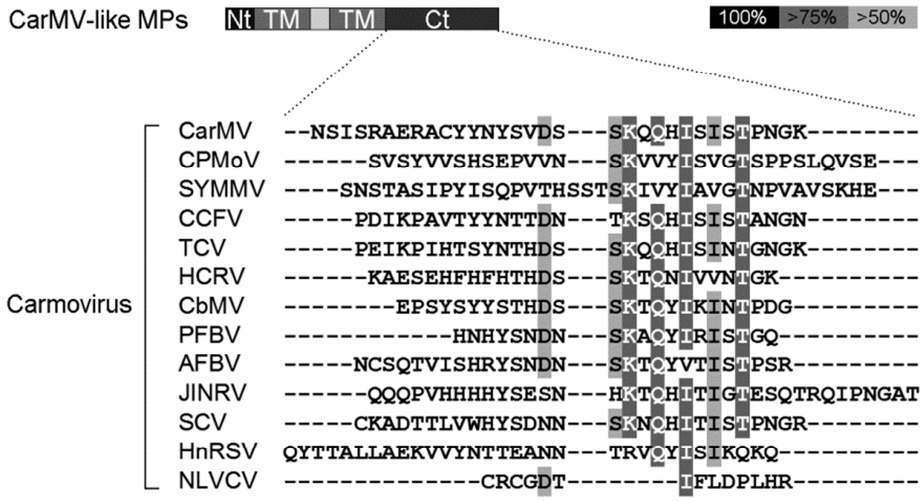

Figure S4. Sequence alignment of the carboxyl region of p7B-related proteins from 13 members of the *Carmovirus* genus.

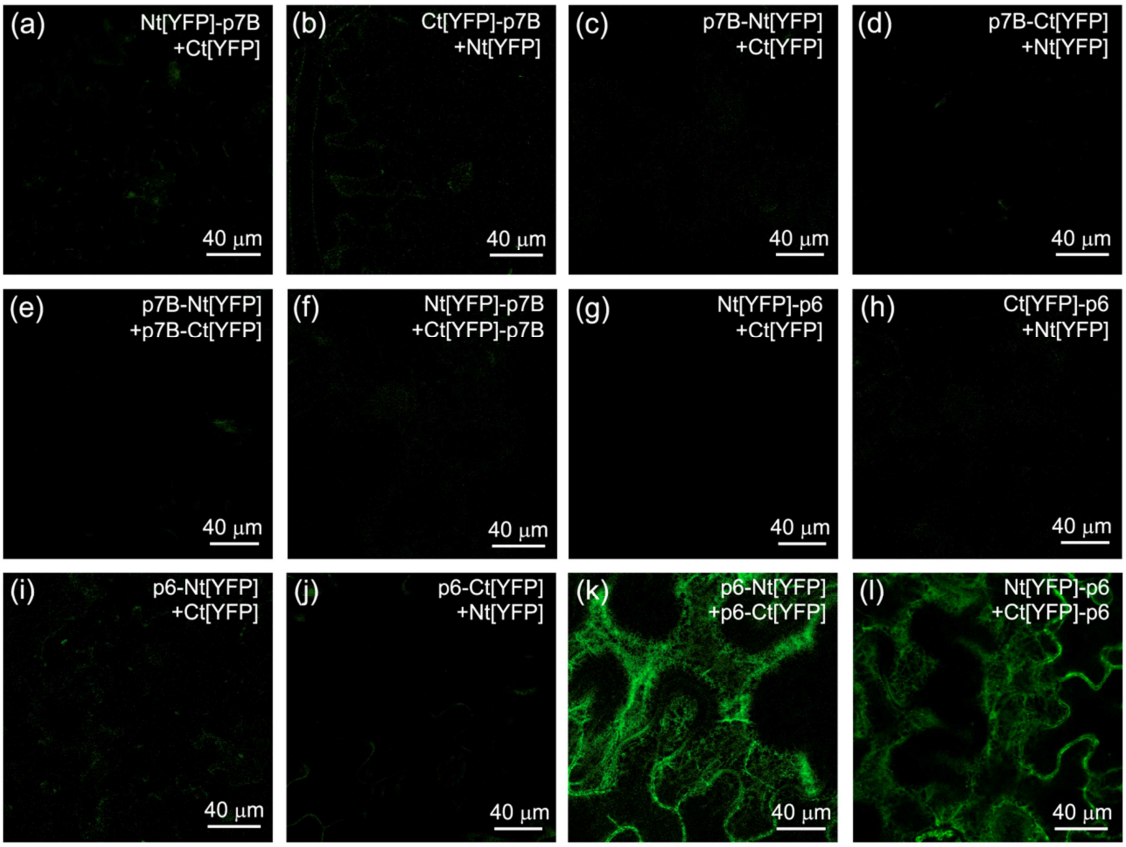

Figure S5. Study on p7B dimerization by bimolecular fluorescence complementation assay.

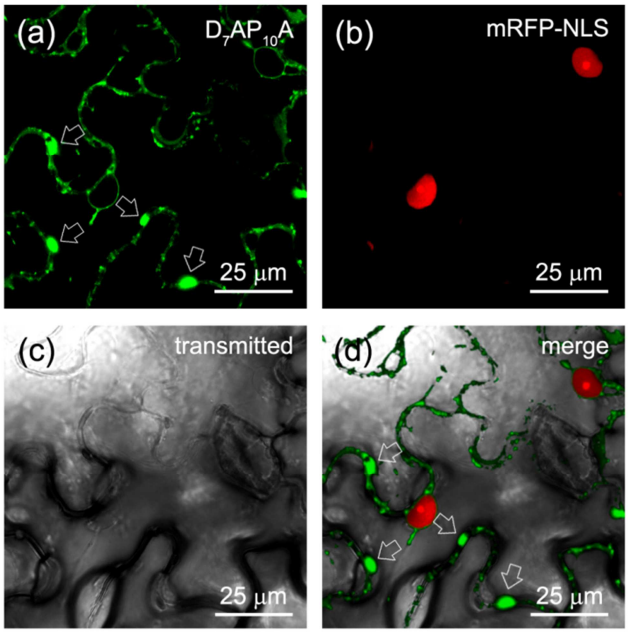

Figure S6. Accumulation of GFP-p7B[$D_7AP_{10}A$] complexes in the cellular periphery by lateral transport along the endoplasmic reticulum.

Table S1. List of oligonucleotides used in this study

cDNA/Mutation	name	sequence
TaV 2a	VP1881	GCGGTGACGTCGAGGAGAATCCTGGGCCCATCTCGCCTTAGGTTTACG
	VP1882	TGTTAGCAGACTTCCTCTGCCCTCTCCACTGCCCTTGTACAGCTCGTCCAT
Coat protein	VP1883	ATCGGGGCC**C**ATGGCGATGGTTAGACGC
	VP1884	ATCGGGGCCCTTAGGCGAGGTAGGCTGT
Nt-deletion	VP1575	GGGCCCATACTTGTACAGCTCGTCCATG
	VP1576	TCTGGAGCGTTGCTTATATTATTTATC
$C_3AC_4AC_5A$	VP1669	TATGGGCCCATGGCTGCTGCCGCTTGCGACTCCAGCCCC
	VP1670	GGGGCTGGAGTCGCAAGCGGCAGCAGCCATGGGCCCATA
$C_6AD_7AS_8A$	VP1671	ATGGCTTGTTGCCGTGCCGCCGCCAGCCCCGGGGATTAC
	VP1672	GTAATCCCCGGGGCTGGCGGCGGCACGGCAACAAGCCAT
$S_9AP_{10}AG_{11}A$	VP1673	TGCCGTTGCGACTCGCCGCCGCGGATTACTCTGGAGCG
	VP1674	CGCTCCAGAGTAATCCGCGGCGGCGGAGTCGCAACGGCA
$D_{12}AY_{13}A$	VP1675	GACTCCAGCCCCGGGGCTGCCTCTGGAGCGTTGCTTATA
	VP1676	TATAAGCAACGCTCCAGAGGCAGCCCCGGGGCTGGAGTC
$D_7AP_{10}A$	VP2208	GGAGGCGCAACGGCAACAAGCCAT
	VP2209	AGCGCCGGGGATTACTCTGGAGCG
Ct-deletion	VP1336	ATTACCTCGCTTAGCTAGCAAGGAAATACTTAC
	VP1337	GTAAGTATTTCCTTGCTAGCTAAGCGAGGTAAT
$N_{37}AT_{38}AY_{39}A$	VP989	CTTAGCTCGCAAGGAGCTGCTGCCGTTCATCACTTCGAT
	VP990	ATCGAAGTGATGAACGGCAGCAGCTCCTTGCGAGCTAAG
$V_{40}AH_{41}AH_{42}A$	VP991	CAAGGAAATACTTACGCTGCTGCCTTCGATAACTCTTCC
	VP992	GGAAGAGTTATCGAAGGCAGCAGCGTAAGTATTTCCTTG
$F_{43}AD_{44}AN_{45}A$	VP993	ACTTACGTTCATCACGCCGCTGCCTCTTCCGTTAAAACA
	VP994	TGTTTTAACGGAAGAGGCAGCGGCGTGATGAACGTAAGT
$S_{46}AS_{47}AV_{48}A$	VP995	CATCACTTCGATAACGCTGCCGCTAAAACACAATACGCT
	VP996	AGCGTATTGTGTTTTAGCGGCAGCGTTATCGAAGTGATG
$K_{49}AT_{50}AQ_{51}A$	VP997	GATAACTCTTCCGTTGCAGCAGCATACGCTGGCATCTCT
	VP998	AGAGATGCCAGCGTATGCTGCTGCAACGGAAGAGTTATC
$Y_{52}A$	VP999	TCCGTTAAAACACAAGCCGCTGGCATCTCTACAAAT
	VP1000	ATTTGTAGAGATGCCAGCGGCTTGTGTTTTAACGGA
$G_{54}AI_{55}AS_{56}A$	VP1001	AAAACACAATACGCTGCCGCCGCTACAAATGGCGATGGT
	VP1002	ACCATCGCCATTTGTAGCGGCGGCAGCGTATTGTGTTTT
$T_{57}AN_{58}AG_{59}A$	VP1003	TACGCTGGCATCTCTGCAGCTGCCGATGGTTAAGGGCCC
	VP1004	GGGCCCTTAACCATCGGCAGCTGCAGAGATGCCAGCGTA
$D_{60}AG_{61}A$	VP1167	GCATCTCTACAATGGCGCTGCTTAGACGCATTAATAATT
	VP1168	AATTATTAATGCGCTTAAGCAGCGCCATTTGTAGAGATGC
$K_{49}A$	VP1665	GATAACTCTTCCGTTGCAACACAATACGCTGGCATCTCT
	VP1666	AGAGATGCCAGCGTATTGTGTTGCAACGGAAGAGTTATC

Table S2. List of virus used for multiple sequence alignment of MNSV p7B related proteins

virus abbreviation	full name	genus
MNSV	*Melon necrotic spot virus*	*Carmovirus*
PSNV	*Pea stem necrosis virus*	
CarMV	*Carnation mottle virus*	
CPMoV	*Cowpea mottle virus*	
SYMMV	*Soybean yellow mottle mosaic virus*	
CCFV	*Cardamine chlorotic fleck virus*	
TCV	*Turnip crinkle virus*	
HCRV	*Hibiscus chlorotic ringspot virus*	
CbMV	*Calibrachoa mottle virus*	
PFBV	*Pelargonium flower break virus*	
AFBV	*Angelonia flower break virus*	
JINRV	*Japanese iris necrotic ring virus*	
SCV	*Saguaro cactus virus*	
HnRSV	*Honeysuckle ringspot virus*	
NLVCV	*Nootka lupine vein clearing virus*	
GaMV	*Galinsoga mosaic virus*	*Gallantivirus*
OLV1	*Olive latent virus 1*	*Alphanecrovirus*
OMMV	*Olive mild mosaic virus*	
TNV strain A	*Tobacco necrosis virus*	
TNV strain D	*Tobacco necrosis virus*	*Betanecrovirus*
BBSV	*Beet black scorch virus*	
LWSV	*Leek white line mosaic virus*	
CMMV	*Cocksfoot mild mosaic virus*	*Panicovirus*

Table S3. *t*-Test for difference between two unpaired means: two-tailed p-value

(a) Half-time of maximum recovery

		DMSO			Latrunculin B			
		$D_7AP_{10}A$	$K_{49}A$	KDEL	wt	$D_7AP_{10}A$	$K_{49}A$	KDEL
DMSO	wt	0.6850*	0.0001	<0.0001	0.1468*	0.0233	<0.0001	<0.0001
	$D_7AP_{10}A$		0.0019	<0.0001	0.4468*	0.1908*	<0.0001	<0.0001
	$K_{49}A$			<0.0001	0.0443	0.1616*	0.0517*	<0.0001
	KDEL				<0.0001	<0.0001	<0.0001	0.3797*
Lat B	WT					0.4965*	0.0002	<0.0001
	$D_7AP_{10}A$						0.0016	<0.0001
	KA							<0.0001

(b) Maximum recovery fluorescence

		DMSO			Latrunculin B			
		$D_7AP_{10}A$	$K_{49}A$	KDEL	wt	$D_7AP_{10}A$	$K_{49}A$	KDEL
DMSO	wt	0.0048	<0.0001	0.0006	0.7767*	<0.0001	<0.0001	<0.0001
	$D_7AP_{10}A$		<0.0001	<0.0001	0.0363	0.0020	<0.0001	<0.0001
	$K_{49}A$			<0.0001	<0.0001	0.0290	0.0539*	<0.0001
	KDEL				0.0449	<0.0001	<0.0001	0.0553*
Lat B	wt					0.0011	<0.0001	0.0054
	$D_7AP_{10}A$						0.6647*	<0.0001
	$K_{49}A$							<0.0001

* Indicates no statistical difference between data set. If the *P*-value for the test is less than 0.05, the null hypothesis of equal means can be rejected

SUPPORTING EXPERIMENTAL PROCEDURES

Construction of binary vectors for bimolecular fluorescence complementation assays.

The recombinant cDNAs corresponding to Nt[YFP]-p7B, Ct[YFP]-p7B, p7B-Nt[YFP] and p7B-Ct[YFP] consisting on an amino-terminal YFP fragment (residues 1-155, referred to as Nt-[YFP]) and a carboxyl-terminal YFP fragment (residues 156-238, referred to as Ct-[YFP]) either fused to the amino or carboxyl terminus of the p7B were obtained by standard procedures. Similar recombinant cDNAs were obtained with the *Beet yellows virus* p6 movement protein. All these recombinant cDNAs together with the Nt[YFP] and Ct[YFP] fragments were inserted in the binary vector pMOG800 under the control of the Cauliflower mosaic virus (CaMV) 35S promoter and used in bimolecular fluorescence complementation experiments. For the simultaneous expression of two

different proteins, individual bacterial cultures containing the corresponding binary vectors were adjusted to a final OD_{600} of 0.2 and mixed before its infiltration in *N. benthamiana* leaves. Plants were kept in growth chambers in 16h light at 25 °C and 8h dark at 22 °C.

Movie S1 and S2. Time-lapse movie depicting the movement of GFP-p7B[$D_7AP_{10}A$] ER-associated complexes.

Movie S3. Time-lapse movie depicting the movement of GFP-p7B[$D_7AP_{10}A$] ER-associated complexes in the presence of brefeldin A.

Movie S4. Time-lapse movie depicting the movement inhibition of GFP-p7B[$D_7AP_{10}A$] complexes and Golgi marker STtmd-ChFP in the presence of latrunculin B.

CAPÍTULO SEGUNDO

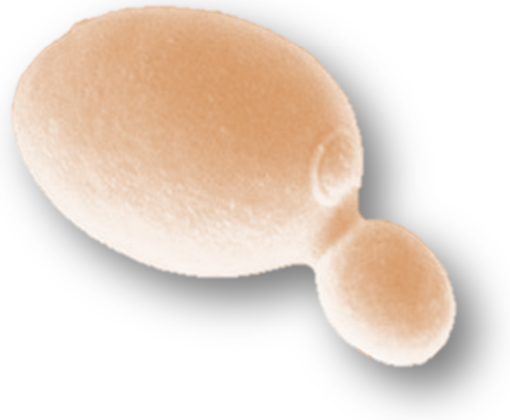

A Y2H study with three DGBp1s identifies three common interacting cellular factors, WRKY36, RPP3A and eIF3g, revealing a possible conserved functionality.

INTRODUCTION

Viral movement is one of the best studied issues in plant virus biology. Its importance relies not only in increasing the general knowledge and unveiling new antiviral applications, but also in providing important insights into the functioning of cellular processes, such as molecular trafficking of cell proteins, natural defense and plant development. To establish systemic infection, plant viruses must be localized to the appropriate subcellular compartment and then transported from initially infected cells to adjacent cells. Next, viral infection is locally extended to the vascular system which finally provides the route to invade distal parts of the plants (Harries and Ding, 2011). Plant viruses have developed a variety of strategies to move from cell to cell, commonly exploiting highly specialized channels that symplastically communicate contiguous cells, namely, plasmodesmata (PD) (Niehl and Heinlein, 2011; Schoelz *et al.,* 2011; Tilsner *et al.,* 2013; Waigmann *et al*., 2004). Movement proteins (MPs) of plant viruses play a central role in the spread of infection in accomplishing several functions. MPs bind viral genome to form mobile nucleoprotein complexes (NPC) (Boevink and Oparka, 2005; Citovsky *et al.,* 1990; Herranz and Pallás, 2004; Marcos *et al.,* 1999b). Cellular mechanisms governing the intracellular trafficking of host proteins are sometimes recruited by MPs to deliver NPCs to the PD, (Boevink and Oparka, 2005; Sánchez-Navarro *et al*., 2006, Verchot-Lubicz, 2005; Wolf *et al.,* 1989). In this regard, it is known that MPs associate with the endogenous scaffold supporting the intracellular transport pathways, mainly cytoskeleton and endomembrane system, and with related host factors (Lucas, 2006). Depending on the virus, MPs interact with additional MPs and with different viral factors such as coat protein. Finally, MPs contribute to plasmodesmata gating, and may even influence RNA silencing suppression (Bayne *et* al., 2005; Genovés et al., 2006; Navarro et al., 2006).

In addition, the ability of viruses to invade plants and to cause systemic infection is also dependent on cellular factors supporting movement, among other processes

(Pallás *et al*.,2011). Consequently, to carry out the above mentioned functions, MPs have inevitably been found to associate with diverse host factors. For example, MPs of various viruses can bind to PD and other components of cell periphery (Chen *et al.,* 2000; Chen *et al.,* 2005; Dorokhov *et al.,* 1999; Gillespie *et al.,* 2002; Kawakami *et al.,* 2004; Lee *et al.,* 2005), cytoskeleton (Brandner *et al.,* 2008; Genovés *et al*.,2009; Sambade *et al.,* 2008; Su *et al.,* 2010), vesicle trafficking associated membrane proteins (Chen *et al*., 2000; Huang *et al.,* 2001; Serra-Soriano *et al.,* 2014), chaperones (Krenz *et al.,* 2010; Shimizu *et al.,* 2009), nuclear components (Matsushita *et al.,* 2002) and others such transcription factors (Desvoyes *et al.,* 2002).

Intracellular and intercellular studies on carmoviruses are scarce, and the main components of the movement-competent complex during intracellular transport of these viruses are as yet unknown. The cell-to-cell movement of the carmoviruses *Turnip crinkle virus* (TCV), *Melon necrotic spot virus* (MNSV), and *Pelargonium flower break virus* (PFBV) requires the coordinated action of two small proteins encoded in the central region of their genomes (Genovés *et al*., 2006; Li *et al.,* 1998; Martínez-Turiño and Hernández, 2011). This couple of proteins, which was initially referred to as the double gene block (DGB) movement proteins (Hull, 2002), is commonly found among the members of the genera *Carmovirus*, *Alphanecrovirus*, *Betanecrovirus*, *Gallantivirus* and *Panicovirus* (Navarro *et al*., 2006; Serra-Soriano *et al*., 2014). DGB was considered the simplest multicomponent transport system due to the small size of both constituent MPs (DGBp1 and DGBp2) (Navarro *et al*., 2006). However, recent studies have shown that the mechanism governing carmovirus movement is more intricate than previously thought.

Different structural and molecular studies performed with DGBp1 of *Carnation mottle virus* (CarMV) (p7) and MNSV (p7A), showed that at N terminus there was an α-helical central region related to the RNA binding capability (Marcos *et al*., 1999b; Navarro *et al*., 2006; Vilar *et al*., 2001; Vilar *et al*., 2005). On the other hand, the DGBp1 C-terminus contains a potential β-sheet folding that may be involved in DGBp1 self-interaction and protein-protein interaction (Genovés *et al*., 2009). In the case of CarMV, subcellular fractionation experiments showed that its DGBp1 was mainly associated with the cell wall fraction (García-Castillo *et al.,* 2003). However MNSV

DGBp1, which RNA-binding activity had been directly connected to cell to cell movement, was localized in motile granules that associate with microfilaments (MFs), showed actin-dependent movement at the cytoplasm and accumulates at the cell periphery (Genovés *et al*., 2009). The second MPs of these viruses (DGBp2) have been classified as CarMV-like or MNSV-like DGBp2s depending on whether they have one or two potential transmembrane domains (TMDs), respectively (Navarro *et al*., 2006; Serra-Soriano *et al*., 2014). CarMV-like DGBp2s, such as those of CarMV and TCV, in addition to MNSV DGBp2 are all three targeted and inserted *in vitro* into ER-derived microsomes by means of a cotranslational/signal recognition particle (SRP)-dependent and translocon-assisted process (Martínez-Gil *et al.,* 2007; Navarro *et al*., 2006; Saurí *et al.,* 2005). MNSV and CarMV-like PFBV DGBp2s have been demonstrated that associate also to plant ER membranes (Genovés *et al.,* 2010; Martínez-Turiño and Hernández, 2011) but only MNSV DGBp2 was shown to be further targeted to Pd via the Golgi apparatus (GA) in a COPII-dependent pathway (Genovés *et al*., 2010). ER export of PFBV DGBp2s to other cellular membranes cannot be excluded since it was occasionally observed in unknown punctate structures in the cytoplasm and close to the plasma membrane (Martínez-Turiño and Hernández, 2011). However, in spite of the large amount of information obtained for this protein, the specific role of DGBp2 in viral transport is still not clear.

Movement-defective plant viruses can be complemented by another in double infections and it is known now that this feature often relies on the fact that MPs can be shared among different viruses (Fajardo *et al.,* 2013; Sánchez-Navarro *et al.,* 2010; Sánchez-Navarro *et al.,* 2006). This apparent lack of specificity makes these viral proteins appropriate for the identification of interacting-host factors that must be commonly used by plant viruses in their own benefit. Identification and functional characterization of these MP-interacting proteins could provide a deeper understanding of the viral life cycle and valuable new targets to ultimately generate viral broad-spectrum resistance. Therefore, in this study we try to identify some of the host factors interacting with MPs of two most studied *Carmovirus* CarMV and MNSV.

MATERIALS AND METHODS

Molecular cloning and plasmids for yeast two hybrid assays

Plasmids containing full-length cDNA genomes of MNSV-Al (Genovés *et al*., 2006), CarMV Dixie (Vilar *et al*., 2001) and TCV-M (Oh *et al.,* 1995) isolates were used as PCR template. The amplification of the corresponding MNSV p7A, CarMV p7 and TCV p8 movement proteins was carried out with the primers listed in Table 1. The resulting MNSV p7A and CarMV p7 cDNAs were cloned into GAL4-based MATCHMAKER Two-Hybrid System yeast plasmids pGBKT7 and pGADT7 with the appropriate restriction enzymes. TCV p8 cDNA was cloned into pGBKT7. pGBKT7 carries the GAL4 binding domain (BD), the Kan^r for selection in *E. coli* and the TRP1 nutritional marker for selection in yeast. pGADT7 contains the GAL4 activation domain (AD), an ampicillin resistance gene (Amp^r) for selection in *E. coli* and a LEU2 nutritional marker for selection in yeast. Hereafter, we will use pBD and pAD to denote constructions made with pGBKT7 and pGADT7, respectively. pBD/p7A$^{\Delta 1\text{-}22}$, pBD/p7A$^{\Delta 23\text{-}44}$ and pBD/p7A$^{\Delta 45\text{-}65}$ deletion mutants lacking either amino acid residues (aa) 1 to 22 (nucleotides [nt] 1 to 66 of the MNSV p7A cDNA sequence), aa 23 to 44 (nt 67 to 132) and aa 45 to 65 (nt 132 to 195), respectively, were obtained by inverse PCR using pBD/p7A as template. pBD/p7A^{fnf}, pBD/p7^{fnf} and pBD/p8^{fnf}, having the three most C-terminal amino acid residues (F63, N64 and F65) mutated to alanine, were obtained by site directed mutagenesis using a QuikChange site-directed mutagenesis kit (Stratagene) and appropriate oligonucleotides according to the manufacturer's instructions. All primers used are listed in Table1.

The identity of the cDNA fragments resulting in positive interactions either with MNSV p7A or CarMV p7 during the yeast two-hybrid screening was found by BLAST searching at The Arabidopsis Information Resource (TAIR) source. The full-length ORF of each gene was obtained using poly(A) messenger RNAs extracted from *Arabidopsis thaliana* (Col-0) plants and SuperScript™ III One-Step RT-PCR System with Platinum® Taq High Fidelity following the manufacture's protocol. The resulting cDNAs were cloned into pGADT7 using appropriate restriction enzymes and oligonucleotides (Table 1).

Table 1. List of clones and primers used in this study.

Plasmid	Insert	Forward primer	Reverse primer
pGBKT7	MNSV p7A	ACGTAAGCTTCCATGGACTCTCAACGAACT	ACGTGGATCCCTAAAAGTTAAAGTTAA
pGBKT7	CarMV p7	AGCTCCATGGATATTGAATCGGAAG	AGCTTGGATCCCTAAAAGTTGAAGTGAATGTG
pGADT7	MNSV p7A	ACGTAAGCTTCCATGGACTCTCAACGAACT	ACGTGGATCCCTAAAAGTTAAAGTTAA
pGADT7	CarMV p7	AGCTCCATGGATATTGAATCGGAAG	AGCTTGGATCCCTAAAAGTTGAAGTGAATGTG
pGBKT7	TCV p8	ACGTCCATGGATCCTGAACGAATTC	ACGTCTGCAGTTAGAAGTTGAAGTTGATTG
pGBKT7	MNSV p7A$^{\Delta 1\text{-}22}$	GGG GGA AAA CAG AAG AAC TCA ATG	GGCCATATGCAGGTCCTCCTC
pGBKT7	MNSV p7A$^{\Delta 23\text{-}44}$	GGAGTTATGGGTGCTAGCAC	GCTGTCACCACGTTCTTTAC
pGBKT7	MNSV p7A$^{\Delta 45\text{-}65}$	TAGGGATCCGTCGACCTGCAG	TTGCTTCGATTCAGAGATAGCATC
pGBKT7	MNSV p7A^{fnf}	ACGTAAGCTTCCATGGACTCTCAACGAACT	ACGTGGATCCCTAAGCGGCAGCGTTAATAGTCACCTTAAT
pGBKT7	CarMV p7^{fnf}	AGCTCCATGGATATTGAATCGGAAG	AGCTGGATCCCTAAGCGGCGGCGTGAATGTGCACCTC
pGBKT7	TCV p8^{fnf}	ACGTCCATGGATCCTGAACGAATTC	ACGTCTGCAGTTAAGCAGCAGCGTTGATTGAGACTTCCAC TTTATC
pGBKT7	At3g02550	ACGTCATATGCGGATGAGCTGTAATGGA	ACGTGGATCCTTAGAGCATAAGCTCAGT
pGBKT7	At3g11400	AGCTCATATGACGATCGATTCGCAGCAA	ACGTGGATCCCTAGGTTGGTCTTGGAGT
pGBKT7	At1g09070	AGCTCCATGGAGTGTAGATCATTGGATCT	AGCTGGATCCTCAGAAATCGAAACCACC
pGBKT7	At4g25890	AGCTCATATGGGAGTATTCACATTCGTA	ACGTGGATCCTTAACCAAAGAGATCGAA
pGBKT7	At3g05010	AGCTCCCGGGGATGGTTGTGCTTGCTGC	AGCTGGATCCTCATATGACTTGATAGTT
pGBKT7	At5g62190	AGCTCATATGGGAGACGCTAGAGACAAC	AGCTGAATTCTTAAGACGGCATGTAAGT
pGBKT7	At1g04870	AGCTCATATGAGGAGCTCCCAAAACGGC	AGCTGGATCCTCACTCTATGAAGTAAGT
pGBKT7	At5g48030	AGCTCATATGTCGGGTAAAGGAGAAGGA	ACGTGGATCCTTAGTCGACCTCCTCGAT
pGBKT7	At5g62300	AGCTCCATGGCGACAGCGTATCAA	ACGTGGATCCCTACGAGTCGGCGAT
pGBKT7	At1g69810	AGCTCATATGATCAAAGAGGAGACCGTT	AGCTGGATCCTTATTGCTGTCCGGAAAG
pGBKT7	At1g10350	GAATTCGAATTCATGGGGGTGGATTACTAC	GGATCCGGATCCTCAGCTTCCACCAAGAAC
pGBKT7	At1g70790	TTAGTCCAATCGTTTTGTG	GATGGAAGATAAACCATTAG
pGBKT7	At1g72370	GAATTCGAATTCATGGCGACTAATGGATCTGC	GGATCCGGATCCTTACTCCCAACCAGCAGCTG
pGBKT7	At2g35635	GAATTCGAATTCATGCAGATCTTCGTCAAAAC	GGATCCGGATCCTCAGAGAAGACCACCCCTAA
pGBKT7	At3g09440	GAATTCGAATTCAATGGCTGGTAAAGGAGAAGG	GGATCCGGATCCTTAGTCGACTTCCTCAATCT
pGBKT7	At5g11170	GATGGGAGACGCTAGAGAC	TTAAGAAGGCATGTAGGT
pMOG800	eIF3g-Nt/Ct[YFP] eIF3g-GFP	AGCTTCATGACGATCGATTCGCAGCAA	ACGTTCTAGAGGTTGGTCTTGGAGT
pMOG800	Nt/Ct[YFP]-eIF3g GFP-eIF3g	AGCTTCATGACGATCGATTCGCAGCAA	ACGTTCTAGACTAGGTTGGTCTTGGAGT
pMOG800	WRKY36-Nt/Ct[YFP] WRKY36-GFP	AGCTACATGTTGAAAGAGGAGACCGTT	ACGTGCTAGCTTGCTGTCCGGAAAG
pMOG800	Nt/Ct[YFP]-WRKY36 GFP-WRKY36	AGCTACATGTTGAAAGAGGAGACCGTT	ACGTGCTAGCTTATTGCTGTCCGGAAAG
pMOG800	RPP3-Nt/Ct[YFP] RPP3-GFP	AGCTCCATGGGAGTATTCACATTCGTA	ACGTGCTAGCACCAAAGAGATCGAA
pMOG800	Nt/Ct[YFP]-RPP3 GFP-RPP3	AGCTCCATGGGAGTATTCACATTCGTA	ACGTGCTAGCTTAACCAAAGAGATCGAA
pMOG800	p7A-Nt/Ct[YFP]	ACGTAAGCTTCCATGGACTCTCAACGAACT	ACGTGGATCCAAAGTTAAAGTTAA
pMOG800	Nt/Ct[YFP]/p7A	ACGTAAGCTTCCATGGACTCTCAACGAACT	ACGTGGATCCCTAAAAGTTAAAGTTAA
pMOG800	p7-Nt/Ct[YFP] p7-GFP	AGCTCCATGGATATTGAATCGGAAGTA	ACGTGCTAGCAAAGTTGAAGTG
pMOG800	Nt/Ct[YFP]-p7 GFP-p7	AGCTCCATGGATATTGAATCGGAAGTA	ACGTGCTAGCCTAAAAGTTGAAGTG
pMOG800	p8-Nt/Ct[YFP] p8-GFP	ACGTCCATGGATCCTGAACGAATTC	ACGTTCTAGAGAAGTTGAAGTTGATTGAGAC
pMOG800	Nt/Ct[YFP]-p8 GFP-p8	ACGTCCATGGATCCTGAACGAATTC	ACGTTCTAGATTAGAAGTTGAAGTTGATTGAGAC

Yeast two hybrid (Y2H) assays

Y2H assays were performed with GAL4-based MATCHMAKER Two-Hybrid System as described in manufacturer's protocol (Clontech) (Fields and Song 1989a). For library screening, recombinant "bait" vectors, pBD-p7A and pBD-p7 were used to transform yeast strain AH109 by the small-scale TRAFO protocol (Gietz and Woods 2002). Transformant cells were selected by culturing on minimal synthetic medium lacking tryptophan (SD-Trp). As "prey", we used an *A. thaliana* cDNA library in GAL4 activation domain vector pGADT7 (Nemeth, 1998). Plasmids from the library were amplified in *E. coli* and purified by Maxiprep. Yeast cells harboring recombinant "bait" plasmids were transformed with the *A. thaliana* library by the large-scale transformation protocol as described by the manufacturer (Clontech). Positive interactions were selected by culturing on high stringency SD medium lacking leucine, tryptophan, adenine and histidine (SD-Ade-His-Leu-Trp). Assays for extracellular α-galactosidase (MEL1) activity were performed by transferring all growing colonies to SD-Ade-His-Leu-Trp+X-α-Gal plates. Plasmids from blue growing colonies were isolated following a phenol-chloroform protocol. In order to eliminate duplicates pAD/library inserts were amplified by PCR and digested with a frequent-cutter restriction enzyme, BsuRI. PCR fragment sizes were analyzed by 2.5% agarose gel electrophoresis. Unique clones were amplified in *E.coli* and sequenced using the T7 and 3'AD sequencing primers.

Some of identified *A. thaliana* genes were cloned into pGADT7 and transformed into reporter AH109 yeast cells containing pBD-p7A, pBD/p7A^{fnf}, pBD/p7, pBD/p7^{fnf}, pBD-p8 or pBD/p8^{fnf}. Positive interactions were analyzed by culturing co-transformants on SD-Ade-His-Leu-Trp+X-α-Gal and, in some cases, on SD-Ade-His-Leu-Trp+X-α-Gal plus 3AT. To confirm the specificity of the interactions, pGADT7 vectors containing *A. thaliana* genes were also transformed in yeast cells harboring "empty" pGBKT7 or yeast cells containing pBD-p53 (tumor protein p53). For the identification of MNSV p7A domain involved in protein-protein interaction, reporter AH109 yeast cells were first transformed with pBD-p7A, pBD/p7A^{fnf}, pBD/p7A$^{\Delta 1\text{-}22}$, pBD/p7A$^{\Delta 23\text{-}44}$, pBD/p7A$^{\Delta 45\text{-}65}$ or pBD-p7, and spread on SD-Trp plates for selection of transformants. Then, colonies were grown in SD-Trp liquid media, pooled and transformed either with pAD-7A or

pAD-p7. Co-transformant cells were selected using plates with SD-Leu-Trp. Positive interactions were analyzed as before.

Molecular cloning for subcellular localization studies and bimolecular fluorescence complementation (BiFC) assays

For subcellular localization studies, the cDNAs corresponding to MNSV p7A, CarMV p7, TCV p8, 60S acidic ribosomal protein P3 (RPP3A, At4g25890), the subunit G of the eukaryotic translation initiation factor 3 (eIF3g, At3g11400) and the WRKY36 transcription factor (At1g69810) were fused *in frame* to the 5´and, when indicated, also to the 3' end of the green fluorescent protein (GFP). For BiFC assay, an amino-terminal fragment of the yellow fluorescent protein (YFP) (residues 1-155, referred to as Nt-[YFP]) and a carboxyl-terminal YFP fragment (residues 156-238, referred to as Ct-[YFP]) were either fused to the amino or carboxyl terminus of the cDNAs corresponding to MNSV p7A, CarMV p7, TCV p8, RPP3A, eIF3g and WRKY36. All these recombinant constructs were inserted between the 35S promoter of *Cauliflower mosaic virus* and the *Solanum tuberosum* proteinase inhibitor terminator (PoPit) into pMOG800 binary vector (Knoester *et al*., 1998).

Agrobacterium tumefaciens-mediated transient expression and bimolecular fluorescence complementation assays

Transient expression assays on *Nicotiana benthamiana* plants were performed as previously described (Genovés *et al*., 2006). Briefly, the binary constructs of interest were introduced into the *Agrobacterium tumefaciens* strain C58C1 by electroporation (GenePulser XcellTM electroporation system, Bio-Rad). Transformed bacteria were grown overnight in a shaking incubator at 28 °C in Luria-Bertani (LB) medium supplemented with the appropriate antibiotic mixture. Cultures were collected by slow-speed centrifugation and adjusted to the required final OD600 value (0.2) with 10 mM $MgCl_2$, 10 mM MES pH 5.6 and 150 µM acetosyringone. These suspensions were infiltrated into two-week-old *N. benthamiana* plants by gentle pressure infiltration into the lower side of the leaves. For co-localization experiments and bimolecular fluorescence complementation experiments requiring the simultaneous expression of two different proteins, individual bacterial cultures containing the corresponding

binary vectors were adjusted to a final OD600 of 0.2 and mixed before leaf infiltration. Plants were kept in growth chambers in 16h light at 25 °C and 8h dark at 22 °C.

Confocal laser scanning microscopy

Subcellular localization of the fluorescent tagged proteins and BiFC imaging was conducted with an inverted Zeiss LSM 780 confocal microscope (Carl Zeiss, Oberkochen, Germany, http://www.zeiss.com). GFP/YFP and dsRFP fluorescence was visualized by 488 and 561 nm laser excitation, respectively. The corresponding emission detection windows were 492–532 and 590–630, respectively.

RESULTS

A highly conserved amino acid triplet at the very carboxyl terminal end is essential for DGBp1 self-interacting.

In previous reports it was demonstrated that MNSV DGBp1, namely p7A, self-interacts both *in vitro* and *in vivo*, as revealed by electrophoretic analysis and BiFC assays, respectively (Genovés *et al*., 2009). However, the protein domain/motif responsible for this interaction was not mapped. For this purpose, were used here a yeast two hybrid (Y2H) approach and a set of deletion and point mutants of MNSV p7A. Y2H is a genetic system wherein the interaction between two proteins of interest is detected via the reconstitution of a transcription factor (Fields and Song, 1989b). In this method, a protein of interest is expressed as a fusion to a GAL 4 DNA-binding domain (BD), while a second protein is expressed as a fusion to a GAL 4 activation domain (AD). After co-expression in yeast, if both proteins interact, the AD and BD could be close enough to activate the reporter genes, via reconstitution of the transcription factor (Fig. 1) (Auerbach and Stagljar, 2005). The major disadvantage is the appearance of false positives, although new two hybrid assays, such as those used here, have reduced it drastically. Yeast strains as AH109 minimize false positives by using three reporters ADE2, HIS3 and MEL1 (Fig. 1) under the control of distinct GAL4 upstream activating sequences (UASs) and TATA boxes. These promoters produce specific responses to GAL4, avoiding false positives consequence of the direct interaction with flanking sequences of GAL4 binding site and those that interact with transcription factors bound to specific TATA boxes. ADE2 and HIS3 reporters provide

strong nutritional selection, allowing selection stringency control. In contrast, MEL 1 is an endogenous gene which encodes α-galactosidase that is a secreted enzyme, so it can be assayed directly on X-α-Gal indicator plates through a blue/white screening.

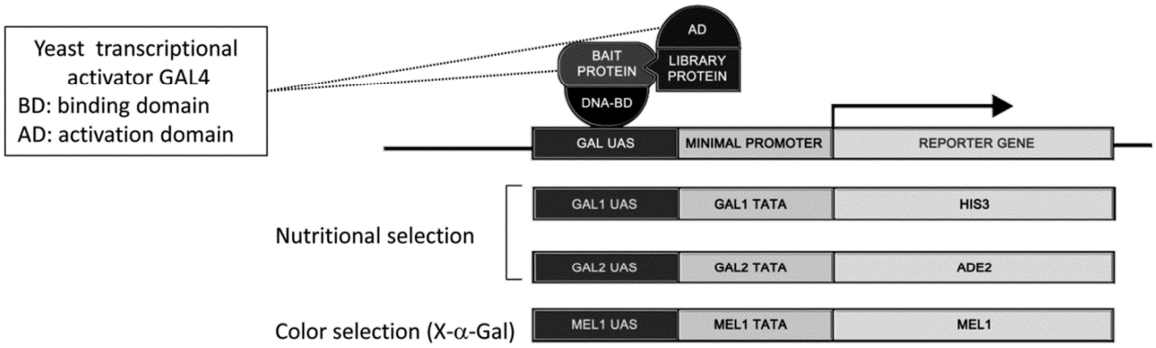

Figure 1. The yeast two-hybrid method and reporter constructs in AH109 strain. The DNA-BD corresponds to amino acids 1–147 of the yeast GAL4 protein, which binds to the GAL UAS upstream of the reporter genes. The AD corresponds to amino acids 768–881 of the GAL4 protein and functions as a transcriptional activator. Strain AH109 includes the ADE2 and HIS3 markers. MEL1 is an endogenous GAL4-responsive gene. The HIS3, ADE2, and MEL1 reporter genes are under the control of three completely heterologous GAL4-responsive UAS and promoter elements GAL1, GAL2, and MEL1, respectively.

First, full length MNSV p7A and CarMV p7 were fused to the activation domain (pAD plasmids) and transformed into yeast cells expressing either p7A or p7 fused to the binding domain (pBD plasmids) as described in Material and Methods. After growing at 28 °C for 5 days on interaction selective medium we found that both MPs not only self-interact but also interact with each other to form p7A-p7 heterodimers (Fig. 2). This is the first time that these interactions have been described suggesting that structural similarities shared by MPs of these genera could respond to common functionality.

In fact, the alignment of the amino acid (aa) sequences of DGBp1s from different genera within *Tombusviridae* family revealed low conservation at the level of primary structure except for a highly conserved group of three aa at the carboxyl terminal end (F63, N64 and F65 positions in MNSV p7A), which is present in almost each aligned protein. In spite of this, the consensus data obtained using seven different computational prediction methods (PHDpsi, PROFsec, SSPro 2.01, Predator, YASPIN,

JNet and PSIPred) available on the SYMPRED prediction server (http://ibivu.cs.vu.nl/programs/sympredwww/) revealed the presence of two highly conserved elements of secondary structure (Fig. 3): a centrally located α-helix domain, which was previously related to RNA binding, and a potential β-sheet folding at the C-terminal end that could be involved in protein-protein interaction.

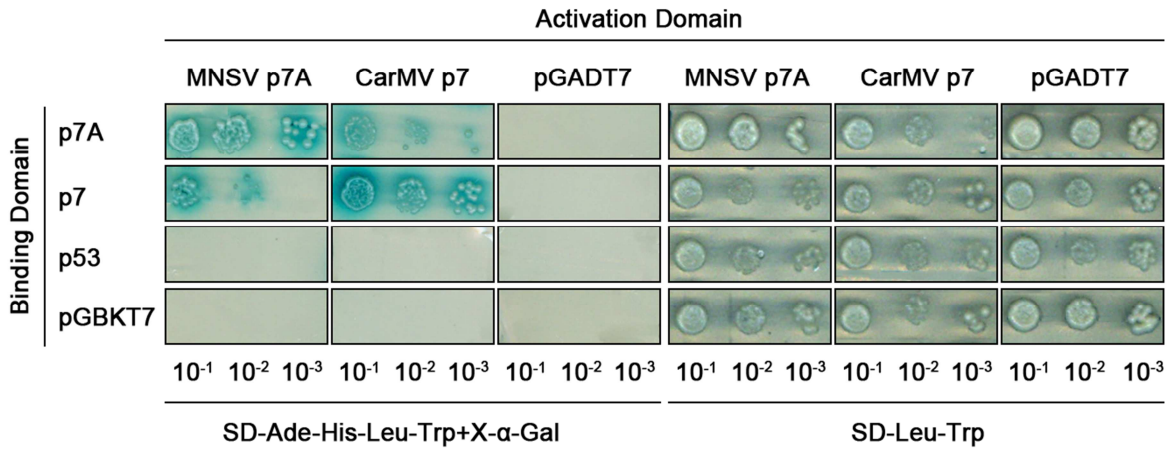

Figure 2. Spot tests for detecting MP-MP interactions by yeast two-hybrid assay. AH109 budding yeast strain carrying the bait plasmid expressing MNSV p7A or CarMV p7 linked to the Gal4 binding domain (BD) was transformed into strains carrying the prey plasmid expressing the Gal4 activation domain (AD) also linked to MNSV p7A or CarMV p7. As a control, the bait and prey strain was transformed into a strain carrying the empty plasmids pGADT7 and pGBKT7 or pBD-p53 as a heterologous protein control. Diploid colonies were applied in three 10x dilution series to rich medium SD-Leu-Trp (right panels) and to selective media SD-Leu-Trp-His-Ade+X-α-Gal (left panels). Growth on selective media indicated MNSV p7A and CarMV p7 self-interaction, and also interaction of MNSV p7A with CarMV p7.

To further delineate the region involved in DGBp1 self-interaction, additional truncated mutants were generated. For this purpose p7A ORF was divided into three sections comprising aa residues 1 to 22 (nucleotides [nt] 1 to 66), aa 23 to 44 (nt 67 to 132) and aa 45 to 65 (nt 132 to 195), and each one deleted in truncated mutants pBD/p7A$^{\Delta 1\text{-}22}$, pBD/p7A$^{\Delta 23\text{-}44}$ and pBD/p7A$^{\Delta 45\text{-}65}$, respectively. Yeast two hybrid assays with wild-type MNSV p7A and CarMV p7 revealed that only the interactions between combinations including mutants pBD/p7A$^{\Delta 45\text{-}65}$, lacking the carboxyl terminal region, were unsuccessful (Fig. 4). However, in some experimental replicates, pAD/p7 and pBD/p7A$^{\Delta 45\text{-}65}$ combination resulted in a reduced colony growing (Fig. 4). Any of the other tested combinations had not effect on the capacity to interact indicating that the region comprised between aa residues 45-65 of MNSV p7A plays an essential role in

MP-MP interaction. Interestingly, this region included the three highly conserved aa residues above mentioned (F63, N64 and F65 in MNSV p7A). To study whether these aa residues were also involved in MP-MP interaction, site-directed mutagenesis was used to produce a new mutant, pBD/p7A^{fnf}, in which the conserved FNF triplet was mutated to alanine. Interestingly, this mutation was enough to block the ability of p7A to self-interact and to interact with p7 (Fig. 4). Therefore, aromatic rings of lateral chains of these conserved residues but not the conserved β-sheet folding at the C-terminal region appear to be required for MP-MP interaction.

Y2H *Arabidopsis thaliana* cDNA library screening with two carmovirus DGBp1s.

To identify possible host factors interacting with MNSV p7A and CarMV p7, we used also the Y2H method to screen an *A. thaliana* cDNA library. As we mentioned above, the library used as pray was expressed as a pool of fusions to GAL4 activation domain vector pGADT7. Recombinant "bait" vectors, pBD-p7A and pBD-p7 were used in two independent library screenings. For this purpose yeast cells either containing pBD-p7A or pBD-p7, were transformed with the *A. thaliana* library as described in Materials and Methods (Fig. 5). The yeast culture was incubated in SD-Ade-His-Leu-Trp where only cells containing interacting proteins can grow. The resulting colonies were transferred to an SD-Ade-His-Leu-Trp+X-α-Gal selective medium and blue colonies were chosen to isolate the library plasmids, which were transferred to *Escherichia coli* DH5α strain for amplification and segregation from bait plasmids. Plasmid duplicities were checked by PCR before sequencing as described in Materials and Methods.

In the case of MNSV p7A screening, 583 colonies were rescued from the library transformation in the first round of selection and plated again on selective media containing X-α-Gal. Those colonies with phenotype Ade$^+$/His$^+$/Mel1$^+$ (colonies showing blue coloring) were then selected (166 colonies) and harboring plasmids isolated. AD/library inserts were analyzed through amplification and restriction of PCR products with a frequent-cutter restriction enzyme. In order to eliminate duplicates, fragment sizes were analyzed in agarose gel electrophoresis. Before digesting, an uncut sample was run to check for colonies which may contain multiple AD/library plasmids. After this analysis 83 plasmids were selected, stored and sequenced. After discarding

repeated or truncated sequences, and those which were not in frame with the AD, we finally identified 22 possible p7A-interacting proteins. Those interactions were tested again in a selective medium. In this case, we include a negative control either containing the empty vector or a non-related protein. From this third round of selection we discard another 5 proteins, those which did not grow or grew in negative controls (data not shown). The 17 final possible p7A-interacting proteins are listed in Table 2.

Table 2. List of putative DGBp1 interacting proteins.

Access number	Name	Function	p7A	p7	Full-length tested
Stress and signaling					
At1g70790	Calcium-dependent lipid-binding (CaLB domain) protein	Abscisic acid-activated signaling pathway	+		+
At1g23140	C2-domain ABA-related 8 protein (CAR8)	Abscisic acid-activated signaling pathway	+	+	
At5g40190	Calmodulin binding protein	Signaling		+	
At1g09070	Soybean gene regulated by cold-2 (SRC2)	Vesicle mediated transport and response to stress	+	+	+
At5g67360	Subtilisin-like serine protease (ARA12)	Development and response to stress	+		
At5g15090	Voltage dependent anion channel 3 (VDAC3)	Development and disease resistance	+	+	
At1g04870	Protein arginine methyltransferase 10 (PRMT10)	Flower developmental regulation	+	+	+
At3g05010	G-protein coupled receptor 2,(CAND2)	Response to molecule of bacterial origin, root morphogenesis	+	+	+
At1g18310	Glycosyl hydrolase family 81 protein	Carbon utilization, cell-wall organization and pathogen defence	+		
Chaperones					
At1g10350	DNA-J heat shock family protein	Protein folding	+	+	+
At5g02500	Heat shock cognate protein 70-1	Response to biotic and abiotic stress	+		
At5g02480	HSP20-like chaperones superfamily protein	Response to heat, high light intensity, and hydrogen peroxide		+	
At5g48030	Gametophitic factor 2 (GFA2); DNAJ family protein	Protein folding		+	+
At3g09440	Heat shock protein 70 (Hsp70)	Response to biotic and abiotic stress		+	+
RNA metabolism					
At5g11170	Dead-box ATP-dependent RNA-helicase 56	RNA metabolism		+	+
At5g62190	Dead-box ATP-dependent RNA helicas (PRH75)	RNA metabolism		+	+
At2g26460	RNA splicing protein (SMU2)	RNA metabolism	+		

At5g11200	ATP-dependent RNA helicase (UAP56B)	RNA metabolism and response to DNA damage	+		
Protein modification					
At4g05320	Polyubiquitin 10	Cellular protein modification process	+		
At2g35330	RING/U-box superfamily protein	Cellular protein modification process		+	
At2g35635	NEDD8-like protein RUB2 (UBQ7)	Cellular protein modification process		+	+
At2g40640	RING/U-box superfamily protein	Protein ubiquitination		+	
At3g48070	RING/U-box superfamily protein	Protein ubiquitination		+	
At5g42220	Ubiquitin-like superfamily protein	Cellular protein modification process		+	
At3g52590	Ubiquitin extension protein (UBQ1)	Cellular protein modification process		+	
Protein translation					
At4g25890*	60S acidic ribosomal protein (RPP3A)	Translational elongation	+	+	+
At3g11400*	G subunit of eukaryotic initiation factor 3 (EIF3g).	Formation of translation preinitiation complex	+	+	+
At3g45030	Ribosomal protein S10p/S20e family protein	Protein translation	+	+	
At1g72370	40S Ribosomal protein SA	Protein translation		+	+
At5g62300	Ribosomal protein S10p/S20e family protein	Protein translation		+	+
Transcription factors					
At3g02550	LOB domain-containing protein 41 (LBD41)	Regulation of transcription	+		+
At1g69810	Transcription factor WRKY36	Regulation of transcription		+	+
Others					
At1g43890	RAB GTPase homologe 18 (ATRAB-18)	Vesicle-targeting specificity		+	
At3g59470	FAR1-related sequences-related factor1 (FRF1)	Response to red or far red light		+	
At5g19090	Heavy metal transport/detoxification protein	Metal ion homeostasis		+	
At5g41600	Reticulon like protein B4 (RTNLB4)	Endoplasmic reticulum tubular network organization		+	
At1g48580	Uncharacterized protein			+	
At1g21740	Uncharacterized protein			+	
At1g20100	Uncharacterized protein			+	
At1g48580	Uncharacterized protein			+	
At1g14630	Uncharacterized protein			+	

We proceeded in the same way with CarMV p7. In this case, we rescued 1124 colonies, which 394 were $Ade^+/His^+/Mel1^+$ in the second round of selection. AD/library inserts were analyzed and after PCR, restriction and gel electrophoresis analysis, 150 library pAD plasmids were sequenced. 50 unique and correct expressed candidates were retested in a third round of selection with negative controls. 15 of them were

discarded because did not grow or grew with both negative controls (data not shown). Finally 33 possible interacting proteins were identified (see Table 2).

On the basis of their probable molecular functions, the interacting proteins were grouped into different groups including stress response and signal transduction, chaperones, RNA metabolism, protein modification and translation, regulation of transcription and others. A last group included proteins of unknown function (Table 2). Interestingly, we found that some of the identified proteins were common in both screenings (Table 2).

Reassessment of interactions using full-length prey proteins

Since genomic libraries contain random fragments of proteins, a screen will find not only full-length interactors, but also interacting subdomains of a given protein. It is possible that a domain is capable of interacting with a bait, but the complete protein is not, for example, since other parts of the protein impede the interaction. Therefore, large-scale library screens probably yield a high number of interactions that do not occur in a physiological context and that must therefore be labeled as false positives. Considering that most of the sequenced pAD inserts corresponded to partial ORFs, we decided to confirm some of possible interactions using full-length proteins. The full-length sequence of each gene was obtained by BLAST searching at The Arabidopsis Information Resource (TAIR) source. In a first round of amplifications we only obtained and cloned in pGADT7 the cDNAs corresponding to 16 putative prey interacting proteins (see Table 2) which were analyzed in this work. The rest of the proteins will remain for future analysis.

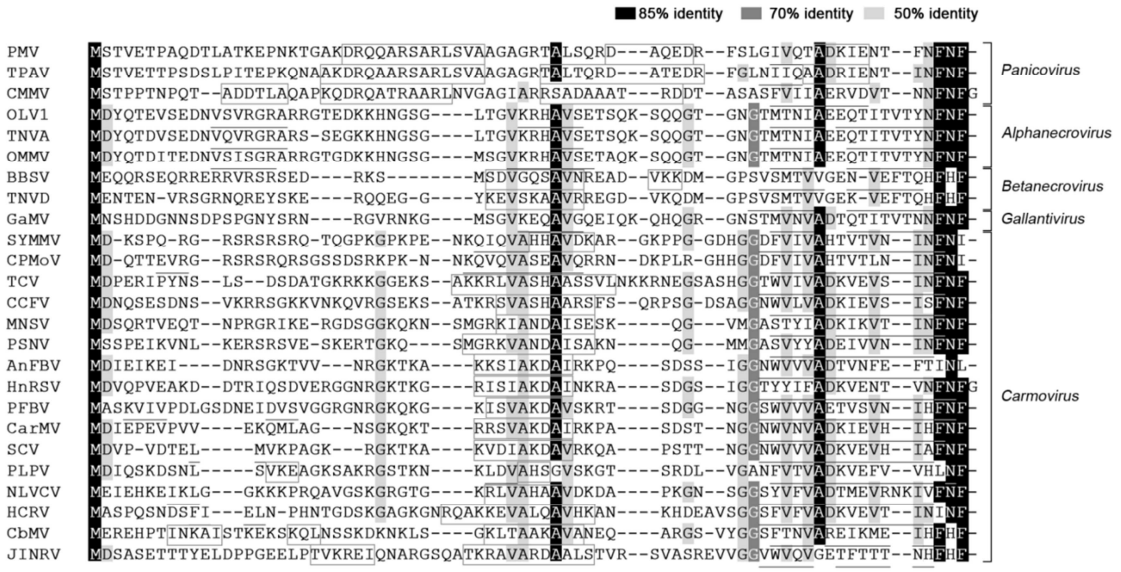

Figure 3. DGBp1 amino acid sequence alignment of members of several genera in *Tombusviride* family. The analysis was conducted using the ClustalW option under the "alignment" tab in MEGA version 6.06 (http://www.megasoftware.net). Identity scores are as indicated by color code. Gaps are represented as contiguous dashes. Amino acid residues predicted to be involved in α-helix are boxed whereas β-sheet structured domains are underlined. Viruses compared are: PMV, *Panicum mosaic virus*; TPAV, *Thin paspalum asymptomatic virus*; CMMV, *Cocksfoot mild mosaic virus*; OLV1, *Olive latent virus 1*; TNVA, *Tobacco necrosis virus A*; OMMV, *Olive mild mosaic virus*; BBSV, *Beet black scorch virus*; TNVD, *Tobacco necrosis virus D*; GaMV, *Galinsoga mosaic virus*; SYMMV, *Soybean yellow mottle mosaic virus*; CPMoV, *Cowpea mottle virus*; TCV, *Turnip crinkle virus*; CCFV, *Cardamine chlorotic fleck virus*; MNSV, *Melon necrotic spot virus*; PSNV, *Pea stem necrosis virus*; AnFBV, *Angelonia flower break virus*; HnRSV, *Honeysuckle ringspot virus*; PFBV, *Pelargonium flower break virus*; CarMV, *Carnation mottle virus*; SCV, *Saguaro cactus virus*; PLPV, *Pelargonium line pattern virus*; NLVCV, *Nootka lupine vein clearing virus*; HCRV, *Hibiscus chlorotic ringspot virus*; CbMV, *Calibrachoa mottle virus* and JINRV, *Japanese iris necrotic ring virus*.

In these Y2H assays, we used as bait both MNSV p7A and CarMV p7 independently of the screening where the interacting prey proteins were identified. We also extend the analysis to the *Turnip crinkle virus* (TCV) p8, since TCV certainly is the most studied member of *Carmovirus* genus. Moreover, TCV but neither MNSV nor CarMV infects *A. thaliana* representing a powerful tool in future analysis. The FNF motif involved in homo and heterodimerization of DGBp1s was mutated to Ala in all three MPs assayed and mutants used also as baits (pBD/p7A^{fnf}, pBD/p7^{fnf}, pBD/p8^{fnf}). In addition to the negative controls pGBDKT7 and pBD-p53, we also used the bLHL transcription factor ILR3 (at5g54680) fused to the AD (pAD-ILR3) and pGADT7. AH109 yeast strain was transformed using a sequential procedure. First, yeast cells previously transformed with bait plasmids (pBD-p7A, pBD-p7, pBD-p8, pBD/p7A^{fnf}, pBD/p7^{fnf}, pBD/p8^{fnf}, pGBDKT7 and pBD-p53) were grown o/n in liquid selection media (SD-Trp) and 1 ml of

each culture was used as yeast background to transform the 16 prey plasmids containing the full-length ORFs. Interactions were tested in SD-Ade-His-Leu-Trp+X-α-Gal but also in SD-His-Leu-Trp+X-α-Gal in order to identify weak interactions and SD-Ade-His-Leu-Trp+X-α-Gal containing 10 mM 3-Amino-1,2,4-triazole (3AT). The 3AT is a competitive inhibitor of the HIS3 protein (His3p). Therefore, the presence of 3AT will select clones with high level of HIS3 which depends on the strength of the interaction between bait and prey (Fields 1993). Finally, SD-Leu-Trp medium was used as growing control.

The results were similar independently of the selective medium used (Fig. 6 only shows those obtained with SD-Ade-His-Leu-Trp+X-α-Gal and SD-Leu-Trp). Only 3 interactions were strongly confirmed, the 60S acidic ribosomal protein P3 (RPP3A, At4g25890), the subunit G of the eukaryotic translation initiation factor 3 (eIF3g, At3g11400) and the WRKY36 transcription factor (At1g69810) (Fig. 6). The rest of preys failed to grow in selective medium or grew in negative controls (some examples are also presented in Fig 6). Interestingly, the three positive interactions were confirmed in all wild-type baits pBD-p7A, pBD-p7 and pBD-p8 but not in mutant baits pBD/p7A^{fnf}, pBD/p7^{fnf}, pBD/p8^{fnf}. These data not only validate the association of the viral MPs with the host protein, but also indicate a common functionality in this interaction that could be shared by all DGBp1s. In addition, the highly conserved FNF motif appears to function as a protein anchor that could be universally extended among these viruses.

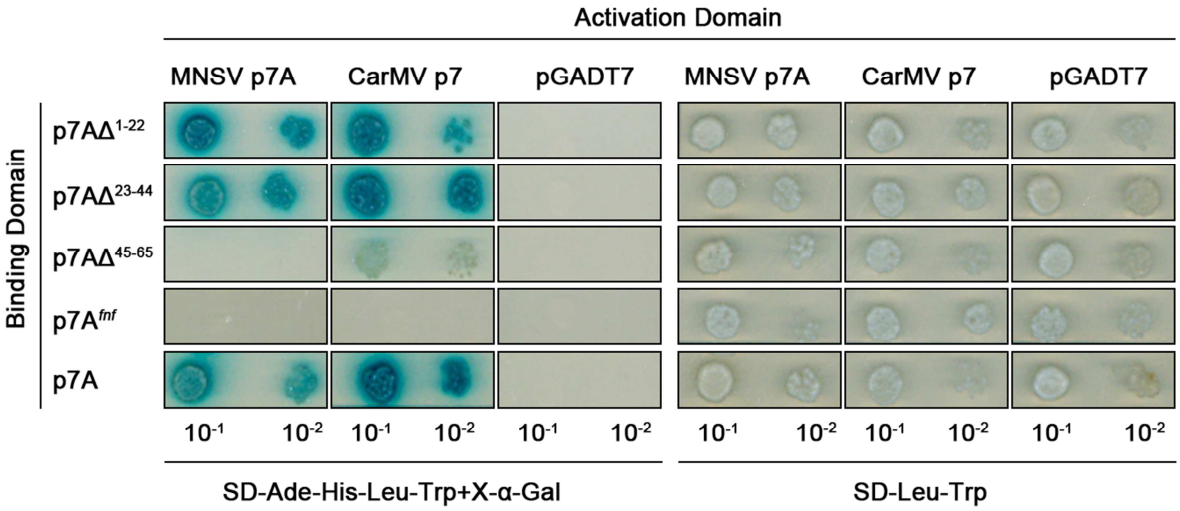

Figure 4. Spot tests for mapping the region of MNSV p7A involved in MP-MP interaction by yeast two-hybrid assay. AH109 budding yeast strain carrying the bait plasmid either expressing MNSV p7A or deletion mutants p7A$^{\Delta 1\text{-}22}$, p7A$^{\Delta 23\text{-}44}$ and p7A$^{\Delta 45\text{-}65}$ lacking either amino acid residues (aa) 1 to 22 (nucleotides [nt] 1 to 66), aa 23 to 44 (nt 67 to 132) and aa 45 to 65 (nt 132 to 195), or mutant pBD/p7A^{fnf} having the three most C-terminal amino acid residues (F63, N64 and F65) mutated to alanine, linked to the Gal4 binding domain (BD) was transformed into strains carrying the prey plasmid expressing the Gal4 activation domain (AD) also linked to MNSV p7A or CarMV p7. As a control, the bait strains were transformed into a strain carrying the empty plasmids pGADT7. Diploid colonies were applied in two 10x dilution series to rich medium SD-Leu-Trp (right panels) and to selective media SD-Leu-Trp-His-Ade+X-α-Gal (left panels). Growth on selective media indicated that MNSV p7A self-interaction was abolished with p7A$^{\Delta 45\text{-}65}$ and p7A^{fnf} but also the interaction of p7A with p7.

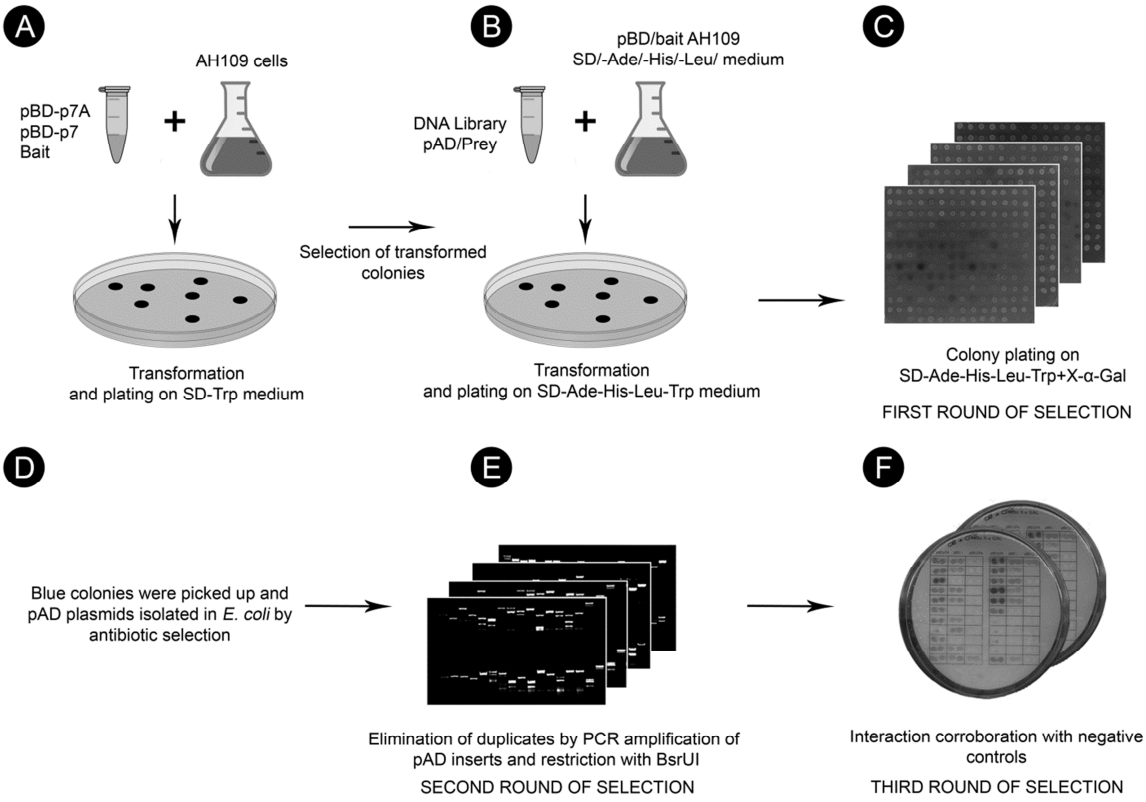

Figure 5. Schematic representation of the *A. thaliana* library transformation and screening protocol used in this work. A) recombinant "bait" vectors, pBD-p7A and pBD-p7 were used to transform yeast strain AH109 by the small-scale TRAFO protocol. Transformant cells were selected by culturing on minimal synthetic medium lacking tryptophan (SD-Trp). B) Plasmids from an *A. thaliana* cDNA library in GAL4 activation domain vector pGADT7 were purified and used as "prey" in large-scale transformation. Positive interactions were selected by culturing on high stringency SD medium lacking leucine, tryptophan, adenine and histidine. C) Assays for extracellular α-galactosidase (MEL1) activity were performed by transferring all growing colonies to SD-Ade-His-Leu-Trp+X-α-Gal plates. D) Plasmids from blue growing colonies were isolated following a phenol-chloroform protocol and pGADT7 library plasmids separated from pGBKT7 bait plasmids by antibiotic selection in *E. coli*. E) Duplicates were eliminated by PCR amplification of pAD/library inserts following a digestion with a frequent-cutter restriction enzyme, BsuRI. PCR fragment sizes were analyzed by 2.5% agarose gel electrophoresis. F) Interactions were reassessed with negative controls.

Subcellular localization studies and evaluation of interactions using bimolecular fluorescence complementation (BiFC) assays

As ultimate confirmation of the three protein-protein interactions above identified, we used bimolecular complementation (BiFC) assay in *Nicotiana benthamiana* as an additional technique. Before that we used green fluorescent protein (GFP) tagging approaches to study the subcellular localization of bait and prey proteins. The p7 and p8 ORFs was fused to the N terminus of the GFP and cloned in plasmids suitable for expressing the recombinant proteins after agroinfiltration in *N.*

benthamiana leaves. In previous works, we showed that p7A-GFP was distributed in cytoplasmic granules associated with actin microfilaments (MFs) but also in punctate structures at the cell periphery (Genovés *et al*., 2009). Similarly, p7-GFP was also located in punctate structures at the cell periphery, but also labelling cytoplasmic filamentous structures or distributed along them as granules of different size (Fig. 7A-C). Co-expression of p7-GFP with either encoding the *Tobacco mosaic virus* (TMV) MP, which also label microtubules (MTs) (Fig. 7D-F) or the mouse talin actin-biding domain (Fig. 7G-I) (Ashby *et al.,* 2006; Boutant *et al.,* 2009) fused to the DsRed fluorescent protein (dsRed-talin) revealed that CarMV MP was associated with MTs. Interestingly, co-expression of p7-GFP with TMV MP-dsRed decreased the green labelling of the filamentous structures indicating that CarMV p7 and TMV MP could compete for the same anchor in MT binding. In contrast to that observed with MNSV p7A and CarMV p7, TCV p8 was localized into the nucleoplasm as was previously described (Cohen *et al.,* 2000), but occasionally forming dense aggregates most likely resulting of excessive protein (Carmo-Fonseca *et al.,* 2010)(Fig. 7J-L).

In the case of the prey proteins, eIF3G, RPP3A and WRKY36 ORFs were also fused to the N or C terminus of the GFP and cloned in plasmids suitable for expressing the recombinant proteins after agroinfiltration in *N. benthamiana* leaves. Subcellular localization was similar independently of the GFP end used to fuse the bait protein (Fig. 8D-F) were distributed in cytoplasmic granules ranging between approximately 0.1 and 1 µm in diameter. As expected, transcription factor WRKY36 was found in the nucleus excluding the nucleolus but also it accumulates to form nuclear bodies or aggregates within the nucleoplasm (Fig 8G-I).

BiFC approach is based on the restoration of the fluorescence when two half-parts of an auto-fluorescent protein reporter, neither of which fluoresces on its own, are brought together by an interaction between proteins fused to each fragment (Aparicio *et al*.,2006). We fused each of the YFP fragments (see Materials and Methods section) to the amino and carboxyl terminus of the bait (p7A, p7 and p8) and prey proteins (eIF3G, RPP3A and WRKY36) to generate Nt [YFP]-Bait/Prey, Ct [YFP]-Bait/Prey, Bait/Prey-Nt[YFP] and Bait/Prey-Ct[YFP] recombinant protein. We screen all putative combinations of fusion proteins for fluorescence complementation: Bait-

Ct[YFP]+Nt[YFP]-Prey, Ct[YFP]-Bait+Nt[YFP]-Prey, Bait-Nt[YFP]+Ct[YFP]-Prey, Nt[YFP]-Bait+Ct[YFP]-Prey, Bait-Ct[YFP]+Prey-Nt[YFP], Ct[YFP]-Bait+Prey-Nt[YFP], Bait-Nt[YFP]+Prey-Ct[YFP] and Nt[YFP]-Bait+ Prey-Ct[YFP]. Four days after the Agrobacterium-mediated co-expression, fluorescent signals were only observed in combinations containing Ct[YFP]-Bait or Nt[YFP]-Bait but not with the other options (data not shown). This situation probably results from the interference of the split YFP fragments on conserved FNF motif in the Bait-Nt[YFP] and Bait-Ct[YFP] recombinant proteins. Interestingly, the fluorescence was distributed among punctate structures at the cell periphery in the case of p7A and p7 but located within the nucleoplasm in the case of p8 (Fig. 9, 10 and 11 shows representative images of Bait-Ct[YFP]+Nt[YFP]-Prey combinations). Therefore, subcellular localization of the interacting partners is more related with that of MPs than that of prey proteins. Moreover, the expression of each recombinant bait and prey protein with the corresponding complementary YFP fragment (either Nt[YFP] or Ct[YFP]) did no produce any detectable fluorescent signal as in the case of Nt[YFP] and Ct[YFP] co-expression (data not shown).

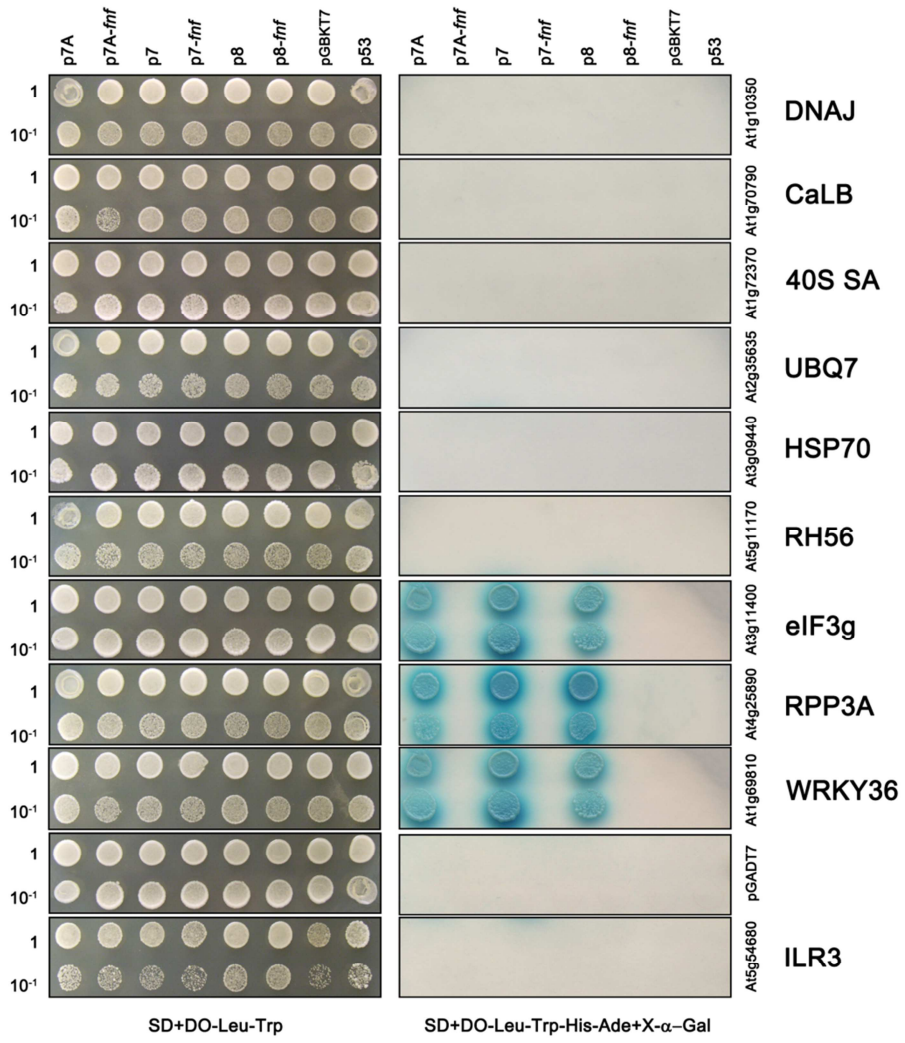

Figure 6. Yeast two hybrid spot test re-evaluation of some MP-host factor interactions using full-length prey proteins. AH109 budding yeast strain carrying the bait plasmid either expressing MNSV p7A, CarMV p7, TCV p8 and the corresponding p7A^{fnf}, p7^{fnf} and p8^{fnf} mutants, linked to the Gal4 binding domain (BD) was transformed into strains carrying the prey plasmid expressing the Gal4 activation domain (AD) linked to the indicated full-length host factors. As a control, the bait strains were transformed into a strain carrying the empty plasmid pGADT7 or pAD-ILR3 expressing a bLHL transcription factor of *A. thaliana* (At5g54680). Diploid colonies were applied in two 10x dilution series to rich medium SD-Leu-Trp (right panels) and to selective media SD-Leu-Trp-His-Ade+X-α-Gal (left panels). Growth on selective media indicated that all three DGBp1s but not the corresponding *fnf* mutants interacted with the 60S acidic ribosomal protein P3 (RPP3A, At4g25890), the subunit G of the eukaryotic translation initiation factor 3 (eIF3g, At3g11400) and the WRKY36 transcription factor (At1g69810). Spot tests of DNA-J heat shock family protein (DNAJ, At1g10350), Calcium-dependent lipid-binding protein (CaLB, At1g70790), 40S Ribosomal protein SA (40S SA, At1g72370) NEDD8-like protein RUB2 (UBQ7, At2g35635), Heat shock protein 70 (Hsp70, At3g09440), Dead-box ATP-dependent RNA-helicase 56 (RH56, At5g11170) are showed as representative examples of negative interactions.

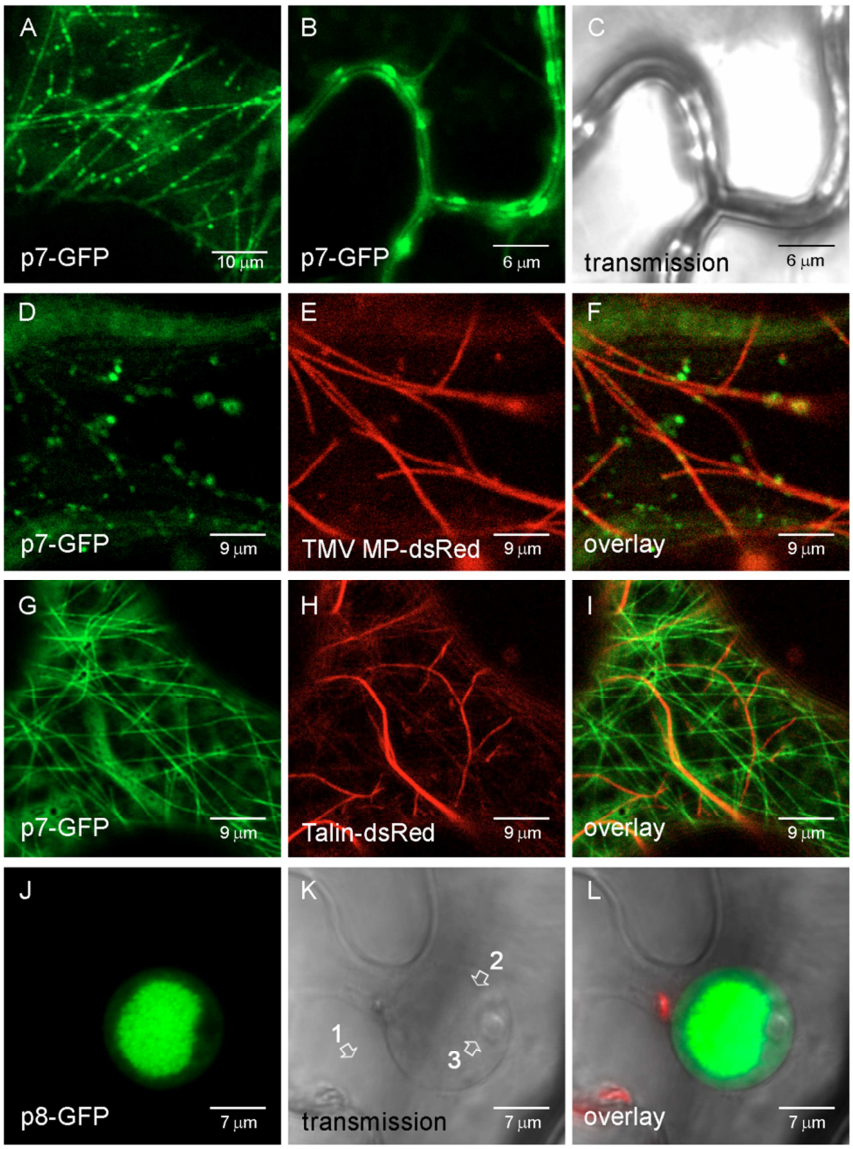

Figure 7. Analysis of the subcellular localization of CarMV p7-GFP and TCV p8-GFP by means of *A. tumefaciens* transient expression in *N. benthamiana* leaves. Confocal laser images were taken approximately 30h after infiltration. A) Fluorescence pattern obtained by p7-GFP expression distributed in filamentous structures and cytoplasmic granules aligned along them. B) Peripheral punctate structures also observed after p7-GFP expression. C) The transmission phase image is presented to clearly show the boundary between two adjacent cells. D-I) Co-expression assays of CarMV p7-GFP with microfilaments (MTs, TMV MP-dsRed) (panels D-F) or microtubules (MFs, Talin-dsRed) (panels G-I) markers. Overlay images of the green fluorescence from p7-GFP (panels D and G) and red fluorescence from TMV MP-dsRed (panel E) and Talin-dsRed (panel H) are displayed in panel F and I, respectively. Co-expression of p7-GFP (panel D) and TMV MP-dsRed (panel E) show a tight association of green cytoplasmic granules with MTs. J-L) TCV p8-GFP subcellular localization in the nucleus but not in nucleolus. The transmission phase image (panel K) is presented to highlight the difference between the cytoplasm (1), nucleus (2) and nucleolus. The overlay image of panels J and K is presented in panel L.

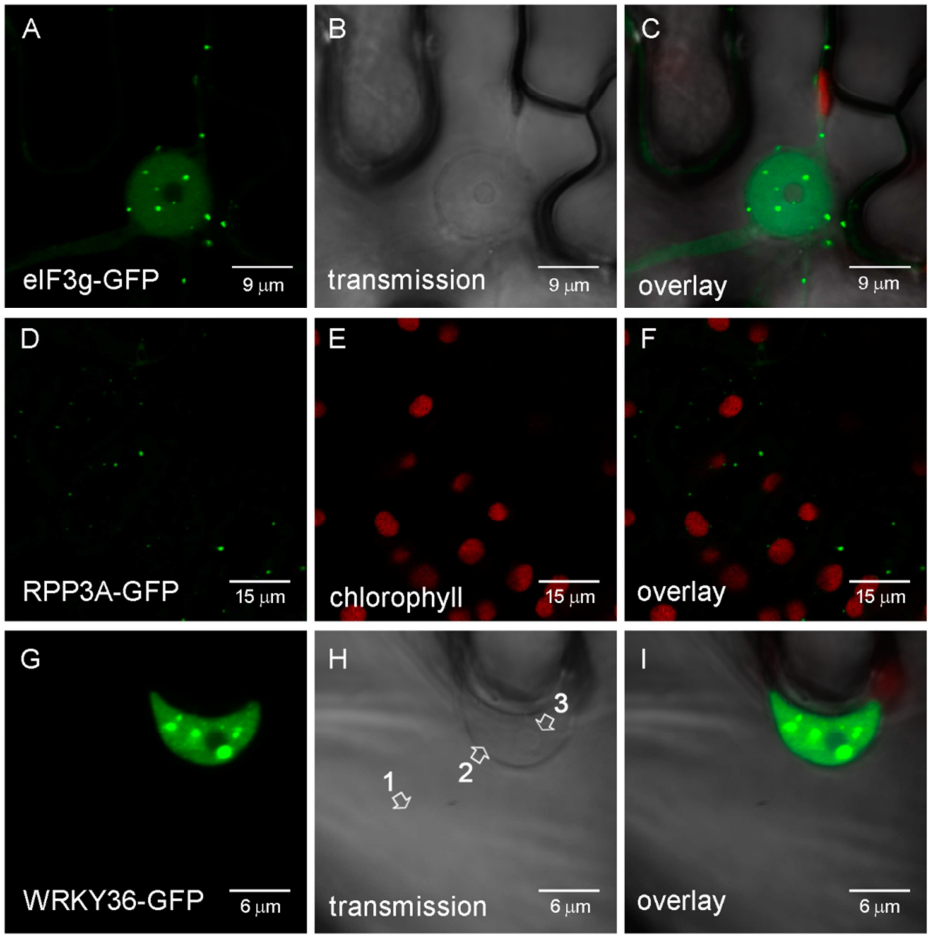

Figure 8. Analysis of the subcellular localization of the 60S acidic ribosomal protein P3 (RPP3A), the subunit G of the eukaryotic translation initiation factor 3 (eIF3g) and the WRKY36 transcription factor fused to the N terminus of the GFP. eIF3G (panel A) and RPP3A (panel D) were distributed in cytoplasmic granules ranging between approximately 0.1 and 1 µm in diameter. A nucleocytoplasm background was occasionally observed in the case of eIF3G. Transmission phase (panel B) and chlorophyll (E) images are displayed to highlight the size of granules compared with the nucleus and chloroplasts (overlays in panel C and F, respectively). G-I) Subcellular localization of the transcription factor WRKY36 into the nucleus showing nuclear bodies or aggregates within the nucleoplasm (Fig 8G-I). The transmission phase image (panel H) is presented to highlight the difference between the cytoplasm (1), nucleus (2) and nucleolus. Overlay image of panels G and H is presented in panel I.

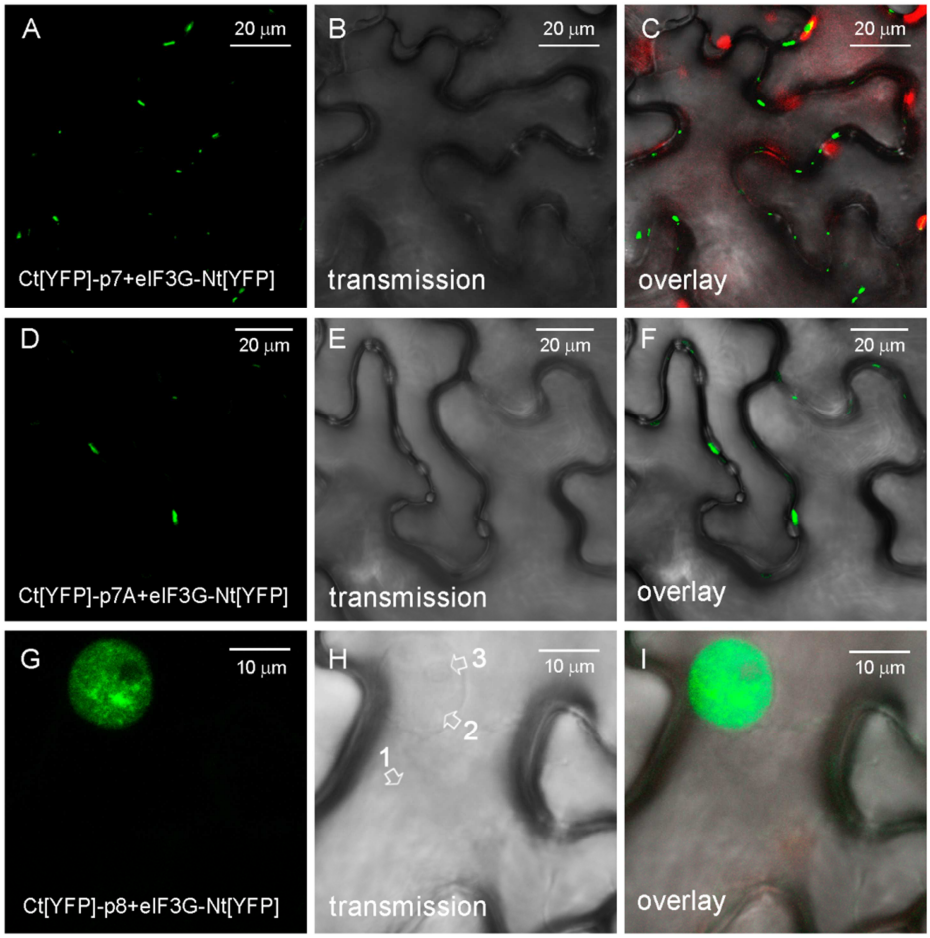

Figure 9. Re-evaluation of MNSV p7A, CarMV p7 and TCV p8 interaction with the subunit G of the eukaryotic translation initiation factor 3 (eIF3g) by bimolecular fluorescence complementation assay in *N. benthamina* leaves. Panels A, D and G show the fluorescence distribution resulting from co-expression of Ct[YFP]-p7, Ct[YFP]-p7A and Ct[YFP]-p8 with eIF3G-N_t[YFP], respectively. Images resulting from the overlay of transmittance mode (panels B, E, H) and green channel are displayed to clearly show the fluorescence resulting from interactions on cell boundaries, in the case of p7 and p7A, (panels C and F) and nucleus in the case of p8 (panel I). For other indications see Fig. 8.

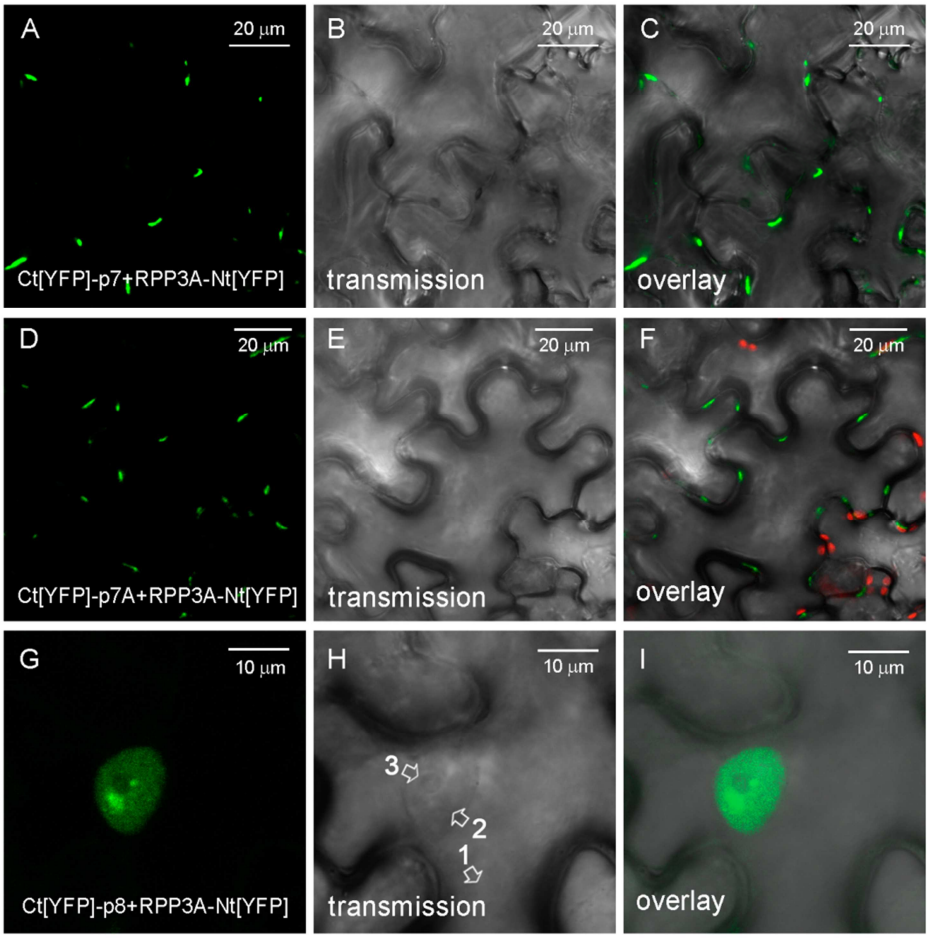

Figure 10. Re-evaluation of MNSV p7A, CarMV p7 and TCV p8 interaction with the the 60S acidic ribosomal protein P3 (RPP3A) by bimolecular fluorescence complementation assay in *N. benthamina* leaves. Panels A, D and G show fluorescence distribution resulting from co-expression of Ct[YFP]-p7, Ct[YFP]-p7A and Ct[YFP]-p8 with RPP3A-N_t[YFP], respectively. Images resulting from the overlay of transmittance mode (panels B, E, H) and green channel are displayed to clearly show the fluorescence resulting from interactions on cell boundaries, in the case of p7 and p7A, (panels C and F) and nucleus in the case of p8 (panel I). For other indications see Fig. 8.

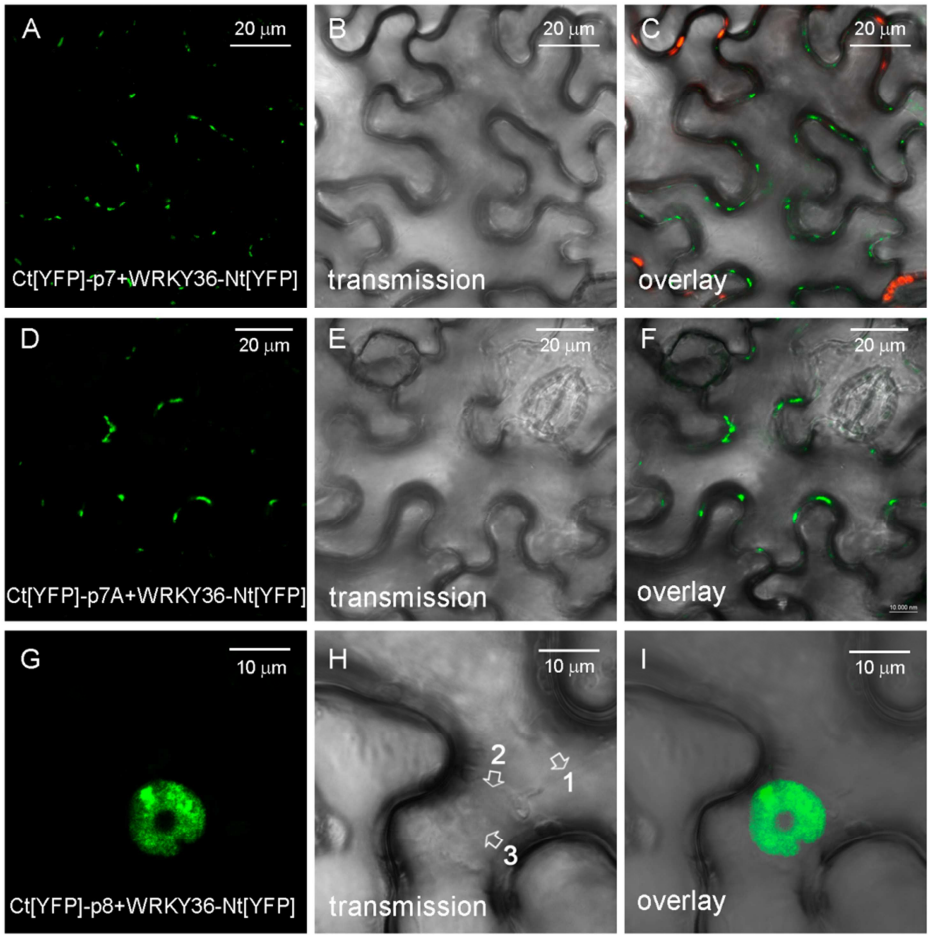

Figure 11. Re-evaluation of MNSV p7A, CarMV p7 and TCV p8 interaction with the WRKY36 transcription factor by bimolecular fluorescence complementation assay in *N. benthamina* leaves. Panels A, D and G show fluorescence distribution resulting from co-expression of Ct[YFP]-p7, Ct[YFP]-p7A and Ct[YFP]-p8 with WRKY36-N_t[YFP], respectively. Images resulting from the overlay of transmittance mode (panels B, E, H) and green channel are displayed to clearly show the fluorescence resulting from interactions on cell boundaries, in the case of p7 and p7A, (panels C and F) and nucleus in the case of p8 (panel I). For other indications see Fig. 8.

DISCUSSION

Knowledge on the molecular basis of viral infection and host defense mechanisms have been recently driven by the high number of plant proteins interacting with viral proteins identified using the Y2H system (Nagy, 2008). Y2H is a very sensitive *in vitro* genetic screening method widely used to study protein-protein interactions. In addition, Y2H is easily scalable, no purification steps are needed and automatization it is also possible. However, the library screening approach is technically laborious and there are some limitations to consider. Potential false negatives arise from the fact that some proteins cannot reliably be expressed in yeast. On the other hand, library

screens often yield small protein fragments that interact nonspecifically with many unrelated baits, so-called false positives. For this reason, large-scale library screens probably yield a high number of interactions that do not occur in a physiological context. To circumvent some of these challenging difficulties, we used two closely related homologous viral movement proteins, MNSV p7A and CarMV p7, to screen the same *A. thaliana* cDNA library and, in further reassessment, we also included a third homologous DGBp1, namely TCV p8. This approach most likely allows the results to be confidently generalized to the rest of related MPs.

Using Y2H and BiFC, as an additional technique, we confirm the interactions of three carmovirus MPs (p7, p7A and p8) with three different host factors: the 60S acidic ribosomal protein P3 (RPP3A, At4g25890), the subunit G of the eukaryotic translation initiation factor 3 (eIF3g, At3g11400) and the WRKY36 transcription factor (At1g69810). eIF3g and RPP3A were common interacting preys rescued in MNSV p7A and CarMV p7 screenings, while the transcription factor WRKY36 initially only interacts with CarMV p7. None of these host proteins appear to be primarily related to viral movement. However, it has been described that many viral proteins are multifunctional and, in this sense, emerging MP roles in different steps of viral cycle have been described; for example, in the manipulation of host susceptibility and suppression of gene silencing (Amari *et al.,* 2012; Morozov and Solovyev, 2012).

To complete its cycle of life, viruses utilize host ribosomes to translate viral mRNAs subverting host protein synthesis functions. Therefore, it is not surprising that viral proteins take control of cellular translation factors, ribosomes and host signaling pathways that control translation (Walsh and Mohr, 2011). Large ribosomal subunits have a lateral protrusion, which is referred to as ribosomal stalk (Gonzalo and Reboud, 2003), composed of acidic proteins P0, P1, and P2 (Wool *et al.,* 1991) and the plant-specific protein P3 (here designed as RPP3) (Bailey-Serres *et al.,* 1997; Szick *et al.,* 1998). P-protein complex is thought to assist in the elongation phase of protein translation (Szick *et al*., 1998) and, in maize seedling, alterations of the ribosomal P-protein complex may be involved in the selective translation of mRNA in flooded roots (Bailey-Serres *et al*., 1997). P proteins can be also present in non-ribosome-related pools (Sánchez-Madrid *et al.,* 1981, Tsurugi and Ogata, 1985, Zinker and Warner,

1976). In this sense, P0 was recently reported to act as an extraribosomal protein that regulates viral RNA functions in *Potato virus* A (PVA) infection by promoting viral translation along with eIF(iso)4E and the viral protein VPg (Hafren *et al.,* 2013). Since DGBp1s are also viral RNA interacting proteins, we can hypothesize that its association with RPP3 could favors specific translation of viral RNAs.

Also involved in the translation initiation machinery and DNA degradation during apoptosis, the eIF3g is a component of the eukaryotic translation initiation factor 3 (eIF-3) complex. The multiprotein eIF3 complex, in concert with eIFs 1, 1A, and 5, promotes recruitment of the eIF2–GTP–Met-tRNAi^{Met} ternary complex to the small ribosomal subunit (40S), generating the 43S preinitiation complex. The eIF4F complex, containing the cap-binding eIF4E and the scaffold protein eIF4G, then mediates recruitment of an mRNA to the 43S with the help of eIF3 and the poly(A)-binding protein (Hinnebusch and Lorsch, 2012, Jackson *et al.,* 2010). On the other hand, apoptosis-inducing factor (AIF) inhibits protein synthesis by interacting with eIF3g during apoptosis (Kim *et al.,* 2006). eIF3g is also cleaved by caspases 3 and 7 and the cleaved eIF3g N-terminus, which is translocated to the nucleus, shows a strong DNase activity (Kim *et al.,* 2013). eIF3g seems to be also required for resumption of scanning of posttermination ribosomes, and together with eIF3i stimulates canonical linear scanning. These processes are critical for translation of a subset of mRNAs encoding tightly regulated genes containing secondary structures at 5', such as those involved in cell cycle regulation, signal transduction, etc. (Cuchalova *et al.,* 2010). From these data, eIF3G can be regarded as an effective target to control host protein translation. Therefore, the interaction of DGBp1s with eIF3g could potentially sequester eIF3g, preventing it from participating in translation of specific messengers and suppressing, for example, plant host defenses, hypersensitive responses (HR), etc.. A situation like that has been already described in infections with the *Measles virus* (MV), a non-segmented, negative-sense RNA virus. In mammalian MV-infected cells, the virus-encoded nucleocapsid protein (N) shuts off host translation through protein-protein interactions with eIF3g, while selective translation of viral mRNA still occurs (Sato *et al.,* 2007).

The *Cauliflower mosaic virus* (CaMV) transactivator (TAV) interacts with both the eIF3g and the 60S ribosomal protein L24 to promote translation reinitiation of viral polycistronic mRNAs (Park *et al.,* 2001). L24 is located at the internal surface of the 60S ribosomal subunit and in the main factor-binding site and its deletion cause deficiencies in the 60S subunit joining step during the initiation of translation. Thus, it was speculated that TAV functions in the recruitment of the 60S ribosomal subunit for the reinitiation event (Thiébeauld, 2007). However, the CaMV genomic expression strategy largely differs from that of carmoviruses. CaMV is a dsDNA virus that transcribes their genome into two RNA species, the polycistronic 35S and the monocistronic 19S. TAV is produced from the monocistronic 19S RNA and is absolutely required for the expression of the rest of the viral proteins from polycistronic 35S RNA, in a process involving ribosomal shunt and TAV controlled reinitation of the translation (Ryabova *et al.,* 2006). In contrast, carmoviruses produce two coding 3'-co-terminal subgenomic messengers (sgRNAs). sgRNA2 is required to express the coat protein and sgRNA1 for expressing both MPs most likely utilizing a leaky scanning mechanism. The components of the replication complex must still be translated from the genomic RNA. (Mandahar, 2006). Therefore, DGBp1s interaction with eiF3g and RPP3·could be related to a viral strategy to control translation of both MPs from bicistronic sgRNA1. Alternatively, it is possible that DGBp1s could act as a transcriptional regulator by interacting with translational elements in order to modify the balance between translation and viral movement depending on which is required at that moment.

The third host protein interacting with DGBp1s identified in this work was the WRKY36 transcription factor. WRKY36 is one of the 74 members of a family of *A. thaliana* proteins containing DNA-binding domains with the conserved amino-acid sequence WRKYGQK (WRKY). WRKY proteins are involved in various physiological plant processes, including seed development, senescence, dormancy and germination, response to biotic and abiotic environmental stresses (Pandey and Somssich, 2009; Rushton *et al.,* 2010). However, far less information is available about the functions of WRKY proteins in antiviral defense than about their functions in defense against bacterial or fungal pathogens. In spite of this, some examples of the implication of these factors in virus infection have been described. After *Tobacco mosaic virus* (TMV)

infection of tobacco or chili pepper, NtWRKY1 and CaWRKYa/d, respectively, were involved in the induction of cell death derived from the HR by regulation downstream gene expression (Huh *et al.,* 2012; Huh *et al.,* 2015; Menke *et al.,* 2005). WRKY8 was involved in the defense response against crucifer-infecting TMV mediating the crosstalk between ABA and ethylene signaling (Xu *et al.,* 2013). In addition, plant viruses can also utilize WRKY factors in their own benefit. *Potato virus* X (PVX) may recruit the NtWRKY1 transcription factor, which binds to the 5' NTR of viral genomic RNA, to maintain the correct balance of viral accumulation during viral infection (Park and Kim, 2012). Interestingly, WRKY proteins are regulated by physical interaction with a wide range of proteins with roles in signaling, transcription, and chromatin remodeling (Chi *et al.,* 2013). In a possible scenario, DGBp1s interaction with WRKY36 could impede, in some extent, the transcriptional reprogramming induced by plant defense against viruses generating an appropriate environment for pathogen survival.

Alternatively, it is possible that DGBp1s bind to WRKY36 to facilitate its own traffic through the PD. Proteins that traffic cell-to-cell are generally named non-cell-autonomous proteins (NCAPs). Most of them are mobile transcription factors that plant cells utilize to transmit intercellular signals (Han *et al.,* 2014). NCAPs also include RNA-binding proteins and MPs such as carmovirus DGBp1s. However, the PD gating capability of DGBp1s has not been reported. Hence, DGBp1s Interaction with a putative mobile transcription factor that brings PD-gating competence could contribute to the subsequent intercellular trafficking of MPs or associated viral complexes.

The application of alanine scanning mutagenesis has demonstrated that only a small subset of residues at a protein-protein interface is essential for binding. Among them, aromatic residues are some of the most typical (Moreira *et al.,* 2013). In fact, conservation of Trp and to a lesser extent, Phe and Met on the protein surface indicates a highly likely protein-protein binding site (Ma *et al.,* 2003). Aromatic residues are usually involved in noncovalent interactions between planar aromatic rings, referred to as π-π interactions or π-stacking, that play an essential role in many fields of chemistry and biochemistry, particularly in global conformational stability, molecular recognition and self-assembly (Gazit, 2002; McGaughey *et al.,* 1998; Meyer

et al., 2003; Profit *et al.,* 2013). Our data demonstrate the importance of the highly conserved FNF motif in self-interaction, interaction with homologous MPs and with host proteins. It is possible that FNF motif act as a common anchor to interact with different host proteins but, alternatively, self-association could produce DGBp1 conformational changes required to interact with host proteins.

The fact that the three DGBp1s analyzed here, which belong to the most widely studied carmoviruses, including CarMV the model virus of the genus, TCV and MNSV, associate with the same host factors suggests a functional strategy that must be conserved among them. Although several possibilities have been discussed here, each interaction identified needs to be confirmed in the context of virus-infected cells before any definitive conclusion can be drawn on relevance for the virus life cycle. Thus, it remains for future studies to experimentally determine the specific function that each interaction plays during the viral infection.

CAPÍTULO TERCERO

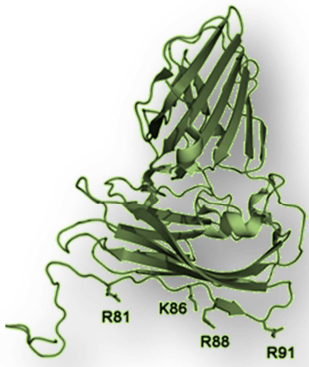

Dissecting the multifunctional role of the N-terminal disordered domain of a plant virus coat protein in RNA packaging, viral movement and interference with antiviral plant defense.

INTRODUCTION

The high misincorporation frequency of viral RNA dependent RNA polymerases and viral deficiency of repair mechanisms are traits that make viral RNA genomes to exhibit extremely high spontaneous mutation rates (10^{-4}/base/replication cycle) (Drake and Holland, 1999). This situation can be seen as an advantage as it allows viruses for fast adaptation to changes; however it also implies a potential risk. Virus populations are extremely vulnerable to a slight increase in deleterious mutations since RNA genomes replicate at or very close to the so-called error threshold. Beyond this limit, viral genomes could incorporate such number of mutations that they do not undergo a further round of replication (Elena and Sanjuan, 2005). To decrease lethality, RNA viruses have evolved to reduce their coding capacity and minimize genome size with overlapping reading frames (Belshaw *et al.,* 2007). Even with the limitations imposed by this genetic "economy", plant viruses, which code for only 4-7 proteins on average, are still capable pathogens. This successful outcome comes from the fact that almost every viral protein has co-evolved with their host to assume a wide array of structural and functional tasks during viral infection.

The molecular hallmark of multifunctionality has been related with the presence of ordered domains combined with some others having a disordered conformation, which can be shaped to bind different ligands (Dunker *et al.,* 2008; Hsu *et al.,* 2013). The viral coat proteins (CP), the main components of nucleocapsid shells, are not exceptions because they have co-existing both types of domains. Indeed, it has been shown that CPs have roles in practically every step of viral biology, including genome replication, interference with plant antiviral defense, local and systemic movement and vector transmission (Callaway *et al.,* 2001; Ni and Cheng Kao 2013; Weber and Bujarski 2015).

Virions of *Melon necrotic spot virus* (MNSV), a member of the genus *Carmovirus* in the *Tombusviridae* family, are comprised of small spherical protein shells (30-nm-

diameter) that encapsidate positive sense, monopartite, single-stranded RNA genomes of approximately 4.3 kb (Hibi and Furuki 1985). Although MNSV genome has the typical arrangement of five ORFs found in carmoviruses (Genovés *et al.,* 2006; Riviere and Rochon, 1990), it shows a particular feature that makes it unique among them. Multiple sequence alignment demonstrated that MNSV possess a coat protein (CP) more similar to that of members of *Tombusvirus* genus than that of *Carmovirus* genus (Riviere *et al.,* 1989). More recently, three-dimensional structure of MNSV has been determined at 2.8 Å resolution, revealing that similarities with tombusvirus CP can be extended from primary to higher levels of protein structure (Wada *et al.,* 2008).

Quaternary organization of MNSV capsids follows a T=3 icosahedral symmetry with 180 copies of three conformational quasi-equivalent CP subunits (A, B and C). Regardless of which type of subunit is considered, the tertiary structure of MNSV CP is composed of three major domains (Fig. 1). Two of them, the middle S domain that builds a robust protein shell around the genome and the C-terminal P domain that projects outward from the capsid as dimers between adjacent subunits (30 C-C and 60 A-B dyads), have been found to adopt an ordered conformation in all tombusvirus, carmovirus and dianthovirus analyzed (Doan *et al.,* 2003; Harrison *et al.,* 1978; Hogle *et al.,* 1986; Katpally *et al.,* 2007; Ke *et al.,* 2004; Morgunova *et al.,* 1994; Sherman *et al.,* 2006). The third domain of the MNSV CP or R-domain consisted of an N-terminal flexible arm of 94 residues (from Met1 to Gly94) that, in A- and B-type subunits, hangs down inside of the viral particle in a disordered way. Its basic nature along with its inner position makes evident that R domain must play an important role in genome binding during encapsidation (Rao, 2006). Otherwise, residues between Asn60 and Gly94 form an ordered arm In C-type subunits which extends from the inner face of the S-domain to icosahedral threefold axes (Fig. 1). Three of such extended arms, each one projected from different C-C dyads, can be connected by hydrogen bonding around threefold axes to form a circular structure called β-annulus, a common element that has been observed in many T=3 icosahedral viruses (Doan *et al*., 2003; Harrison *et al*., 1978; Hogle *et al*., 1986; Katpally *et al*., 2007; Ke *et al*., 2004; Wada *et al*., 2008). Unlike what was initially thought, β-annulus was reported to be a consequence rather than an elicitor of capsid assembly that, in any case, provided additional stability to the

viral particles (Hui and Rochon, 2006; Pappachan *et al.,* 2008; Satheshkumar *et al.,* 2005). Obviously MNSV CP plays also multiple non-structural roles during the virus life cycle. It enhances viral local spread most likely by interfering with post-transcriptional RNA silencing mechanisms (Genovés *et al*., 2006) and mediates virion attachment to the surface of *Olpidium bornovanus* zoospores to be transmitted externally (Mochizuki *et al.,* 2008; Ohki *et al.,* 2010). The P domain was proved to be involved in compatibility with the fungal vector, but no other studies that relate the various structural CP domains to other possible functions such as virion assembly and suppression of RNA silencing have been reported until now. R domain of MNSV CP contains up to 16 basic residues and therefore, is the most plausible candidate to be involved in the interaction with RNA during encapsidation. In addition, sequestration of small RNAs has been proposed as a general strategy employed by viral suppressors of RNA silencing (VSR) to inhibit antiviral plant defense (Incarbone and Dunoyer, 2013).

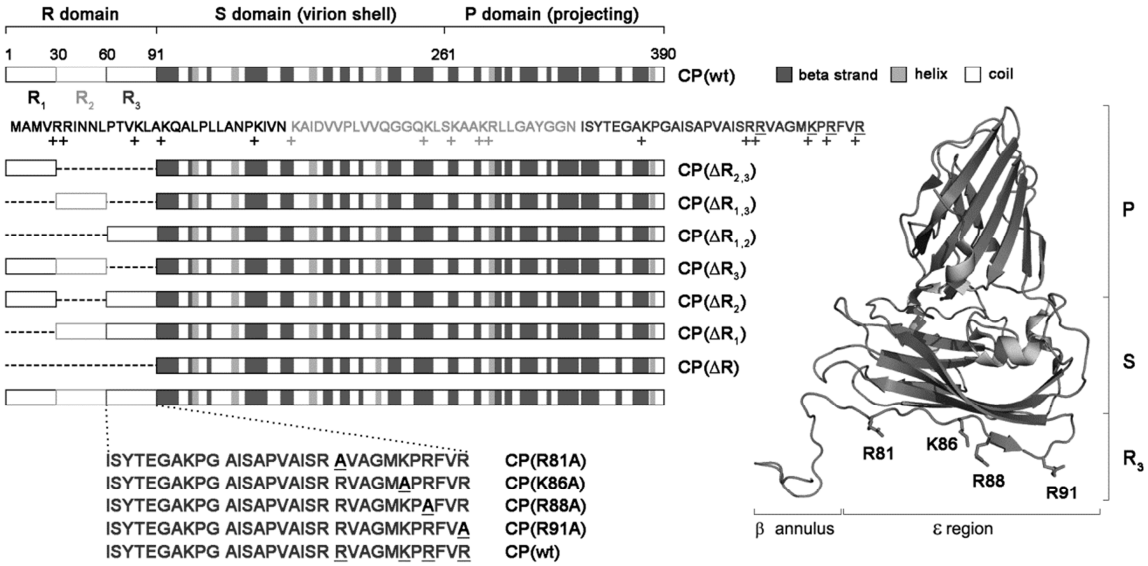

Fig. 1. Linear order of the structural domains of MNSV CP (R, S and P) and location of R1 (black lined boxes), R2 (grey lined boxed) and R3 (dark grey lined boxes) subdomains in which MNSV CP R domain was divided in this study is shown at the top. The color code for secondary structure elements is as indicated. Amino acid sequence corresponds to the first 91 amino acids of disordered R domain. Positively charged residues Lysine/Arginine are highlighted with the symbol "+", and sequences corresponding to each R subdomain are colored according to the code assigned above. A schematic representation of MNSV CP R domain mutants used in this study is shown below. Dashes correspond to deleted amino acids and, at the bottom, letters underlined within R3 subdomain sequence correspond to positions changed in Ala substitution mutations. On the right, a ribbon drawing of C subunit of MNSV CP is displayed. In C type subunit, R3 subdomain was comprised of a β annular structure and a downstream sequence termed "ε" region in other icosahedral viruses. Spatial distribution of side chains of basic residues mutated within R3 subdomain is shown. Secondary structure elements of ordered S and P domains are indicated by twisted (α-helix) and arrowed (β-strand) ribbons.

Taking into account this background, the present study was designed to explore the role of the R domain of MNSV CP in RNA binding and how this capability can modulate different steps of the viral biology. The affinity for long and small RNAs of wild-type CP and that of a series of deletion and point mutations within the R domain was determined *in vitro* by estimating kinetic parameters. The resulting mutants were also examined for their competence in viral RNA package, local spread, systemic movement and interference with antiviral RNA silencing. Our results demonstrated that RNA binding mediated by the R domain plays a pivotal role in virion assembly, viral counter defense and viral movement through the plant. These findings reinforce the common assumption that disordered arms are highly essential for multifunctionality of viral CPs, and in determining the survival of icosahedral plant viruses.

MATERIALS AND METHODS

Plasmid construction for protein expression and protein purification procedure

For protein production in bacteria, pG-CPwt was obtained through the insertion of the MNSV CP sequence into pGEX-KG (GE Healthcare Life Sciences). Viral gene was PCR-amplified from previously constructed pMNSV(Al) (DQ339157) (Genovés *et al*., 2006) and fused *in frame* after the glutathione S-transferase (GST) gene. pG-CP(wt) was used as PCR template to obtain all CP mutants except for construct encompassing CP($\Delta R_{1,3}$) which was obtained from pG-CP(ΔR_1) (see Fig. 1 for a detailed representation of the mutants used in this study). For making deletions an inverse PCR strategy was employed using divergent phosphorylated primers located in opposite sides of the region to be removed. Next, the resulting amplified products were self-ligated. Point-mutations were introduced by site-directed mutagenesis using the QuickChange XLSite-Direct Mutagenesis Kit following manufacturer's instructions (Agilent Technologies). Primer pair sequences are shown in Table S1.

All plasmids were introduced into *E. coli* BL21(DE3)pLysS cells by electroporation and grown under chloramphenicol and ampicillin selection in Luria-Bertani (LB) medium at 37 °C. After 3 h under *shaking incubation* conditions, protein expression was induced at 18 °C for 14-16 h by isopropyl thio-β-galactoside (IPTG) addition to a

final concentration of 1 mM. Cells were harvested, washed twice and resuspended in 0.05 original volume of 1X PBS (140 mM NaCl, 2.7 mM KCl, 10 mM Na_2HPO_4, 1.8 mM KH_2PO_4, pH 7.3). Cell lysis was induced by repeated freezing and thawing (around 3-5 cycles) and proteins purified under non-denaturing conditions by affinity chromatography with glutathione-Sepharose 4B as indicated by the manufacturer's batch/column protocol (GE Healthcare Life Sciences). Protein concentration was determined with the Bio-Rad protein assay reagent using a series of bovine serum albumin (BSA) standards of known concentration.

Nucleic acid binding assay

Protein-RNA binding studies were performed by means of electrophoretic mobility shift assay (EMSA) as previously described (Herranz and Pallas, 2004). A digoxigenin-labelled RNA, which included the nucleotide sequence comprised between the positions 2443 and 2828 of MNSV(Al), was synthesized by *in vitro* transcription. A constant amount of this RNA (5 ng) was heat denatured for 5 min at 85 °C, cooled to room temperature and incubated for 30 min on ice with increasing amounts of each recombinant protein in a 30 µl transcription. A constant amount of this RNA (5 ng) was heat denatured for 5 mir, pH 8.0). Samples were electrophoresed on a 1% agarose gel in 1X TAE (40 mM Tris-acetate, 1 mM EDTA, pH 8.0), capillary-transferred to positively-charged nylon membranes (Roche Diagnostic GmbH) in the presence of 10X SSC (1,5M NaCl, 0,15M sodium citrate) and cross-linked (700 x 100 µJ/cm2). Viral RNA detection was conducted using CSPD chemiluminescent substrate (Roche Diagnostic GmbH) as previously described (Pallás *et al*., 1998). Bands were visualized using the Luminescent Image Analyzer LAS-3000 (Fujifilm) and densitometry was performed using Fujifilm Multigauge 3.0 software.

The apparent dissociation constant (K_a) for protein-RNA binding, which correspond to the concentration of the protein at which half of RNA amount is bound, was calculated on the basis of densitometry data and using a Hill transformation as described in (Marcos *et al.,* 1999a). EMSA for each recombinant protein was repeated between three and five times to ensure reproducibility and accurate linear regression of Hill transformation (R-squared values higher than 0.9).

In some experiments, digoxigenin-labelled single- and double-stranded small RNAs (21, 22 and 24 nt long) were used in binding assays. Single-stranded small RNAs were obtained by *in vitro* transcription using T7 RNA polymerase. To do this, DNA oligonucleotides consisting of the reverse-complement of both the sequence of interest at the 5' and the T7 RNA polymerase promoter at the 3' were used as templates for transcription after making them double-stranded by PCR (Table S1). The antisense sRNAs were obtained using DNA oligonucleotides including the sequence of interest followed by the reverse-complement of the T7 RNA polymerase promoter (Table S1). Double-stranded small RNA molecules were formed by annealing equimolar mixtures of complementary single-stranded RNAs in 20 µl of hybridization buffer (80% deionized formamide, 100 mM sodium citrate, 300 mM sodium acetate and 1 mM EDTA, pH 6.4). The mix was heat denatured at 95°C for 5 min, and hybridization was performed over a period of 2 h at 42°C. Non-hybridized RNAs were removed by PAGE separation and further purification. Binding assay and densitometry were conducted as described above with the exception that samples were subjected to 5% PAGE in TAE 1X buffer and wet-transferred onto nylon membranes.

Plasmid construction for encapsidation assays and experimental procedure

The capacity of CP mutants to form nucleoprotein shells was examined by purifying virions from *Cucumis melo* L. subsp. melo cv. Galia cotyledons agroinfiltrated with MNSV infectious clones. To make binary vectors harboring either CP(wt) or each CP mutant, the full-length genome of MNSV was amplified from pMNSV(Al) (Genovés *et al*., 2006) and cloned between the *Cauliflower mosaic virus* (CaMV) 35S promoter and the potato proteinase inhibitor II terminator (PoPit) into a modified pBSIIKS(+) (Agilent Technologies). The resulting p35-MNSV(Al) plasmid was the basis to introduce all CP deletions and R81A point-mutation as was done before for pGEX (see primer pairs in Table S1). Next, each expression cassette was amplified using M13 forward and reverse primers and cloned into pMOG800 binary vector (Knoester *et al.,* 1998).

All MNSV binary constructs were introduced into the *Agrobacterium tumefaciens* strain C58C1 by electroporation and the transformed bacteria were grown overnight. Cultures were collected by slow-speed centrifugation and adjusted to a final OD_{600} of 1

with 10 mM $MgCl_2$, 10 mM MES pH 5.6 and 150 µM acetosyringone. Bacterial suspensions were infiltrated into one-week-old melon plants by gentle pressure infiltration in the abaxial side of the cotyledons. For this and the rest of assays performed in this study, plants were kept in a growth chamber at 22 °C during a 8 h dark period and 25 °C during a 16 h light period, *e*xcept when otherwise indicated. Two weeks later, virions were purified as described (Diez *et al.,* 1998) with slight modifications. Briefly, thirty melon cotyledons (approximate 10 g) agroinfiltrated with each construct were collected and homogenized in liquid nitrogen. A small quantity of the resulting powder (100 mg) was used for total RNA extraction with TRIzol Reagent. The rest of the homogenate was poured into a tube containing 20 ml of 0.2 M sodium acetate, pH 5.0, mixed by shaking and centrifuged at 7,700×g. After supernatant filtering, virions were pelleted by centrifugation at 146,000×g for 2 h through a 20% sucrose cushion and resuspended in 50 µl of 10 mM Tris-HCl, pH 7.3. 10-fold serial dilutions of all virions stocks were dotted onto PVDF membranes (GE Healthcare Life Sciences) which were subsequently used to determine the relative amounts of virions by dot-blot immunodetection. For this purpose, membrane manufacture's immunodetection protocol was followed using a rabbit polyclonal antibody against the MNSV (Loewe Biochemica GmbH). For virions analysis, samples were eletrophoresed through 1% agarose gel in TAE1X and blotted overnight onto positively-charged nylon membranes as described before. For total RNA extracts, 2 µg of each sample were electrophoresed in denaturing 1.2% agarose gel (3% formaldehyde, 40 mM MOPS, 10 mM sodium acetate and 1mM EDTA, pH 7.0). Viral RNA detection was performed by overnight hybridization as previously described (Pallás *et al*., 1998) using a 500 nt length digoxigenin labelled-riboprobe complementary to the 3' end region of the MNSV CP gene. The complete assay was repeated three times.

Plasmid construction for cell-to-cell movement assays and experimental procedure

To measure the cell-to-cell movement extent, the previously constructed p35-MNSV(Al)/GFP vector was used (Serra-Soriano *et al.,* 2014). MNSV(Al)/GFP RNA express both GFP and CP from a bicistronic gene (GFP-CP) which product is processed during translation by means of the self-cleaving 2A peptide of *Thosea asigna virus* (TaV) (GSGEGRGSLLTCGDVEENPGP) (Kim *et al.,* 2011) (Fig. 4A). A cloning strategy

relying on the use of BveII type IIs endonuclease was used to introduce all CP deletion mutants and R81A point-mutation. The 3' end of the CP sequence between 2816 and 3566 genome position from p35-MNSV(Al)/GFP was deleted by inverse PCR using oligonucleotides that contain both BveII recognition site (Table S1 in bold) and a restriction site designed to avoid the introduction of non-viral sequences (Table S1 in italic). The resulting PCR product was used as cloning vector to introduce the amino terminal regions of each CP mutant that were amplified from the set of pGEX clones obtained before. Expression cassettes from all constructs were amplified using M13 forward and reverse primers and cloned into pMOG800 binary vector.

Cell-to-cell movement was monitored as previously described by examining the formation of fluorescent foci (Serra-Soriano *et al*., 2014). The binary constructs were agroinfiltrated (OD_{600} of 0.2) into fully expanded leaves from 2-week-old melon plants. In preliminary experiments and using the wild type construct, OD_{600} was tuned to reduce the number of infection foci preventing the fluorescence induction in the whole leaf. Three independent experiments were performed in which ten leaves from five plants per construct were used each time. Images of fluorescent infection foci were taken at 6 and 12 days post-infiltration using a Leica MZ12 fluorescent stereomicroscope (Leica microsystems). Infected areas were measured using FIJI free software (http://fiji.sc/Fiji) and data were analyzed using MS Excel (Microsoft). Separation of fluorescent areas resulting from fusion of several infection foci was done either manually or using the FIJI watershed option. GraphPad Prism 6 software and Student's t-test (p value<0.05) was used to determine the statistical significance of results. For a detailed description of the protocol see also (Navarro *et al.,* 2014).

Plasmid construction for systemic movement assays and experimental procedure

The effect of CP mutations on MNSV systemic movement was evaluated by using *N. benthamiana*. For this purpose, pMNSV(Al) construct was modified by replacing its 3'-UTR from that of the isolate MNSV-264 that possesses an avirulence determinant in this region allowing the infection of non-cucurbit species (Diaz *et al.,* 2004). The resulting plasmid, referred here as pMNSV(Al/264), was the basis to introduce all CP mutant deletions and R81A point mutation. The procedure and primers (Table S1)

were the same used before to obtain p35-MNSV(Al) mutants. *N. benthamiana* seedlings were inoculated with *in vitro* T7 RNA polymerase transcripts (9 plants per pMNSV(Al/264) mutant). Total RNA extracted from inoculated and upper non-inoculated leaves that were collected one and two weeks later, respectively, was analyzed by Northern blot as described before. Three independent experiments were performed in the same conditions.

Plasmid construction for systemic RNA silencing suppression assays and experimental procedure

To study the effect of MNSV CP and R domain mutants in systemic RNA silencing suppression, an agroinfiltration assay using GFP transgenic *N. benthamiana* plants (line 16c) was performed as previously described (Hamilton *et al.,* 2002). MNSV CP(wt), deletion mutants and CP(R81A) mutant were cloned between the CaMV 35S promoter and PoPit in pMOG800, introduced into C58C1 cells and grown overnight at 28°C in LB with rifampin and kanamycin. pMOG(GFP) expressing eGFP was used to trigger the silencing of the GFP transgene of 16c *N. benthamina* plants. In coinfiltration experiments, equal volumes (OD_{600} of 0.5) of an *A. tumefaciens* culture containing pMOG(GFP) was mixed immediately before infiltration with each individual *A. tumefaciens* culture bearing either MNSV CP(wt), deletion mutants or CP(R81A) mutant. Control plants were infiltrated with a mixture consisting of equal volumes of *A. tumefaciens* cultures carrying pMOG(GFP) or empty pMOG800. Five independent experiments were performed, including in each one the infiltration on three plants per construct. Growing conditions included a repetitive two-step cycle of 10 h of darkness at 18°C and 14 h of light at 20°C. Depending on the experiment, 20-30 days after, when silencing of GFP was completely achieved in control plants (pMOG(GFP)/pMOG800), photographs were taken under long-wavelength UV light (UVGL-58 Handheld UV lamp; UV Products) by using a tripod and a Nikon D3000 digital camera at F11 aperture value and 1/10s shutter speed (Yaegashi *et al.,* 2012).

Plasmid construction for pathogenicity of *Potato virus X* derivatives in *N. benthamiana* assays and assay procedure

PVX-derivatives containing the CP(wt), deletion mutants and R81A point-mutation were constructed cloning the corresponding ORFs downstream of the duplicated PVX coat protein promoter in pGR107 (Jones *et al.,* 1999). After electroporation, each of the construct was propagated in *A. tumefaciens* strain C58C1 containing the helper plasmid pSoup, grown to OD_{600} of 0.5, and infiltrated into *N. benthamiana* plants. Three weeks later, the plants were photographed and non-infiltrated leaves collected for total RNA extraction and Northern blot analysis. Viral RNA detection was performed by overnight hybridization with a 500 nt length digoxigenin labelled-riboprobe complementary to the 3' end region of the PVX CP gene. The experiment was repeated three times.

RESULTS

Mutations in the R domain affect *in vitro* RNA-binding properties of MNSV CP

Here, we follow the terminology of Wada and colleagues (Wada et al., 2008) which defined the R domain of MNSV CP as the region comprised between positions 1 and 94. Thus, it also includes the so-called arm region that in C-type subunits is made by the β-annulus structure and downstream residues hereafter termed ε region (Fig. 1) (Hui and Rochon, 2006; Reade et al., 2010). Multiple sequence alignment of the N-terminal region (around 94 residues) of MNSV CP with that of all sequenced tombusvirus was performed (Fig. S2). The comparison showed that only the last 30 residues, which approximately matched to the arm region, were highly conserved. However, the number of basic residues that contribute to the positively charged environment of the R domain was similar in all sequences and oscillated between 14 and 17. It was also evident that most of them were particularly clustered upstream from the arm region and inside the ε region.

Electrophoretic mobility shift assays (EMSA) were first conducted to estimate the ability of the MNSV CP (CP(wt)) to bind RNA in solution. CP(wt) was cloned into pGEX-KG plasmid for expression as *in frame* fusion to the C-terminus of the glutathione S-transferase (GST) gene. To avoid denaturing conditions during protein purification and

to increase protein solubility we were forced to use the GST-CP fusion in RNA binding assays. A constant amount of a viral RNA transcript was incubated with increasing quantities of CP(wt). First panel in Fig. 2 shows a representative shift gel where the disappearance of the free RNA band was evident from 10 ng upwards, indicating the formation of a protein-RNA complex. The resulting complex barely entered the matrix gel and, consequently, it was hardly transferred onto a nylon membrane through the bottom of gel wells. To perform consistent binding kinetic analysis, RNA-protein complex formation was measured as the disappearance of the band corresponding to unbound RNA (Carey, 1991; Marcos *et al*., 1999a). Preliminary shift gels with five different sense RNA transcripts covering MNSV full-genome indicated that GST-CP(wt) did not preferentially recognize a particular nucleotide sequence (data not shown). Therefore, for binding kinetics analysis, we used, in this and further experiments, a transcript of 500 nt comprising both viral movement protein genes.

A Hill transformation was applied to data to plot the log [(1-x)/x] versus the log[CP(wt)], where x is [RNA]unbound/[RNA]total. The apparent dissociation constant (K_a, defined as the concentration of protein at half-saturtion) was calculated from the linear regression of the mean values from at least three independent experiments (Fig. S1) (Herranz and Pallás, 2004; Marcos *et al*., 1999a; Navarro, *et al*., 2006). K_a of CP(wt) was estimated to be 0.92 nM which is in the same order of magnitude of those calculated for some viral CPs (Aparicio *et al.,* 2003; Jansen *et al.,* 1998) but considerably lower than others (Baer *et al.,* 1994; Skuzeski and Morris, 1995).

Deletion of the amino acids at positions 1 to 91 in CP(ΔR) mutant resulted in RNA interaction losing even at a high protein concentration (Fig. 2) corroborating the role of R domain in RNA binding. To further identify the regions of R domain involved in such interaction, we defined three different R subdomains, each comprised of 30 residues with 5-6 positive charges (R1, R2 and R3) (Fig 1). Next, we engineered a series of mutations in which one or two of these subdomains were deleted (Fig 1).

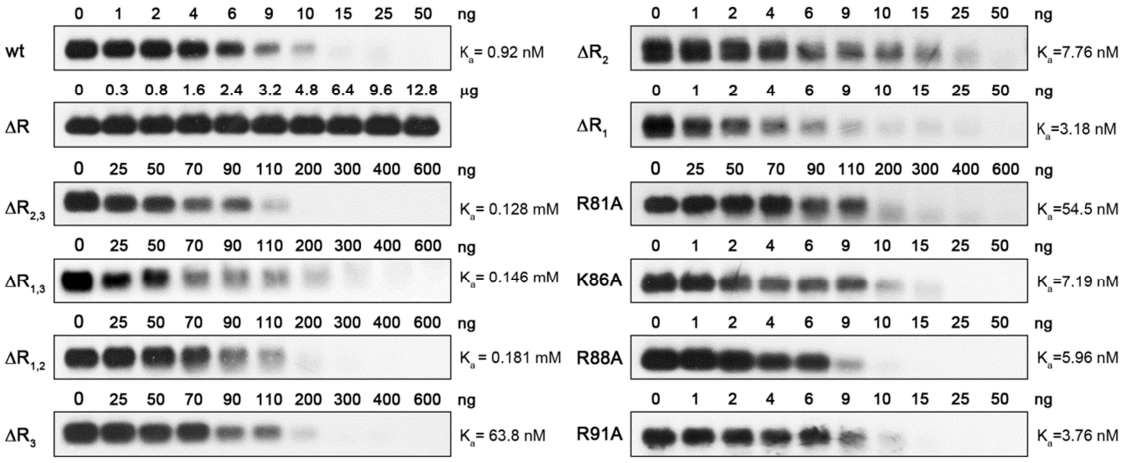

Fig. 2. Analysis of RNA binding activity of MNSV CP and R domain mutants by EMSA. Increasing amounts of either GST-CP or each GST recombinant R domain mutant were mixed with a constant amount (5 ng) of a digoxigenin labelled viral transcript of 500 nt. Unbound RNA and RNA-protein complexes were separated in non-denaturing 1% agarose gels and transferred to nylon membranes. After chemiluminescent detection of viral RNAs, bands corresponding to unbound RNA were quantified and the apparent dissociation constant calculated using a Hill transformation of data (Ka, concentration of the protein required to give 50% saturation). Complexes were hardly transferred to membranes since they barely enter the gel; therefore, only disappearance of unbound RNA from representative EMSAs is shown.

None of these last deletions rendered MNSV CP incompetent for RNA binding, although affinity was always weakened (Fig. 2 and S1). As expected, the highest detrimental effect was observed in CP($\Delta R_{2,3}$), CP($\Delta R_{1,3}$) and CP($\Delta R_{1,2}$) mutants, all of them having two subdomains deletion. Regardless of which subdomain was preserved, Kas were comparable and estimated to be between 139 and 196 times higher than that of CP(wt) (0.128, 0.146 and 0.181 mM for CP($\Delta R_{2,3}$), CP($\Delta R_{1,3}$) and CP($\Delta R_{1,2}$), respectively). For mutants having only one subdomain deletion, K_a of CP(ΔR_1) was 3.18 nM, only 3.5 times higher than that of CP(wt) while it slightly increased in CP(ΔR_2) (K_a 7.76 nM, 8.4 times higher). In contrast, deletion of R_3 subdomain had a much drastic effect increasing the K_a of CP(ΔR_3) (K_a 63.8 nM) up to 70 times that of CP(wt). From these data, it is apparent that R_3 subdomain plays the most important role in RNA binding albeit in the presence of upstream residues either from R_1 or R_2 subdomains.

A second set of constructs was intended to establish the specific contribution in RNA binding of specific basic residues of ε region within R_3 subdomain. Mutations to Ala were introduced in four of the most protein surface-exposed positively charged positions of ε region. All of them had deleterious effects on RNA binding, but the

magnitude varied significantly. CP(R91A), which affects a low conserved Arg, leads to a slightly 4-fold reduction in RNA affinity (K_a 3.76 nM). Interestingly, single substitution of MNSV-specific Arg81 (CP(R81A)) had a more severe impact on RNA binding (K_a 54.5 nM) than mutations in fully conserved Lys86 (CP(K86A) and Arg88 (CP(R88A) (K_a 7.19 nM and 5.96 nM, respectively). Actually, K_a of CP(R81A) was in the same order of magnitude to K_a of CP(ΔR_3) that lacks the full-length R_3 subdomain (60 and 70-fold increase with respect to CP(wt), respectively) indicating that Arg81 has a wide participation in RNA binding within ε region.

The conserved region of the R domain of MNSV CP is necessary but not sufficient for package of full-length viral genome during infection

To know whether results obtained in *in vitro* RNA binding assays can be generalized to *in vivo* packaging of viral RNAs, the ORFs of MNSV CP(wt), R subdomains deletion mutants, CP(ΔR) and CP(R81A) (Fig. 1) were subcloned into a MNSV infectious binary vector (Fig 3A). We used an agroinfiltration approach to differentiate the effect of mutations on RNA package into virions from those due to cell-to-cell movement deficiencies. Cotyledons of melon were chosen to be agroinfiltrated as virion accumulation in this tissue was higher than in leaves (Fig. S3) (Serra-Soriano *et al.,* 2015). Assembled particles were also separated from free CPs through a 20% sucrose cushion.

All mutants were found to produce viral or viral-like particles (VLP) dense enough to reach the bottom of a 20 % sucrose cushion as revealed by dot-blot immunodetection using an antibody against MNSV virions (Fig. 3B). CP titer of purified particles was measured by serial dilution and, in the majority of mutants, signal intensities were reduced in more than 100-fold that of wild-type, indicating that any modification of the R domain greatly decreased particle assembly efficiency. Next, viral RNA packaging competency was determined by Northern blot analysis using a CP riboprobe. Equal amounts of viral particles, which were estimated by dot-blot immunodetection, were subjected to agarose gel electrophoresis in native conditions to preserve virion structure throughout the run. Only mutants harboring CP($\Delta R_{1,2}$), CP(ΔR_2), CP(ΔR_1) or CP(R81A) mutations were able to encapsidate viral RNAs. However, all four yielded hybridization signal intensities lower than that obtained in wild-type

infection, suggesting that RNA package into virions was significantly reduced (Fig. 3C). Interestingly, all these mutants still maintain the R_3 subdomain that was previously shown, in this work, to play an essential role in *in vitro* RNA binding. Although CP(R81A) mutation had less effect on viral RNA package into virions than expected, these findings are in high correlation with *in vitro* results.

It is feasible that reduced encapsidation levels or absence of hybridization signals is due to a deficiency in viral RNAs accumulation during plant infection. To assess this possibility, a small quantity (100 mg) of the ground infected cotyledons used before to purify viral particles was reserved to perform total RNA extractions. After electrophoresis in agarose gel, Northern blot analysis showed that all mutants accumulate both genomic (gRNA) and subgenomic (sgRNA) viral RNAs at levels comparable or higher than that of wild type (Fig. 3D). This observation demonstrates that the results obtained before are not primary due to diminished viral RNA accumulation in infected tissue.

Northern blot analysis of RNAs extracted from particles produced by CP($\Delta R_{1,2}$), CP(ΔR_2), CP(ΔR_1), CP(R81A) and CP(wt) only showed detectable levels of full-length genomic RNA in the case of CP(R81A) and CP(wt) (Fig. 3E). Three viral RNA species smaller than MNSV genome were also observed in these mutants. The two lower molecular weight species likely correspond to both MNSV sgRNAs (1.9 and 1.6 kb). The biggest RNA (approximately 2 kb) may represent a defective interfering RNA (DI RNA) that was occasionally observed in Northern blot analysis of total RNA from infected tissue (e.g. see Fig 3D) or could it simply be the result of gRNA degradation.

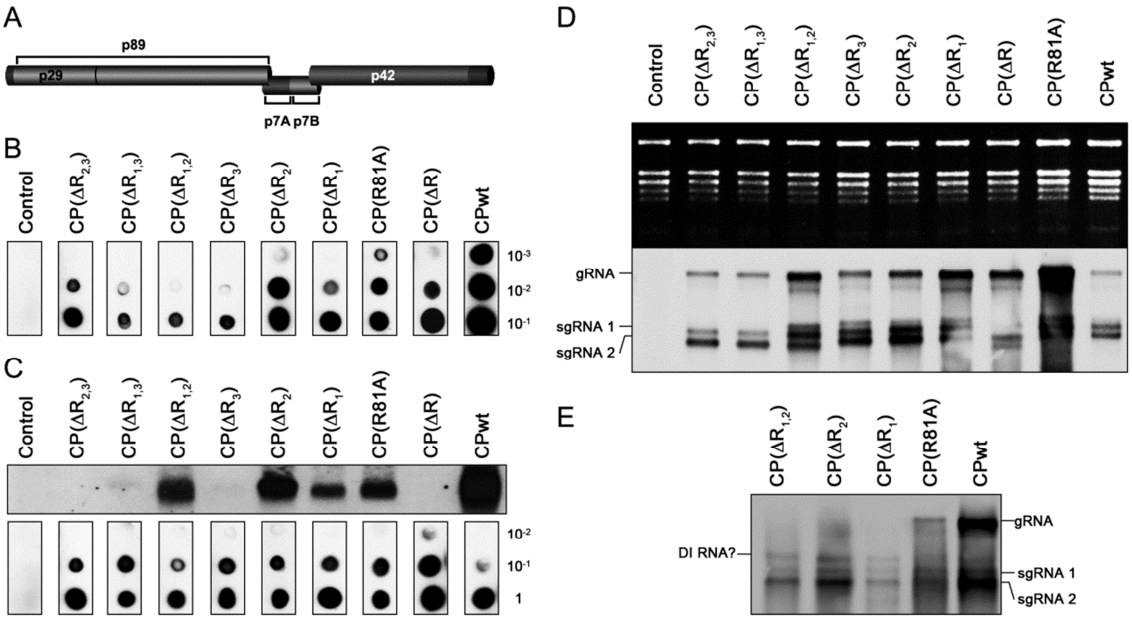

Fig. 3. Effects of MNSV CP R domain mutations on viral RNA encapsidation. (A) Schematic diagram of the MNSV genome organization. The 5' proximal ORF has the potential to encode an auxiliary protein of 29 kDa (p29) ending in an amber codon. Read-through during translation would result in the synthesis of an RNA dependent RNA polymerase of 89 kDa(p89). Two small centrally located ORFs encode two movement-related proteins of 7 kDa (p7A and p7B), while the fifth ORF codes for the coat protein. (B) Dot-blot immunodetection of viral particles produced by the indicated MNSV CP R domain mutants. Virions were purified through a 20% sucrose cushion from melon cotyledon extracts and serial dilutions applied to a PVDF membrane. Detection was performed using a rabbit polyclonal antibody against MNSV virions. (C) Northern blot analysis of MNSV RNAs associated to virions produced by MNSV CP R domain mutants. After native agarose gel electrophoresis, viral particles were transferred to nylon membrane and hybridized to a digoxigenin-labelled MNSV-specific riboprobe. Loaded samples were adjusted to have approximately equal amounts of virions as revealed by the Dot-blot immunodetection analysis included below. (D) Denaturing agarose gel electrophoresis of total RNA isolated from cotyledon extracts infected with the indicated mutants. After membrane blotting, Northern blot analysis was performed as above. Position of MNSV genomic and both subgenomic RNAs is indicated. E) Northern blot analysis of RNAs isolated from purified virions produced by CP(ΔR1,2), CP(ΔR2), CP(ΔR1), CP(R81A) and CP(wt). Position of a putative defective interfering RNA (DI RNA) or gRNA degradation product is indicated.

The R domain of MNSV CP modulates cell-to-cell movement independently of its role in encapsidation

We previously demonstrated that RNA encapsidation was not a prerequisite for MNSV cell-to-cell movement since local spread was decreased but not inhibited when the CP gene was replaced by GFP (Genovés *et al*., 2006). We also showed that transport efficiency was recovered when either MNSV CP or a heterologous viral suppressors of RNA silencing (VSRs) was provided *in trans* suggesting a role for MNSV CP in eluding host defense (Genovés *et al*., 2006). However, virion contribution to MNSV cell-to-cell movement cannot be entirely excluded since encapsidation capability of non-genome-translated CPs was not evaluated. From the results obtained

here, viruses harboring R domain mutants appear to not encapsidate full-length genome. Therefore, to compare the ability of these mutants to move from cell to cell with that of wild type under equal conditions, each CP variant was introduced into a MNSV binary vector that take advantage of the TaV 2A catalytic peptide to express both GFP and CP genes under the same viral promoter (Fig. 4A). This recombinant MNSV resulted to be not competent for packaging most likely due to its larger genome size, a situation that has been reported for the related carmovirus *Turnip crinkle virus* (TCV) (Qu and Morris, 1997; Serra-Soriano *et al*., 2014).

Cell-to-cell movement was monitored at 6 and 12 days post-infiltration (dpi) by measuring the area of fluorescent infection foci in six fully expanded melon leaves per mutant (Navarro *et al*., 2014; Serra-Soriano *et al*., 2014). Each bar diagram in Fig. 4B represents the average of foci size means from three independent experiments (approximately 600 foci per mutant). At 6 dpi, the wild-type virus induced fluorescent foci of 0.230±0.006 mm^2 on average size; in contrast, movement was significantly (*p* value <0.0001) reduced in almost all mutants which formed infection foci with mean sizes ranging from 0,091±0,015 to 0.146±0.017 mm^2. Only mutant harboring CP(ΔR_1) produced foci significantly (p<0.0001) higher than those of wild-type (0.333±0.035 mm^2). At 12 dpi the situation was similar, wild-type and CP(ΔR_1) mutant infections progressed to reach infection foci sizes 5-fold higher than before (1.24±0.02 and 1.75±0.19 mm^2, respectively). The rest of mutants showed infection foci smaller than those of wild-type (Fig. 4B and 4C). Statistical analysis indicated that the mean area of the infection foci formed by these mutants were significantly different from that of the wild-type (p≤0.0008) except for CP(R81A) mutant (p=0.53) (1.24±0.02 vs 1.13±0.03 mm^2). Similarly to RNA binding results obtained before, single deletion mutants harboring R_3 subdomain and CP(R81A) mutant had also the smallest deleterious effect on cell-to-cell movement.

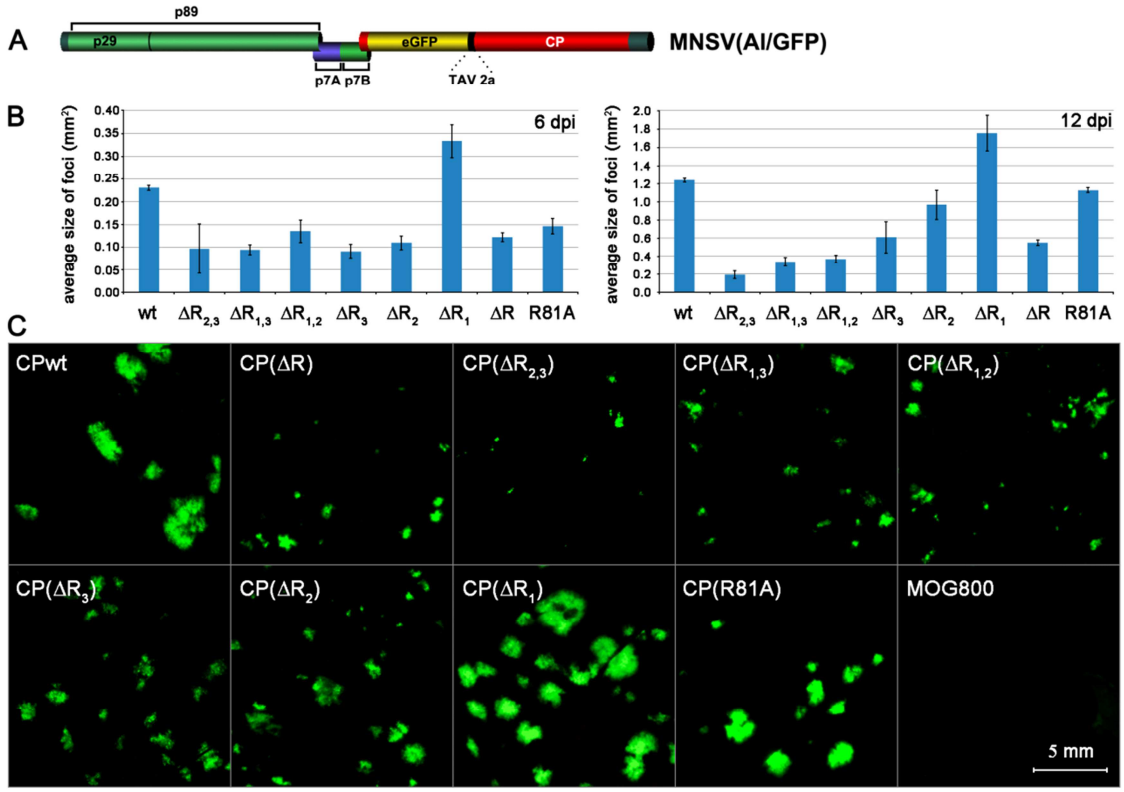

Fig. 4. Influence of mutations in MNSV CP R domain on viral cell-to-cell movement in *C. melo*. A) Schematic representation of recombinant MNSV(AI)/GFP genome cloned into pMOG800 under the control of the CaMV 35S promoter. eGFP and CP were simultaneously expressed using the 'self-cleaving' TAV 2a peptide. Viral and fluorescent protein names are indicated. (B) Quantification of cell-to-cell movement of wild-type MNSV(AI)/GFP and CP R domain mutants. Recombinant binary vectors were agroinfiltrated into C. melo leaves and, after imaging, fluorescent areas corresponding to infection foci were measured at 6 and 12 days post-infiltration. The results are presented as the average of infection foci size means from three separated experiments. (C) Representative images of fluorescent infection foci produced by wild-type MNSV(AI)/GFP and indicated CP R domain mutants at 12 days post-inoculation. Infiltration of bacteria carrying empty pMOG800 was used as negative control for autofluorescence.

Mutations within the R domain of MNSV CP reduced drastically viral RNA accumulation and limited long-distance movement in *N. benthamiana*

None of our available MNSV infectious constructs were competent to efficiently infect *C. melo* at systemic level. Therefore, we were forced to use *N. benthamiana* plants as experimental host to examine the requirements of the R domain for long-distance movement. We used a modified version of pMNSV(AI) (Genovés *et al*., 2006) in which parental 3' UTR was replaced with that of isolate MNSV-264 (Fig. 5A) (Diaz *et al*., 2004). Inoculation of *in vitro* transcripts of MNSV(AI/264) resulted in a high percentage of systemic infections (>90%) (Fig. 5C). Moreover, one interesting finding was that our attempts to purify viral particles either from inoculated or from symptomatic non-inoculated leaves were unsuccessful (Fig. S3B), indicating that long-

distance movement of MNSV(Al/264) in *N. benthamiana* occurs independently of encapsidation. A similar hypothesis has been already proposed for MNSV systemic movement in melon (Serra-Soriano *et al*., 2015).

N. benthamina seedlings were inoculated with *in vitro* transcripts of wild-type MNSV(Al/264) and R domain CP mutant (9 plants per clone). One week later, only plants inoculated with wild-type MNSV(Al/264) and CP(ΔR_1) mutant showed local symptoms (Fig. 5B). However, the percentage of plants infected with CP(ΔR_1) mutant that, two weeks later, developed symptoms in non-inoculated leaves (Fig. 5B) was considerably lower than wild-type (approximately 33% vs 89%). Northern-blot analysis of the non-inoculated leaves revealed that viral RNA accumulation in plants infected with wild-type MNSV(Al/264) was similar in some cases to that of CP(ΔR_1) mutant but higher in the majority of them (Fig. 5C). Inoculated leaves were similarly analyzed and after short exposure time, only RNAs of wild-type MNSV(Al/264) and CP(ΔR_1) mutant were detected (Fig. 5D). Hybridization signals were comparable in their intensity but note that, to avoid signal saturation, the quantity of total RNA from plants infected with wild-type MNSV(Al/264) run in agarose gels was 10-fold lower than in the rest of mutants. Although RNA accumulation was drastically reduced, a much longer exposure time revealed that all mutants appear to replicate as indicated by detection of faint hybridization signals corresponding to both genomic and sgRNAs (Fig. S4).

From these results, it is evident that difference in RNA accumulation among mutants was too large to be attributed only to variations in cell-to-cell movement. To minimize the influence of movement in viral RNA accumulation, we constructed binary vectors of wild-type MNSV(Al/264) and some representative mutants such as CP(ΔR_1), CP(ΔR) and CP(R81A) to be agroinfiltrated in *N. benthamiana* leaves. Results of Northern blot analysis of total RNAs extracted from agroinfiltrated leaves were similar to those obtained in infections resulting from transcript inoculation (Fig. 5E). In contrast to that we observed in melon, mutations in the R domain appear to reduce drastically virus accumulation and/or replication in *N. benthamiana*. Consequently, movement of virus through the plant may be also affected. Only CP(ΔR_1) mutant seems to occasionally reach the level of viral accumulation required to infect

systemically, most likely overcoming antiviral plant defense in a process where the presence/absence of both R_2 and R_3 subdomains switches the outcome.

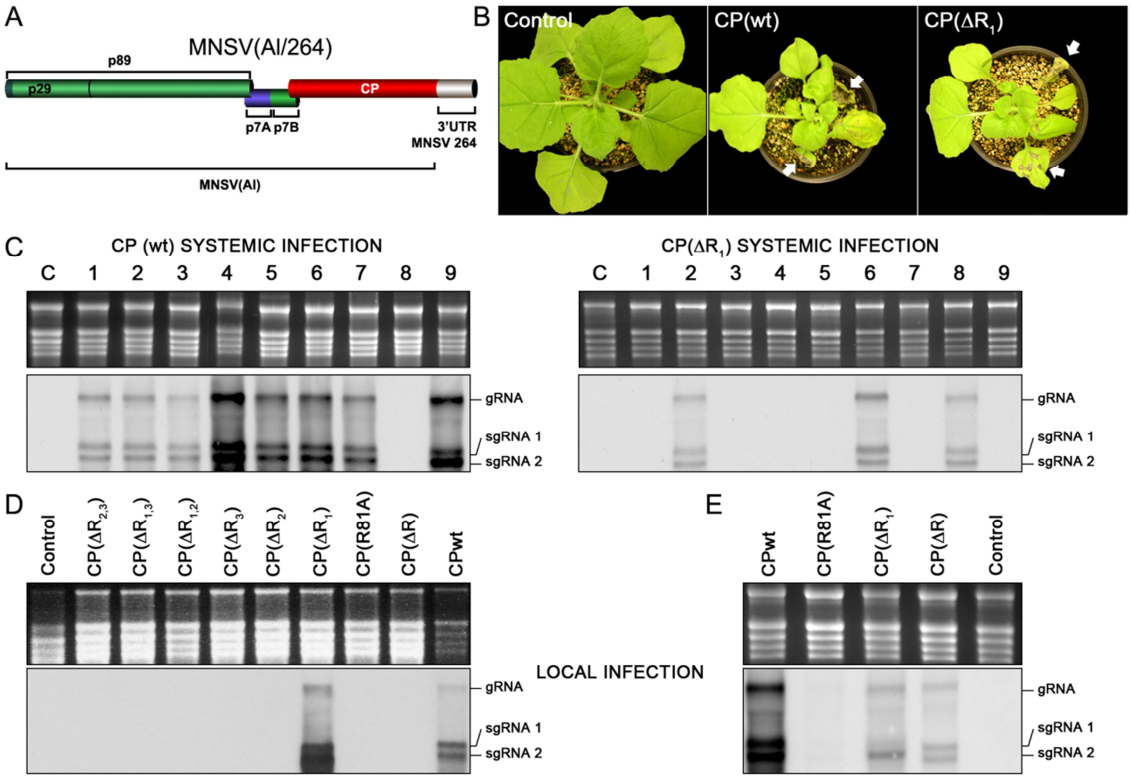

Fig. 5. Influence of mutations in MNSV CP R domain on viral long-distance movement and viral RNA accumulation in *N. benthamiana*. (A) Schematic representation of recombinant MNSV(Al/264) genome organization. (B) Local (indicated by arrows) and systemic symptoms of *N. benthamiana* plants inoculated either with in vitro-synthesized RNAs of MNSV(Al/264) wild-type or CP(ΔR1) mutant. Healthy control plants were mock-inoculated with phosphate buffer. Photographs were taken two weeks after inoculation. (C) Detection of MNSV RNAs in upper non-inoculated leaves of nine *N. benthamiana* plants (one plant per line) either inoculated with MNSV(Al/264) wild-type (on the left) or CP(ΔR1) mutant (on the right) RNAs. (D) Detection of MNSV RNAs in inoculated leaves of a representative *N. benthamiana* plant infected with MNSV(Al/264) wild-type and the indicated mutants. Mock-inoculated control plants were included in Northern blot analysis (E) Detection of viral RNAs in leaves of representative *N. benthamiana* plants agroinfiltrated with binary constructs either containing MNSV(Al/264) wild-type genome or that of CP(ΔR), CP(R81A) or CP(ΔR1) mutant. Northern blot assays were performed using a digoginenin-labelled MNSV-specific riboprobe. The corresponding denaturing agarose gel electrophoresis stained with ethidium bromide is shown.

Enhanced pathogenicity and increased viral RNA accumulation in PVX infections after expression of MNSV CP is dependent on the R domain region between amino acids 31-91

We next wanted to reevaluate the VSR activity of MNSV CP using an assay based on enhanced *Potato virus X* (PVX) pathogenicity when an additional VSR is provided *in cis* (Voinnet *et al.,* 1999). We also assessed the relevance of the R domain, and

especially that of the R_2 and R_3 subdomains, in MNSV CP silencing suppression phenotype. We hence introduced the sequences coding for wild-type MNSV CP and mutated CP(ΔR_1), CP(ΔR_2), CP(ΔR_3), CP(ΔR) and CP(R81A) into a PVX-derived binary vector (Lacomme and Chapman, 2008). PVX-permissive host *N. benthamiana* was agroinfiltrated and three weeks later, plants were imaged (Fig. 6A). Those plants infected with PVX that expressed either wild-type MNSV CP (PVX-CP(wt)) or mutated CP(ΔR_1) (PVX-CP(ΔR1)) showed severe stunting and necrosis (Fig. 6A). In contrast, phenotype of plants infected with PVX-CP(ΔR) was more comparable to that of control infections with empty PVX. In both cases infected plants only displayed mild symptoms that progressively disappeared in upper leaves. Plants infected either with PVX-CP(ΔR_2) or PVX-CP(ΔR_3) showed a slightly more severe symptomatology than PVX-CP(ΔR) and finally, plants infected with PVX-CP(R81A) had increased symptomatology but without reaching the severity observed in PVX-CP(wt) and PVX-CP(ΔR1). Total RNAs from non-agroinfiltrated leaves were also analyzed by Northern blot with a PVX CP specific riboprobe (Fig. 6B). Hybridization signals revealed substantially more accumulation of viral RNAs in plants infected either with PVX-CP(wt) or PVX-CP(ΔR1) than in those infected with control PVX and with each of the PVX variants examined. Therefore, VSR function is dependent on R domain and, specifically, on the region embracing both R_2 and R_3 subdomains

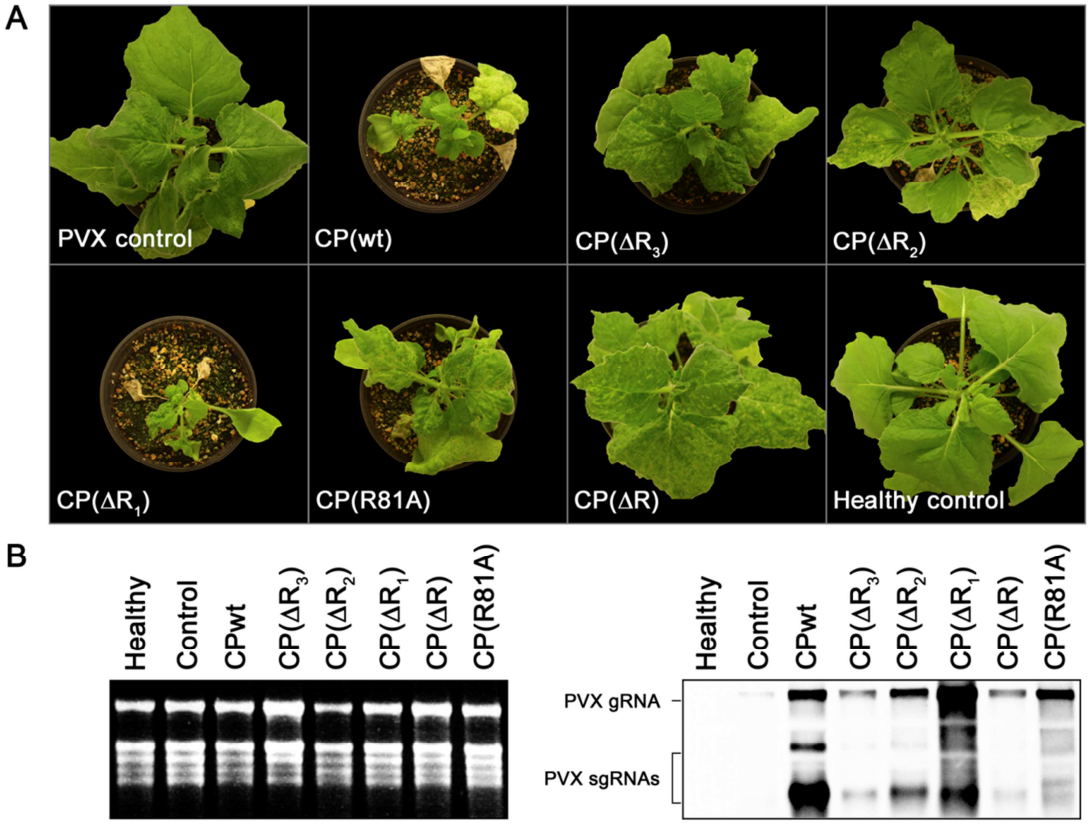

Fig. 6. Increasing of PVX pathogenicity and viral RNA accumulation is facilitated by MNSV CP R domain. (A) Symptoms of infection with "empty" PVX or PVX expressing MNSV CP (wild-type or the indicated mutants) in *N. benthamiana* plants. Images were taken three weeks after agroinfiltration. (B) Northern blot analysis with PVX CP specific riboprobe of total RNAs of representative *N. benthamiana* plants systemically infected with "empty" PVX or PVX expressing MNSV CP (wild-type or the indicated mutants). Healthy control plants were agroinfitrated with bacteria carrying empty pMOG800.

MNSV CP binds Dicer-like small RNAs through the R domain region between amino acids 31-91.

To study MNSV CP binding to small RNAs, we performed gel shift assays and kinetic analysis essentially as hereinbefore described. We first used MNSV CP(wt) and *in vitro* transcripts either of 21, 22 or 24 nt to determine the optimal protein concentration at which to perform further comparisons with R domain mutants. Increasing quantities of GST-CP(wt) lowered the amount of free single stranded RNAs (ssRNAs) independently of its size and resulted in the formation of ssRNA-CP complexes that, as occurred before, barely enter the gel (Fig. 7A). Disappearance of free ssRNAs of 21 and 22 nt began to be more evident at higher protein concentrations than in the case of ssRNAs of 24 nt. This observation was reflected in the values of the corresponding apparent dissociation constants (Fig 7B). Kas for the binding of MNSV CP to 21 and 22 nt ssRNAs were similar and it was estimated to be 180 nM. In contrast,

a four-fold increase of affinity for the binding of MNSV CP to 24nt sRNAs was found (K_a 50 nM). These results may indicate that MNSV CP binds ssRNAs in a size-selective manner, and suggest a preference for 24 nt ssRNAs.

To examine whether the loss of silencing suppressor activity coincides with loss of binding affinity to siRNA molecules, GST-recombinant R domain mutants were compared with GST-CP(wt) in gel mobility shift assays. Next experiments were performed using a single protein concentration. Therefore, to avoid misinterpretations of binding specificity (Ryder *et al.,* 2008) and to guarantee that complex formation was not limited by protein availability, we used a concentration (600 nM) at which unbound RNA practically disappeared in the assays performed above. ssRNAs of 21, 22 and 24 nt but also the corresponding RNAs duplexes (dsRNAs) containing 2-nt 3' end overhangs were incubated with GST-CP(wt) and GST-recombinant R domain mutants (Fig. 8A and 8B, respectively). EMSAs revealed that only GST-CP(wt) and GST-CP(ΔR1) showed binding activity to single and double stranded RNAs of 21, 22 and 24 nt, whereas the rest of mutants failed to form complexes with either type of RNA tested (Fig. 4B). These results indicate that the R domain region between amino acid 31-91 is required for silencing suppression and binding of siRNAs and, consequently, corroborate our initial assumption that both properties should be closely linked.

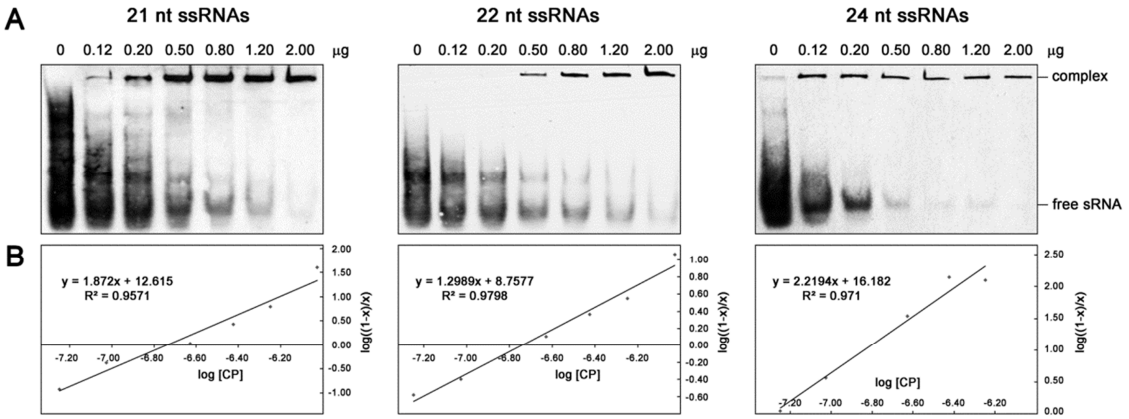

Fig. 7. Analysis of small RNA (sRNA) binding activity of MNSV CP(wt) by EMSA. (A) Gel retardation assays of single stranded viral transcripts (ssRNAs) of 21, 22 or 24 nt with GST-CP(wt). Bands corresponding to unbound sRNA were quantified to calculate the apparent dissociation constant. (B). Hill plots of sRNA binding activity of GST-CP(wt). A Hill transformation was applied to data to graphically represent the log [(1-x)/x] versus the log[CP], were x is the ratio of unbound RNA to total RNA. Lines represent the best fit determined by least square analysis of the mean values from at least three separated experiments. The corresponding equation and R-squared value are given in each graph.

MNSV CP inhibition of systemic RNA silencing triggered by sense GFP RNA is also dependent on the R domain region between amino acids 31-91

When RNA silencing was triggered by sense GFP RNA using GFP transgenic *N. benthamiana* plants (line 16c), MNSV CP exhibited a weak suppressor activity of transgene silencing in local infiltrated leaves (Genovés *et al*., 2006). However, effects on upper non-infiltrated leaves were not examined. To determine whether MNSV CP could interfere with systemic RNA silencing, five 16c plants were infiltrated with a mix of two *A. tumefaciens* cultures either expressing GFP or CP(wt). Bacteria carrying binary vectors either expressing each R domain deletion mutant, CP(R81A) mutant or an unrelated protein, which was used as positive control for systemic silencing, were also included into assay. Three independent experiments were performed. Development of GFP systemic silencing was monitored, under UV light, following the appearance and spread of red chlorophyll autofluorescence. In all control plants, the upper noninfiltrated leaves started to lose green GFP fluorescence around major veins at approximately 10-12 dpi. At 25-30 dpi, the whole plant lost green fluorescence and became completely red under UV light (Fig. 9). Almost all plants (around 90%) coinfiltrated with GFP plus CP(wt) or GFP plus CP(ΔR_1) retained green fluorescence in noninfiltrated leaves at 30 dpi. In contrast, plants infiltrated with GFP plus either of remaining seven mutants behaved similarly to control plants (Fig. 9). None of the analyses described at present has been conclusive about molecular form of the mobile RNA that triggers systemic silencing but siRNAs have become the most plausible option. These results are in line with those obtained in siRNA binding experiments indicating that MNSV CP could suppress systemic RNA silencing by small RNA sequestering.

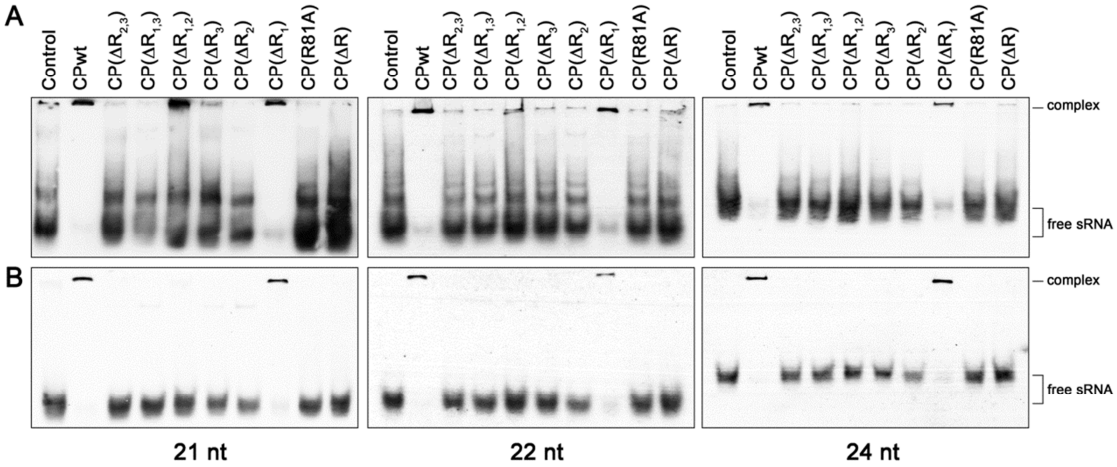

Fig. 8. Comparison of small RNA (sRNA) binding activities of MNSV CP(wt) and R domain mutants by EMSA. Single stranded RNAs (ssRNA) of 21, 22, or 24 nt (A) and the corresponding RNAs duplexes (dsRNA) containing 2-nt 3' end overhangs (B) were incubated with 600 nM of GST-CP(wt) or the indicated GST-recombinant R domain mutants. No protein was included in the control mix.

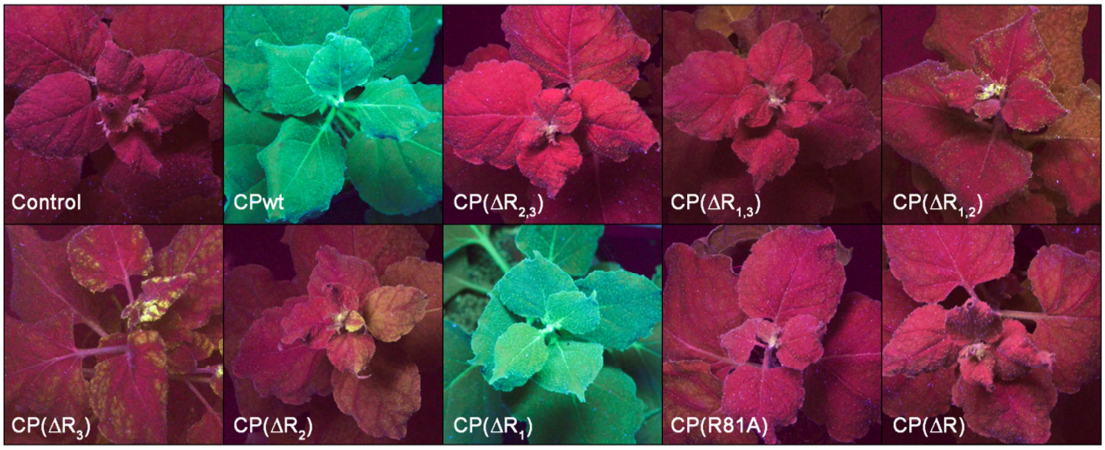

Fig. 9. Effects of MNSV CP and R domain mutants on systemic GFP silencing. At the 4 leaf stage, GFP transgenic *N. benthamiana* plants (line 16c) were coinfiltrated with agrobacteria expressing eGFP plus MNSV CP wild type and the indicated mutants. 25-30 days later, photographs were taken under long-wavelength UV light.

DISCUSSION

To survive under high mutation rates, RNA plant viruses have evolved small genome sizes that strongly constrain the gain of function by gene duplication or lateral gene transfer (Belshaw *et al*., 2007). More often than not, the solution to this pressure consists on the acquirement of new activities by viral proteins already performing other roles in virus biology. It is commonly assumed that competence to multifunctionality depends on the presence of intrinsically disordered domains

(Dunker *et al*., 2008). In this sense, N-terminal regions of some spherical (+)-RNA plant virus CPs are suitable candidates since they have been difficult to resolve in crystallographic structures, indicating most likely its flexibility and spatially disordered conformation (Doan *et al*., 2003; Harrison *et al*., 1978; Hogle *et al*., 1986; Katpally *et al*., 2007; Ke *et al*., 2004; Morgunova *et al*., 1994; Wada *et al*., 2008). To provide new insights into these multifunctional regions, we have examined the N-terminal region or R domain of MNSV CP for its relevance in multiple and essential processes in the viral life cycle.

In this work, we showed that MNSV CP binds with high affinity to long ssRNAs without detectable sequence specificity. We also demonstrated that RNA binding exclusively depends on the R domain since RNA interaction was completely eliminated after deletion of the very 94 N-terminal amino acid residues. Although there were significant variations between RNA affinities among the rest of R domain mutants, they were proved to be insufficient to abolish *in vitro* RNA binding ability. This indicates that, at least in solution, all 16 basic residues located along the R domain can potentially contribute to interact with negatively charged RNA backbones. However, the presence of the R_3 subdomain appeared to be more relevant in single than in double subdomain deletion mutants since the deletion of this subdomain had a significantly stronger effect in the RNA-binding affinity than the deletion of either R1 or R2 subdomains (compare the corresponding Ka in Fig. 2). Consistently with these results, the presence of R3 subdomain was proven to be required for virion assembly (Fig. 3B, 3C).

Experimental evidences suggest that the role of R_3 subdomain in virion RNA binding cannot be ascribed basically to neutralization of the negative charge of the RNA through the basic residues of the ε region (Hui and Rochon, 2006). Interaction among CP subunits during *in vivo* assembling may facilitate the formation of the intrinsic β-annulus element and ε region, which are known that contribute to virion stability, RNA binding and subunit quasi-equivalence in related viruses. By taking this assumption, we tried to explain our results on the basis of recent structural data of related tombusvirus. Neutron diffraction studies on *Tomato bushy stunt virus* (TBSV) and cryo-transmission electron microscopy structures of *Cucumber necrosis virus* (CNV)

revealed that tombusvirus particles were internally organized in four alternating concentric shells of protein and RNA (Katpally *et al*., 2007; Timmins *et al.,* 1994). The outer protein shell corresponded to the S and P domains while the second internal protein shell was formed by most of disordered N-terminal region. Most of viral RNA was very tightly packed between both protein shells, showing higher density under C-C dyads than under A-B dyads. In contrast, RNA density was lacking close to the highly hydrophobic β-annulus elements at the threefold axis. High structural homology among MNSV and TBSV CPs has been reported (Wada *et al*., 2008). In fact, the ε region of MNSV CP is also highly basic, containing five positively charged residues, while only a basic residue is found in the β-annulus sequence. This led us to assume that MNSV capsid may display a TBSV-like internal architecture and similar distribution of the RNA density under the inner surface of the outer protein shell, supporting the major role of the ε region in MNSV RNA encapsidation.

It has been shown that removal of an extended N-terminal region facilitates CP to assemble into 60 subunits T=1 particles that are significantly smaller than the native T=3 particles (Hsu *et al.,* 2006; Kakani *et al.,* 2008; Katpally *et al*., 2007; Kumar *et al.,* 1997; Larson *et al.,* 2005; Sangita *et al.,* 2004). Thus, deletion of R_1, R_2 or both subdomain could modify T=3 symmetry of MNSV virions, resulting in smaller capsids large enough to ensure encapsidation of sgRNAs but not full-length genomes. This assumption could explain why MNSV RNAs of approximately 4.3 kb were only recovered from wild-type and CP(R81A) mutant virions, which have the complete R domain, but not from other deletion mutants. In this sense, recombinant TCV RNAs larger than parental genomes were unsuccessfully encapsidated (Dong *et al.,* 1998). As another possible explanation, N-terminal deletions could compromise inner shell formation affecting morphology and/or stability of T=3 particles. Without ruling out the possibility that inner shell can be also required in recognition of MNSV RNAs as observed in EMSAs, unsuccessful encapsidation of full-length genome could result from an increased accessibility of nucleases inside the unstable mutant particles, as previously proposed for CNV (Reade *et al*., 2010).

We previously showed that the potential role of MNSV CP as VSR was barely demonstrated by a standard bioassay on transgenic 16c *N. benthamiana* (Genovés *et*

al., 2006). The results obtained here indicate that MNSV CP suppression of viral induced silencing, which has biological significance for viral infection, seems to be more evident than suppression of transgene induced silencing. Similar discrepancy has been already reported for others VSRs and it is most likely due to the fact that PVX assay more closely mimics wild-type conditions produced by cytoplasmic RNA viruses (Powers *et al.,* 2008). The link between the VSR activity and their effects on the pathogenic process has been well documented (see García and Pallás, 2015 for review) Here we demonstrated that VSR function is dependent on R domain and, specifically, on the region embracing both R_2 and R_3 subdomains. In encapsidation independent movement assays, only CP(ΔR1) mutant showed a phenotype similar to that observed in wild-type infections. Therefore, the same region of MNSV R domain required for VSR activity was essential for efficient viral movement through the whole plant, indicating that defects in combating the host defense system are likely causing restrictions in cell-to-cell movement and systemic infection and a pathogenic phenotype.

Interestingly, deletion of the R_1 subdomain significantly increased cell-to-cell movement in melon leaves although decreased the number of systemically infected *N. benthamiana* plants. In CNV, the N-terminal 39 amino acids of the CP can function as a mitochondrial targeting peptide (mTP) resulting in a proteolytic cleavage of the R domain near the R/arm junction (equivalent to the R_2/R_3 subdomain junction in MNSV) (Hui *et al.,* 2010). These researchers proposed that mitochondrial targeting of CNV CP could determine its destiny towards assembly or disassembly during infection. We have also experimental evidences that dual targeting to mitochondria and chloroplast followed by proteolytic cleavage of the R domain occurs in MNSV CP(wt) but not in CP(ΔR1) mutant (unpublished results). Although more studies are required, CP(wt) suppressor activity could be compromised in CP(wt) by proteolytic cleavage but not in CP(ΔR1) mutant. Thereby, more CP(ΔR1) protein could be fated to act as VSR facilitating local spread. In contrast, the reduced systemic infection by this mutant in *N. benthamiana* plants was most likely due to the observed host specific defects in RNA accumulation/replication, which might cause delayed virus entry into the vascular system.

Double-stranded RNAs mainly derived from cytoplasmic viral replication intermediates are targeted by Dicer-like nucleases (DCL) that cut them into small interfering RNAs duplexes (siRNA) of about 21 to 24 nt (Pumplin and Voinnet, 2013). One strand of the duplex is integrated into a multiprotein complex termed RISC (RNA-induced silencing complex) and guide Argonaute proteins (AGO), the main RISC component, for homologous RNA degradation. To evade this plant defense mechanism, different VSRs have evolved to target any step and/or component of the RNA silencing pathway; e.g., many VSRs, which contain RNA binding domains with positively charged basic amino acids, inhibit RISC assembling through sequestration of small RNA duplexes (Burgyán and Havelda, 2011; Lakatos *et al.,* 2006; Merai *et al.,* 2006). Two observations made us to speculate that binding siRNAs could be the molecular mechanism by which MNSV CP interferes with RNA silencing: first, viral-derived siRNAs, mainly of 21 nt, accumulated to abundant levels in infected plants, suggesting that MNSV CP does not prevent siRNA production *in vivo* (Donaire *et al.,* 2009; Herranz *et al.,* 2015); second, we demonstrated here that suppressor activity of MNSV CP *in vivo* was dependent on basic R domain. Shift mobility gels showed that purified MNSV CP can bind DCL-produced sRNAs *in vitro* independently of their size. Moreover, our mutational analysis revealed a positive correlation between the ability to bind sRNAs *in vitro* and the capacity to suppress RNA silencing *in vivo*, strongly indicating that MNSV CP interfere with viral RNA degradation by sequestering sRNAs. It has been shown that 24 nt rather than 21 nt sRNAs were selectively mobile through the systemic pathway, at least from a GFP transgene and from selected endogenous loci (Melnyk *et al.,* 2011). Our results demonstrated that MNSV CP showed higher affinity for sRNAs of 24 nt, a functional feature that could be involved in blocking the spread of the mobile systemic signal of RNA silencing. Remarkably, the capability to systemically infect *N. benthamiana* plants strongly correlated with the VSR activity (Figs. 5,8,9) supporting the conclusion that the silencing suppression function of carmovirus CPs is the primary requirement for systemic spread (Cao *et al.,* 2010; Zhang and Simon 2003).

Tough MNSV belongs to genus *Carmovirus*, its CP is more similar to those of genus *Tombusvirus* in the extent of sequence similarity, length of the R and P domains and tridimensional structure (Riviere *et al*., 1989, Wada *et al*., 2008). These findings

indicate that MNSV CP gene could have been acquired during a recombinant process. In this regard, tombusviruses and carmoviruses have been predicted to be highly recombinant compared to viruses of the other genera in *Tombusviridae* family (Boulila, 2011). Moreover, recombination may occur between viruses belonging to different genera and particularly in the coat protein-encoding gene (Boulila, 2011). Such a recombinant event was largely studied for CNV and MNSV (Riviere and Rochon, 1990). In the family *Tombusviridae*, CPs of carmoviruses and P19 protein, which is entirely nested within the movement protein of tombusviruses, have been described as major suppressors of RNA silencing (Burgyán and Havelda, 2011). In contrast, CPs of tombusviruses are lacking of VSR activity. In fact, MNSV CP lacks the GW motif that is present in carmovirus CPs and in the only member of the recently proposed *Pelarspovirus* genus (Azevedo *et al.,* 2010; Pérez-Cañamás and Hernández, 2015). The GW motif mimics the GW/WG repetitive motif of cellular AGO interacting proteins and, in the case of TCV CP, it has been proposed to avoid sRNA loading into AGO1 by interacting with nonloaded AGO1. In addition to this protein-protein interaction, carmovirus CPs have been postulated to bind viral sRNAs as an alternative mechanism of RNA silencing (Merai *et al*., 2006). This binding relies on specific basic amino acids within the S domain of the CP (Cao *et al*., 2010). Our results demonstrate the peculiarity of the MNSV CP in its mode of action for its RNA silencing activity. Moreover, the relevance of GW motif in sRNA binding has been also demonstrated (Azevedo *et al*., 2010; Pérez-Cañamás and Hernández, 2015). In the absence of P19-like proteins or *bona fide* carmovirus CP, MNSV CP could have acquired VSR activity by adapting its N-terminal disordered region to interact with different RNA molecules such as siRNAs. As MNSV encapsidation and suppression functions rely on same functional domain of the CP, they should be mutually exclusive processes. Therefore, further studies are needed to identify the physiological or molecular switch that determines the fate of MNSV CP toward encapsidation or RNA silencing suppression.

SUPLEMENTARY INFORMATION

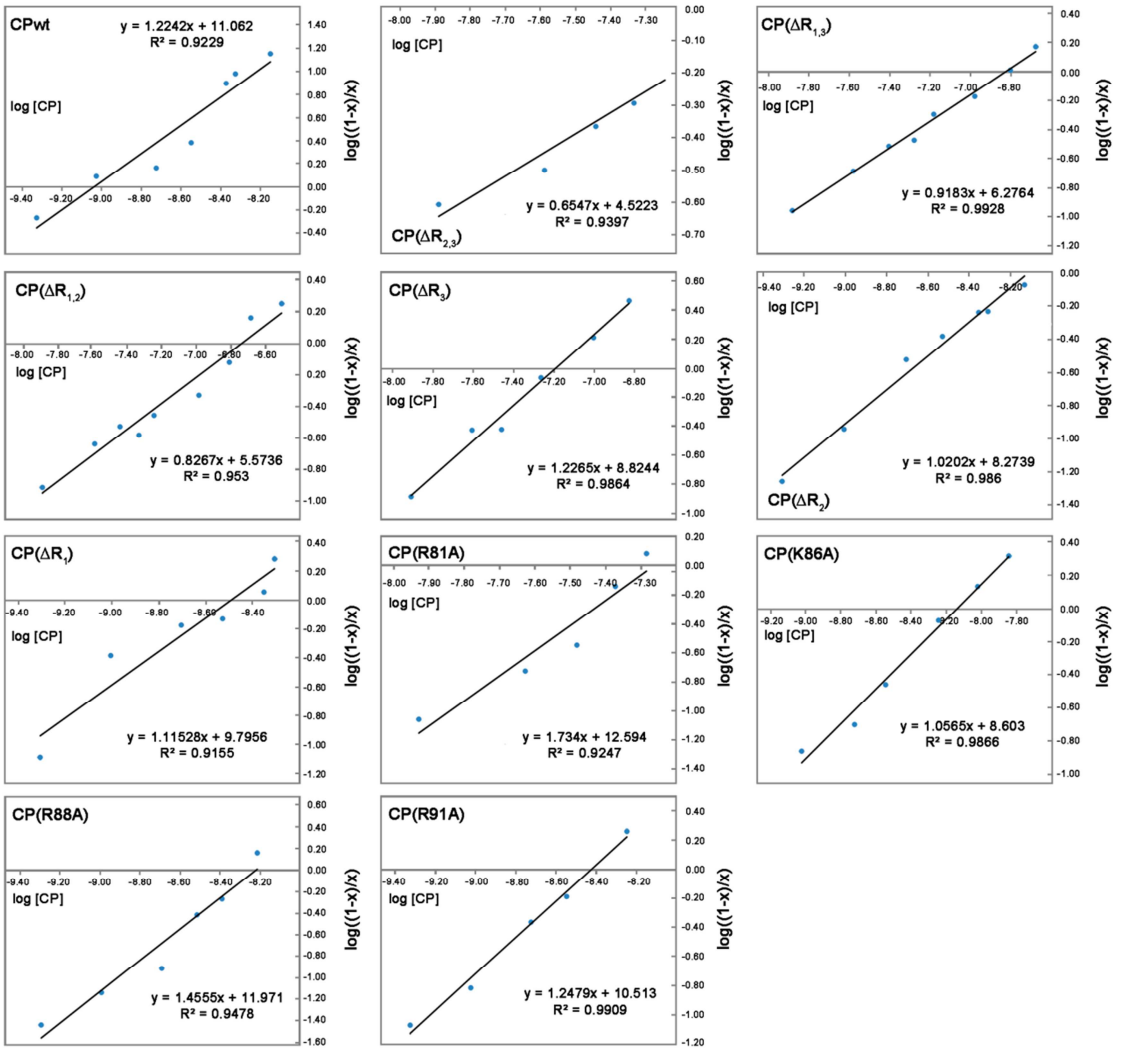

Fig S1. Hill plots of RNA binding activity of GST-CP(wt) and GST recombinant R domain mutants. A Hill transformation was applied to data to graphically represent the log [(1-x)/x] versus the log[CP], were x is the ratio of unbound RNA to total RNA. EMSA for each recombinant protein was repeated between three and five times to ensure reproducibility and accurate linear regression of Hill transformation. Lines represent the best fit determined by least square analysis of the mean values from at least three measures (R-squared values higher than 0.9). The corresponding equation and R-squared value are given in each graph.

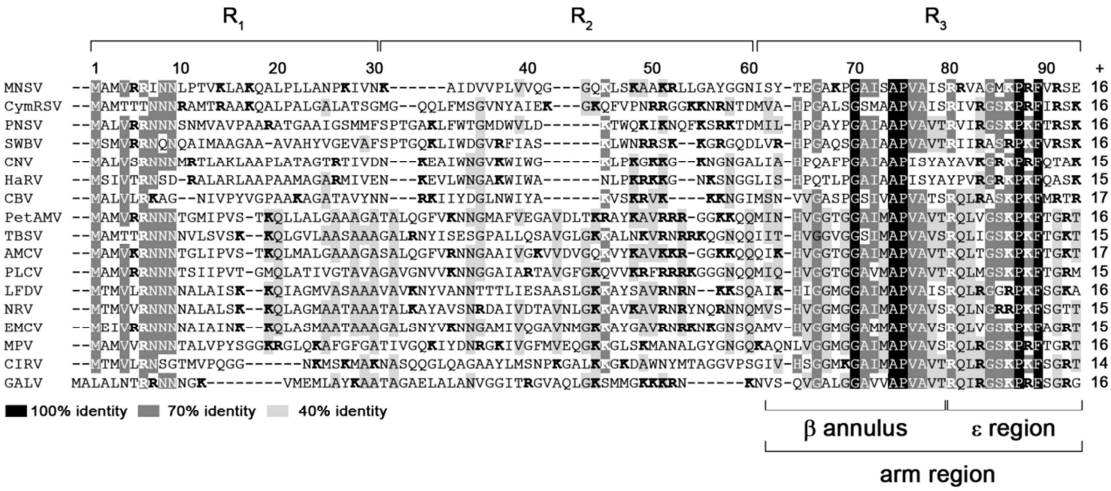

Fig. S2. Amino acid sequence alignment of coat protein N-terminal regions of *Melon necrotic spot virus* (MNSV) and all available members of genus *Tombusvirus*. The analysis was conducted using the ClustalW option under the "alignment" tab in MEGA version 6.06 (http://www.megasoftware.net). Identity scores are as indicated by color code. Gaps are represented as contiguous dashes. Location of positively charged residues Lysine/Arginine is highlighted in bold, and their total number indicated on the right of each aligned sequence. Numbering is based on CP amino acid sequence of isolate MNSV(Al) (DQ339157). R_1, R_2 and R_3 subdomain distribution, which was assigned in this study, is also indicated on top. The different tombusviruses compared are: CymRSV, *Cymbidium ringspot virus*; PNSV, *Pelargonium necrotic spot virus*; SWBV, *Sitke waterborne virus*; CNV, *Cucumber necrosis virus*; HaRV, *Havel River virus*; CBV, *Cucumber Bulgarian virus*; PetAMV, *Petunia asteroid mosaic virus*; TBSV, *Tomato bushy stunt virus*; AMCV, *Artichoke mottled crinkle virus*; PLCV, *Pelargonium leaf curl virus*; LFDV, *Limonium flower distortion virus*; NRV, *Neckar River virus*; EMCV, *Eggplant mottled crinkle virus*; MPV, *Moroccan pepper virus*; CIRV, *Carnation Italian ringspot virus*; and GALV, *Grapevine Algerian latent virus*.

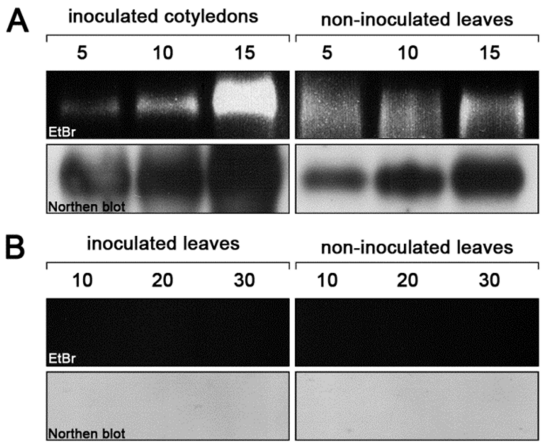

Fig. S3. Purification of virions from MNSV-infected *C. melo* and *N. benthamiana* tissues using 20% sucrose cushion at two-week post-inoculation. (A) Native gel electrophoresis stained with ethidium bromide and Northern blot analysis of MNSV virions purified from 20 g of both *C. melo* inoculated cotyledons (on the left) and *C. melo* symptomatic non-inoculated leaves (on the right). Infection were performed by inoculation of MNSV(Al) virions in both cotyledons. The final volume was 0.5 ml and 5, 10 and 15 µl were run. (B) Native gel electrophoresis stained with ethidium bromide and Northern blot analysis of extracts obtained from 20 g of both inoculated (on the left) and symptomatic non-inoculated *N. benthamiana* leaves (on the right). Infection were performed by inoculation of MNSV(Al/264) transcripts in three leaves per plant. The final resuspension volume was 0.5 ml and 10, 20 and 30 µl were run in this case.

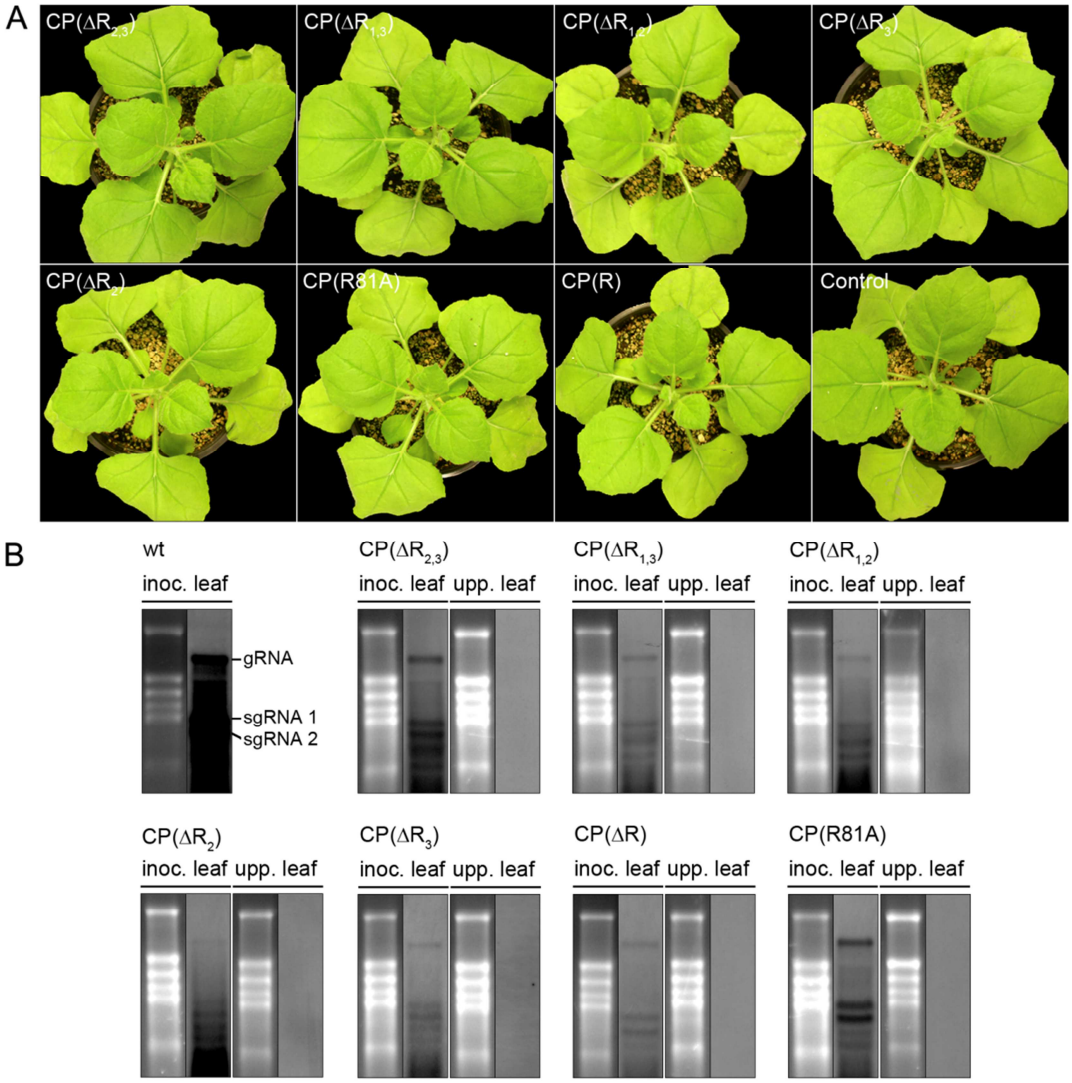

Fig. S4. Influence of mutations in MNSV CP R domain on viral long-distance movement and viral RNA accumulation in *N. benthamiana.* (A) Photographs of *N. benthamiana* plants taken two weeks after inoculation with *in vitro*-synthesized RNAs of the indicated MNSV(Al/264) mutants. Healthy control plants were mock-inoculated with phosphate buffer. (B) Detection of MNSV RNAs in inoculated and upper non-inoculated leaves of representative *N. benthamiana* plants infected with RNAs of the indicated MNSV(Al/264) mutants. Different exposure times were required to finally detect viral RNAs of all mutants. Northern blot assays were performed using a digoginenin-labelled MNSV-specific riboprobe. The corresponding denaturing agarose gel electrophoresis stained with ethidium bromide is shown.

Table S1. List of oligonucleotides used in this study

genome position	name	sequence	mutation	template
pGEX-KG				
2816-2832	VP282 (s)	atcg**GGATCC**ATGGCGATGGTTAGACG (BamHI)	-	pMNSV(AI)
3988-3972	VP469 (a)	atcg**AAGCTT**TTAGGCGAGGTAGGCTG (HindIII)		
2906-2929	VP2046 (s)	AAAGCTATAGATGTGGTTCCTTTG	CP(ΔR_1)	pG-CPwt
pGEX-KG GST	VP2067 (a)	GGATCCACGCGGAACCAG		
2996-3022	VP2171 (s)	ATTTCGTACACTGAGGGTGCCAAACCA	CP(ΔR_2)	pG-CPwt
2905-2885	VP2047 (a)	ATTTACAATTTTAGGGTTCGC		
3086-3106	VP1897 (s)	CGATCGGAAGGATCTGTGAAG	CP(ΔR_3)	pG-CPwt
2995-2969	VP1896 (a)	GTTGCCTCCATAAGCGCCAAGCAATCG		
3086-3106	VP1897 (s)	CGATCGGAAGGATCTGTGAAG	CP($\Delta R_{2,3}$)	pG-CPwt
2905-2885	VP2047 (a)	ATTTACAATTTTAGGGTTCGC		
3086-3106	VP1897 (s)	CGATCGGAAGGATCTGTGAAG	CP($\Delta R_{1,3}$)	pG-CP(ΔR_1)
2995-2969	VP1896 (a)	GTTGCCTCCATAAGCGCCAAGCAATCG		
2996-3022	VP2171 (s)	ATTTCGTACACTGAGGGTGCCAAACCA	CP($\Delta R_{1,2}$)	pG-CPwt
pGEX-KG GST	VP2067 (a)	GGATCCACGCGGAACCAG		
3086-3106	VP1897 (s)	CGATCGGAAGGATCTGTGAAG	CP(ΔR)	pG-CPwt
pGEX-KG GST	VP2067 (a)	GGATCCACGCGGAACCAG		
3045-3066	VP1681 (s)	CTATTAGTCGGGCAGTGGCTGG	CP(R81A)	pG-CPwt
3066-3045	VP1682 (a)	CCAGCCACTGCCCGACTAATAG		
3061-3083	VP1683 (s)	GGCTGGTATGGCGCCTAGGTTTG	CP$_I$K86A)	pG-CPwt
3083-3061	VP1684 (a)	CAAACCTAGGCGCCATACCAGCC		
3065-3090	VP1685 (s)	GGTATGAAGCCTGCGTTTGTTCGATC	CP(R88A)	pG-CPwt
3090-3065	VP1686 (a)	GATCGAACAAACGCAGGCTTCATACC		
3074-3099	VP1687 (s)	CCTAGGTTTGTTGCATCGGAAGGATC	CP(R91A)	pG-CPwt
3099-3074	VP1688 (a)	GATCCTTCCGATGCAACAAACCTAGG		
MNSV(AI) and MNSV(AI/264)				
2906-2929	VP2046 (s)	AAAGCTATAGATGTGGTTCCTTTG	CP(ΔR_1)	MNSV(AI)/(AI/264)
2830-2810	VP2319 (a)	GCTAACCATCGCCATTTGTAG		
2996-3022	VP2171 (s)	ATTTCGTACACTGAGGGTGCCAAACCA	CP(ΔR_2)	MNSV(AI) /(AI/264)
2905-2885	VP2047 (a)	ATTTACAATTTTAGGGTTCGC		
3086-3106	VP1897 (s)	CGATCGGAAGGATCTGTGAAG	CP(ΔR_3)	MNSV(AI)/(AI/264)
2995-2969	VP1896 (a)	GTTGCCTCCATAAGCGCCAAGCAATCG		
3086-3106	VP1897 (s)	CGATCGGAAGGATCTGTGAAG	CP($\Delta R_{2,3}$)	MNSV(AI)/(AI/264)
2905-2885	VP2047 (a)	ATTTACAATTTTAGGGTTCGC		
3086-3106	VP1897 (s)	CGATCGGAAGGATCTGTGAAG	CP($\Delta R_{1,3}$)	MNSV(AI)-CP(ΔR_1) /(AI/264)-CP(ΔR_1)
2995-2969	VP1896 (a)	GTTGCCTCCATAAGCGCCAAGCAATCG		
2996-3022	VP2171 (s)	ATTTCGTACACTGAGGGTGCCAAACCA	CP($\Delta R_{1,2}$)	MNSV(AI)/(AI/264)
2830-2810	VP2319 (a)	GCTAACCATCGCCATTTGTAG		
3086-3106	VP1897 (s)	CGATCGGAAGGATCTGTGAAG	CP(ΔR)	MNSV(AI)/(AI/264)
2830-2810	VP2319 (a)	GCTAACCATCGCCATTTGTAG		
2996-3022	VP2171 (s)	ATTTCGTACACTGAGGGTGCCAAACCA	CP(R81A)	MNSV(AI)/(AI/264)
2905-2885	VP2047 (a)	ATTTACAATTTTAGGGTTCGC		
MNSV(AI/GFP)				
TaV 2a	VP2689 (s)	ccgc**ACCTGC**acgt*ACCG*CCCATGGTGATCTTTATGTCG (BveI)	Vector	MNSV(AI/GFP)
3542-3566	VP2688 (a)	ggcg**ACCTGC**acgt*GGGC*CCAGGATTCTCCTCGACGTCA (BveI)		
3546-3542 3086-3106	VP2690 (s)	ccgc**ACCTGC**acgt*GCCCC*GATCGGAAGGATCTGTGAAG (BveI)	CP(ΔR)	pG-CP(ΔR)
3546-3542	VP2691 (s)	ccgc**ACCTGC**acgt*GCCC*ATTTCGTACACTGAGGGTGCC (BveI)	CP($\Delta R_{1,2}$)	CP($\Delta R_{1,2}$)

2995-3016 3546-3542 2906-2926	VP2692 (s)	ccgc**ACCTGC**acgt*GCCC*AAAGCTATAGATGTGGTTCCT (BveI)	CP($\Delta R_{1,3}$)/ CP(ΔR_1)	pG-CP($\Delta R_{1,3}$)/ pG-CP(ΔR_1)
3546-3542 2816-2836	VP2693 (s)	ccgc**ACCTGC**acgt*GCCC*ATGGCGATGGTTAGACGCATT (BveI)	CP(wt)/ CP($\Delta R_{2,3}$)/ CP(ΔR_3)/ CP(ΔR_2)	pG-CP(wt)/ pG-CP($\Delta R_{2,3}$)/ pG-CP(ΔR_3)/ pG-CP(ΔR_2)
3545-3521	VP2694 (a)	ggcg**ACCTGC**acgt*CGGT*GTCACCAGCACCAGAGTAAGT (BveI)		
sRNAs				
3182-3202	VP2424(a)	GGCAAGTATAGAGTCAATCCC**TATAGTGAGTCGTATTAG** (T7 promoter)		
3200-3182	VP2425(s)	GATTGACTCTATACTTGCCCC**TATAGTGAGTCGTATTAG** (T7 promoter)		
3182-3202	VP2426(a)	GGCAAGTATAGAAGTCAATCCC**TATAGTGAGTCGTATTAG** (T7 promoter)		
3200-3182	VP2427(s)	GATTGACTTCTATACTTGCCCC**TATAGTGAGTCGTATTAG** (T7 promoter)		
3182-3202	VP2428(a)	GGCAAGTATAGATAAGTCAATCCC**TATAGTGAGTCGTATTAG** (T7 promoter)		
3200-3182	VP2429(s)	GATTGACTTATCTATACTTGCCCC**TATAGTGAGTCGTATTAG** (T7 promoter)		

Sequences in bold refer to cleavage site of indicated restriction enzyme or T7 promoter sequence

Underlined letters correspond to inserted nucleotides, (s) sense (a) antisense

CAPÍTULO CUARTO

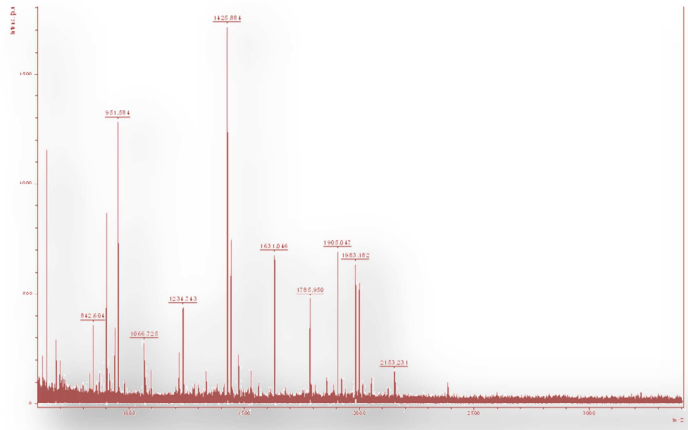

Este capítulo ha dado lugar a la siguiente publicación:

Serra-Soriano M, Navarro JA, Genoves A, Pallas V. 2015. Comparative proteomic analysis of melon phloem exudates in response to viral infection. J Proteomics 124:11-24.

Comparative proteomic analysis of melon phloem exudates in response to viral infection

INTRODUCTION

The phloem is a highly specialized conducting tissue of vascular plants whose major role was initially considered to be the movement and distribution of photo-assimilates, sugars and organic compounds, between autotrophic and heterotrophic tissues. It was soon evident that phloem also contained hormones and a wide range of macromolecules, including RNAs and proteins, that could act as mobile signals to regulate a variety of developmental processes and environmental responses (Atkins *et al.,* 2011; Dinant and Suárez-López, 2012; Pallás and Gómez, 2013; Turgeon and Wolf, 2009; Turnbull and Lopez-Cobollo, 2013). The floral transition, the tuber production in potato, the systemic acquired resistance (SAR) against bacteria, fungi and viruses and systemic wound response (SWR) against chewing insects are well-known processes triggered by phloem-mobile signals such as proteins, mRNAs and hormones (Banerjee *et al.,* 2006; Schilmiller and Howe, 2005; Vlot *et al.,* 2008; Zeevart, 2008). In addition, graft-transmissible small RNAs (siRNAs and miRNAs) appear to spread systemically the so-called RNA silencing (Dunoyer *et al.,* 2010; Voinnet *et al.,* 1998). All these examples, and others, make clear that phloem is more than just a system for nutrient circulation in plants and, indeed, it must be considered as a complex network of integrative long-distance communication (Lough and Lucas, 2006; van Bel*et al.,* 2013).

Most plant viruses are well known to use the phloem, mainly the sieve elements (SE), to spread throughout all parts of the plant from the roots to the leaves, fruits, seeds and even pollen (Hipper *et al.,* 2013; Vuorinen *et al.,*2011). Thus, interference with viral long-distance transport in the phloem could contribute to an effective reduction of disease incidence. The phloem plays a key role in plant protection producing and transporting multitude of stress and defense proteins as well as an antioxidant defense system (Gaupels and Vlot, 2012; Kher, 2006; Walz *et al.,* 2002). Some proteins specifically involved in viral-resistance processes have been also identified in phloem. The tobacco cadmium-ion-induced GRP protein (cdiGRP), which is localized in the cell wall of SE and companion cells (CC), blocks the entry of a

tobamovirus into SE from vascular bundles by increasing callose deposition (Ueki and Citovsky, 2002). In addition, the corresponding proteins of *Arabidopsis thaliana* RTM1 and RTM2, two of the five dominant genes involved in resistance to several potyvirus, are specifically localize to SE (Chisholm *et al.,* 2001). On the other hand, phloem proteins have been also shown to facilitate the transport of endogenous (Ruiz-Medrano *et al.,* 1999; Xoconostle-Cazares *et al.,* 1999; Yoo *et al.,* 2000), viral (Requena *et al.,* 2006) and subviral (Gómez and Pallás, 2001, 2004; Gómez *et al.,* 2005; Owens *et al.,* 2001) RNAs as well as to potentially facilitate viral transmission by aphids (Bencharki *et al.,*2010). Thus, the understanding of many plant defense processes against viruses as well as the requirements for host susceptibility will require a detailed knowledge of which proteins are differently accumulated in the phloem during the progress of a viral infection.

The recent application of quantitative "second generation" proteomic techniques, such as differential in gel electrophoresis (DIGE), has significantly facilitated the study of plant-virus interactions through proteomic analysis (see DiCarli *et al.,* 2012 for review). By the other hand, the number of proteins identified in proteomic investigations of the phloem sap is significantly increasing (Anstead *et al.,* 2013; Batailler *et al.,* 2012; Giavalisco *et al.,* 2006; Kehr, 2006; Lin *et al.,* 2009), In this scenario, it is paradoxical that the studies dealing with the comparison of the phloem sap proteome during viral infection were limited to only one (Malter and Wolf, 2011). In that work, authors, using conventional 2D electrophoresis, observed that the infection of melon by *Cucumber mosaic virus* (CMV) induced the up-accumulation of a limited number of phloem proteins including the major latex protein (MLP), an enolase, a translationally controlled tumor protein homolog (TCTP), the heatshock cognate protein 70 and a fifth additional unknown protein (Malter and Wolf, 2011). As could be expected, all of annotated proteins were associated with stress responses.

Yield losses caused by *Melon necrotic spot virus* (MNSV) have great economic impact in melon (*Cucumis melo*)-growing regions worldwide and, at present, the only resistance found to MNSV in melon is that controlled by the single recessive gene *nsv* (Nieto *et al.,* 2006; Truniger *et al.,* 2008). As most plant viruses, the systemic spread of MNSV in melon plants occurs through phloem tissue (Gosalvez-Bernal *et al.,* 2008;

Vuorinen *et al.,* 2011). To better understand the underlying processes that are taking place during MNSV infection of melon which, at the same time, may provide new targets/markers for resistance or susceptibility processes we used a proteomic approach to study and identify phloem proteins differentially accumulated between MNSV-infected and non-infected melon plants. A total of 1046 spots were detected to match across all replicates by two-dimensional difference gel electrophoresis (2D-DIGE) (Larbi and Jefferies, 2009) and 25 were statistically significant differentially accumulated. Most of them corresponded to proteins involved in redox homeostasis and cell death. The identification of these proteins offer new insights into the repertoire of mechanisms that may occurs during plant-virus interaction.

MATERIALS AND METHODS

Plant material, virus inoculation and phloem sampling

Cucumis melo L. subsp. melo cv. Galia plants were kept in a growth chamber, at constant temperature of 23 °C under a 16/8 h light/dark cycle. 6-10 day-old plants were infected by mechanical inoculation of fully expanded cotyledons with purified virions of MNSV-Al isolate (Gosalvez *et al.,* 2003). Mock plants were inoculated with buffer 10 mM Tris-HCl pH 7.3. Phloem sap was collected from well-watered plants 15 days post-inoculation. Briefly, the main stem was cut with a sterile razor between the shoot apex and the first leaf from the top. The exudate was collected using sterile micropipette tips (10 µl) and immediately mixed with 9 volumes of phloem sap collection buffer (7 M urea, 2 M thiourea, 4% 3-[3-chloramidopropyl dimethylammonio]-1-propanesulfonate or CHAPS, and 67 mM DTT). All buffers and samples were kept on ice during phloem sap sampling.

Protein purification and labelling

Four independent assays were performed each of them including 200 MNSV-infected and 40 mock-inoculated melon plants. Phloem exudates collected in each assay were separately pooled according to its origin from healthy (H) or infected (I) plants. Finally, we obtained eight phloem sap samples (H1,H2, H3, H4, I1, I2, I3 and I4) (See experimental system in Supplementary Fig. 1). Total proteins from each pool were

separately purified with 2-D Clean-Up kit (GE Healthcare Life Sciences; Piscataway, NJ, USA) to remove salts and other contaminants that could interfere with the following labeling and gel electrophoresis. Proteins samples were washed and concentrate by precipitation with four volumes of acetone. Pellets were then resuspended in 2D-DIGE labeling buffer (7 M urea, 2 M thiourea, 4% CHAPS, 20 mM Tris pH 8.5). Protein concentration was determined with the Sigma Bradford Reagent using a series of bovine serum albumin (BSA) solutions as protein concentration standards. Total protein yield ranges from 0.086 to 0.65 µg (BSA equivalents)/µl of phloem exudate for healthy plants and from 0.33 to 0.68 µg (BSA equivalents)/µl of phloem exudate for infected plants.

The pH of each sample (H1 to H4 and I1 to I4) containing approximately 50 µg (BSA equivalents) of phloem proteins was adjusted between 8 and 8.5 before they were labeled with CyDye DIGE Fluor saturation dyes (Cy3 and Cy5) (GE Healthcare Life Sciences; Piscataway, NJ, USA). The labeling was carried out adding to each sample 400 pmol of the corresponding cyanine dye (Cy3 or Cy5) for 60 min on ice in darkness. The labeling reaction was stopped by adding 10 nmol of lysine for 10 min. H1, H3, I2 and I4 samples were labeled with Cy3 and H2, H4, I1 and I3 with Cy5. The dye swapping was applied to decrease/eliminate differences due to the variability in labeling efficiency. A mix of equal amount of all samples, four infected and four healthy, was mixed to obtain the internal standard (IS) which was labeled with cyanine dye Cy2 to be run on every gel for quantitative comparisons.

Two dimensional difference gel electrophoresis (2D-DIGE)

2D-DIGE analyses were performed at the proteomic lab facilities at the IBMCP (CSIC-UPV) in Valencia, Spain. A total of four gels were run in a set to obtain statistical analysis of changes in protein abundance between phloem sap from healthy and MNSV infected plants. Each pair of Cy3- and Cy5-labeled protein samples (Cy3-labelled H1+Cy5-labelled-I1, Cy5-labelled-H2+ Cy3-labelled-I2, Cy3-labelled-H3+ Cy5-labelled-I3 and Cy5-labelled-H4+ Cy3-labelled-I4) were mixed together with the IS as described in the Supplementary Fig. 1 and Fig. 2. The four samples (150 µg/BSA equivalents of phloem proteins each one) were resuspended into 65 mM DTT and 1% carrier

ampholytes and applied to immobilized broad range strip gels (Immobiline DryStrip pH 3-11 NL, 24 cm, GE Healthcare Life Sciences; Piscataway, NJ, USA), previously rehydrated overnight with 8 M urea, 4% CHAPS, 1% carrier ampholytes and 12 µl/ml of DeStreak rehydration solution (GE Healthcare Life Sciences; Piscataway, NJ, USA). Isoelectric focusing (IEF) was performed at 20 °C using a gradual increase in voltage up to 8000 V. The program included 300 V for 4 h, 1000 V for 6 h and 8000 V for 3 h to reach a total focusing time of 32 kVh. After IEF, gel strips were equilibrated in 50 mM Tris-HCl pH 8.8, 6 M urea, 30% glycerol and 2% SDS in two steps of 15 min. First step included 2% DTT while 2.5% iodoacetamide was added in the second one. Equilibrated strips were loaded onto 12.5% SDS-PAGE to separate proteins according to their molecular weight. Electrophoresis was carried out at 2 W/gel for about 1h and then 15 W/gel for 6h. All four gels were run simultaneously.

Gel imaging and statistical analysis of the data

Gel imaging was carried out after electrophoresis by fluorescence scanning of cyanine dye-labelled proteins using a Typhoon Trio scanner (GE Healthcare Life Sciences; Piscataway, NJ, USA). The appropriate excitation and emission wavelengths for each Cy2-, Cy3- and Cy5-labelled proteins were used. All images resolution was 200 µm pixel size. The photomultiplier tube voltage was set from 500 to 600 V using normal sensitivity. Scanned images were cropped identically and simultaneously using ImageQuant tools (GE Healthcare Life Sciences; Piscataway, NJ, USA) to exclude non-essential information. Once processed, comparative analysis of the images was performed using two different modules of the DeCyder 2D software version 6.5 (GE Healthcare Life Sciences; Piscataway, NJ, USA). The DIA (Difference In-gel Analysis) module was used to co-detect spot boundaries of H, I and IS groups at each replicate gel. Spot volumes were calculated and normalized versus the volume of the corresponding spot present in the IS of the same gel (standardized abundance). The degree of difference in the standardized abundance between H and I spots was expressed as the average ratio (standardized volume ratio between the two protein spot groups). Gel-to-gel matching of protein spots, followed by statistical analysis of protein abundance change across all the replicates was performed using the DeCyder BVA (Biological Variation Analysis) module. The IS image (Cy2) with the highest number

of spots (1046 spots) was assigned as master image and its spot boundary map was used as template. Statistical significance of the average ratio was analyzed by paired Student's t-test. Protein spots exhibiting differential accumulation with reproducibly (at least in three of the four replicates) and statistical significance $p<0.05$ were selected for further identification by MS/MS or LC-MS/MS. The variability of the data and the Principal Component Analysis (PCA) were determined with DeCyder Extended Data Analysis (EDA) module.

Protein identification by mass spectrometry (MS/MS and LC-MS/MS)

After analysis, gels were stained with silver solution for picking spots of interest. Selected stained spots were excised from the gel with a razor blade and then digested overnight with sequencing grade modified trypsin (Promega) (Shevchenko *et al.,* 1996). Protein identification was performed by the proteomics facility of the Principe Felipe Research Center (CIPF, Valencia, Spain) which is a member of ProteoRed (http://www.proteored.org). The digested peptides were analyzed using a matrix-assisted laser desorption time-of-flight 4700 Proteomics Analyzer with TOF/TOF Optics (Applied Biosystems; Foster City, CA, USA), in positive reflector mode (200 shots per spot). Five of the most intense ions were selected automatically excluding those that correspond to known contamination. MS/MS data was acquired using the default 1kV MS/MS method installed by the manufacturer. Database searches on NCBInr with taxonomic restriction *Viridiplantae* (green plants) (date 2010/02/23) and EST_cucurbitaceae (date 2010/04/01) were performed using the Mascot search engine (Matrix Science, London, UK) via GPS explorer software (Applied Biosystems; Foster City, CA, USA). Mascot protein scores greater than 68 were considered significant with a p value < 0.05. Searches were done with tryptic specificity allowing one missed cleavage and a tolerance on the mass measurement of 100 ppm in MS mode and 0.5 Da for MS/MS ions. Carbamidomethylation of Cys was used as a fixed modification and oxidation of Met and deamidation of Asn and Gln as variable modifications. The samples without a positive identification were analyzed by LC-MS/MS using the Ultimate 3000 nano-LC system HPLC (Thermo Scientific; Amsterdam, NL) and the QSTAR XL nanoESI Q-TOF hybrid mass spectrometer (AB Sciex; Concord, ON, Ca). Samples were loaded onto a PepMap C18 trap column (300 µm x 5 mm, Thermo

Scientific; Amsterdam, NL) at a flow rate of 30 µl/min during 10 min. Peptides were then put into a PepMap C18 analytical column (3 µm, 100 Å, 75 µm x 15 cm; Thermo Scientific; Amsterdam, NL) and eluted at a flow rate of 200 nl/min using a 5-45% linear ACN gradient at 200 nl/min over 90 min. Spectral information was sent to Mascot search engine via Mascot Daemon client using the search parameters and databases defined before (Matrix Science; London, UK). Mascot protein scores greater than 38 were considered significant with a *p* value < 0.05. The last version of *Cucumis melo* genome (v3.5.1) developed and provided by the Spanish Melonomics project (https://melonomics.net/) [42] was used to obtain the functional identification and the complete sequences of the identified proteins. For this purpose a local blastp with the list of MS/MS peptides was used. Phytozome v10 (http://phytozome.jgi.doe.gov/pz/portal.html) and *Cucumis sativus v1.0* genome were used when indicated. The Blast2GO program was used to analyze the gene ontology annotation of the proteins (Conesa *et al.,* 2005).

RNA extraction and RT-PCR analyses

Total RNA was either isolated from 100 µl of phloem sap or from 1 g of leaves tissue of healthy and MNSV-infected melon plants using the TRIzol reagent (Life Technologies; Carlsbad, CA, USA). RT-PCRs were carried out using Invitrogen SuperScript®III One-Step RT-PCR system with Platinum®Taq DNA Polymerase (Life Technologies; Carlsbad, CA, USA). RT-PCR amplifications were performed in 10 µl reaction mixtures with 5 µl of 2x Reaction Mix buffer provided by the supplier, 0.1 µg of total RNA, 0.5 µM of each primer, 10 units of RNase inhibitor and 0.4 µl of enzyme mix. The program used for PCR was 50 °C for 30 min and 95 °C for 2 min followed by 35 cycles at 95 °C for 15 s, 55 °C-68 °C for 30 s (depending on the Tm value of primers) and 68 °C for 30 s; the reaction was terminated with a 10 min extension step at 68°C. The PCR products were separated on a 2% agarose gel stained with ethidium bromide. Pairs of oligonucleotides were designed to amplify the mRNA from six of the proteins identified before, the CmF308 phloem translocable transcript (Omid *et al.,* 2007) as phloem positive control and the RuBisCO small subunit (RBCS) mRNA (Giavalisco *et al.,* 2006; Ruiz-Medrano *et al.,* 1999) as phloem negative control (Supplementary Table 1).

SDS-PAGE and Western blot

The purified proteins were analyzed on 12 % SDS-PAGE under reducing conditions either followed by Coomassie Brilliant Blue staining or Western blot analysis. For Western blot, gels were electrophoretically transferred onto polyvinylidine difluoride membranes (GE Healthcare Life Sciences; Piscataway, NJ, USA). After protein transfer, the membranes were treated with the blocking buffer followed by incubation either with anti-RuBisCO or MNSV virion antibodies. Then, the bands were visualized using the Pierce ECL western blotting substrate (Thermo Scientific; Amsterdam, NL).

RESULTS

Collection of melon phloem exudate

Plant species belonging to the *Cucurbitaceae* family, such as melon, have become model plants for proteome analysis of phloem stream because of the significant amounts of uncontaminated phloem exudate that can be easily collected from incisions in the stem (Cho *et al.,* 2010; Lin *et al.,* 2009; Malter and Wolf, 2011; Walz *et al.,* 2004). This holds true especially for healthy plants but after MNSV infection, melon plants suddenly wilt and lose vigor resulting in a considerable reduction of phloem flow. Herein, a large number of systemically infected plants (approximately 200 plants per biological replicate, BR) were necessary in order to obtain sufficient amount of exudate. In contrast, significantly fewer healthy plants were used (healthy/infected plants ratio 1:5). Two weeks after inoculation, only MNSV-inoculated melon plants with visible symptoms, mainly curly young leaves with chlorotic/necrotic spotting were chosen for exudate collection (Figure 1A). Systemically infected plants that suddenly wilted were discarded. Phloem sap was obtained from 3-leaf stage plants cutting the stem internode which is between the first and the second leaf (white arrow in Figure 1A). Different bioassays were carried out until sufficient amount of proteins to perform four biological replicates (BR) was obtained (see Materials and Methods).

On the other hand, to rule out the possibility of phloem sap contamination by injured neighboring cells during the initial stem cutting, we checked for the presence/absence of RuBisCO large subunit in infected and healthy phloem sap samples (Dafoe *et al.,* 2009; Giavalisco *et al.,* 2006). On western blots, RuBisCO large

subunit (approximately 55 kDa, Figure 1B) was highly abundant in leaf but could not be detected in phloem samples confirming the purity of the isolated proteins.

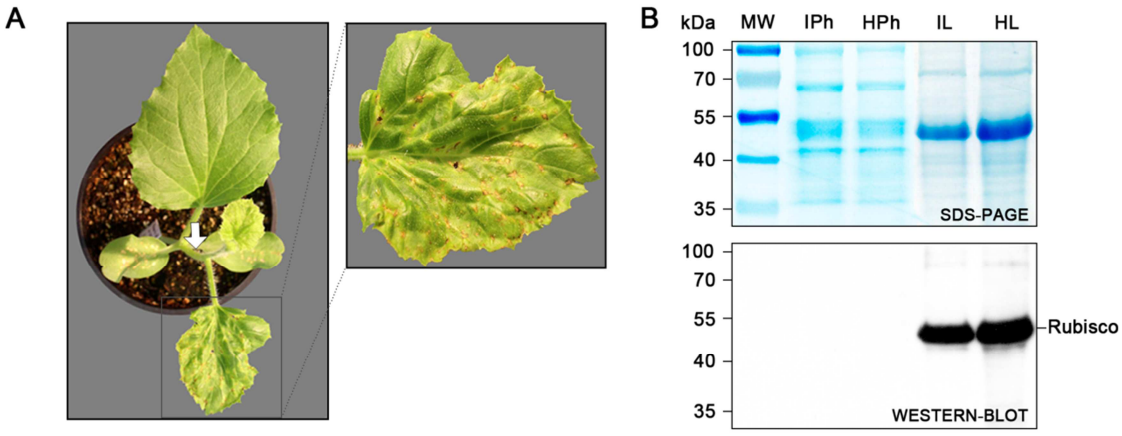

Figure 1. A) The image on the left shows a 3-leaf stage melon plant taken 15 days after MNSV infection. The white arrow points to the stem internode between the first and second leaf that was sectioned to collect the phloem exudate. The image on the right is a magnification of the second leaf showing disease symptoms. B) Comparison between phloem sap (Ph) and leaf (L) proteins from MNSV-infected (I) and healthy (H) melon plants using Coomassie stained SDS-PAGE and western blot with antibodies against the large subunit of RuBisCO. The position of the RuBisCO protein and the molecular weight in kDa of the pre-stained protein marker (MW) are indicated.

Differentially accumulated phloem sap proteins by 2D-DIGE and MS

Two-dimensional difference gel electrophoresis (2D DIGE) was used to compare protein profiles of phloem exudate collected from stem sections of healthy and MNSV-infected melon plants. In order to increase reproducibility and statistical identity significance, a total of 4 BRs were prepared combining the samples as indicated in the Figure 2. Each BR was applied to a 24 cm, 3-11 pH linear gradient strip gels, as first dimension, and then loaded onto a 12.5% polyacrylamide SDS-PAGE, as the second one. BRs contained also a pooled internal standard which effectively eliminates gel-to-gel variation and avoid the use of technical replicates. Moreover, IS was used to derive statistical data between gels (Figure 2).

Upon software-aided automatic detection, background subtraction, quantification, normalization and inter-gel matching of fluorescent images, a systematic statistical analysis (Student's t-test significance $p<0.05$) of all replicates determined that from a total of 1046 matched spots across all four gels, only 25 had significant changes in abundance in at least three of the four independent BRs. Principal component analysis

(PCA) was applied to the entire set of variable spots taking into account the four BRs. First principal component revealed a separation between samples from MNSV-infected exudates and those from healthy controls (Supplementary Fig. 2). Therefore, the 25 variable spots were excised from gels (Figure 3) and subjected to MS/MS and LC-MS/MS. Three of the spots (white numbers in Figure 3) did not produce positive identification neither using MS/MS nor LC-MS/MS but the rest of the 22 processed spots (13 of them up-accumulated and 9 down-accumulated) lead to the identification of 19 single proteins with no contamination with other putative co-migrating protein species. MASCOT search was initially performed against the NCBInr and EST_Cucurbitaceae databases using the Mascot algorithm and common contaminants like keratins were not found. However, functional description of most of them as well as the complete amino acid sequence was lacking (Supplementary Table 2). During the course of this study the complete genome of *C. melo* was accessible through the MELONOMICS website (http://melonomics.net) (García-Mas *et al.,* 2012). Thus, we performed an additional blastp against the *C. melo* genome (v3.5.1) with the list of peptides identified by mass spectrometry (Supplementary Table 3 and Supplementary Table 4 provide all peptides information for protein identification) and using the server cluster of our bioinformatics core resource. Protein sequences with top hit scores obtained were confirmed to match with the sequence of peptides obtained before (Supplementary File 1) and the functional description was determined by Melonomics database searching (Supplementary Table 2). All protein spots were properly classified by function except that from spot 1014 that produced a positive match with no functional description in melon genome and showed also no significant homology with known *A. thaliana* sequences (The Arabidopsis Information Resource, TAIR). In this case, BLAST search was repeated with the MELO3C01086691 sequence (corresponding to spot 1014) using phytozome v10 portal and *Cucumis sativus v.10* genome leading finally to the functional annotation of the spot 1014 as an EF hand family calcium-binding protein (Score 199, 1.3e-66, identity 89.2%) (Supplementary Table 2). Table 1 reports the spot number, accession number according to Melonomics database, functional description as provided by melonomics/phytozome, mean value of the standardized ratio between healthy and infected groups, Student's t-test *p*-value obtained for every matched spot-set, comparing the average and standard deviation of

protein abundance for a given spot between the healthy and infected groups, Mascot protein scores, number of matched peptides, percentage of sequence coverage and theoretical MW and pI.

The suite of proteins identified in our analysis was generally consistent with reports from other species indicating that are phloem constituents, and obvious contaminants were not apparent (Table 2). Only two of the differentially accumulated proteins had never been described to be present in the phloem before: the carboxylesterase 6 (spots 588 and 592), a protein with homology to the tobacco hypersensitivity-related hsr203J (Pontier *et al.,* 1994), and the fumarylacetoacetate hydrolase 1 (spot 935), a novel defense/stress-related gene (Kottapalli *et al.,* 2007; Lee *et al.,* 2010). In certain instances two spots were matched to a unique protein: the carboxylesterase 6 (CXE6) (spots 588 and 592), the phospholipid hydroperoxide glutathione peroxidase 6 (GPX6) (spots 1017 and 1019) and the aldose-1-epimerase (AEP) (spots 517 and 553). This situation has been commonly assumed to be due to the presence of different protein species with different maturation states, degradation and/or post-translational modifications (Gorg *et al.,* 2004). Interestingly, CXE6 588 and GPX6 1017 spots were up-accumulated while CXE6 592 and GPX6 1019 spots were down-accumulated. Likewise, similar situation has been also observed in other previously reported proteomic studies where the same identified proteins matched with both up and down-accumulated spots (Neilson *et al.,* 2011; Xu *et al.,* 2013) Both AEP 517 and 553 spots were up-accumulated.

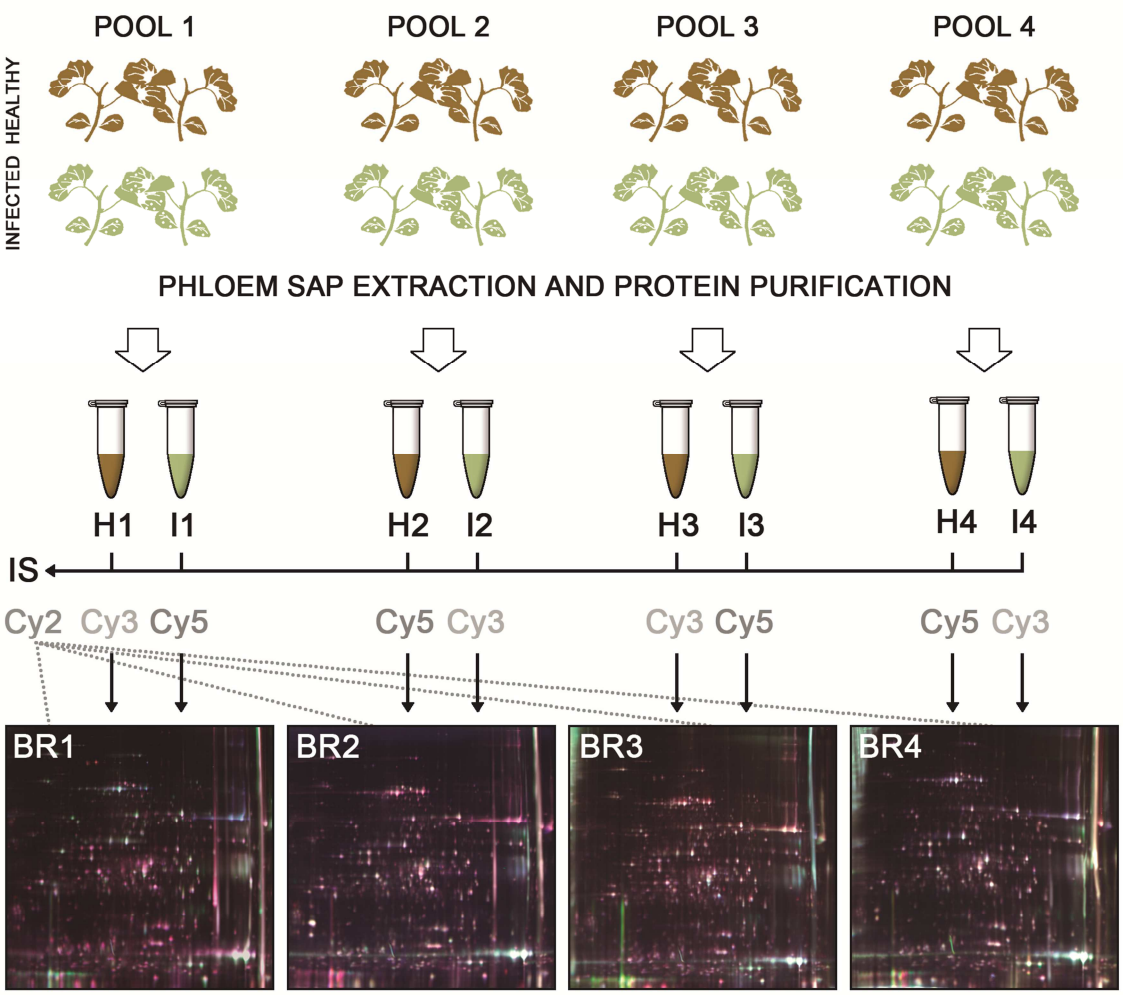

Figure 2. Schematic outline of the 2D DIGE study used to compare protein profiles of phloem exudate collected from stem sections of healthy and MNSV-infected melon plants. Healthy (H) and infected (I) purified protein from phloem sap different collection date were divided into 4 subgroups and labelled with cyanine dye (Cy3 or Cy5). To remove experimental gel-to-gel variation, aliquots of all samples were mixed to create a pooled internal standard (IS) that was labelled with cyanine dye Cy2. The samples were combined as indicated in the figure to generate four biological replicates (BR) and then separated by 2D-DIGE. An overlay of the three fluorescence images of each BR is shown.

Gene ontology classification of differentially accumulated proteins

On the basis of the gene ontology (GO) annotations, the differently accumulated phloem proteins were grouped into their probable biological processes (Supplementary Figure 3) and molecular functions (Supplementary Figure 4) using percentages of second level GO terms. GO analysis revealed the participation of 16 putative proteins in 8 biological processes. Among them, metabolic processes were the most represented with 15 gene products (35%) mainly involved in carbohydrate (7 GO

terms), lipid (2 GO terms), protein (2 GO terms) and nitrogen compound (2 genes) primary metabolic process and catabolic process (6 GO terms). The second largest group corresponded to putative proteins encoded by 11 genes (26%) and involved in cellular process. Response to stimulus which included stress and abiotic stimulus was the third largest group (10% and 4 GO terms) whereas the other biological processes were represented at a much lower scale.

In terms of molecular function, the most represented functions were catalytic activity and binding, accounting for 55% (15 GO terms) and 41% (11 GO terms) of the total annotations, respectively, and only followed by enzyme regulator activity (4%). Under catalytic activity most of the sequences were related with hydrolase activity (5 GO terms) and transferase activity (3 GO terms). Concerning the binding function, the largest group (6 GO terms) was that of binding to small molecules such as nucleotides. There were no relevant differences in GO classification between up-accumulated and down-accumulated groups of proteins (Figures S1 and S2) except for a small enrichment of GO terms associated with hydrolase activity in the former.

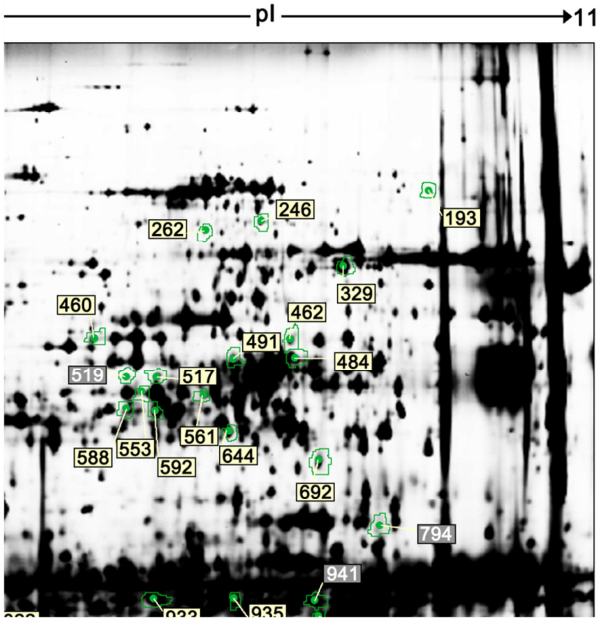

Figure 3. Image corresponding to the silver staining of one of the three 2D DIGE biological replicates selected to protein spot picking. The 25 differently accumulated protein spots observed after MNSV infection in phloem sap are outlined and tagged with their respective spot numbers. The three spots tagged with white numbers did not produce mass spectrum neither using MS/MS nor LC-MS/MS but the rest of the 22 processed spots (black numbers) was properly identified as it is shown in Table 1.

Analysis of the phloem exudate for the presence of the mRNAs of some identified proteins by RT-PCR

It was anticipated that protein synthesis did not take place in mature enucleate SE and that proteins herein should be synthesized in the neighboring companion cells to further enter into the translocation stream. However, after the identification in phloem sap of a large number of proteins involved in translation, this common notion must be reassessed considering feasible the translation of some phloem proteins from phloem sap mRNAs (Lin *et al.,* 2009). In this sense, grafting experiments also revealed that only six of 43 mRNA molecules were able to traffic long distances indicating that not all phloem sap transcripts are constituents of the whole-plant communication network but must be involved in local functions (Omid *et al.,* 2007). Knowledge of which phloem proteins encoding-mRNAs are also found into SE with its corresponding polypeptide and if they are also regulated in some way may provide valuable information on this topic.

In order to verify if the levels of phloem proteins that were differentially accumulated during MNSV infection correlated with global changes in gene expression, total RNAs from leaf and phloem sap samples of either control or MNSV-infected plants were subjected to a qualitative RT-PCR validation of six selected genes (Figure 4). CXE6 and GPX6 were chosen for the singular up and down-accumulation observed at each of the two spots where such proteins were identified. T-Complex protein 1 (TCP1), polyadenylate-binding protein 2 (PAB2) and 3-ketoacyl-CoA synthase 7 (KCS7) were all of them down-accumulated. Finally, FAH was taken as an example of an up-accumulated protein. Moreover, CXE6 and FAH were specially chosen because none of them was identified in phloem exudates before. The melon Aux/IAA transcript CmF-308 was used as a down-regulated phloem mRNA positive control (Omid *et al.,* 2007). *CXE6* and *KCS7* transcriptional expression was slightly reduced in MNSV infected leaf but the rest of the selected genes levels showed no significant differences. In contrast, the amount of the four transcripts that were detected in phloem was considerably reduced in infected phloem samples except that of FAH that showed similar levels in healthy and infected samples (Figure 4). KCS7 transcript was not detected in phloem. As an additional quality control, phloem RNAs were analyzed by RT-PCR with primers

against the coding sequence of the green tissue-specific Rubisco small subunit (RBCS) mRNA (Giavalisco *et al.,* 2006; Xoconostle-Cazares *et al.,* 1999). Although *RBCS* transcripts were readily detected when using RNA leaf extracts as template they were not detected within the RNAs obtained from the phloem exudates (Fig. 4). This experiment established that contamination produced during the harvesting process originating from tissues outside of the SE must have been present at a low level. From these results one can argue that some transcripts could be loaded and translated into the SE. Thus, selective regulation of the phloem entry of these mRNA could result in a rapid variation of the stationary steady of the corresponding phloem proteins. On the other hand, it is known that protein kinases and glycosylation enzymes are present in phloem exudates (Nakamura *et al.,* 1995; Rodriguez-Medina *et al.,* 2011). Thus, phloem protein turnover/post-translational modifications might account for the up and down-accumulation of CXE6 and GPX6 spots.

Validation of the absence of the MNSV coat protein in phloem

Since the viral CP is required in abundance for encapsidation, it commonly appears as a prominent spot in 2D gels mass spectrometry that in some instances has been used for virus detection and identification (Casado-Vela *et al.,* 2006). However, our 2D DIGE comparative study did not reveal the MNSV CP (p42) (Riviere *et al.,* 1989) as a differentially accumulated protein most likely suggesting that it may be absent in phloem sap or, alternatively, present in very low abundance. In order to verify this observation, we checked several phloem protein samples by western blot. Proteins from cotyledons and young symptomatic leaves of MNSV-infected melon plants (15 dpi) and similar samples from healthy plants were included into the analysis. Commercial antibodies directed against the MNSV CP recognized the corresponding polypeptide, at approximately 42 kDa, which was highly abundant in infected cotyledons but significantly less accumulated in leaf. In contrast, CP was never detected in phloem samples (Figure 5).

Table 1. Summary of phloem sap proteins differentially accumulated during MNSV infection of melon plants

Spot	Melon accession	Protein identification in melon	Mascot score	Ratio (a)	p-value (b)	Matched peptides	Sequence coverage (%)	MW (kDa) (c)	pI (d)
Cell death-related proteins									
262	MELO3C004636P1	T-Complex protein 1/cpn60 chaperonin	80	-1.58	0.017	3	7	57.20	5.77
491	MELO3C010898P1	Serine protease inhibitor (SERPIN)	133	1.51	0.035	8	19.8	42.79	6.27
561	MELO3C009549P1	Putative deoxyribonuclease TATDN1	90	1.2	0.013	4	17.3	36.20	5.81
588	MELO3C011389P1	Carboxylesterase 6	105	1.39	0.0048	2	42.5	37.15	5.52
592	MELO3C011389P1	Carboxylesterase 6	375	-1.39	0.032	4	59.5	37.15	5.52
935	MELO3C006680P1	Fumarylacetoacetate hydrolase 1	42	1.79	0.025	1	7.3	23.72	6.21
1022	MELO3C026618P1	3-ketoacyl-CoA synthase 7	40	-2.18	0.032	1	2.7	49.90	9.10
Proteins involved in redox homeostasis									
246	MELO3C008985P1	Glucose-6-phosphate 1-dehydrogenase	64	-1.42	0.047	2	10.7	29.23	8.40
329	MELO3C020429P1	Serine hydroxymethyltransferase	231	-1.4	0.042	4	42.9	52.00	6.77
462	MELO3C002816P1	Obg-like ATPase 1	105	1.35	0.045	4	12.9	44.37	6.36
644	MELO3C014584P1	Dihydroflavonol 4-reductase	86	1.24	0.015	5	14.5	35.53	6.00
1017	MELO3C005666P1	Phospholipid hydroperoxide glutathione peroxidase 6	90	-1.37	0.033	1	41.9	26.76	9.20
1019	MELO3C005666P1	Phospholipid hydroperoxide glutathione peroxidase 6	158	1.57	0.049	12	37.3	26.76	9.20
Other stress related proteins									
460	MELO3C018626P1	12-oxophytodienoate reductase	84	1.72	0.049	3	17.5	42.02	5.94
517	MELO3C017363P1	Aldose 1-epimerase	49	1.35	0.018	1	3	37.17	5.65
553	MELO3C017363P1	Aldose 1-epimerase	152	1.35	0.041	5	13.4	37.17	5.65
692	MELO3C005621P1	Rhamnose biosynthetic enzyme	104	-1.23	0.0049	6	20	33.57	6.25
975	MELO3C011984P3	Polygalacturonase	51	-1.57	0.033	2	12.5	23.44	6.44
Putative virus-interacting proteins									
193	MELO3C018462P1	Polyadenylate-binding protein 2	56	-1.42	0.045	2	5.5	70.59	6.39
262	MELO3C004636P1	T-Complex protein 1/cpn60 chaperonin	80	-1.58	0.017	3	7	57.20	5.77
484	MELO3C024519P1	Fructose-1,6-bisphosphate aldolase	239	1.16	0.013	9	26.8	38.44	6.96
933	MELO3C011172P1	Proteasome subunit beta type 6	154	1.33	0.012	3	44.3	19.08	5.74
1014	MELO3C010866P1	EF hand family calcium-binding protein *	56	1.36	0.012	2	20.4	12.17	5.77

(a) *Mean value of the standardized volume ratio. Up-accumulation/ down-accumulation is indicated by positive/negative ratio values, respectively*
(b) *p-value obtained from t-Student test ($p<0.05$).*
(c) (d)*Theoretical MW and pI*

4. Discussion

In this study we used the 2D DIGE to compare changes in protein accumulation between phloem exudates from healthy and MNSV-infected melon plants. Our results revealed that MNSV infection did not lead to highly dramatic changes in the overall phloem sap protein profile but this finding has been previously reported to be usual in similar stress-related studies that were performed with common 2D gels on phloem proteome. Infection of melon by CMV revealed increased accumulation of no more than five proteins [35] and only two sieve-tube sap proteins, pop3/SP1 protein, and a thaumatin-like protein, were reported to accumulate in poplar (*Populus deltoides*) in response to wounding [47]. On the other hand, drought treatment in cucumber and pumpkin induced an increase in sieve-tube exudate activity of several antioxidant enzymes (superoxide dismutase, dehydroascorbate reductase, peroxidase) [17, 18]. One can argue that phloem responses to stress may be dependent on activity modifications of enzymes already present at a steady state level in sieve tubes. Considering that using 2D DIGE we detected significantly more differential changes than in previous works, it seems to be too early to draw such a conclusion with the few published papers. Therefore, the emergence of the 3rd generation of proteomics methods will help drive us towards new major advances on this subject.

On the other hand, it is clear from our results that the majority of the differentially accumulated proteins were linked to redox homeostasis and cell death. Other few proteins were related with acid jasmonic synthesis, energy metabolism and cell wall modification under stress conditions and putative viral complex interacting proteins.

Table 2. Presence of the differentially accumulated phloem proteins in MNSV-infected melons in previously characterized phloem proteomes from other species

Spot	Protein/function	*Cucurbita*[a,b] *maxima*	*Cucumis*[b] *sativus*	*Brassica*[c] *napus*	*Brassica*[d] *oleracea*	*Oriza*[e] *sativa*	*Arabidopsis*[f] *thaliana*	Hybrid[g] poplar	*Lupinus*[h] *albus*
588/592	Carboxylesterase 6								
935	Fumarylacetoacetate hydrolase 1								
1019/1017	Glutathione peroxidase 6	gi|148615524				gi|115447759			AAP69867
553	Aldose 1-epimerase	FG227041_1 gi|15242099					At3g17940		
460	12-oxophytodienoate reductase						At1g76680*		
933	Proteasome subunit beta type 6	FG227184_1	AAG25896		At4g31300				XP002510414
1014	EF hand family calcium-binding protein	gi|157358048							
484	Fructose-bisphosphate aldolase 5	FG227018_2		At3g52930	At3g52930		At2g21330 At4g38970		NP001118453
561	Putative deoxyribonuclease TATDN1	FG227314_3							
644	Cinnamoyl CoA reductase-like protein	FG227808_3	NP913999		At5g19440				
491	Serine protease inhibitor (SERPIN)	gi|9937311				gi|115454103	At1g47710		
462	Obg-like ATPase 1	FG226976_3		At1g30580					
262	T-Complex protein 1/cpn60 chaperonin	FG227673_1							
692	Rhamnose biosynthetic enzyme	FG227180_4							
193	Polyadenylate-binding protein 2	gi|7528270							
1022	3-ketoacyl-CoA synthase 7	FG227260_2 gi|1129145 gi|393707			At2g33150 At5g46290				
975	Polygalacturonase	FG227297_3					At3g14040		
329	Serine hydroxymethyltransferase	FG227611_3					At4g13930*	829808	
246	Glucose-6-phosphate 1-dehydrogenase	gi|3021510*			At5g40760*			736146	

[a] Lin *et al.*, 2009; [b] Walz *et al.*, 2004; [c] Giavalisco *et al.*, 2006; [d] Anstead *et al.*, 2013; [e] Aki *et al.*, 2008; [f] Batailler *et al.*, 2012; [g] Dafoe et al., 2009; [h] Rodriguez-Medina *et al.*, 2011

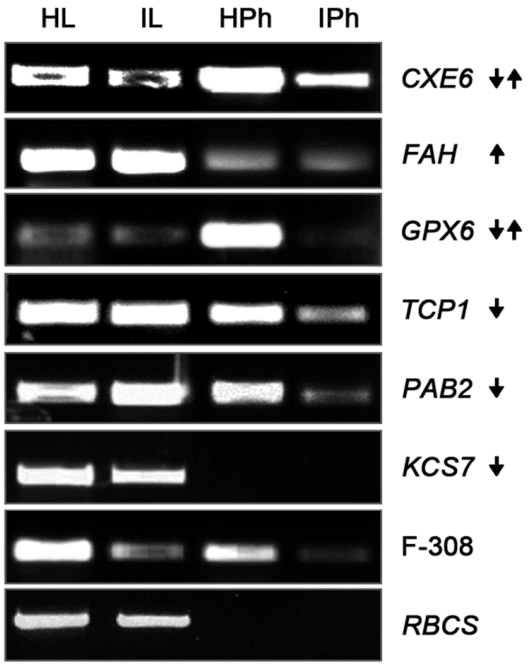

Figure 4. Detection by RT-PCR of the encoding mRNA corresponding to six selected proteins that were differently accumulated in phloem sap after MNSV infection. Leaf (L) and phloem sap (Ph) RNAs from MNSV-infected (I) and healthy (H) melon plants were used as templates. CXE6: carboxylesterase 6 mRNA. GPX6: Phospholipid hydroperoxide glutathione peroxidase 6 mRNA. FAH: Fumarylacetoacetate hydrolase mRNA. TCP1: T-Complex protein 1/cpn60 chaperonin mRNA. PAB2: Polyadenylate-binding protein 2 mRNA. KCS7: 3-ketoacyl-CoA synthase 7 mRNA. F-308: melon Aux/IAA transcript CmF-308. RBCS: RuBisCO small subunit mRNA. The arrows pointing up and down indicate up and down-accumulation, respectively.

Proteins involved in redox homeostasis

Plants appear to purposefully generate ROS as byproducts of various metabolic pathways but also as signaling molecules to control various processes such as pathogen defense, cell death and development (Apel and Hirt, 2004). Therefore, plants are provided with mechanisms to control the redox homeostasis and, in this way, the role of phloem in the maintenance of the redox balance has been supported by the fact that SEs of cucurbit plants contains a complete set of functional antioxidant proteins (Walz *et al.,* 2004). Among previously described proteins, we found increased abundance of both positive and negative regulators of oxidative stress response. The phospholipid hydroperoxide glutathione peroxidase (PHGPx) functions in scavenging of phospholipids hydroperoxides and acts as a cytoprotective protein under oxidative, salt and heat stresses (Chen *et al.,* 2004; Dixon *et al.,* 2002; Navrot *et al.,* 2006). The dihydroflavonol 4-reductase (DFR) is a key enzyme in the anthocyanin biosynthesis that uses NADPH as cofactor therefore affecting NAD homeostasis (Hayashi *et al.,*

2005). In addition, anthocyanins have been described to show essential physiological functions, such as antioxidative, antimutagenic and anticancer activities (Wang *et al.,* 2013. In contrast to the previous enzymes, it has been reported that up-regulation of Obg-like ATPases may act as a negative regulator of oxidative stress response in mammalians, prokaryotes and plants most likely to prevent defense response from provoking excessive self-damaging (Cheung *et al.,* 2010; Wenk *et al.,* 2012; Zhang *et al.,* 2009.

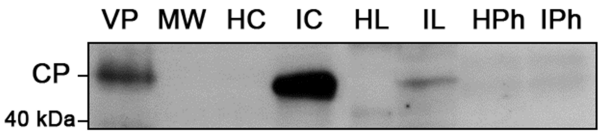

Figure 5. Comparison between phloem sap (Ph), leaf (L) and cotyledon (C) proteins from MNSV-infected (I) and healthy (H) melon plants using western blot with antibodies against the coat protein of MNSV. The position of the coat protein (CP) and the molecular weight in kDa of the protein marker (MW) is indicated. Proteins from purified MNSV viral particles (VP) were used as control.

Conversely, the activity and levels of some ROS detoxifying enzymes (like ascorbate peroxidases and catalases) may be repressed in different plant-pathogen interactions. This suppression of ROS detoxifying mechanisms is crucial for the onset of programmed cell death (Apel and Hirt, 2008). In this sense, the serine hydroxymethyltransferase (SHMT) that functions in the photorespiratory pathway and the glucose-6-phosphate dehydrogenase (G6PDH) that is responsible for the first reaction of the pentose phosphate pathway were both down-accumulated. Deficiency of SHMT interferes with the activation of defense responses and increase oxidative stress (Moreno *et al.,* 2005) while G6PDH is the main responsible for the production of cellular NADPH and for preserving the cellular balance of glutathione that is essential in resistance to oxidative stress in plants (Wang *et al.,* 2008. Changes in the accumulation of these redox-related enzymes may be involved in fine-tuned modulation of the ROS-antioxidant interaction which in phloem has a dual function: maintenance of redox states in SE and ROS-mediated signaling.

Cell death-related proteins

In many non-host and incompatible host plant-microbe interactions, the oxidative burst precedes a form of localized cell death (LCD) which includes the induction of defense-associated genes, proteolytic and nucleolytic events and the initiation of death-associated signals such as calcium, ROS, salicylic acid, and sphingolipids. This phenomenon is collectively known as the hypersensitive response (HR) (Zurbriggen *et al.,* 2010). HR was thought to be designed to restrict pathogen advance but it is known that during susceptible interactions many virulent pathogens also induce cell death with apoptotic features (Greenberg and Yao, 2004).

Thus, the two previously undetected phloem proteins identified in this study were both up-accumulated and considered negative regulators of cell death: a carboxylesterase (CXE) that showed 65% of identity with the HR-specific marker HSR203J of *N. tabacum* and a fumarylacetoacetate hydrolase (FAH) that catalyzes the final step in tyrosine degradation pathway. Transgenic plants with non-functional HSR203J showed intensified HR and greater pathogens resistance (Gershater and Edwards, 2007. Likewise, disruption of FAH leads to the accumulation of tyrosine degradation intermediates that are toxic for plant cell and cause cell death (Han *et al.,* 2013). Also up-accumulated, the serine protease inhibitor (serpin) has been found in *A. thaliana*, rice, pumpkin and melon exudates. Serpins have been shown to mainly act on serine proteases but also on caspases, metacaspase-like proteins and papain cysteine proteases. Indeed, when sufficient AtSerpin1 is present in the cytoplasm, cell death is prevented suggesting that plant serpins may have an essential role in plant defense regulating the host immune response (Lampl *et al.,* 2010; Law *et al.,* 2006; Li *et al.,* 2013). In addition, it has been suggested that phloem proteinase inhibitors may play a role in protecting phloem-mobile RNA-binding proteins from proteolysis during their long-distance journey from the source to sink regions of the plant (Lin *et al.,* 2009). Remarkably, these proteinase inhibitors have been shown to form part of the ribonucleoprotein complexes potentially involved in RNA trafficking (Ham *et al.,* 2014). Finally, we found also down-accumulation of 3-ketoacyl-CoA synthase (KCS), an enzyme that is involved in very long chain fatty acid synthesis, the precursors for the sphingolipids. Recent studies indicated that multiple steps of the sphingolipids

biosynthetic pathway are activated by infection resulting in cell death and resistance (Hause *et al.,* 2003). Therefore both up-accumulation of the former three proteins and down-accumulation of KCS are all of them related with cell death inhibition as would be expected for a susceptible interaction such as that of melon with MNSV.

By contrast, up-accumulation of the deoxyribonuclease TATDN1 could be associated with the nucleolytic events that occur during cell death. In general nucleases are involved in host defense against foreign nucleic acid molecules (Hsia *et al.,* 2005), even some PR proteins have DNase and RNase activity (Guevara-Morato et al 2010; Pereira *et al.,* 2014). However TATDN1 has been described as a conserved nuclease directly implicated in apoptotic DNA fragmentation in yeast and *Caenorhabditis elegans* (Yang *et al.,* 2012). Another evidence of cell death may be the down-accumulation of the TCP1/cpn60 protein, a chaperonin required for the correct folding and subsequent assembly of polypeptides into functional oligomeric enzymes. It was reported that TCP1/cpn60 may be a target of metacaspase 9 (AtMC9), a cell-death related protease in *A. thaliana* (Xu *et al.,* 2008). Interestingly, the proteolytic activity of AtMC9 is regulated among other possibilities by AtSerpin1 (Vercammen *et al.,* 2006).

Other stress related proteins

The transport of oxylipin signal jasmonic acid (JA) through the phloem has been shown to be induced in response to pathogen infection. Several JA biosynthetic enzymes (allene oxide synthase, allene oxide cyclase, and lipoxygenase) have been located in tomato SE suggesting that JA is not only transported but also synthesized, at least in part, within phloem cells (Hause *et al.,* 2003). Lipoxygenase has been also found in cucurbit phloem exudates but the 12-oxophytodienoate reductase 3 (OPR3), the enzyme that catalyzes the NADPH-dependent reduction of 12-oxophytodienoic acid (OPDA), have been located only in *A. thaliana* SEs (Batailler *et al.,* 2012; Walz *et al.,* 2004). In the present study, we also found up-accumulation of an OPR-like protein that could be involved in positive feedback regulation of JA biosynthesis in phloem cells as proposed for AtOPR3 (Li *et al.,* 2013). Evidence that oxylipins may be positive

regulators of cell death responses induced by compatible virus infections that lead to systemic necrosis has been reported (García-Marcos *et al.,* 2013).

Additionally, the abundance of the spots corresponding to two proteins involved in the generation of energy and carbohydrate metabolism, aldose 1-epimerase (AEP) and fructose-1,6-bisphosphate aldolase (FBPA), was also increased. Expression of both proteins has been shown to undergo changes in response to many biotic and abiotic stresses but its specific role remains unclear (Caplan *et al.,* 2009; Fan *et al.,* 2009; Gilardoni *et al.,* 2010; Trapphoff *et al.,* 2009; Zhang *et al.,* 2011). They could participate in increasing the availability of substrates required for increased metabolic activity but alternatively, AEP may reinforce cell wall in response to water stress conditions. It is known that, under drought, properties of the cell wall can be modified by the synthesis of polysaccharides such as homogalacturonan, rhamnogalacturonan-II and rhamnogalacturonan-I with lateral chains of arabinans, galactans and highly branched arabinogalactans that are able to influence the hydration properties of the wall (Piro *et al.,* 2003). In our case, rearrangement of cell wall polysaccharides was evident by the reduced accumulation of a rhamnose biosynthetic enzyme and a polygaracturonase, two proteins related with pectic polysaccharides metabolism. It is possible that wilt and vigor loss in MNSV-infected plants could be sensed as water deficit triggering the drought response. In this sense, it has been demonstrated that plants infected with RNA viruses exhibited significantly improved tolerance to desiccation indicating an activation of the drought response (Xu *et al.,* 2008).

Putative virus-interacting proteins

Although MNSV RNAs were previously detected by Northern-blot analysis of total RNAs isolated from phloem sap of infected plants (Herranz *et al.,* 2015), our efforts to detect the MNSV CP using specific antibodies failed indicating that the CP might not be a component of the viral movement complex, whose composition is still far to be resolved. However, CP was demonstrated to be required for MNSV systemic movement (Genovés *et al.,* 2006), pointing towards an essential role of the CP either in phloem uploading or in suppression of systemic plant defense response.

Interestingly, three of the differently accumulated phloem proteins found in the present study, the fructose-1,6-biphosphate aldolase, a proteasome subunit beta type 6, and the chaperonin TCP1/cpn60, were previously identified by mass spectrometry from the complexes formed by a plant virus (*Rice yellow mottle virus*, RYMV) and the proteins of its natural host (rice) (Brizad *et al.,* 2006). Brizard *et al.,* demonstrated that host proteins were still in viral complexes after high salt concentration extraction suggesting that their interaction with virus particles was strongly specific. Whether these proteins are components of the viral movement complex (VMC) that moves through the phloem and its specific role remains to be elucidated. In addition, the polyadenylate-binding proteins (PABP), an abundant type of translation initiation factors that binds to the polyadenylated end of mRNA, have been shown to enhance the translation of uncapped and nonpolyadenylated RNAs of *Red clover necrotic mosaic virus* (RCNMV) by its interaction with a cap independent translation enhancer element (CITE) (Iwakawa *et al.,* 2012). MNSV as RCNMV belongs to the *Tombusviridae* family and both have a functional CITE (Miras *et al.,* 2014; Truniger *et al.,* 2008). Therefore, MNSV may also require PAPB for the translation of its proteins in vegetative tissues where virus replicates and this situation could indirectly affect the levels of PABP in phloem. Remarkably, PABP has been previously detected in the phloem of *C. maxima* (Lin *et al.,* 2009) and it can be considered as part of a set of phloem RNA-binding proteins (Ham *et al.,* 2014; Lin *et al.,* 2009; Pallás and Gómez, 2013) potentially involved in the vascular translocation of viral or endogenous RNAs.

CONCLUSIONS

The results of this study show that MNSV produces changes in melon phloem composition of proteins. We could identify 19 phloem proteins which abundance was altered during MNSV infection. Two of them were not reported before in proteomic approaches but all the rest was previously described in the phloem sap of other related and non-related species. From these analyses it can be concluded that the majority of the differently accumulated proteins can be considered to be involved in controlling both redox balance during oxidative stress and defense. In accordance with the compatible interaction between MNSV and melon plants, some of them were related, direct or indirectly, to cell death or HR response suppression. Further studies

may be needed to fully understand the role of these proteins during viral systemic infection.

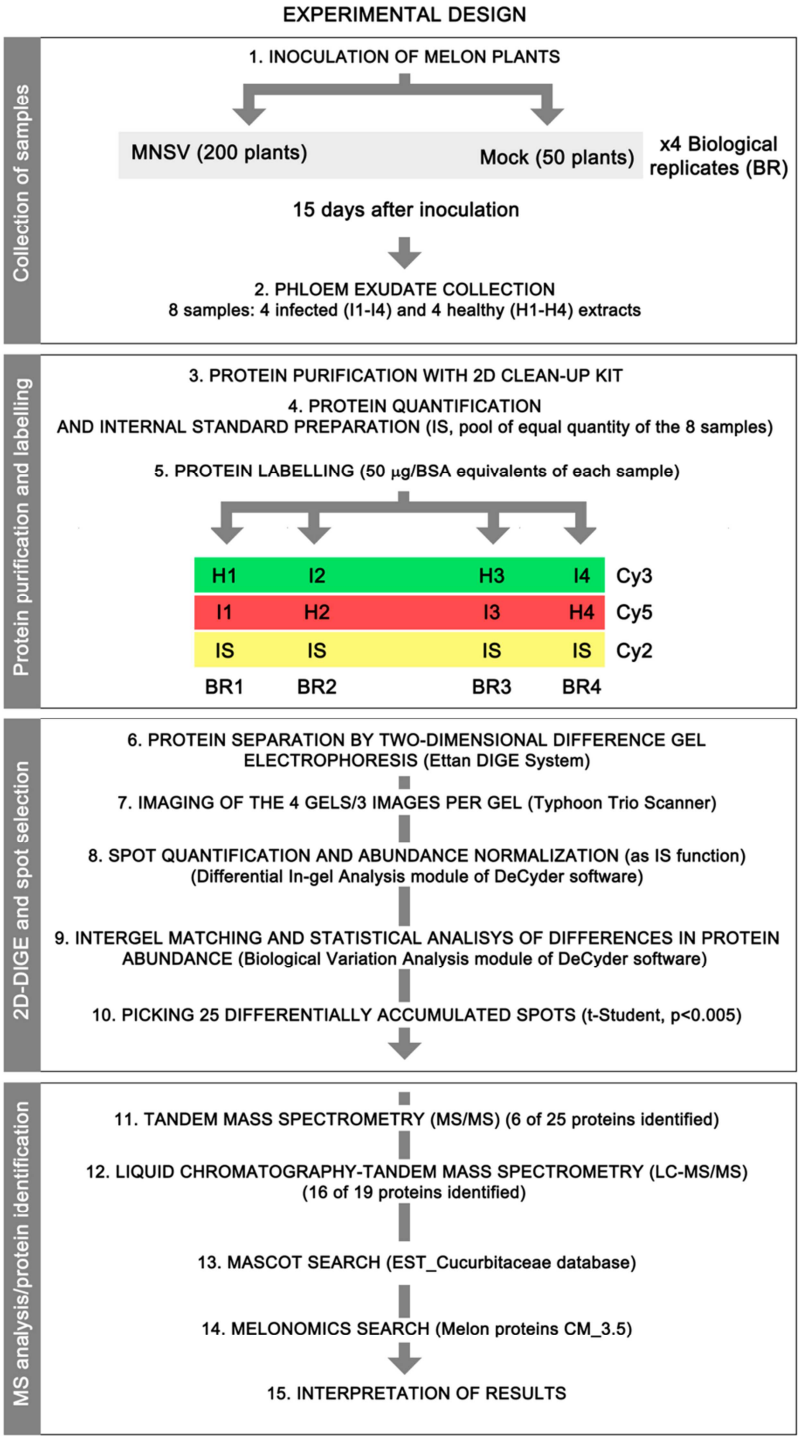

Supplementary Figure 1. Schematic picture of the experimental system used for the identification of differentially accumulated proteins in phloem exudates of melon plants during MNSV infection.

SUPPORTING INFORMATION

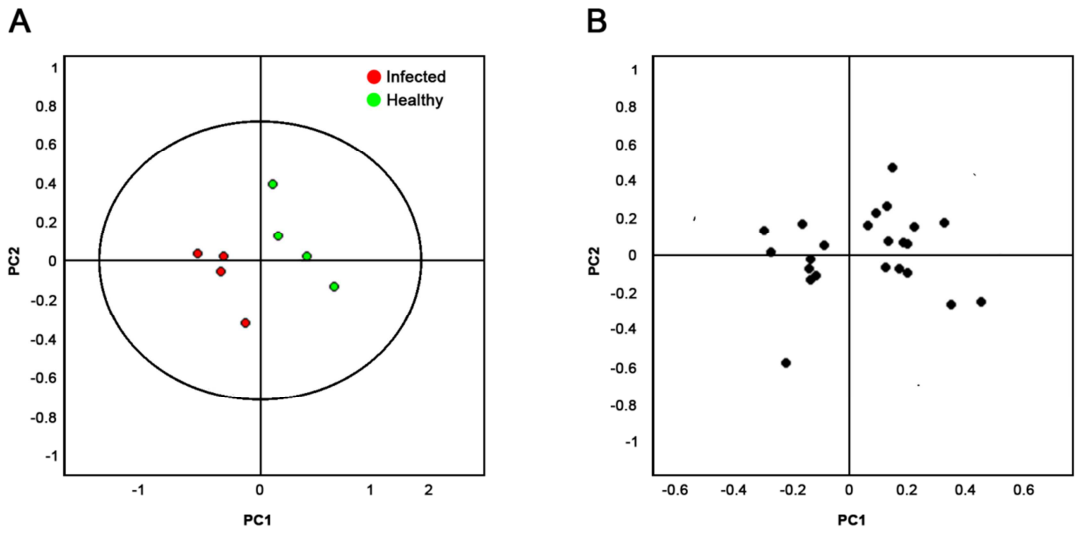

Supplementary Figure 2. Principal component analysis (PCA) applied to the samples (A) and the whole set of differential spots (B).

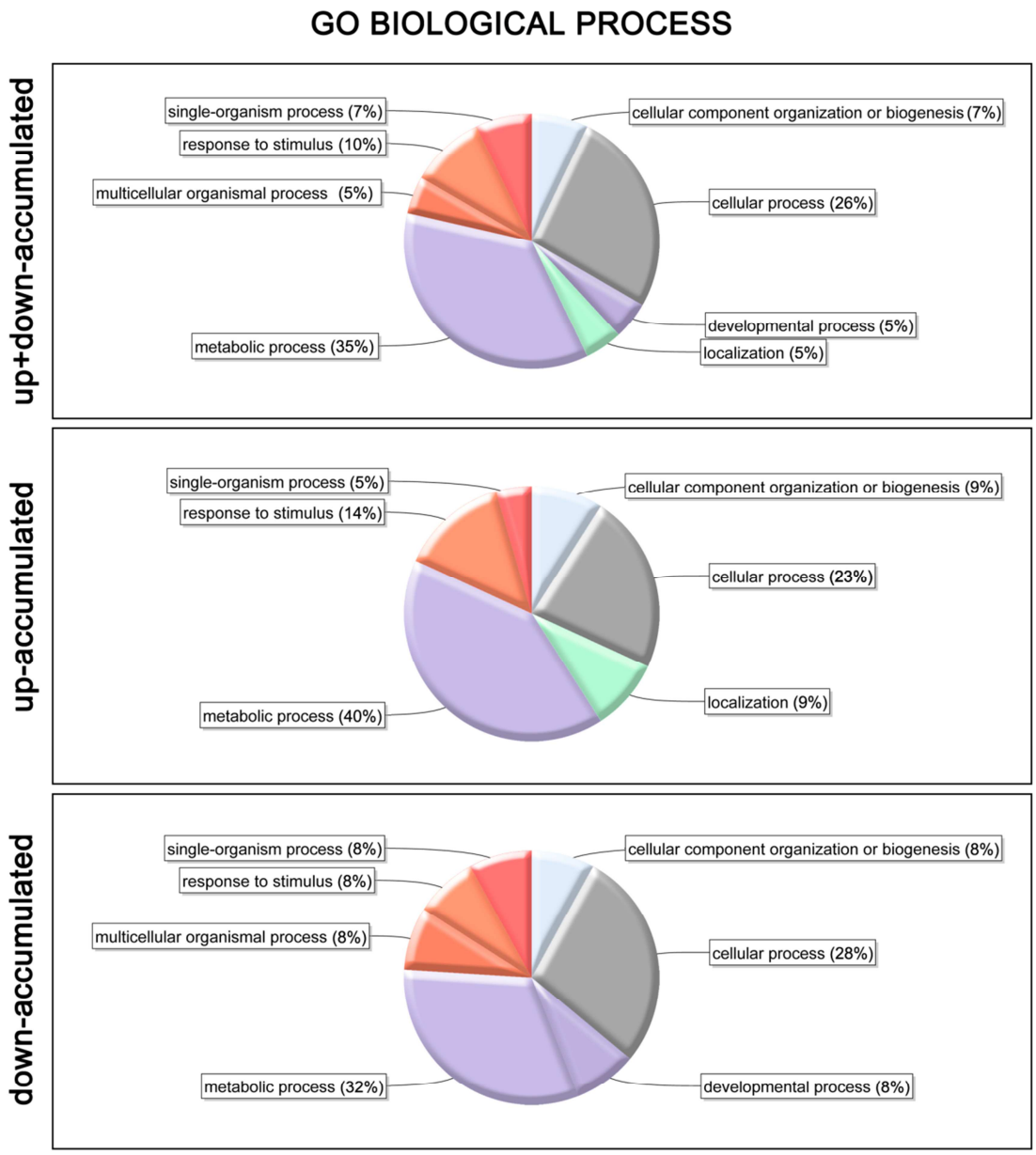

Supplementary Figure 3. Ontology analysis of the differently accumulated phloem proteins after MNSV infection grouped into their probable biological processes using percentages of second level GO terms.

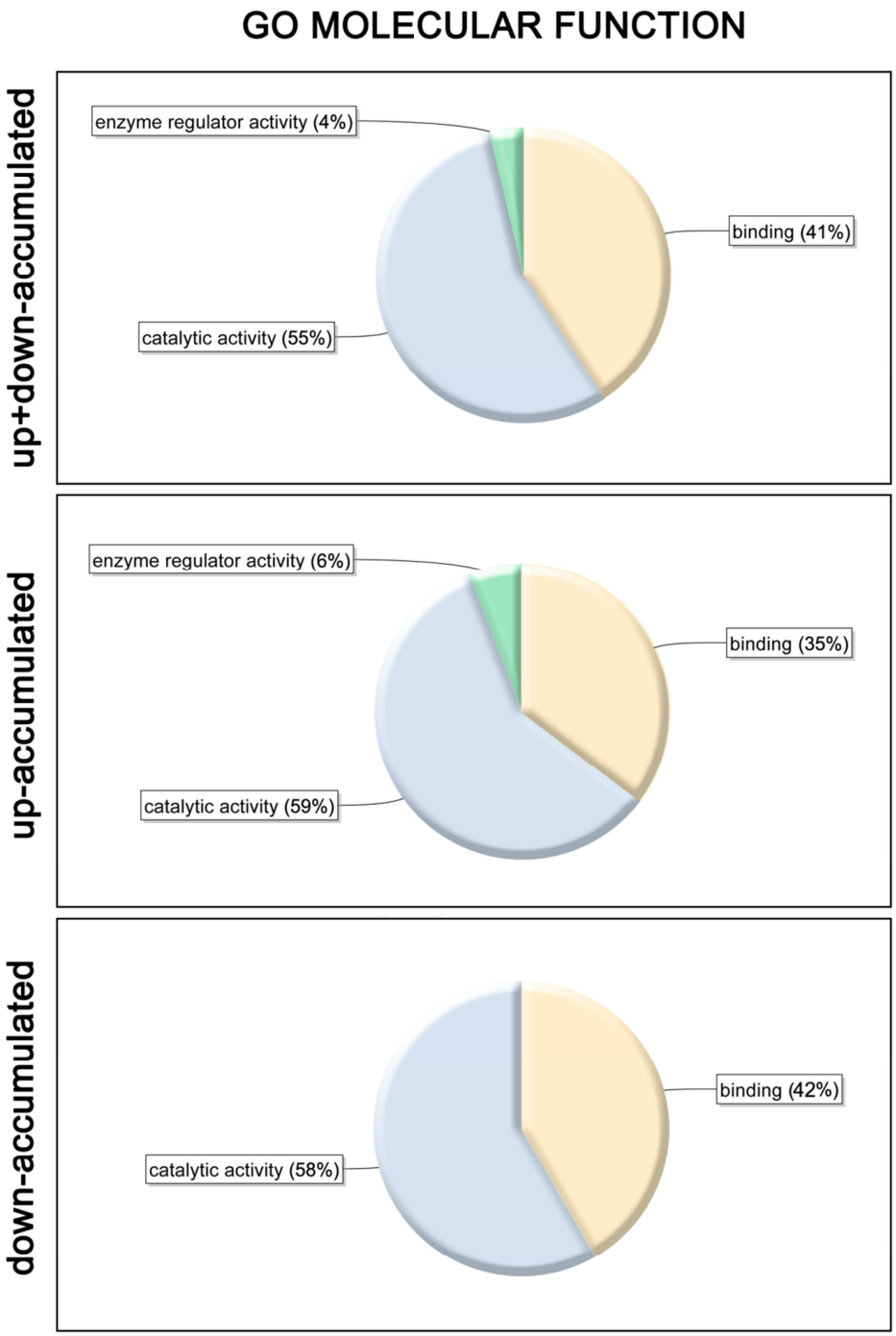

Supplementary Figure 4. Ontology analysis of the differently accumulated phloem proteins after MNSV infection grouped into their probable molecular functions using percentages of second level GO terms.

Supplementary Table 1. Sequences of the primers used for the RT-PCR analyses

Spot number	Accession number	Forward primer	Reverse primer
193	MELO3C019525P1	GGATGTGCTGAACTTTACC	GATTTACCATCAGCATCCC
262	MELO3C004636P1	GGAAGCGGACGGTTGATG	AGCATTGACCCCTTTATA
588/592	MELO3C011389P1	GATCGGACCTGGACTGGAC	CCGATTGAAGCCACTTGAG
935	MELO3C006680P1	TGAAACCCACGTCGTCTTAC	TCACCTTCTGACCTGCCTTC
1017/1019	MELO3C005666P2	CGCTCTCTTCTCACAAGAA	AATTCGAATTAGTCAAGCC
1022	MELO3C026618P1	CAAGAGAAGAGATTGAAAT	AGCCTGGTGATTGGATCCC
F-308[a]	EB715302	TTTGTATGGATGGCGCACCT	CATTGCTCTTGGGGCAAGTC
RBCS[b]	MELO3C012252P1	ATGGCTTCATCCATTCTCTC	GGAGATGTGTAGAATCTTGG

[a] ***F-308 correspond to a phloem translocable Aux/IAA transcript from melon***

[b] ***RuBisCO small subunit***

Supplementary Table 2. Identification of phloem sap proteins differentially accumulated during MNSV infection of melon plants in EST_cucurbitaceae, NCBInr and Melonomics databases.

Spot	EST_cucurbitaceae	Organism	NCBInr	Organism	Functional annotation in NCBInr	MELONOMICS	Functional annotation in *C. melo*
Cell death-related proteins							
262	gi|79133570	*C. melo*	gi|15242093	*A. thaliana*	TCP-1/cpn60 chaperonin	MELO3C004636P1	T-Complex protein 1/cpn60 chaperonin
491	gi|157726911	*C. melo*	gi|58416137	*C. sativus*	Serine protease inhibitor (SERPIN)	MELO3C010898P1	Serine protease inhibitor (SERPIN)
561	gi|157727668	*C. melo*	gi|42572645	*A. thaliana*	TatD related DNase	MELO3C009549P1	Putative deoxyribonuclease TATDN1
588	gi|157721170	*C. melo*	NS	NS	NS	MELO3C011389P1	Carboxylesterase 6
592	gi|157721170	*C. melo*	NS	NS	NS	MELO3C011389P1	Carboxylesterase 6
935	gi|157707335	*C. melo*	-	-	-	MELO3C006680P1	Fumarylacetoacetate hydrolase 1
1022	gi|659130038	*C. melo*				MELO3C026618P1	3-ketoacyl-CoA synthase 7
Proteins involved in redox homeostasis							
246	gi|62894232	*C. sativus*	gi|149938954	*A. chinensis*	Glucose-6-phosphate 1-dehydrogenase	MELO3C008985P1	Glucose-6-phosphate 1-dehydrogenase
329	gi|229067196	*C. maxima*	NS	NS	NS	MELO3C020429P1	Serine hydroxymethyltransferase
462	gi|229064807	*C. maxima*	gi|147766666	*V. vinifera*		MELO3C002816P1	Obg-like ATPase 1
644	gi|157707670	*C. melo*	gi|32490317	*O. sativa*		MELO3C014584P1	Dihydroflavonol 4-reductase
1017	gi|157719665	*C. melo*	NS	NS	NS	MELO3C005666P1	Phospholipid hydroperoxide glutathione peroxidase 6
1019	gi|79136257	*C. melo*	gi|544437	*C. sinensis*	Phospholipidhydroperoxide glutathione peroxidase	MELO3C005666P1	Phospholipid hydroperoxide glutathione peroxidase 6
Other stress related proteins							
460	gi|157707106	*C. melo*	NS	NS	NS	MELO3C018626P1	12-oxophytodienoate reductase
517	gi|157713813	*C. melo*	-	-	-	MELO3C017363P1	Aldose 1-epimerase
553	gi|157713813	*C. melo*	-	-	-	MELO3C017363P1	Aldose 1-epimerase
692	gi|229066325	*C. maxima*	gi|50252992	*O. sativa*	dTDP-D-glucose 4,6-dehydratase-like	MELO3C005621P1	Rhamnose biosynthetic enzyme
975	gi|198409986	*C. lanatus*	-	-	-	MELO3C011984P3	Polygalacturonase
Putative virus-interacting proteins							
193	-	-	gi|225428865	*V. vinifera*	Polyadenylate-binding protein 2	MELO3C018462P1	Polyadenylate-binding protein 2
262	gi|79133570	*C. melo*	gi|15242093	*A. thaliana*	TCP-1/cpn60 chaperonin	MELO3C004636P1	T-Complex protein 1/cpn60 chaperonin
484	gi|79138046	*C. melo*	gi|786178	*O. sativa*	Fructose-1,6-bisphosphate aldolase	MELO3C024519P1	Fructose-1,6-bisphosphate aldolase
933	gi|79134356	*C. melo*	NS	NS	NS	MELO3C011172P1	Proteasome subunit beta type 6
1014	gi|37572213	*C. melo*	-	-	-	MELO3C010866P1	EF hand family calcium-binding protein *

-, negative identification; NS, non search

** Functional identification of the protein using "phytozome" blast of MELO3C010866P1protein sequence against C. sativus genome Cucsa232880.1*

SUPPLEMENTARY TABLE 3. Spots and list of peptides identified by MALDI-TOF-TOF (4700 PA)										
Spot (a)	**Protein/function (b)**	**Accession (c)**	**Start (d)**	**End (d)**	**Observed (e)**	**Mr (expt) (e)**	**Mr (calc) (e)**	**Delta (f)**	**Score (g)**	**Peptide sequence (h)**
329	Serine hydroxymethyltransferase	MELO3C020429P1	68	83	1991.8872	1990.8799	1990.8730	0.0069	80	R.YYGGNEFIDEIENLCR.S
			68	85	2235.1533	2234.1460	2234.0061	0.1399	_	R.YYGGNEFIDEIENLCRSR.A
			124	145	2261.1116	2260.1043	2260.0946	0.0098	_	R.IMGLDLPSGGHLTHGYYTSGGK.K
			147	160	1618.8512	1617.8439	1617.8290	0.0149	_	K.ISATSIYFESLPYK.V
			161	172	1330.7156	1329.7083	1329.6088	0.0995	_	K.VDSATGFIDYDK.L
			184	194	1206.6344	1205.6271	1205.6226	0.0045	25	K.LIICGGSAYPR.D
			184	200	2012.9713	2011.9640	2011.9574	0.0066	7	K.LIICGGSAYPRDWDYAR.F
			251	257	873.4362	872.4289	872.4214	0.0075	_	R.AGMIFYR.K
			320	332	1378.7130	1377.7057	1377.7074	-0.0017	_	K.ANAVALGNYLMNK.G
			336	359	2603.4380	2602.4307	2602.4230	0.0077	_	K.LVTGGTENHLVLWDLRPLGLTGNK.V
			336	362	2959.5461	2958.5388	2958.6290	-0.0902	_	K.LVTGGTENHLVLWDLRPLGLTGNKVEK.L
			363	373	1349.6584	1348.6511	1348.6479	0.0032	_	K.LCDLCNITVNK.N
			363	389	2848.4216	2847.4143	2847.4007	0.0137	_	K.LCDLCNITVNKNAVFGDSSALAPGGVR.I
			374	389	1517.7731	1516.7658	1516.7633	0.0025	83	K.NAVFGDSSALAPGGVR.I
			390	398	903.4777	902.4704	902.4644	0.0061	_	R.IGAPAMTSR.G
			399	414	1931.0095	1930.0022	1929.9948	0.0074	70	R.GLVEKDFEQIAEFLHR.A
			404	414	1404.7059	1403.6986	1403.6833	0.0153	_	K.DFEQIAEFLHR.A
			429	435	877.4937	876.4864	876.5069	-0.0204	_	K.LLKDFNK.G
460	12-oxophytodienoate reductase 2	MELO3C018626P1	33	40	882.5657	881.5584	881.5698	-0.0114	12	R.IVLAPLTR.Q
			43	59	2081.0596	2080.0523	2080.0126	0.0397	_	R.SYNNVPQQHAILYYSQR.A
			43	62	2383.9536	2382.9463	2383.1444	-0.1980	_	R.SYNNVPQQHAILYYSQRATK.G
			159	172	1716.8988	1715.8915	1715.8842	0.0073	17	R.LRTDEIPQIVNDFR.L
			161	172	1447.7148	1446.7075	1446.6990	0.0085	_	R.TDEIPQIVNDFR.L
			221	237	1816.9486	1815.9413	1815.9366	0.0048	30	R.FALEVVEAVVNEIGGDR.V
588	Carboxylesterase 6	MELO3C011389P1	6	16	1244.7472	1243.7399	1243.6924	0.0475	_	K.SLVLDVSGWLR.L
			17	34	2035.0538	2034.0465	2033.9694	0.0771	_	R.LYDDGSVDRTWTGPPEVK.F
			35	53	2084.1196	2083.1123	2083.0374	0.0750	10	K.FVAESVPPHDEFIDGVAVR.D
			54	64	1229.7102	1228.7029	1228.6411	0.0618	_	R.DLVIDQNSGLR.V
			112	123	1367.7526	1366.7453	1366.6914	0.0539	_	K.SAEAICVSVYLR.R
			166	184	1899.0712	1898.0639	1898.0009	0.0630	_	R.VFLIGDSSGGNLVHSVAAR.A
			185	207	2329.3955	2328.3882	2328.2953	0.0929	_	R.AGETDLAPLKLAGGIPIHPGFVR.A
			195	207	1333.8154	1332.8081	1332.7666	0.0416	17	K.LAGGIPIHPGFVR.A
			213	242	3289.8445	3288.8372	3288.6951	0.1421	_	K.SEIENPQSPFLTLDMVDKFLNLALPVGSSK.D
592	Carboxylesterase 6	MELO3C011389P1	6	16	1244.7297	1243.7224	1243.6924	0.0300	_	K.SLVLDVSGWLR.L
			17	25	1039.4963	1038.4890	1038.4618	0.0272	_	R.LYDDGSVDR.T
			17	34	2035.0256	2034.0183	2033.9694	0.0489	_	R.LYDDGSVDRTWTGPPEVK.F
			35	53	2084.0938	2083.0865	2083.0374	0.0492	60	K.FVAESVPPHDEFIDGVAVR.D

			35	64	3294.7209	3293.7136	3293.6679	0.0457	_	K.FVAESVPPHDEFIDGVAVRDLVIDQNSGLR.V
			54	64	1229.6809	1228.6736	1228.6411	0.0325	_	R.DLVIDQNSGLR.V
			65	73	1116.6927	1115.6854	1115.6702	0.0152	_	R.VRIYLPEVK.C
			112	123	1367.7355	1366.7282	1366.6914	0.0368	46	K.SAEAICVSVYLR.R
			112	124	1523.8398	1522.8325	1522.7925	0.0400	_	K.SAEAICVSVYLRR.A
			125	142	1979.0875	1978.0802	1978.0272	0.0531	_	R.APEHRLPAQIEDGFSALK.W
			130	142	1388.7760	1387.7687	1387.7347	0.0340	_	R.LPAQIEDGFSALK.W
			143	165	2717.1804	2716.1731	2716.3383	0.1652	_	K.WLQSVALGNEIEPWIVEKADFNR.V
			161	184	2502.3315	2501.3242	2501.2774	0.0468	_	K.ADFNRVFLIGDSSGGNLVHSVAAR.A
			166	284	1899.0557	1898.0484	1898.0009	0.0475	60	R.VFLIGDSSGGNLVHSVAAR.A
			185	194	1014.5671	1013.5598	1013.5393	0.0205	_	R.AGETDLAPLK.L
			185	207	2329.3547	2328.3474	2328.2953	0.0521	_	R.AGETDLAPLKLAGGIPIHPGFVR.A
			195	207	1333.8080	1332.8007	1332.7666	0.0342	63	K.LAGGIPIHPGFVR.A
			213	242	3290.8042	3289.7969	3289.6791	0.1178	_	K.SEIENPQSPFLTLDMVDKFLNLALPVGSSK.D
			231	242	1245.7418	1244.7345	1244.7128	0.0217	_	K.FLNLALPVGSSK.D
933	Proteasome subunit beta type 6	MELO3C011172P1	24	33	930.5276	929.5203	929.4930 0.	0.0273	_	K.GGVVLGADSR.T
			34	43	1067.5524	1066.5451	1066.5407	0.0044	_	R.TSTGVYVANR.A
			51	59	1139.5559	1138.5486	1138.5441	0.0046	28	K.LTDNVYVCR.S
			60	74	1554.7943	1553.7870	1553.7321	0.0549	20	R.SGSAADSQIVSDYVR.H
			75	91	1955.0786	1954.0713	1954.0537	0.0176	43	R.HFLHQHTIQLGQPATVK.V
			92	105	1560.8351	1559.8278	1559.8671 -	-0.0392	_	K.VAANLVRLLAYNNK.D
1017	Phospholipid hydroperoxide glutathione peroxidase	MELO3C005666P1	134	165	3596.6018	3595.5945	3595.6248	-0.0302	_	K.GHGFEILAFPCNQFGGQEPGSNEEIVQFACTR.F
			168	188	2338.1868	2337.1795	2337.1640	0.0155	_	K.AEYPIFDKVDVNGNNAAPLYK.F
			176	191	1765.7509	1764.7436	1764.8933	-0.1497	_	K.VDVNGNNAAPLYKFLK.S
			192	203	1179.6326	1178.6253	1178.6295	-0.0041	_	K.SSKGGLFGDAIK.W
			195	203	877.4906	876.4833	876.4705	0.0129	_	K.GGLFGDAIK.W
			195	208	1539.8140	1538.8067	1538.7881	0.0186	_	K.GGLFGDAIKWNFSK.F
			209	220	1376.7284	1375.7211	1375.7095	0.0116	26	K.FLVDKDGNVVDR.Y
			221	232	1306.7147	1305.7074	1305.6816	0.0258	_	R.YAPTTSPLSIEK.D

(a) Assigned spot number as indicated in Fig. 3
(b) Identified protein of *Cucumis melo*
(c) Accesion number code refers to Melonomics database (melon genome v3.5.1)
(d) Start and end positions of peptides in *Cucumis melo* proteins
(e) Observed and predicted peptide masses
(f) Mass error between experimental and theoretical peptide mass
(g) Ions score
(h) Sequences of the peptides assigned to the proteins

SUPPLEMENTARY TABLE 4. Spots and list of peptides identified by NanoLC nano ESI-QTOF										
Spot (a)	**Protein/function (b)**	**Accession (c)**	**Start (d)**	**End (d)**	**Observed (e)**	**Mr (expt) (e)**	**Mr (calc) (e)**	**Ppm (f)**	**Score(g)**	**Peptide (h)**
193	Polyadenylate-binding protein 2	MELO3C019525P1	69	85	937.9264	1873.8383	1873.8595	-11	19	R.SLGYGYVNYSNPQDAAR.A
			352	366	764.3499	1526.6852	1526.7001	-10	36	R.GSGFVAFSTPDEASR.A
246	Glucose-6-phosphate 1-dehydrogenase	MELO3C008985P1	167	178	713.3433	1424.6720	1424.6936	-15	38	R.YQGVTIPEAYER.L
			227	237	586.2864	1170.5583	1170.5768	-16	30	R.GPAEADELLEK.A
262	T-Complex protein/Cpn60 chaperonin	MELO3C004636P1	68	77	533.2860	1064.5575	1064.5614	-4	18	K.SLHIDNPAAK.V
			372	383	660.8121	1319.6096	1319.6218	-9	25	R.GASHHVLDEAER.S
			428	436	509.2624	1016.5102	1016.5039	6	36	K.SHAIEAFSR.A
462	Obg-like ATPase 1	MELO3C002816P1	10	28	604.8539	1207.6933	1207.6673	22	30	K.EAPAERPILGR.F
			27	37	533.8402	1065.6658	1065.6546	10	24	K.IGIVGLPNVGK.S
			38	46	512.7932	1023.5718	1023.5601	11	42	K.STLFNTLTK.L
			327	340	743.3840	1484.7535	1484.7260	19	29	K.APQAAGTIHTDFEK.G
484	Fructose-bisphosphate aldolase	MELO3C024519P1	25	38	666.8347	1331.6548	1331.6933	-29	44	K.GILAADESTGTIGK.R
			25	39	744.8887	1487.7628	1487.7944	-21	73	K.GILAADESTGTIGKR.L
			40	52	737.8678	1473.7210	1473.7423	-14	42	R.LSSINVENVETNR.R
			83	94	623.3546	1244.6946	1244.7129	-15	24	K.TAAGKPFVDVLK.E
			95	103	435.2491	868.4836	868.5018	-21	16	K.EGGVLPGIK.V
			95	106	606.3408	1210.6670	1210.6921	-21	5	K.EGGVLPGIKVDK.G
			133	139	415.1890	828.3634	828.3766	-16	23	K.YYEAGAR.F
			149	168	1048.0061	2093.9977	2094.0341	-17	52	K.IGPNEPSQLSINENANGLAR.Y
			204	210	412.7168	823.4190	823.4262	-9	11	R.VLAACYK.A
491	Serine proteinase inhibitor (Serpin)	MELO3C010898P1	9	19	556.3184	1110.6223	1110.6033	17	60	R.SHGDVAIAITK.H
			20	27	469.2903	936.5660	936.5392	29	37	K.HLLLNEAK.A
			112	119	483.2769	964.5392	964.5229	17	24	K.QVVDTLYK.A
			122	128	404.7241	807.4336	807.4127	26	43	K.LSQADFK.T
			131	144	774.8948	1547.7751	1547.7467	18	46	K.AVEVTSEVNSWAEK.Q
			208	219	723.3916	1444.7686	1444.7350	23	40	K.NKQYIATFEGFK.V
			210	219	602.3180	1202.6215	1202.5972	20	14	K.QYIATFEGFK.V
			220	226	390.2454	778.4763	778.4589	22	13	K.VLGLSYK.Q
517	Aldose 1-epimerase	MELO3C017363P1	115	123	560.8155	1119.6164	1119.5924	21.4	37	K.GENPSITF.K
553	Aldose 1-epimerase	MELO3C017363P1	57	68	655.3354	1308.6563	1308.6649	-7	40	K.GLAPYFGCIVGR.V
			107	114	526.7674	1051.5203	1051.5338	-13	10	K.VWQLSEYK.K
			115	124	560.7949	1119.5752	1119.5924	-15	38	K.KGENPSITFK.Y
			116	124	496.7552	991.4958	991.4975	-2	38	K.GENPSITFK.Y
			215	225	628.8112	1255.6079	1255.6085	-0	25	K.GTPFDFTSEKK.D
561	Deoxyribonuclease TATDN1	MELO3C009549P1	26	38	708.3744	1414.7342	1414.7204	10	21	K.QYHAADIAAVLSR.A
			47	58	630.8401	1259.6656	1259.6721	-5	28	R.IIVTGGSLEESR.E
			70	80	643.8310	1285.6474	1285.6602	-10	63	R.LFCTVGVHPTR.C

			155	166	698.3070	1394.5995	1394.6136	-10	66	R.AAAEDFCDIVER.N
644	Dihydroflavonol 4-reductase	MELO3C014584P1	35	45	584.3386	1166.6627	1166.6407	19	21	K.ASVRNPADPIK.T
			39	58	697.0460	2088.1161	2088.0963	9	48	R.NPADPIKTAHLLSLDGAAER.L
			46	58	677.3648	1352.7151	1352.7048	8	58	K.TAHLLSLDGAAER.L
			162	168	454.7657	907.5168	907.5167	0	33	K.LWYVLSK.T
			169	180	703.8619	1405.7093	1405.6990	7	46	K.TLAEEAAWNFVR.E
692	Rhamnose biosynthetic enzyme	MELO3C005621P1	89	102	759.8999	1517.7853	1517.7872	-1	84	R.TNVVGTLTLADVCR.E
			157	165	584.7735	1167.5325	1167.5342	-1	26	K.NYENVCTLR.V
			168	178	608.8064	1215.5982	1215.5918	5	40	R.MPISSDLSNPR.N
			184	189	405.2300	808.4455	808.4443	1	22	K.ITRYEK.V
			263	271	496.2378	990.4610	990.4618	-1	59	R.SNNELDATK.L
			289	296	512.2834	1022.5522	1022.5549	-3	40	K.YVFKPNQK.T
935	Fumarylacetoacetate hydrolase 1	MELO3C006680P1	119	132	740.3874	1478.7602	1478.7617	-1	42	K.GQDTFTPISSVLSK.T
975	Polygaracturonase	MELO3C011984P3	184	194	637.3694	1272.7242	1272.7231	1	26	K.SLFVHVPLFSK.I
			203	215	724.3504	1446.6863	1446.7177	-22	24	R.FVHSLLEAIASTC.-
1014	EF hand family calcium-binding protein	MELO3C010866P1	6	12	423.2581	844.5017	844.5130	-13	29	R.SQLKLTR.D
			95	105	618.8091	1235.6037	1235.6081	-4	27	K.VPAQKPCHDGK.S
1019	Phospholipid hydroperoxide glutathione peroxidase 6	MELO3C005666P1	81	89	517.2803	1032.5460	1032.5240	21	30	K.TSVHDFTVK.D
			81	92	674.3531	1346.6916	1346.6830	6	45	K.TSVHDFTVKDAK.G
			93	102	541.2646	1080.5146	1080.5087	5	39	K.GNDVDLSAYK.G
			93	104	633.8315	1265.6485	1265.6252	18	42	K.GNDVDLSAYKGK.V
			204	213	629.3313	1256.6481	1256.6441	3	23	R.FKAEYPIFDK.V
			204	226	872.1325	2613.3758	2613.3115	25	12	R.FKAEYPIFDKVDVNGNNAAPLYK.F
			214	226	688.3647	1374.7149	1374.6779	27	48	K.VDVNGNNAAPLYK.F
			233	241	439.2504	876.4862	876.4705	18	43	K.GGLFGDAIK.W
			247	258	689.3724	1376.7302	1376.6936	27	30	K.FLVDKDGNVVDR.Y
			247	270	889.1487	2664.4243	2664.3647	22	11	K.FLVDKDGNVVDRYAPTTSPLSIEK.D
			259	270	653.8516	1305.6887	1305.6816	5	48	R.YAPTTSPLSIEK.D
			259	273	824.9540	1647.8935	1647.8719	13	25	R.YAPTTSPLSIEKDVK.K
1022	3-ketoacyl-CoA synthase 7	MELO3C026618P1	224	233	529.2975	1056.5805	1056.6179	-35	26	R.MGGAAILLSN.K

(a) Assigned spot number as indicated in Fig. 3
(b) Identified protein of Cucumis melo
(c) Accesion number code refers to Melonomics database (melon genome v3.5.1)
(d) Start and end positions of peptides in Cucumis melo proteins
(e) Observed and predicted peptide masses
(f) Error expressed as parts per million
(g) Ions score
(h) Sequences of the peptides assigned to the proteins

DISCUSIÓN GENERAL

La infección de una planta susceptible por parte de un virus se inicia con la entrada/replicación del mismo en el interior de celular. La progenie viral es entonces transportada hacia las células vecinas a través de los plasmodesmos (PDs). Este transporte incluye los denominados movimientos intra e intercelular que básicamente están facilitados y regulados por las proteínas de movimiento (MPs). Las MPs utilizan el sistema de endomembranas y el citoesqueleto del huésped para moverse por el interior celular, y en algunos casos son dependientes de la ruta de secreción de macromoléculas. Posteriormente, el virus alcanza las partes distales de la planta mediante el movimiento sistémico, para el cual es necesaria la entrada y salida del sistema vascular (principalmente del floema). Este movimiento a larga distancia, que en muchos casos es facilitado por la proteína de cubierta (CP), también es esencial para la transmisión de los virus puesto que garantiza la accesibilidad de las partículas víricas a sus vectores naturales. Sin embargo, para completar este ciclo biológico, el virus ha de ser capaz de evadir la respuesta de defensa que en muchos casos limita su movimiento. En general, la respuesta del huésped se basa en dos mecanismos diferentes, los genes de resistencia y el silenciamiento génico de RNA. La forma más habitual de contrarrestar el silenciamiento de RNA por parte de los virus es mediante la expresión de factores proteicos o supresores (*viral suppressors of RNA silencing*, VSR) que actúan bloqueando a diferentes niveles las rutas de defensa (Csorba *et al.,* 2015). Los virus codifican pues en sus genomas múltiples proteínas (MPs, CPs y VSRs, entre otras) implicadas, directa o indirectamente, en mediar el movimiento del virus por la planta y la propagación de la infección viral. El estudio de las mismas y de sus interacciones con los componentes celulares del huésped pueden ayudar a esclarecer los mecanismos moleculares en los que intervienen. Además, tal y como ha ocurrido anteriormente para otras ramas de la Virología, el estudio del transporte del RNA viral ha contribuido y puede seguir haciéndolo aun mas al descubrimiento de principios básicos de la biología más allá de constituir la base para el desarrollo de nuevas estrategias de control.

El género *Carmovirus* representa al menos 19 especies de virus de plantas que afectan a numerosas especies cultivadas, en muchos casos con una gran repercusión económica. Este género se caracteriza por poseer en la parte central de su genoma dos

ORFs que codifican dos pequeñas MPs, denominadas generalmente DGBp1 y DGBp2 (*double gene block of proteins*, DGBps). En un principio se propuso un modelo de movimiento en el que la DGBp1 se encargaría de la unión del RNA viral mientras que la DGBp2 anclada a la membrana, facilitaría el transporte del complejo DGBp1-RNA hacia la periferia celular. Sin embargo, estudios recientes con las MPs del virus de las manchas necróticas del melón (MNSV) han puesto de manifiesto que este sistema es más complejo y que podría no ser aplicable a todos los miembros del género (Navarro *et al.,* 2006). Además, la participación de la CP del MNSV tanto en el movimiento local como sistémico del virus así como la de los posibles factores celulares implicados en ambos procesos no ha sido caracterizada con detalle. Por tanto, en la presente tesis doctoral se ha intentado continuar y extender los trabajos anteriores realizando una serie de estudios que incluyen el análisis funcional y estructural de varios factores virales implicados en el movimiento de los carmovirus en sus tres etapas principales: intracelular, intercelular y sistémico, la identificación de algunos de los factores celulares implicados en las mismas y las alteraciones proteómicas que ocurren a nivel vascular durante la infección viral.

Transporte de p7B (DGBp2 de MNSV) durante las etapas tempranas de la ruta de secreción celular: secuencia mínima necesaria y requerimiento de movilidad lateral en el RE.

La asociación de las proteínas virales a los componentes celulares tiene un papel fundamental en el ciclo vital de los virus de plantas (Sanfaçon, 2005; Netherton *et al.,* 2007; Hwang *et al.,* 2008). Los virus son capaces de utilizar el sistema de endomembranas y el citoesqueleto para moverse por el interior celular. En algunos casos este movimiento hacia el PD es dependiente de la ruta de secreción, como es el caso de la p7B del MNSV. Esta MP necesita la intervención de las vesículas COPII para salir del retículo endoplasmático (RE) y dirigirse al aparato de Golgi. El mecanismo de formación de las vesículas y sus componentes han sido ampliamente estudiados (Hawes and Satiat-Jeunemaitre, 2005; Yang *et al.,* 2005; Hanton *et al.,* 2005, Hanton *et al.,* Hanton *et al.,* 2006, Hanton *et al.,* 2007, Hanton *et al.,* 2009; Aniento *et al.,* 2006; Matheson *et al.,* 2006; Kang and Staehelin, 2008; Zhang *et al.,* 2010; Lerich *et al.,*

2012). Sin embargo, los motivos/señales que dirigen la salida del RE de las proteínas de membrana no están todavía claros.

En estudios anteriores se observó que la estructura de p7B (Navarro *et al.,* 2006; Genovés *et al* 2009, 2010) presenta 3 regiones o dominios diferenciados: un extremo Nt o RC (de región citoplásmica) corto que presenta un giro β, un dominio transmembrana (TMD) localizado en la región central en forma de α-hélice y un segmento Ct o RL (de región luminal) con cierto plegamiento en hojas β. Por tanto, presenta un solo fragmento transmembrana y una topología de tipo II, lo que implica que su Nt se orienta hacia el citoplasma. No posee una secuencia o péptido señal de transporte al RE que se procese pero se demostró que el TMD de p7B era suficiente para dirigir el transporte y la inserción en la membrana del RE pero no su posterior transporte al aparato de Golgi (Genovés *et al.,* 2010, 2011). Estos resultados previos sugieren que la salida del RE debe estar dirigida por otros elementos localizados en motivos de la región citoplasmica (RC) y/o de la región luminal (RL). A través de un estudio de mutagénesis dirigida observamos que para la salida del RE de p7B se necesita la acción conjunta de 4 residuos (DSSP) del RC expuestos al citosol y una lisina del LR (K49) orientada hacia el lumen. Mediante alineamiento múltiple comprobamos que estos dos motivos están conservados en MPs homólogas a p7B de otros miembros de la familia *Tombusviridae,* indicando su relevancia funcional en el transporte intracelular de esta proteína y, por tanto, en el ciclo de vida viral.

Una característica común de muchas señales de salida del RE es la presencia de residuos cargados, como en el caso de la lisina 49 de p7B. En principio, estos resultados contradicen el hecho, al parecer más generalizado, de que las proteínas con un fragmento transmembrana destinadas a ser secretadas sólo poseen señales citoplasmáticas de salida del RE. Esta es una situación lógica puesto que estas señales tienen que ser reconocidas activamente por los componentes de las vesículas COPII (sar1 y/o sec24) que desencadenan la formación de las mismas y que son citoplasmáticos (Aniento *et al.,* 2006; Robinson *et al.,* 2007). En muy pocos casos de proteínas con más de un fragmento transmembrana se ha descrito una doble participación de señales de secuencia situadas tanto en el extremo Nt como el Ct. Sin embargo, en la mayoría de estos casos, la topología de la proteína permite que ambos

motivos sean citoplasmáticos. En levaduras y mamíferos sí encontramos algunos ejemplos como la guanosina difosfatasa (Dancourt and Barlowe, 2009) o p23 (Blum and Lepier, 2008) respectivamente, en los que existen determinantes de salida compartidos en el Nt, TMD y Ct luminal, sin embargo es la primera vez que se describe en plantas.

Por otra parte la salida de proteínas de secreción del RE depende principalmente de las vesículas COPII. Éstas emergen desde las regiones especializadas del RE llamadas ERES (*endoplasmic reticulum exit sites*) (Hanton *et al.,* 2005; Mateson *et al.,* 2006; Lerich *et al.,* 2012) hacia el aparato del Golgi. Su ensamblaje se inicia con la activación de la proteína sec12 (aunque en plantas su participación es discutida), que se encuentra en la membrana del RE y que a su vez recluta y activa a Sar1. Sar1 sufre entonces un cambio conformacional exponiendo una α-hélice anfipática que le facilita el anclaje a la membrana para así reclutar el heterodímero Sec23/24. La disposición tridimensional de los distintos sitios de unión de la proteína transportada respecto a estos componentes, Sar1 y Sec24, y otras proteínas accesorias sugiere que tanto las interacciones químicas como la correcta orientación de los grupos funcionales es lo que determina la selección de carga (Lee and Miller, 2007; Quintero *et al.,* 2010). Esto concordaría con la importancia de la disposición de los residuos del motivo DSSP en forma de giro β. Dentro de este motivo, la prolina está altamente conservada y entre las posiciones -1 y -4 con respecto a esta prolina existe siempre una carga negativa, principalmente un Asp. Este giro β, permite acercar ambos residuos lo suficiente para formar un puente de hidrógeno estabilizando la estructura. El hecho de que esté tan conservada apuntaría a que es necesaria para la interacción directa o indirecta con los componentes del COPII. Esta estructura secundaria podría favorecer una orientación espacial de las cadenas laterales de los residuos del giro β adecuada para la interacción con el/los sitio/s de unión del receptor como ocurre con algunos receptores y transportadores en mamíferos (Bansal and Gierasch, 1991; Eberle *et al.,* 1991; Aroeti *et al.,* 1993; Dargemont *et al.,* 1993; Sun *et al.,* 2003). Sin embargo, las señales luminales, como la lisina 49 de p7B, requieren componentes adicionales que comuniquen el dominio luminal de la proteína transportada con los componentes citosólicos necesarios para la formación de las vesículas COPII. De hecho, algo similar

ocurre con algunos de los miembros de la familia Cornichon (Bökel *et al.,* 2006; Dancourt and Barlowe, 2010). Estas proteínas son receptores auxiliares transmembrana que interaccionan con las señales luminales de determinadas proteínas. Estos adaptadores transmembrana parecen estar bastante conservados en eucariotas sin embargo no existe evidencia experimental de su existencia en plantas hasta ahora. Los estudios realizados con el mutante adicional GFP-p7B [$D_7AP_{10}A$] permitieron confirmar su asociación con un marcador del aparato de Golgi después del tratamiento con latrunculina B, un inhibidor de la polimerización de microfilamentos. Esta observación sugiere que el mutante, los componentes asociados a él y el aparato de Golgi utilizan el mismo mecanismo para desplazarse por la superficie del RE. Lo más probable es que las estructuras asociadas al mutante representen una especie de precomplejo detenido en una etapa previa a la formación del complejo COPII como consecuencia de un defecto en la interacción con algún componente necesario. En este sentido el mutante $D_7AP_{10}A$ fue incapaz de inducir la formación *de novo* de ERES. Además no podemos descartar la posibilidad de que estas estructuras posiblemente sean consecuencia de la interacción con el posible adaptador transmembrana.

Por otro lado, los estudios realizados con el mutante $K_{49}A$ revelaron que interfiere en los estadios tempranos de la ruta de secreción de la planta, dado que su expresión provoca cambios drásticos en la morfología del RE muy parecidos a los que produce la brefeldina A (BFA), un inhibidor del tráfico anterógrado entre el RE y el aparato de Golgi. Además, los análisis mediante FRAP indicaron que esta lisina es esencial para la difusión lateral de p7B en la membrana del RE indicando que el posible adaptador transmembrana debe ser capaz de unir también a la proteína directa o indirectamente al citoesqueleto de actina, promoviendo su movimiento y concentración.

Con todos estos datos hemos propuesto un modelo en el que después de la inserción y correcto plegamiento de la proteína en la membrana del RE, el RL de p7B interacciona a través del residuo K49 con un adaptador transmembrana asociado al citoesqueleto de actina para su movimiento y concentración en el RE-cortical (Figura 9, capítulo 2). El motivo citoplasmático en RC sería necesario para el ensamblaje de la vesícula COPII, aunque el mecanismo exacto todavía estaría por determinar.

Un estudio con Y2H y tres DGBp1s identifica tres factores celulares que interaccionan con ellas, WRKY36, RPP3A y eIF3g, revelando una posible similitud funcional conservada en los carmovirus.

La capacidad de los virus para invadir una planta y provocar una infección sistémica, depende en gran parte de la interacción con los factores celulares. Una de las principales y más críticas etapas dentro del ciclo viral es el movimiento, en el que las MPs desempeñan un papel central. Éstas son capaces de reclutar factores y mecanismos celulares para llevar a cabo sus funciones (Wolf *et al.,* 1989; Boevink and Oparka, 2005; Verchot-Lubicz, 2005; Sánchez-Navarro *et al.,* 2006; Lucas, 2006). La técnica de doble híbrido en levadura (Y2H) ha sido ampliamente utilizada para el estudio de interacciones proteína-proteína, dada su sensibilidad, fácil manejo, escalabilidad y que no necesita pasos posteriores de purificación. Aunque también presenta inconvenientes principalmente relacionados con los falsos positivos y falsos negativos debido a las restricciones que ofrece la levadura en cuanto a expresión de proteínas heterólogas, en este trabajo hemos intentado minimizarlos utilizando dos proteínas homólogas para rastrear la misma librería de cDNAs de *Arabidopsis thaliana*. En concreto, utilizamos dos proteínas de movimiento del grupo DGBp1 del género de los *Carmovirus*, la p7 del virus del moteado del clavel (CarMV) y la p7A del MNSV.

Mediante Y2H y BiFC (como técnica alternativa para confirmar las interacciones) encontramos 3 factores que interaccionaban con ambas MPs: la proteína P3 de la subunidad ribosomal 60S (RPP3A, At4g25890), la subunidad G del factor de inicio de la traducción eIF3 (eIF3g, At3g11400) y el factor de transcripción WRKY36 (At1g69810). Para tratar de generalizar los resultados, se volvieron a comprobar las interacciones con una tercera DGBp1 homóloga, la p8 del virus del arrugamiento del nabo (TCV), lo que nos permitió confirmar las interacciones de las tres MP con los tres factores celulares. Estos factores están más bien relacionados con procesos como traducción, apoptosis y mecanismos de defensa celulares que, aunque en última instancia afectan al movimiento del virus, no parecer estar directamente implicados en éste. Sin embargo, estos resultados son consistentes con las hipótesis recientes en las que se sugiere que las MPs pueden participar en múltiples etapas del ciclo viral como en la

supresión del silenciamiento o en la susceptibilidad del huésped (Amari *et al.,* 2012; Morozov and Solovyev, 2012).

Para completar su ciclo biológico los virus necesitan utilizar la maquinaria de traducción celular y con el fin de poder competir con los mRNAs celulares algunas proteínas virales son capaces de controlar los ribosomas, ciertos factores y rutas implicadas en la traducción (Walsh and Morh, 2011). La subunidad grande del ribosoma posee una protrusión lateral (Gonzalo and Reboud, 2003) compuesta por un complejo de tres proteínas P (P0, P1y P2). Exclusivamente en plantas se encuentra una cuarta proteína denominada P3 (Bailey-Serres *et al.,*1997; Szick *et al.,*1998). Este complejo P está implicado en la elongación (Szick *et al.,* 1998) y, en algunos casos, en la traducción selectiva de mRNAs, como se ha descrito en raíces de maíz en inundación (Bailey-Serres *et al.,* 1997). Considerando que las DGBp1s son las proteínas virales que interaccionan con el RNA viral, todo parece indicar que la asociación con RPP3 podría favorecer la traducción del RNA viral.

Por otra parte, eIF3g participa en una multitud de procesos relacionados con la traducción además de otros implicados en apoptosis. En primer lugar forma parte del complejo multimérico necesario para la formación del complejo de iniciación 43S. Una vez formado, eIF3g junto con eIF4e, eIF4g y PABP reclutan el mRNA y lo dirigen hacia el complejo 43S. En segundo lugar interviene, junto con eIF3i, en la traducción de un subconjunto de mRNAs estrechamente regulados que poseen estructuras secundarias, e intervienen en procesos tales como el ciclo celular o señalización (Cuchalova *et al.,* 2010). Finalmente, también se ha observado que interacciona con un factor de inducción de la apoptosis (AIF), inhibiendo así la síntesis proteica durante la apoptosis (Kim *et al.,* 2006). Todas estas funciones le convierten en un candidato ideal para controlar distintos procesos de la traducción celular, por lo que la interacción de las DGBP1s con eIF3g podría evitar que este factor esté disponible para realizar sus funciones, tales como la traducción de mRNAs específicos de procesos como la respuesta hipersensible (HR) o de defensas celulares, evitando así que se desencadene la respuesta de la planta. Otra posible interpretación es que actúe de manera análoga a como lo hace el activador TAV del virus del mosaico de la coliflor (CaMV). El factor viral TAV interacciona con eIf3g y la proteína de la subunidad ribosomal 60S L24 para

facilitar la traducción de sus mRNAs policistrónicos (Park *et al.,* 2001). Sin embargo, el tipo de genoma y el mecanismo de expresión del CaMV es muy diferente de los carmovirus (Mandahar ,2006). Parece más plausible que la interacción con ambos factores pueda estar relacionada con alguna estrategia viral para controlar la traducción de ambas MPs del sgRNA1. En conjunto podría actuar como un regulador transcripcional interaccionando con diferentes elementos de la traducción para decantar el balance hacia la traducción o el movimiento viral dependiendo de la etapa en la que se encuentre.

La tercera proteína identificada es un factor de transcripción, WRKY36. En *A. thaliana*, pertenece a una familia de 74 miembros involucrados en varios procesos fisiológicos de la planta, como el desarrollo de semillas, senescencia, germinación y respuesta a estreses bióticos y abióticos (Pandey and Somssich, 2009; Ruchton *et al.,* 2010). Sin embargo, no existe mucha información en la que se relacionen estos factores de transcripción WRKY con la defensa antiviral. Existen algunos ejemplos, todos muy recientes, como el caso de NtWRKY1 y CaWRKYa/d relacionados con la HR o el WRKY8 involucrado en la respuesta de defensa tras la infección por el virus del mosaico del tabaco (TMV) (Menke *et al.,* 2005; Huh *et al.,* 2012; Huh *et al.,* 2015). También se ha encontrado que el PVX utiliza NtWRKY1 para mantener la concentración de RNA genómico durante la infección (Park y Kim, 2012). En cualquier caso, las proteínas WRKY están reguladas mediante interacciones con un amplio espectro de proteínas con papeles en señalización, transcripción y remodelado de cromatina (Chi *et al.,* 2013). Esto sugiere que la interacción con DGBp1 y WRKY36 pueda alterar de alguna forma la reprogramación transcripcional inducida por la planta y así contrarrestar sus mecanismos de defensa. Otra posible interpretación es que las DGBp1s se unan a WRKY36 para facilitar su paso a través de los Pds. Las proteínas que circulan entre células suelen llamarse NCAPs (*non-cell autonomous proteins*) y muchas de ellas son factores de transcripción móviles que utilizan las plantas para transmitir señales intercelulares (Han *et al.,* 2014). Por el momento no se ha descrito que las DGBp1 intervengan en la modificación del límite de exclusión molecular del PD por lo que no se descarta la posibilidad de que usen factores de transcripción móviles para pasar de una célula a otra, siendo WRKY36 un posible candidato.

Finalmente identificamos un dominio de tres residuos (FNF) en el extremo 3' de estas MPs, altamente conservado entre DGBp1 homólogas. Demostramos que es indispensable para la interacción con los tres factores celulares caracterizados, además de para la dimerización. Muy probablemente los anillos aromáticos de los dos residuos de fenilalanina del motivo FNF se encuentren implicados en apilamientos de tipo π-π. Este tipo de interacciones generan enlaces no covalentes especialmente relevantes en mantener la estabilidad global de una proteína, el reconocimiento molecular y el autoensamblaje (McGaughey *et al.,* 1998; Gazit, 2002; Meyer *et al.,* 2003; Profit *et al.,* 2013). Este motivo podría funcionar directamente como un punto de anclaje general para múltiples factores. En otra posibilidad, el motivo FNF sería esencial para la homodimerización. La unión entre MPs podría introducir cambios conformacionales que facilitarían la interacción con las proteínas del huésped. La observación de que los tres factores encontrados interaccionen con las DGBps de tres de los carmovirus mejor estudiados, siendo uno de ellos el CarMV la especie tipo del género, sugiere una similitud funcional conservada entre estos virus.

Análisis del papel multifuncional del dominio Nt desestructurado de la proteína de cubierta del MNSV en la encapsidación del RNA, el movimiento viral y en la defensa antiviral de la planta.

Otra de las proteínas que desempeña un papel importante dentro del movimiento viral es la CP. Además, interviene en otras muchas etapas dentro del ciclo viral como, encapsidación, replicación del genoma, interferencia con el sistema de defensa de la planta y de la transmisión por el vector (Weber and Bujarski, 2015; Ni and Cheng-Kao, 2013; Callaway *et al.,* 2001). Esta multifuncionalidad muchas veces va asociada a dominios desestructurados (Dunker *et al.,* 2008) como en el caso del dominio R de la proteína de cubierta del MNSV. Para determinar si la multifuncionalidad de la CP radica, al menos en parte, en este dominio analizamos su posible implicación en varios procesos del ciclo de vida viral.

En primer lugar, pudimos demostrar que la capacidad de unión a RNAs de cadena simple (ssRNAs), aparentemente sin especificidad de secuencia, depende exclusivamente de la región R ya que el mutante de deleción al que se le eliminaron los 94 residuos amino terminales que comprenden este dominio perdió completamente

su capacidad de unir RNA. Aunque encontramos variaciones significativas entre las afinidades por el RNA entre los mutantes de deleción parcial del dominio R o los mutantes puntuales, en ningún caso se perdió la capacidad de unión, con lo que los 16 residuos cargados a lo largo del dominio R pueden potencialmente intervenir en la interacción con el esqueleto fosfodiester del RNA. Sin embargo, la participación del subdominio R3 fue más relevante en los mutantes en los que se delecionó solo un subdominio que en aquellos en los que se delecionaron dos. Sin embargo, el subdominio R3 fue imprescindible en la encapsidación del RNA viral.

La importancia del dominio R3 en la unión al RNA no parece radicar exclusivamente en la neutralización de las cargas positivas por el RNA (Hui and Rochon ,2006). Estudios realizados sobre las partículas víricas de dos tombusvirus, el virus del mosaico del pepino (CNV) y el virus del enanismo arbustivo del tomate (TBSV) (Katpally *et al.,* 2007; Timmins *et al.,* 1994), muestran que los viriones están organizados internamente en cubiertas concéntricas alternas de proteína y RNA (Figura 16, apartado 1.7.4 de la introducción). La cubierta exterior corresponde a los dominios S y P mientras que la segunda cubierta interna está compuesta por la región Nt desordenada. Además, el RNA se concentra en mayor medida bajo las díadas C-C, cuyos extremos Nt se conectan mediante puentes de hidrógeno formando una estructura circular llamada anillo β (Harrison *et al.,* 1978; Hogle *et al.,* 1986; Doan *et al.,* 2003; Ke *et al.,* 2004; Katpally *et al.,* 2007; Wada *et al.,* 2008), aunque el RNA no se sitúa cerca de esta estructura. Por otra parte la interacción entre las subunidades de la CP facilita la formación de los anillos β y la región ε (ambos elementos incluidos en el subdominio R3) ya que estas regiones contribuyen a la estabilidad del virión y a la unión del RNA. Estas observaciones junto con el hecho de que la CP del MNSV y la del TBSV poseen una alta homología (Wada *et al.,* 2008), sugieren que el virión del MNSV podría poseer una disposición interna similar al TBSV y esto a su vez reafirmaría los resultados obtenidos donde la región ε posee una mayor relevancia en la encapsidación del RNA de MNSV.

Por otro lado, se realizaron estudios de encapsidación durante una infección en planta para comprobar si los resultados obtenidos en los ensayos de unión a RNA “in vitro” eran extensibles a la situación “in vivo”. Cualquier alteración en el dominio R

redujo drásticamente la eficiencia del ensamblaje de partículas dado que en todos los mutantes analizados recuperamos partículas densas, en principio viriones, su concentración era mucho menor que en la wt. Sin embargo, estas partículas contenían los dos RNAs subgenómicos (sgRNA1 y sgRNA2) junto con un tercer RNA viral defectivo pero no el RNA genómico de 4,3 Kb que sólo se recuperó en el mutante R81A y en el wt. Esto podría deberse a que al eliminar parte del dominio R se puede modificar la simetría T=3 del icosaedro pudiéndose formar partículas defectivas tipo T=1, más pequeñas que la nativa, y que no permiten la encapsidación del gRNA al ser éste demasiado grande (Kumar *et al.,*1997; Sangita *et al.,*2004; Larson *et al.,*2005; Hsu *et al.,*2006; Katpally *et al.,*2007; Kakani *et al.,*2008). Sin embargo, el ensayo Northern Blot reveló la presencia de una única especie electroforética, indicio de una simetría T=3 en todos los viriones con capacidad de unir RNA. Parece más plausible que las deleciones parciales del Nt comprometan la morfología interna del virión (Figura.16, apartado 1.7.4) o la estabilidad de las partículas T=3 y que, sin descartar la participación de la capa proteica del interior del virión en el reconocimiento de los RNAs del MNSV, esto lo haga más accesible a nucleasas, como ocurre con el CNV (Reade *et al.,* 2010).

En estudios previos utilizando una aproximación típica con plantas de *N. benthamiana* que expresaban constitutivamente la GFP (línea 16c) se observó que la CP del MNSV podría actuar como un supresor viral del silenciamiento de RNA (VSR) (Genovés *et al.,* 2006). Para determinar si existía alguna relación entre el domino R y esta función VSR utilizamos una estrategia diferente basada en el incremento de síntomas y título viral en infecciones con variantes del virus X de la patata que expresan una proteína de interés. Los resultados obtenidos indicaron la supresión del silenciamiento de RNA mediada por la CP del MNSV durante la infección con PVX fue mucho más evidente que la supresión del silenciamiento del transgen de GFP. Se han observado discrepancias similares para otros VSRs probablemente debido a que el ensayo con PVX se aproxima más a las condiciones en las que un VSR de un virus de RNA citoplasmático debería actuar. Los ensayos con los mutantes de la CP confirmaron que la función VSR depende del dominio R, concretamente de los subdominios R2 y R3. Muchos de los mecanismos de silenciamiento se desencadenan con la aparición de dsRNAs, principalmente los derivados de la replicación citoplasmática del virus.

Estudios recientes de secuenciación masiva en plantas de melón han puesto de manifiesto que los siRNAs de 21 nt derivados del MNSV se acumulan mayoritariamente en plantas infectadas, sugiriendo que la CP del MNSV no evita su formación *in vivo* (Donaire *et al.,* 2009; Herranz *et al.,* 2015). Por otra parte hemos demostrado que la actividad supresora de la CP del MNSV *in vivo* depende del dominio R. Estas dos observaciones hacen pensar que el mecanismo que emplea la CP para interferir con el silenciamiento de RNA sea mediante la unión a siRNAs. Para comprobar esta hipótesis realizamos ensayos EMSA con las CPs del MNSV purificadas, tanto mutantes como wt. La CP(wt) fue capaz de unir siRNAs de simple y doble cadena independientemente de su tamaño (21, 22 y 24 nt) con una mayor afinidad por los de 24 nt. Además, el análisis mutacional reveló una correlación positiva entre la interacción con siRNAs *in vitro* y la capacidad de suprimir el silenciamiento de RNA *in vivo* sugiriendo que la CP del MNSV interfiere la degradación del RNA viral secuestrando siRNAs virales mediante la región Nt que abarca los subdominios R2 y R3. Por otro lado, se ha demostrado que los siRNAs de 24 nt, más que los de 21 nt, se transportan sistémicamente de manera selectiva al menos en el caso de un transgen y de determinados locus endógenos (Melnyk *et al.,* 2011). Dada la mayor afinidad de la CP del MNSV por los siRNAs de 24 nt, un mecanismo de actuación plausible sería aquel en el que la CP del MNSV actuaría bloqueando la señal sistémica de silenciamiento de RNA.

En ensayos de movimiento local, la deleción del subdominio R1 produjo un aumento considerable en el avance de la infección del MNSV en melon.

En el CNV, los 39 residuos situados en el extremo Nt de la CP pueden funcionar como un péptido señal de transporte a mitocondrias (mTP) lo que provoca el procesamiento del extremo Nt del CNV cerca de una región equivalente a la zona situada entre los subdominios R2 y R3 del MNSV (Hui *et al.,* 2010). Según los autores este fenómeno serviría para controlar el balance entre la encapsidacion y la desencapsidación durante la infección. En nuestro laboratorio se disponen de datos experimentales que también confirman el transporte a mitocondrias y cloroplastos con el posterior procesamiento de la CP del MNSV pero no del mutante CP(ΔR1) (datos no publicados). Aunque se requiere un estudio con más detalle, en el caso del mutante CP(ΔR1) podría destinarse más proteína a actuar como VSR, dado que conserva los

subdominos R2 y R3, facilitando el avance de la infección local. Además la misma región, R2 y R3, es esencial para el movimiento viral sistémico tal y como se desprende de los ensayos de movimiento independientes de la encapsidación. En estos ensayos el único que mostró un fenotipo similar al virus wt fue el mutante CP(ΔR1) aunque se produjo una reducción en el número de infecciones sistémicas. Este fenómeno podría deberse a las deficiencias en la replicación y/o acumulacion viral específicas de huésped que retrasarían la entrada en el sistema vascular.

A pesar de que el MNSV pertenece al género *Carmovirus*, su CP presenta una mayor semejanza con las CPs de los miembros del género *Tombusvirus* en lo referente a similitud de secuencia, longitud de los dominios R y P y estructura tridimensional (Riviere *et al.,* 1989; Wada *et al.,* 2008). Estas características sugieren que la CP del MNSV puede haber sido adquirida durante un fenómeno de recombinación. En este sentido se han publicado estudios de secuencias virales que predicen que tombusvirus y carmovirus pueden sufrir muchos más procesos de recombinación que el resto de los virus de otros géneros dentro de la familia *Tombusviridae* (Boulila, 2011). Estos eventos de recombinación han sido estudiados, por ejemplo, en el caso del CNV y el MNSV (Riviere and Rochon, 1990). En la familia *Tombusviridae*, las CPs de los carmovirus y la proteína P19 de los tombusvirus constituyen los dos principales tipos de supresores del silenciamiento de RNA. Sin embargo, las CPs de los tombusvirus carecen de actividad VSR. De hecho, la CP del MNSV carece del motivo GW presente en las CPs de los carmovirus y en el único miembro del genero *Pelarspovirus* (Azevedo *et al.,* 2010; Perez-Cañamás and Hernández, 2015). El motivo GW mimetiza el motivo repetitivo GW/WG de las proteínas celulares que interaccionan con AGO y que, en el caso de la CP del TCV, se ha propuesto que interacciona con AGO1 antes de la carga de siRNAs impidiendo su activación. Además de esta interacción proteína-proteína, se ha postulado también que las CPs de los carmovirus son capaces de unir siRNAs como un mecanismo alternativo de supresión del silenciamiento (Merai *et al.,* 2006). Esta unión depende de residuos básicos específicos que se localizan en en el domino S de la CP (Cao *et al.,* 2010) pero también del motivo GW (Azevedo *et al.,* 2010; Perez-Cañamás and Hernández, 2015). En ausencia de proteínas similares a P19 o de CPs de carmovirus “bona fide”, la CP del MNSV puede haber adquirido su capacidad de actuar

como VSR adaptando su región Nt desestructurada para interaccionar con diferentes moleculas de RNA tales como los siRNAs. Debido a que la encapsidación y las funciones de supresión recaen dentro del mismo dominio de la CP del MNSV, ambos procesos deben ser mutuamente excluyentes. Por tanto, la identificación del interruptor fisiológico y/o molecular que gobierna el destino de la CP hacia la encapsidación o hacia la supresión del silenciamiento necesita nuevos estudios que profundicen en estos procesos.

Análisis proteómico comparativo del exudado floemático de melón en respuesta a una infección viral.

El floema constituye la ruta que la mayoría de virus de plantas utilizan para dispersarse por toda la planta, pero además, es la vía de transporte de las señales de defensa que se producen para hacer frente al avance de la infección. Para tratar de aportar nuevos datos sobre el mecanismo que utiliza el MNSV para moverse sistémicamente, y obtener una mejor comprensión de las estrategias de infección y los mecanismos de defensa del huésped realizamos un estudio comparativo del proteoma del exudado floemático de melón en respuesta a la infección viral. Para ello utilizamos la técnica de electroforesis bidimensional diferencial en gel (2D-DIGE).

Los resultados obtenidos indicaron que la infección viral no producía grandes cambios, ni cualitativos ni cuantitativos, en el patrón de proteínas del exudado floemático. Aunque parezca sorprendente, en estudios similares con geles bidimensionales se observó que este fenómeno se encuentra generalizado en situaciones de estrés. Por ejemplo, la infección de melón con el virus del mosaico del pepino (CMV) induce la acumulación de unas cinco proteínas mientras que las carolinas (*Populus deltoides*) responden a herida acumulando solo dos proteínas, pop3/SP1 y taumatina, en el exudado floemático (Dafoe *et al.,* 2009; Malter and Wolf, 2011;). Por otro lado, en pepino y calabaza, el déficit hídrico induce un aumento de la actividad de varios enzimas antioxidantes en el phloema (superóxido dismutasas, dehidroascorbato reductasas y peroxidasas) (Walz *et al.,* 2002; Gaupels and Vlot, 2012). Se podría plantear la idea de que la respuesta a estrés en el floema se traduce en una modificación de la actividad enzimática basal más que en un cambio en la

abundancia de proteínas. Sin embargo, usando 2D DIGE, hemos sido capaces de detectar un mayor número de proteínas que presentan cambios en su abundancia relativa, comparado con las publicaciones anteriores. Por tanto, parece precipitado sacar esta conclusión con los pocos trabajos publicados al respecto. Con toda certeza, la reciente aparición de la tercera generación de aproximaciones proteómicas facilitará el avance en esta área de investigación.

En general este estudio muestra que la infección de MNSV provoca cambios en la abundancia relativa de 19 proteínas en el exudado floemático de melón, dos de ellas no habían sido descritas previamente en estudios proteómicos: la carboxilesterasa (CXE) y la fumarilacetoacetato hidrolasa (FAH) ambas incrementan su abundancia siendo consideradas reguladores negativos de la muerte celular (Gershater and Eduars, 2007; Han *et al.,*2013). El resto de proteínas están implicadas principalmente en estrés oxidativo (tanto producción como desintoxicación) o relacionadas directa o indirectamente con muerte celular o en la supresión de la respuesta hipersensible, muy probablemente debido a que se trata de una infección compatible. Además, estos resultados apoyan la hipótesis de que el floema está implicado activamente en la defensa contra patógenos. Un posible mecanismo de señalización frente a una infección viral podría ser el cambio en la concentración de ciertas proteínas que actúen como señalización y/o como parte de las defensas de la planta.

a) Proteínas implicadas en mantener el balance de oxido-reducción.

Las plantas generan especies reactivas del oxígeno o ROS (*reactive oxygen species*) como subproductos de varias rutas metabólicas pero también como moléculas de señalización para el control de diversos procesos tales como la defensa frente a patógenos, la muerte celular y el desarrollo (Apel and Hirt, 2004). El papel de floema en el mantenimiento del equilibrio redox ha sido apoyado por el hecho de que el exudado floemático de las cucurbitáceas contiene una elevada proporción de proteínas antioxidantes funcionales (Walz *et al.,* 2004). Entre las proteínas diferenciales, se observó un incremento en la abundancia de reguladores, tanto positivos como negativos, de la respuesta al estrés oxidativo. La fosfolípido hidroperóxido glutatión peroxidasa (PHGPx) metaboliza los hidroperóxidos de

fosfolípidos y actúa como una proteína citoprotectora bajo estrés oxidativo, salino y por calor (Dixon *et al.,* 2002; Chen *et al.,* 2004; Navrot *et al.,* 2006). La dihidroflavonol 4-reductasa (DFR) es una enzima clave en la biosíntesis de antocianinas que utiliza NADPH como cofactor, por lo tanto afecta a la homeostasis del NAD (Hayashi *et al.,* 2005). Además, se ha descrito que las antocianinas presentan actividad antioxidante, antimutagénica y anticancerígena (Wang *et al.,* 2013). A diferencia de las anteriores proteínas, la sobreexpresión de ATPasas tipo Obg puede actuar como un regulador negativo de la respuesta al estrés oxidativo en mamíferos, procariotas y plantas, probablemente para evitar que la respuesta de defensa provoque un daño excesivo en la propia planta. (Zhang *et al.,* 2009; Cheung *et al.,* 2010; Wenk *et al.,* 2012)

Por el contrario, la actividad y los niveles de algunas enzimas desintoxicantes de ROS (como ascorbato peroxidasas y catalasas) disminuyen en diferentes interacciones planta-patógeno. Esta supresión de los mecanismos de desintoxicación es crucial para el inicio de la muerte celular programada (Apel *et al.,* 2004). En este sentido, la serina hidroximetil transferasa (SHMT), que funciona en la vía fotorespiratoria, y la glucosa-6-fosfato deshidrogenasa (G6PDH), que es responsable de la primera reacción de la vía de las pentosas fosfato, presentaron una disminución en sus niveles de abundancia. La deficiencia de SHMT interfiere con la activación de las respuestas de defensa y aumenta el estrés oxidativo (Moreno *et al.,* 2005) mientras que la G6PDH es la principal responsable de la producción del NADPH celular y de preservar el equilibrio celular de glutatión, esencial en la resistencia al estrés oxidativo en las plantas (Wang *et al.,* 2008). Los cambios en la acumulación de estas enzimas relacionadas con la homeostasis redox pueden estar implicados en la modulación de los niveles de ROS que en el floema tiene una doble función: el mantenimiento de los estados redox y la señalización.

b) Proteínas relacionadas con la muerte celular.

En muchas interacciones planta-microorganismo incompatibles, la explosión oxidativa que precede la muerte celular localizada (LCD), incluye la inducción de genes de defensa asociados a eventos proteolíticos y nucleolíticos y a la aparición de señales moleculares tales como el calcio, ROS, el ácido salicílico, y los esfingolípidos. Este

fenómeno se conoce colectivamente como respuesta hipersensible (HR) (Zurbriggen *et al.,* 2010). Inicialmente se pensó que la HR estaba diseñada única y exclusivamente para restringir el avance de patógenos. Sin embargo, se sabe que, durante las interacciones susceptibles, muchos patógenos virulentos también inducen la muerte celular con las características de la apoptosis (Greenberg and Yao, 2004).

Las dos proteínas del floema no detectadas previamente identificadas en este estudio presentaban un incremento en su abundancia y se consideran ambas como reguladores negativos de la muerte celular: la carboxilesterasa (CXE) mostró un 65% de identidad con el marcador de HR específico de *N. tabacum* denominado HSR203J y la fumarilacetoacetato hidrolasa (FAH) cataliza la etapa final en la vía de degradación de la tirosina. Se ha descrito que las plantas transgénicas con un HSR203J no funcional muestran una intensificación de la HR y una mayor resistencia a patógenos (Gershater y Edwards, 2007). Del mismo modo, la supresión de la actividad FAH conduce a la acumulación de intermediarios de degradación de la tirosina que son tóxicos para la célula vegetal causando la muerte celular (Han *et al.,*2013). Por otro lado, la serpina, un inhibidor de las serin proteasas, se ha encontrado también sobreacumulado en exudados floemáticos de *A. thaliana*, arroz, calabaza y melón. Las serpinas actúan principalmente sobre las serin proteasas, pero también sobre las caspasas, algunas proteínas semejantes a las metacaspasas y las papaína cisteína proteasas. De hecho, la presencia de una cantidad suficiente de AtSerpin1 en el citoplasma evita la muerte celular lo que sugiere que las serpinas pueden desempeñar un papel esencial en defensa al regular la respuesta inmune del huésped (Law *et al.,* 2006; Lampl *et al.,* 2010; Li *et al.,*2013). Además, se ha sugerido que los inhibidores de las proteinasas del floema pueden desempeñar un papel en la protección frente a la proteolisis de las proteínas de unión a RNAs floemáticos móviles durante su viaje de larga distancia desde las regiones fuente a las sumidero (Lin *et al.,*2009). Además, se ha demostrado que estos inhibidores de proteinasas forman parte de los complejos ribonucleoproteicos que podrían estar implicados en el tráfico de RNA (Ham *et al.,* 2014). Por último, los niveles de una 3-cetoacil-CoA sintasa (KCS) disminuyeron. Esta enzima participa en la síntesis de los ácidos grasos de cadena larga que constituyen los precursores de los esfingolípidos. Muchas etapas de la ruta biosintética de los

esfingolípidos son activadas por la infección generando muerte celular y resistencia (Hause *et al.,* 2003). Tanto la acumulación de las primeras tres proteínas como la reducción de esta última se podría relacionar con una inhibición de la muerte celular, como cabría esperar para un huésped susceptible a MNSV.

Por el contrario, el aumento de la desoxirribonucleasa TATDN1 podría estar asociado con los eventos nucleolíticos que se producen durante la muerte celular. En general, las nucleasas están involucradas en la defensa del huésped contra las moléculas de ácidos nucleicos ajenas (Hsia *et al.,* 2005), incluso algunas proteínas PR (*pathogenesis related*) pueden tener actividad DNasa y RNasa (Guevara-Morato *et al.,* 2010; Pereira *et al.,* 2014). Sin embargo TATDN1 es una nucleasa conservada directamente implicada en la fragmentación apoptótica de DNA en levadura y *Caenorhabditis elegans* (Yang *et al.,* 2012). Otra evidencia de muerte celular puede ser la baja acumulación de la proteína TCP1/cpn60, una chaperonina esencial para el correcto plegamiento y posterior ensamblaje de las diferentes subunidades de los enzimas oligoméricos. Curiosamente, TCP1/cpn60 es una posible diana de la metacaspasa 9 (AtMC9), una proteasa relacionada con la muerte celular en *A. thaliana* cuya actividad proteolítica puede ser regulada, entre otras posibilidades, por AtSerpin1 (Vercammen *et al.,* 2006; Xu *et al.,* 2008).

c) Proteínas con capacidad de interaccionar con el virus

En estudios previos se demostró que la CP era necesaria para el movimiento sistémico (Genovés *et al.,* 2006). En este trabajo además de corroborarlo hemos demostrado que es dependiente de los subdominios R2 y R3 y que el mecanismo más plausible sería a través del bloqueo de la señal sistémica de silenciamiento, favoreciendo así la entrada en el sistema vascular y con ello el movimiento sistémico del virus. Sin embargo no existe evidencia experimental sobre la participación directa de la CP como virión o como parte de un complejo móvil (VMC, *viral movement complex*) en este movimiento a larga distancia por el floema. En estudios previos se confirmó mediante análisis Northern blot que los RNAs del MNSV se acumulaban en el exudado floemático de melón infectado (Herranz *et al.,* 2015). Sin embargo, la CP no se detectó en el exudado floemático, por este motivo no se encontraba entre las proteínas diferenciales obtenidas mediante 2D-DIGE. Este resultado fue confirmado en

estudios posteriores con anticuerpos específicos y sugiere que la CP no formaría parte del VMC cuyos componentes aún no han sido identificados.

En este sentido, tres de las proteínas acumuladas diferencialmente han sido previamente descritas como componentes de complejos virales: la fructosa 1,6 bifosfatasa aldolasa, la subunidad β del proteasoma y la chaperonina TCP1/cnp60 (Brizard *et al.,* 2006). El papel específico de estas proteínas como componentes del VMC que se mueve a través del floema queda por esclarecer. Otra proteína identificada es la proteína de unión a poliadeninas o PABP, un factor de iniciación de la traducción que se une a la cola poli A durante la traducción para estabilizar el mRNA. PABP favorece la traducción de los RNAs sin estructura CAP ni poliadenilados del virus del mosaico necrótico del trébol rojo (RCNMV) mediante su unión a un elemento de secuencia que potencia la traducción independiente de la estructura CAP (CITE) (Iwakama *et al.,*2012). Al igual que el MNSV, el RCNMV también es un miembro de la familia *Tombusviridae* y ambos poseen un elemento CITE funcional (Truniger *et al.,* 2008; Miras *et al.,* 2014). Es posible que el MNSV también necesite la PABP para la traducción de sus proteínas y el incremento de la concentración en las partes vegetativas haga que incremente su concentración en el floema. Además, esta proteína se ha detectado en el floema de calabaza y puede ser considerado como parte de un conjunto de proteínas floemáticas de unión a RNA potencialmente implicados en la translocación vascular de RNAs virales o endógenos (Lin *et al.,* 2009; Pallás and Gómez, 2011; Ham *et al.,* 2014).

CONCLUSIONES

-Se han determinado los requerimientos de secuencia necesarios para la salida del RE hacia el AG en la ruta de secreción temprana de una proteína de movimiento viral. Los residuos implicados de esta proteína transmembrana se localizan tanto en el Nt citosólico como el Ct luminal, siendo uno de los primeros ejemplos descritos en plantas. Con los datos obtenidos se ha propuesto un nuevo modelo en el que después de la inserción y correcto plegamiento de la proteína en la membrana del RE, el Ct luminal de p7B interaccionaría a través del residuo K49 con un adaptador transmembrana asociado al citoesqueleto de actina para su movimiento y concentración en el RE-cortical. El motivo citoplasmático en Nt sería necesario para el ensamblaje de la vesícula COPII.

-Mediante ensayos de doble híbrido y de BiFC se ha podido identificar tres proteínas celulares capaces de interaccionar con tres DGBp1 procedentes de tres carmovirus diferentes (MNSV, TCV y CarMV). Estos factores celulares son la proteína P3 del ribosoma 60S (RPP3A), la subunidad g del factor de iniciación de la traducción 3 (eIF3g) y el factor de transcripción WRKY36. Además, mediante ensayos de mutagénesis se demostró que el dominio de unión de estas DGBp1 es un dominio Ct (FNF) conservado. La observación de que estas tres proteínas interaccionen con los mismos factores claramente sugiere un posible mecanismo conservado en los carmovirus.

-Mediante el análisis del motivo desestructurado Nt (R) de la CP del MNSV, utilizando varias aproximaciones bioquímicas y celulares se ha podido demostrar la multifuncionalidad de esta proteína dentro del ciclo vital del virus. Mediante ensayos de EMSA se ha observado que este dominio, concretamente el subdominio R3, interviene tanto en la unión de vRNA como en la encapsidación. Además, se ha relacionado la capacidad de unir sRNAs del dominio R3 con la supresión del silenciamiento, a través de un potencial bloqueo de la señal sistémica de silenciamiento.

-Se ha demostrado que el MNSV produce cambios en la composición del proteoma del floema del melón. Mediante estudios de 2DE-DIGE se han identificado 19 proteínas cuya concentración se ve alterada durante la infección del MNSV, dos de las cuales (la carboxilesterasa y la fumarilacetoacetato hidrolasa) no habían sido descritas previamente en estudios proteómicos. La mayoría de proteínas encontradas están relacionadas con el estrés oxidativo y la respuesta hipersensible o muerte celular. Estos resultados sugieren un papel activo del floema en la defensa contra patógenos mediante la regulación de la concentración de ciertas proteínas que actúen como señalización y/o como parte de las defensas de la planta.

BIBLIOGRAFÍA

Adenot, X., Elmayan, T., Lauressergues, D., Boutet, S., Bouché, N., Gasciolli, V., and Vaucheret, H. (2006). DRB4-dependent TAS3 trans-acting siRNAs control leaf morphology through AGO7. *Curr Biol* 16:927-932.

Aki, T., Shigyo, M., Nakano, R., Yoneyama, T. and Yanagisawa, S. (2008). Nano scale proteomics revealed the presence of regulatory proteins including three FT-like proteins in phloem and xylem saps from rice. *Plant Cell Physiol* 49:767-790.

Ahlquist, P. (2006). Parallels among positive-strand RNA viruses, reverse-transcribing viruses and double-stranded RNA viruses. *Nat Rev Microbiol* 4:371-382.

Amari, K., Boutant, E., Hofmann, C., Schmitt-Keichinger, C., Fernandez-Calvino, L., Didier, P., Lerich, A., Mutterer J., Thomas C., Heinlein M., Mély Y., Maule A. and Ritzenthaler C. (2010). A family of plasmodesmal proteins with receptor-like properties for plant viral movement proteins. *PLoS Pathog* 6:e1001119.

Amari, K., Vazquez, F. and Heinlein, M. (2012). Manipulation of plant host susceptibility: an emerging role for viral movement proteins? *Front Plant Sci*3:10.

Amari, K., Lerich, A., Schmitt-Keichinger, C., Dolja, V.V. and Ritzenthaler, C. (2011). Tubule-guided cell-to-cell movement of a plant virus requires class XI myosin motors. *PLoS Pathog*. 7:e1002327.

Andreeva, A. V., Zheng, H., Saint-Jore, C. M., Kutuzov, M. A., Evans, D. E. and Hawes, C. R. (2000). Organization of transport from endoplasmic reticulum to Golgi in higher plants. *Biochem Soc Trans* 28:505-512.

Andreev, I. A., Kim, S. H., Kalinina, N. O., Rakitina, D. V., Fitzgerald, A. G., Palukaitis, P. and Taliansky, M. E. (2004). Molecular interactions between a plant virus movement protein and RNA: force spectroscopy investigation. *J Mol Biol* 339:1041-1047.

Andret-Link, P. and Fuchs, M. (2005). Transmission specificity of plant viruses by vectors. *J Plant Pathol* 87:153-165.

Aniento, F., Matsuoka, K. and Robinson, D. (2006). ER-to-Golgi transport: the COPII-pathway. In The plant endoplasmic reticulum. Plant cell monograph Vol 4 (Robinson, D. ed). Berlin/Heidelberg: Springer, pp. 99-124.

Aniento, F. and Robinson, D.G. (2005). Testing for endocytosis in plants. *Protoplasma* 226:3-11.

Anstead, J. A., Hartson, S. D. and Thompson, G.A. (2013). The broccoli (Brassica oleracea) phloem tissue proteome. *BMC Genomics* 14:764.

Aparicio, F., Pallás, V. and Sánchez-Navarro, J. (2010). Implication of the C terminus of the prunus necrotic ringspot virus movement protein in cell-to-cell transport and in its interaction with the coat protein. *J Gen Virol* 91:1865-1870.

Aparicio, F., Sánchez-Navarro, J. and Pallás, V. (2006). In vitro and in vivo mapping of the Prunus necrotic ringspot virus coat protein C-terminal dimerization domain by bimolecular fluorescence complementation. Journal of General Virology 87: 1745-1750

Aparicio, F., Vilar, M., Pérez-Payá, E. and Pallás, V. (2003). The coat protein of prunus necrotic ringspot virus specifically binds to and regulates the conformation of its genomic RNA. Virology 313:213-223.

Apel K, and Hirt H. (2004). Reactive oxygen species: metabolism, oxidative stress, and signal transduction. *Annu Rev Plant Biol* 55:373-399.

Aroeti, B., Kosen, P. A., Kuntz, I. D., Cohen, F. E. and Mostov, K. E. (1993). Mutational and secondary structural analysis of the basolateral sorting signal of the polymeric immunoglobulin receptor. *J. Cell Biol* 123:1149-1160.

Ashby, J., Boutant, E., Seemanpillai, M., Groner, A., Sambade, A., Ritzenthaler, C., and Heinlein, M. (2006). Tobacco mosaic virus movement protein functions as a structural microtubule-associated protein. *J virol* 80:8329-8344.

Asurmendi, S., Berg, R. H., Koo, J. C., and Beachy, R. N. (2004). Coat protein regulates formation of replication complexes during tobacco mosaic virus infection. *Proc Natl Acad Sci U S A* 101:1415-1420.

Atkins, C. A., Smith, P. M. and Rodriguez-Medina, C. (2011). Macromolecules in phloem exudates-a review. *Protoplasma* 248:165-172.

Atkins, D., Hull, R., Wells, B., Roberts, K., Moore, P. and Beachy, R. N. (1991). The Tobacco mosaic virus 30K movement protein in transgenic tobacco plants is localized to plasmodesmata. *J Gen Virol* 72:209-211.

Auerbach, D. and Stagljar, I. (2005). Yeast Two-Hybrid Protein-Protein Interaction Networks. Pages 19-31 in: Proteomics and Protein-Protein Interactions, Springer.

Avisar, D., Abu-Abied, M., Belausov, E., Sadot, E., Hawes, C., and Sparkes, I. A. (2009). A comparative study of the involvement of 17 Arabidopsis myosin family members on the motility of Golgi and other organelles. *Plant Physiol* 150:700-709.

Avisar, D., Prokhnevsky, A. I., Makarova, K. S., Koonin, E. V. and Dolja V. V. (2008). Myosin XI-K is required for rapid trafficking of Golgi stacks, peroxisomes, and mitochondria in leaf cells of *Nicotiana benthamiana*. *Plant Physiol* 146:1098-1108.

Azevedo, J., García, D., Pontier, D., Ohnesorge, S., Yu, A., García, S., Braun, L., Bergdoll, M., Hakimi, M. A., Lagrange, T. and Voinnet, O. (2010). Argonaute quenching and global changes in Dicer homeostasis caused by a pathogen-encoded GW repeat protein. *Genes Dev* 24:904-915.

Baer, M. L., Houser, F., Loesch-Fries, L. S. and Gehrke, L. (1994). Specific RNA binding by amino-terminal peptides of alfalfa mosaic virus coat protein. *EMBO J* 13:727-735.

Bailey-Serres, J., Vangala, S., Szick, K. and Lee, C.H. (1997). Acidic phosphoprotein complex of the 60S ribosomal subunit of maize seedling roots. Components and changes in response to flooding. *Plant Physiol* 114:1293-1305.

Banerjee, A. K., Chatterjee, M., Yu, Y., Suh, S. G., Miller, W. A. and Hannapel, D. J. (2006). Dynamics of a mobile RNA of potato involved in a long-distance signaling pathway. *Plant Cell* 18:3443-3457.

Bansal, A. and Gierasch, L. M. (1991). The NPXY internalization signal of the LDL receptor adopts a reverse-turn conformation. *Cell* 67:1195-1201.

Barajas, D., Xu, K., de Castro Martín, I. F., Sasvari, Z., Brandizzi, F., Risco, C. and Nagy, P. D. (2014). Co-opted oxysterol-binding ORP and VAP proteins channel sterols to RNA virus replication sites via membrane contact sites. *PLoS Pathog* 10:10.

Barlowe, C. (2003). Signals for COPII-dependent export from the ER: what's the ticket out?. *Trends Cell. Biol* 13:295-300.

Batailler, B., Lemaitre, T., Vilaine, F., Sánchez, C., Renard, D., Cayla, T., Beneteau, J. and Dinant, S. (2012). Soluble and filamentous proteins in Arabidopsis sieve elements. *Plant Cell Environ* 35:1258-1273.

Batten, J. S., Turina, M. and Scholthof, K. B. (2006). Panicovirus accumulation is governed by two membrane-associated proteins with a newly identified conserved motif that contributes to pathogenicity. *Virol J* 3:12.

Baulcombe, D. (2004). RNA silencing in plants. *Nature 431*:356-363.

Bayne, E. H., Rakitina, D. V., Morozov, S. Y. and Baulcombe, D. C. (2005). Cell-to-cell movement of Potato Potexvirus X is dependent on suppression of RNA silencing. *Plant J* 44:471-482.

Bazzini, A. A., Hopp, H. E., Beachy, R. N., and Asurmendi, S. (2007). Infection and coaccumulation of tobacco mosaic virus proteins alter microRNA levels, correlating with symptom and plant development. *Proc Natl Acad Sci U S A* 104:12157-12162.

Becker, F., Buschfeld, E., Schell, J. and Bachmair, A. (1993). Altered response to viral infection by tobacco plants perturbed in ubiquitin system. *Plant J* 3:875-881.

Beffa, R. and Meins, F. (1996). Pathogenesis-related functions of plant β-1, 3-glucanases investigated by antisense transformation—a review. *Gene* 179:97-103.

Belkhadir, Y., Nimchuk, Z., Hubert, D. A., Mackey, D. and Dangl, J. L. (2004). Arabidopsis RIN4 negatively regulates disease resistance mediated by RPS2 and RPM1 downstream or independent of the NDR1 signal modulator and is not required for the virulence functions of bacterial type III effectors AvrRpt2 or AvrRpm1. *Plant Cell* 16:2822-2835.

Belshaw R, Pybus OG and Rambaut A. (2007). The evolution of genome compression and genomic novelty in RNA viruses. *Genome Res* 17:1496-1504.

Bencharki, B., Boissinot, S., Revollon, S., Ziegler-Graff, V., Erdinger, M., Wiss, L., Dinant, S., Renard, D., Beuve, M., Lemaitre-Guillier, C. and Brault, V. (2010). Phloem protein partners of Cucurbit aphid

borne yellows virus: possible involvement of phloem proteins in virus transmission by aphids.*Mol Plant Microbe Interact* 23:799-810.

Bencharki, B., El Yamani, M., and Zaoui, D. (2000). Assessment of transmission ability of barley yellow dwarf virus-PAV isolates by different populations of Rhopalosiphum padi and Sitobion avenae. European Journal of Plant Pathology, 106(5), 455-464.

Berna, A., Gafny, R., Wolf, S., Lucas, W. J., Holt, C. A. and Beachy, R. N. (1991). The TMV movement protein: role of the C-terminal 73 amino acids in subcellular localization and function. *Virology* 182:682-689.

Betti, C., Lico, C., Maffi, D., D'Angeli, S., Altamura, M. M., Benvenuto, E., Faoro, F., and Baschieri, S. (2012). Potato virus X movement in *Nicotiana benthamiana*: new details revealed by chimeric coat protein variants. *Mol Plant Pathol* 13:198-203.

Blackman, L. M., Boevink, P., Santa Cruz, S., Palukaitis, P. and Oparka, K. J. (1998). The movement protein of cucumber mosaic virus traffics into sieve elements in minor veins of Nicotiana clevelandii. *Plant Cell* 10:525-537.

Blum, R. and Lepier, A. (2008). The luminal domain of p23 (Tmp21) plays a critical role in p23 cell surface trafficking. *Traffic* 9:1530-1550.

Boevink, P. and Oparka, K. J. (2005). Virus-host interactions during movement processes. *Plant Physiol* 138:1815-1821.

Boevink, P., Oparka, K., Santa Cruz, S., Martin, B., Betteridge, A. and Hawes, C. (1998). Stacks on tracks: the plant Golgi apparatus traffics on an actin/ER network. *Plant J* 15:441-447.

Bol, J. F. (1999). Alfalfa mosaic virus and ilarviruses: involvement of coat protein in multiple steps of the replication cycle. *J Gen Virol* 80:1089-1102.

Bol, J. F. (2008). Role of capsid proteins. In Plant Virology Protocols (pp. 21-31). Humana Press.

Boulila, M. (2011). Positive selection, molecular recombination structure and phylogenetic reconstruction of members of the family Tombusviridae: Implication in virus taxonomy. *Genet Mol Biol* 34:647-660.

Boutant, E., Fitterer, C., Ritzenthaler, C., and Heinlein, M. (2009). Interaction of the Tobacco mosaic virus movement protein with microtubules during the cell cycle in tobacco BY-2 cells. *Protoplasma* 237:3-12.

Brandizzi, F. and Barlowe, C. (2013). Organization of the ER-Golgi interface for membrane traffic control. *Nature Rev* 14:382-392.

Brandizzi, F., Frangne, N., Marc-Martin, S., Hawes, C., Neuhaus, J. M. and Paris, N. (2002a). The destination for single-pass membrane proteins is influenced markedly by the length of the hydrophobic domain. *Plant Cell* 14:1077-1092.

Brandizzi, F., Snapp, E. L., Roberts, A. G., Lippincott-Schwartz, J. and Hawes, C. (2002b). Membrane protein transport between the endoplasmic reticulum and the Golgi in tobacco leaves is energy dependent but cytoskeleton independent: evidence from selective photobleaching. *Plant Cell* 14:1293-1309.

Brandner, K., Sambade, A., Boutant, E., Didier, P., Mely, Y., Ritzenthaler, C., and Heinlein, M. (2008). Tobacco mosaic virus movement protein interacts with green fluorescent protein-tagged microtubule end-binding protein 1. *Plant Physiol* 147:611-623.

Bransom, K. L., Weiland, J. J., Tsai, C. H. and Dreher, T. W. (1995). Coding density of the Turnip yellow mosaic virus genome: roles of the overlapping coat protein and p206-readthrough coding regions. *Virology* 206:403-412.

Brizard, J. P., Carapito, C., Delalande, F., Van Dorsselaer, A. and Brugidou, C. (2006). Proteome analysis of plant-virus interactome comprehensive data for virus multiplication inside their hosts. *Mol Cell Proteomics* 5:2279-2297.

Bue, C. A. and Barlowe, C. (2009). Molecular dissection of Erv26p identifies separable cargo binding and coat protein sorting activities*. J Biol Chem* 284:24049-24060.

Brodersen, P. and Voinnet, O. (2006). The diversity of RNA silencing pathways in plants. *Trends Genet* 22:268-280.

Bucher, G. L., Tarina, C., Heinlein, M., Di Serio, F., Meins, F. and Iglesias, V. A. (2001). Local expression of enzymatically active class I β-1, 3-glucanase enhances symptoms of TMV infection in tobacco. *Plant J* 28:361-369.

Burgyán, J. and Havelda, Z. (2011). Viral suppressors of RNA silencing. *Trends Plant Sci* 16:265-272.

Callaway A, Giesman-Cookmeyer D, Gillock ET, Sit TL, and Lommel SA. (2001). The multifunctional capsid proteins of plant RNA viruses. Annu Rev Phytopathol 39:419-460.

Campo, S., Carrascal, M., Coca, M., Abian, J., and San Segundo, B. (2004). The defense response of germinating maize embryos against fungal infection: a proteomics approach. *Proteomics*, *4*(2), 383-396.

Cañizares, M. C., Marcos, J. F. y Pallás, V. (2001). Molecular variability of twenty-one geographically distinct isolates of Carnation mottle virus (CarMV) and phylogenetic relationships within the Tombusviridae family. *Arch Virol* 146:2039-2051.

Cao M, Ye X, Willie K, Lin J, Zhang X, Redinbaugh M.G, Simon AE, Morris T. J., and Qu F. (2010). The capsid protein of Turnip crinkle virus overcomes two separate defense barriers to facilitate systemic movement of the virus in Arabidopsis. J Virol 84:7793-7802.

Caplan, J. L., Zhu, X., Mamillapalli, P., Marathe, R., Anandalakshmi, R. and Dinesh-Kumar, S. P. (2009). Induced ER chaperones regulate a receptor-like kinase to mediate antiviral innate immune response in plants. Cell Host Microbe 2009;6:457-69.

Carey, J. (1991). Gel retardation. *Methods Enzymol* 208:103-117.

Carmo-Fonseca, M., Berciano, M. T. and Lafarga, M. (2010). Orphan nuclear bodies. Cold Spring Harbor Perspectives in Biology 2:a000703.

Casado-Vela, J., Selles, S. and Martínez, R. B. (2006). Proteomic analysis of tobacco mosaic virus-infected tomato (Lycopersicon esculentum M.) fruits and detection of viral coat protein. *Proteomics* 6 Suppl 1:S196-206.

Chapman, E. J. and Carrington, J. C. (2007). Specialization and evolution of endogenous small RNA pathways. *Nat Rev Genet* 8:884-896.

Citovsky, V., Knorr, D., Schuster, G. and Zambryski, P. C. (1990). The P30 movement protein of tobacco mosaic virus is a single-strand nucleic acid binding protein. *Cell* 60:637-647.

Citovsky, V., Wong, M. L., Shaw, A. L., Prasad, B. V. and Zambryski, P. (1992). Visualization and characterization of Tobacco mosaic virus movement protein binding to single-stranded nucleic acids. *Plant Cell* 4:397-411.

Citovsky, V., Zaltsman, A., Kozlovsky, S. V., Gafni, Y. and Krichevsky, A. (2009). Proteasomal degradation in plant–pathogen interactions. In *Seminars in cell and developmental biology* (Vol. 20, No. 9, pp. 1048-1054). Academic Press.

Cohen, Y., Qu, F., Gisel, A., Morris, T. J. and Zambryski, P. C. (2000). Nuclear localization of *Turnip crinkle virus* movement protein p8. *Virology* 273:276-285.

Cuchalova, L., Kouba, T., Herrmannova, A., Danyi, I., Chiu, W. L. and Valasek, L. (2010). The RNA recognition motif of eukaryotic translation initiation factor 3g (eIF3g) is required for resumption of scanning of posttermination ribosomes for reinitiation on GCN4 and together with eIF3i stimulates linear scanning. *Mol Cell Biol* 30:4671-4686.

Chen, L., Zhang, L., Li, D., Wang, F. and Yu, D. (2013). WRKY8 transcription factor functions in the TMV-cg defense response by mediating both abscisic acid and ethylene signaling in Arabidopsis. *Proc Natl Acad Sci U S A* 110:E1963-1971.

Chen, M. H., Tian, G. W., Gafni, Y. and Citovsky, V. (2005). Effects of calreticulin on viral cell-to-cell movement. *Plant Physiol* 138:1866-1876.

Chen, M. H., Sheng, J., Hind, G., Handa, A. K., and Citovsky, V. (2000). Interaction between the tobacco mosaic virus movement protein and host cell pectin methylesterases is required for viral cell-to-cell movement. *EMBO J* 19:913-920.

Chen, S., Vaghchhipawala, Z., Li, W., Asard, H. and Dickman, M. B. (2004). Tomato phospholipid hydroperoxide glutathione peroxidase inhibits cell death induced by Bax and oxidative stresses in yeast and plants. *Plant Physiol* 135:1630-1641.

Cheung, M.-Y., Xue, Y., Zhou, L., Li, M.-W., Sun, S.S.-M. and Lam H.-M. (2010). An Ancient P-Loop GTPase in Rice Is Regulated by a Higher Plant-specific Regulatory Protein. *J Biol Chem* 285:37359-37369.

Chi, Y., Yang, Y., Zhou, Y., Zhou, J., Fan, B., Yu, J. Q. and Chen, Z. (2013). Protein-protein interactions in the regulation of WRKY transcription factors. *Mol Plant* 6:287-300.

Chisholm, S. T., Parra, M. A., Anderberg, R. J. and Carrington, J. C. (2001). Arabidopsis RTM1 and RTM2 genes function in phloem to restrict long-distance movement of tobacco etch virus. *Plant Physiol* 127:1667-1675.

Cho, W. K., Chen, X. Y., Rim, Y., Chu, H., Kim, S., Kim, S. W., Park, Z. Y. and Kim, J. Y. (2010). Proteome study of the phloem sap of pumpkin using multidimensional protein identification technology. *J Plant Physiol* 167:771-778.

Chou, Y. L., Hung, Y. J., Tseng, Y. H., Hsu, H. T., Yang, J. Y., Wung, C. H., Lin, N. S., Meng, M., Hsu, Y. H. and Chang, B.Y. (2013). The stable association of virion with the triple-gene-block protein 3-based complex of Bamboo mosaic virus. *PLoS Pathog* 9:e1003405

Christensen, N., Tilsner, J., Bell, K., Hammann, P., Parton, R., Lacomme, C. and Oparka, K. (2009). The 5′ cap of tobacco mosaic virus (TMV) is required for virion attachment to the actin/endoplasmic reticulum network during early infection. *Traffic* 10:536-551.

Conesa, A., Gotz, S., García-Gómez, J. M., Terol, J., Talon, M. and Robles, M. (2005). Blast2GO: a universal tool for annotation, visualization and analysis in functional genomics research. *Bioinformatics* 21:3674-3676.

Csorba, T., Kontra, L. and Burgyán, J. (2015). viral silencing suppressors: Tools forged to fine-tune host-pathogen coexistence. *Virology* 479:85-103.

Culver, J. N. (2002). Tobacco mosaic virus assembly and disassembly: determinants in pathogenicity and resistance. *Annu Rev Phytopathol* 40:287-308.

Dafoe, N. J., Zamani, A., Ekramoddoullah, A. K., Lippert, D., Bohlmann, J. and Constabel, C. P. (2009). Analysis of the poplar phloem proteome and its response to leaf wounding.*J Proteome Res* 8: 2341-2350.

Dancourt, J. and Barlowe, C. (2009). Erv26p-dependent export of alkaline phosphatase from the ER requires lumenal domain recognition. *Traffic* 10:1006-1018.

Dancourt, J. and Barlowe, C. (2010). Protein sorting receptors in the early secretory pathway. *Annu Rev Biochem* 79:777-802.

Dargemont, C., Le Bivic, A., Rothenberger, S., Iacopetta, B. and Kuhn, L. C. (1993). The internalization signal and the phosphorylation site of transferrin receptor are distinct from the main basolateral sorting information. *EMBO J* 12:1713-1721.

daSilva, L. L., Snapp, E. L., Denecke, J., Lippincott-Schwartz, J., Hawes, C. and Brandizzi, F. (2004). Endoplasmic reticulum export sites and Golgi bodies behave as single mobile secretory units in plant cells. *Plant Cell* 16:1753-1771.

Dawson WO. 1992. Tobamovirus-plant interactions. Virology 186:359–67.

Deom, C. M., He, X. Z., Beachy, R. N. and Weissinger, A. K. (1994). Influence of heterologous Tobamovirus movement protein and chimeric-movement protein genes on cell-to-cell and long-distance movement. *Virology* 205:198-209.

Deshaies, R. J. (1999). SCF and Cullin/Ring H2-based ubiquitin ligases. *Annu Rev Cell Dev Biol* 15:435-467.

Desvoyes, B., Faure-Rabasse, S., Chen, M. H., Park, J. W., and Scholthof, H. B. (2002). A novel plant homeodomain protein interacts in a functionally relevant manner with a virus movement protein. *Plant Physiol* 129:1521-1532.

Diaz, J. A., Nieto, C., Moriones, E., Truniger, V., Aranda, M. A. (2004). Molecular characterization of a Melon necrotic spot virus strain that overcomes the resistance in melon and nonhost plants. *Mol Plant Microbe Interact* 17:668-675.

Díaz-Vivancos, P., Clemente-Moreno, M. J., Rubio, M., Olmos, E., García, J. A., Martínez-Gómez, P. and Hernández, J. A. (2008). Alteration in the chloroplastic metabolism leads to ROS accumulation in pea plants in response to plum pox virus. *J Exp Bot* 59:2147-2160.

Di Carli, M., Benvenuto, E. and Donini, M. (2012). Recent insights into plant-virus Interactions through proteomic analysis. *J Proteome Res* 11:4765-4780.

Di Carli, M., Villani, M. E., Bianco, L., Lombardi, R., Perrotta, G., Benvenuto, E., & Donini, M. (2010). Proteomic analysis of the plant− virus interaction in Cucumber mosaic virus (CMV) resistant transgenic tomato. *J Proteome Res* 9:5684-5697.

Díez, J., Marcos, J. F. and Pallás V. (1998). Carmovirus isolation and RNA extraction. *Methods Mol Biol* 81:211-217.

Dinant, S. and Suárez-López, P. (2012). Multitude of long-distance signal molecules acting via phloem In: Witzany G, Baluška F, editors. Biocommunication of Plants: Springer Berlin Heidelberg; p. 89-121.

Ding, B., Haudenshield, J. S ., Hull, R. J., Wolf, S., Beachy, R. N. and Lucas, W. J. (1992. Secondary plasmodesmata are specific sites of localization of the Tobacco mosaic virus movement protein in transgenic tobacco plants. *Plant Cell* 4:915-928.

Dixon, D. P., Lapthorn, A. and Edwards, R. (2002). Plant glutathione transferases. *Genome Biol* 3:REVIEWS3004.

Doan, D. N., Lee, K. C., Laurinmaki, P., Butcher, S., Wong, S. M. and Dokland, T. (2003). Three-dimensional reconstruction of hibiscus chlorotic ringspot virus. *J Struct Biol* 144:253-261.

Dolja, V. V. (2003). *Beet yellows virus*: the importance of being different. *Mol Plant Pathol* 4:91-98.

Dolja, V. V., Kreuze, J. F., and Valkonen, J. P. (2006). Comparative and functional genomics of closteroviruses. Virus Res 117:38-51.

Donaire, L., Wang, Y., Gonzalez-Ibeas, D., Mayer, K. F., Aranda, M. A. and Llave, C. (2009). Deep-sequencing of plant viral small RNAs reveals effective and widespread targeting of viral genomes. *Virology* 392:203-214.

Dong, X. F., Natarajan, P., Tihova, M., Johnson, J. E. and Schneemann, A. (1998). Particle polymorphism caused by deletion of a peptide molecular switch in a quasiequivalent icosahedral virus. *J Virol* 72:6024-6033.

Dorokhov, Y. L., Makinen, K., Frolova, O. Y., Merits, A., Saarinen, J., Kalkkinen, N., Atabekov, J. G. and Saarma, M. (1999). A novel function for a ubiquitous plant enzyme pectin methylesterase: the host-cell receptor for the tobacco mosaic virus movement protein. *FEBS Lett* 461:223-228.

Drake, J. W. and Holland, J. J. (1999). Mutation rates among RNA viruses. *Proc Natl Acad Sci U S A* 96:13910-13913.

Drugeon, G. and Jupin, I. (2002). Stability in vitro of the 69K movement protein of Turnip yellow mosaic virus is regulated by the ubiquitin-mediated proteasome pathway. *J Gen Virol* 83:3187-3197.

Duff-Farrier, C. R., Bailey, A. M., Boonham, N. and Foster, G. D. (2015). A pathogenicity determinant maps to the N-terminal coat protein region of the Pepino mosaic virus genome. *Mol Plant Pathol* 16:308-315.

Dukhovny, A., Yaffe, Y., Shepshelovitch, J. and Hirschberg, K. (2009). The length of cargo-protein transmembrane segments drives secretory transport by facilitating cargo concentration in export domains. *J Cell Sci* 122:1759-1767.

Dunker, A. K., Silman, I., Uversky, V. N. and Sussman, J. L. (2008). Function and structure of inherently disordered proteins. *Curr Opin Struct Biol* 18:756-764.

Dunoyer, P., Brosnan, C. A., Schott, G., Wang, Y., Jay, F., Alioua, A., Himber, C. and Voinnet, O. (2010). An endogenous, systemic RNAi pathway in plants. *EMBO J* 29:1699-1712.

Eberle, W., Sander, C., Klaus, W., Schmidt, B., von Figura, K. and Peters, C. (1991). The essential tyrosine of the internalization signal in lysosomal acid phosphatase is part of a beta turn. *Cell* 67:1203-1209.

Edreva, A. (2005). Pathogenesis-related proteins: research progress in the last 15 years. *Gen Appl Plant Physiol* 31: 105-124.

Elena, S. F. and Sanjuan, R. (2005). Adaptive value of high mutation rates of RNA viruses: separating causes from consequences. *J Virol* 79:11555-11558.

Elvira, M. I., Galdeano, M. M., Gilardi, P., García-Luque, I., and Serra, M. T. (2008). Proteomic analysis of pathogenesis-related proteins (PRs) induced by compatible and incompatible interactions of pepper mild mottle virus (PMMoV) in Capsicum chinense L3 plants. *J Exp Bot* 59:1253-1265.

Fajardo, T. V., Peiro, A., Pallás, V. and Sánchez-Navarro, J. (2013). Systemic transport of Alfalfa mosaic virus can be mediated by the movement proteins of several viruses assigned to five genera of the 30K family. *J Gen Virol* 94:677-681.

Fan, J.; Chen, C., Yu, Q., Brlansky, R. H., Li, Z. G. and Gmitter, F. G., Jr. (2011). Comparative iTRAQ proteome and transcriptome analyses ofsweet orange infected by "Candidatus Liberibacter asiaticus". *Physiol Plant* .143:235−245.

Fan, W., Zhang, Z. and Zhang, Y. (2009). Cloning and molecular characterization of fructose-1,6-bisphosphate aldolase gene regulated by high-salinity and drought in Sesuvium portulacastrum. *Plant cell reports* 28:975-984.

Fernández-Calvino, L., Faulkner, C., and Maule, A. (2011). Plasmodesmata as active conduits for virus cell-to-cell movement. In Recent Advances in Plant Virology. Caranta, C., Aranda, M. A., Tepfer, M. and López-Moya, J. J. Editors. Caister Academic Press, Norfolk, UK, pp 47-74.

Fields, S. (1993). The two-hybrid system to detect protein-protein interactions. *Methods* 5:116-124.

Fields, S. and Song, O. (1989). A novel genetic system to detect protein-protein interactions. *Nature* 340:245-246.

Gagne, J. M., Downes, B. P., Shiu, S. H., Durski, A. M. and Vierstra, R. D. (2002). The F-box subunit of the SCF E3 complex is encoded by a diverse superfamily of genes in Arabidopsis. *Proc Natl Acad Sci U S A* 99:11519-11524.

García-Castillo, S., Sánchez-Pina, M.A. and Pallás, V. (2003). Spatio-temporal analysis of the RNAs, coat and movement (p7) proteins of Carnation mottle virus in Chenopodium quinoa plants. *J Gen Virol* 84:745-749.

García, J. A. and Pallás, V. (2015). Viral factors involved in plant pathogenesis. *Curr Opin Virol* 11:21-30.

García-Marcos, A., Pacheco, R., Manzano, A., Aguilar, E. and Tenllado, F. (2013). Oxylipin biosynthesis genes positively regulate programmed cell death during compatible infections with the synergistic pair potato virus X-potato virus Y and Tomato spotted wilt virus. *J Virol* 87:5769-5783.

García-Mas, J., Benjak, A., Sanseverino, W., Bourgeois, M., Mir, G., Gonzalez, V. M., Hénaff, E., Câmara, F., Cozzuto, L., Lowy, E., Alioto, T., Capella-Gutiérrez, S., Blanca, J., Cañizares, J., Ziarsolo, P., Gonzalez-Ibeas, D., Rodríguez-Moreno, L., Droege, M., Du, L., Alvarez-Tejado, M., Lorente-Galdos, B., Melé, M., Yang, L., Weng, Y., Navarro, A., Marques-Bonet, T., Aranda, M. A., Nuez, F., Picó, B., Gabaldón, T., Roma, G., Guigó, R., Casacuberta, J. M., Arús, P., Puigdomènech, P. (2012). The genome of melon (Cucumis melo L.). *Proc Natl Acad Sci U S A* 109:11872-11877.

Gaupels, F., Vlot, A. C. (2012). Plant Defense and Long-Distance Signaling in the Phloem. In: Thompson GA, van Bel, A. J., editor. Phloem: Molecular Cell Biology, Systemic Communication, Biotic Interactions. Oxford: Wiley-Blackwell; p. 227-47.

Gazit, E. (2002). A possible role for pi-stacking in the self-assembly of amyloid fibrils. *FASEB J.* 16:77-83.

Genovés, A., Navarro, J. A. and Pallás, V. (2006). Functional analysis of the five Melon necrotic spot virus genome-encoded proteins. *J Gen Virol* 87:2371-2380.

Genovés, A., Navarro, J. A. and Pallás, V. (2009). A self-interacting carmovirus movement protein plays a role in binding of viral RNA during the cell-to-cell movement and shows an actin cytoskeleton dependent location in cell periphery. *Virology* 395:133-142.

Genovés, A., Navarro, J. A. and Pallás, V. (2010). The intra- and intercellular movement of Melon necrotic spot virus (MNSV) depends on an active secretory pathway. *Mol Plant Microbe Interact* 23:263-272.

Genovés, A., Pallás, V. and Navarro, J. A. (2011) Contribution of topology determinants of a viral movement protein to its membrane association, intracellular traffic, and viral cell-to-cell movement. *J Virol* 85:7797-7809.

Gershater, M. C., Edwards, R. (2007). Regulating biological activity in plants with carboxylesterases. *Plant Sci* 173:579-588.

Giavalisco, P., Kapitza, K., Kolasa, A., Buhtz, A. and Kehr, J. (2006). Towards the proteome of Brassica napus phloem sap. *Proteomics* 6:896-909.

Gietz, R. D. and Woods, R. A. (2002). Transformation of yeast by lithium acetate/single-stranded carrier DNA/polyethylene glycol method. *Methods Enzymol* 350:87-96.

Gilardoni, P. A., Schuck, S., Jungling, R., Rotter, B., Baldwin, I. T. and Bonaventure, G. (2010). SuperSAGE analysis of the Nicotiana attenuata transcriptome after fatty acid-amino acid elicitation (FAC): identification of early mediators of insect responses. *BMC Plant Biol* 10:66.

Gillespie, T., Boevink, P., Haupt, S., Roberts, A.G., Toth, R., Valentine, T., Chapman, S. and Oparka, K. J. (2002). Functional analysis of a DNA-shuffled movement protein reveals that microtubules are dispensable for the cell-to-cell movement of tobacco mosaic virus. *Plant Cell* 14:1207-1222.

Giribaldi, M., Purrotti, M., Pacifico, D., Santini, D., Mannini, F., Caciagli, P., Rolle, L., Cavallarin, L., Giuffrida, M. G. and Marzachì, C. (2011). A multidisciplinary study on the effects of phloem-limited viruses on the agronomical performance and berry quality of Vitis vinifera cv. Nebbiolo. *J Proteomics* 75:306-315.

Gómez-Aix, C., García-García, M., Aranda, M. A. and Sánchez-Pina, M. A. (2015). Melon necrotic spot virus replication occurs in association with altered mitochondria. *Mol Plant Microbe Interact* 28:387-97.

Gómez, G. and Pallás, V. (2001). Identification of an in vitro ribonucleoprotein complex between a viroid RNA and a phloem protein from cucumber plants. *Mol Plant Microbe Interact* 14:910-913.

Gómez G, Pallás V. (2004). A long-distance translocatable phloem protein from cucumber forms a ribonucleoprotein complex in vivo with Hop stunt viroid RNA. *J Virol* 78:10104-10110.

Gómez, G., Torres, H. and Pallás, V. (2005). Identification of translocatable RNA-binding phloem proteins from melon, potential components of the long-distance RNA transport system. *Plant J* 41:107-116.

Gonzalo, P. and Reboud, J. P. (2003). The puzzling lateral flexible stalk of the ribosome. *Biol Cell* 95:179-193.

Gorg, A., Weiss, W., Dunn, M. J. (2004). Current two-dimensional electrophoresis technology for proteomics. *Proteomics* 4:3665-3685.

Gosalvez-Bernal, B., Genovés, A., Navarro, J. A., Pallás, V. and Sánchez-Pina, M. A. (2008). Distribution and pathway for phloem-dependent movement of Melon necrotic spot virus in melon plants. *Mol Plant Pathol* 9:447-461.

Gosalvez, B., Navarro, J. A., Lorca, A., Botella, F., Sánchez-Pina, M. A. and Pallás, V. (2003). Detection of melon necrotic spot virus in water samples and melon plants by molecular methods. *J Virol Methods* 113:87-93.

Greenberg, J. T. and Yao, N. (2004). The role and regulation of programmed cell death in plant-pathogen interactions. *Cell Microbiol* 6:201-211.

Guenoune-Gelbart, D., Elbaum, M., Sagi, G., Levy, A. and Epel, B. L. (2008). Tobacco mosaic virus (TMV) replicase and movement protein function synergistically in facilitating TMV spread by lateral diffusion in the plasmodesmal desmotubule of *Nicotiana benthamiana*. *Mol Plant Microbe Interact* 21:335-345.

Guevara-Morato, M. Á., García de Lacoba, M., García-Luque, I. and Serra, M. T. (2010). Characterization of a pathogenesis-related protein 4 (PR-4) induced in Capsicum chinense L3 plants with dual RNase and DNase activities. *J Exp Bot* 61:3259-3271.

Hacker, D. L., Petty, I. T., Wei, N. and Morris, T. J. (1992). Turnip crinkle virus genes required for RNA replication and virus movement. *Virology* 186:1-8.

Hafren, A., Eskelin, K. and Makinen, K. (2013). Ribosomal protein P0 promotes Potato virus A infection and functions in viral translation together with VPg and eIF(iso)4E. *J Virol* 87:4302-4312.

Ham, B. K., Li, G., Jia, W., Leary, J. A., Lucas, W. J. (2014). Systemic delivery of siRNA in pumpkin by a plant PHLOEM SMALL RNA-BINDING PROTEIN 1-ribonucleoprotein complex. *Plant J* 80:683-694.

Hamilton, A., Voinnet, O., Chappell, L. and Baulcombe, D. (2002). Two classes of short interfering RNA in RNA silencing. *EMBO J* 21:4671-4679.

Han, C., Ren, C., Zhi, T., Zhou, Z., Liu, Y., Chen, F., Peng, W. and Xie, D. (2013). Disruption of fumarylacetoacetate hydrolase causes spontaneous cell death under short-day conditions in Arabidopsis. *Plant Physiol* 162:1956-1964.

Han, X., Kumar, D., Chen, H., Wu, S. and Kim, J. Y. (2014). Transcription factor-mediated cell-to-cell signalling in plants. *J Exp Bot* 65:1737-1749.

Hanton, S. L., Bortolotti, L. E., Renna, L., Stefano, G. and Brandizzi, F. (2005). Crossing the divide - Transport between the endoplasmic reticulum and Golgi apparatus in plants. *Traffic* 6:267-277.

Hanton, S. L., Chatre, L., Renna, L., Matheson, L.A. and Brandizzi, F. (2007a) De novo formation of plant endoplasmic reticulum export sites is membrane cargo induced and signal mediated. *Plant Physiol* 143:1640-1650.

Hanton, S. L., Matheson, L. A. and Brandizzi, F. (2006). Seeking a way out: export of proteins from the plant endoplasmic reticulum. *Trends Plant Sci* 11:335-343.

Hanton, S. L., Matheson, L. A., Chatre, L. and Brandizzi, F. (2009). Dynamic organization of COPII coat proteins at endoplasmic reticulum export sites in plant cells. *Plant J* 57:963-974.

Hanton, S. L., Matheson, L. A., Chatre, L., Rossi, M. and Brandizzi, F. (2007b). Post-Golgi protein traffic in the plant secretory pathway. *Plant Cell Rep* 26:1431-1438.

Harries, P. and Ding, B. (2011). Cellular factors in plant virus movement: at the leading edge of macromolecular trafficking in plants. *Virology* 411:237-243.

Harries, P. A., Palanichelvam, K., Yu, W., Schoelz, J. E. and Nelson, R. S. (2009). The Cauliflower mosaic virus protein P6 forms motile inclusions that traffic along actin microfilaments and stabilize microtubules. *Plant Physiol* 149:1005-1016.

Harries, P. A., Schoelz, J. E. and Nelson, R. S. (2010). Intracellular transport of viruses and their components: utilizing the cytoskeleton and membrane highways. *Mol Plant Microbe Interact* 23:1381-1393.

Harrison, S. C., Olson, A. J., Schutt, C. E., Winkler, F. K. and Bricogne, G. (1978). Tomato bushy stunt virus at 2.9 A resolution. *Nature* 276:368-373.

Haupt, S., Cowan, G. H., Ziegler, A., Roberts, A. G., Oparka, K. J. and Torrance, L. (2005). Two plant-viral movement proteins traffic in the endocytic recycling pathway. *Plant Cell* 17:164-181.

Hause, B., Hause, G., Kutter, C., Miersch, O. and Wasternack, C. (2003). Enzymes of jasmonate biosynthesis occur in tomato sieve elements. *Plant Cell Physiol* 44:643-648.

Hawes, C. (2012). The ER/Golgi Interface - Is There Anything in-between?. *Front Plant Sci* 3:73.

Hawes, C., Osterrieder, A., Hummel, E. and Sparkes, I. (2008). The plant ER-Golgi interface. *Traffic* 9:1571-1580.

Hawes, C. and Satiat-Jeunemaitre, B. (2005). The plant Golgi apparatus--going with the flow. *Biochim Biophys Acta* 1744:93-107.

Hayashi, M., Takahashi, H., Tamura, K., Huang, J., Yu, L. H., Kawai-Yamada, M., Tezuka, T. and Uchimiya, H. (2005). Enhanced dihydroflavonol-4-reductase activity and NAD homeostasis leading to cell death tolerance in transgenic rice. *Proc Natl Acad Sci U S A* 102:7020-7025.

Heinlein, M. and Epel, B. L. (2004). Macromolecular transport and signaling through plasmodesmata. *Int Rev Cytol* 235:93-164.

Heinlein, M., Epel, B. L., Padgett, H. S. and Beachy, R. N. (1995). Interaction of Tobamovirus movement proteins with the plant cytoskeleton. *Science* 270:1983-1985.

Heinlein, M., Padgett, H. S., Gens, J. S., Pickard, B. G., Casper, S. J., Epel, B. L. and Beachy, R. N. (1998). Changing patterns of localization of the Tobacco mosaic virus movement protein and replicase to the endoplasmic reticulum and microtubules during infection. *Plant Cell* 10:1107-1120.

Herr, A. J., and Baulcombe, D. C. (2004). RNA silencing pathways in plants. In *Cold Spring Harbor symposia on quantitative biology* (Vol. 69, pp. 363-370). Cold Spring Harbor Laboratory Press.

Herranz, M. C. and V. Pallás (2004). RNA-binding properties and mapping of the RNA-binding domain from the movement protein of Prunus necrotic ringspot virus. *J Gen Virol* 85:761-768.

Herranz, M. C., Sánchez-Navarro, J. A., Saurí, A., Mingarro, I. and Pallás V. (2005). Mutational analysis of the RNA-binding domain of the Prunus necrotic ringspot virus (PNRSV) movement protein reveals its requirement for cell-to-cell movement. *Virology* 339: 31-41.

Herranz, M. C., Navarro, J. A., Sommen, E. and Pallás, V. (2015). Comparative analysis among the small RNA populations of source, sink and conductive tissues in two different plant-virus pathosystems. *BMC Genomics* 16:117.

Herranz, M. C., Pallás, V. and Aparicio, F. (2012). Multifuncional roles for the N-terminal vasic motif of Alfalfa mosaic virus coat protein: nucleolar/cytoplasmic shuttling, modulation of RNA-binding activity and virion formation. *Mol. Plant Microbe Interact* 25:1093-1103.

Hibi, T. and Furuki, I. (1985). Melon necrotic spot virus, CMI/AAB Descriptions of Plant Viruses, vol 302. Association of Applied Biologists, Warwick, UK.

Hinnebusch, A. G. and Lorsch, J. R. (2012). The mechanism of eukaryotic translation initiation: new insights and challenges. Cold Spring Harbor perspectives in biology 4.

Hipper, C., Brault, V., Ziegler-Graff, V. and Revers, F. (2013). Viral and cellular factors involved in Phloem transport of plant viruses. *Front Plant Sci* 4:154.

Hirashima, K. and Watanabe, Y. (2001). Tobamovirus replicase coding region is involved in cell-to-cell movement. *J Virol* 75:8831-8836.

Hirashima, K. and Watanabe, Y. (2003). RNA helicase domain of tobamovirus replicase executes cell-to-cell movement possibly through collaboration with its nonconserved region. *J Virol* 77:12357-12362.

Hogle, J. M., Maeda, A. and Harrison, S. C. (1986). Structure and assembly of turnip crinkle virus. I. X-ray crystallographic structure analysis at 3.2 A resolution. *J Mol Biol* 191:625-638.

Hsia, K. C., Li, C. L. and Yuan, H. S. (2005). Structural and functional insight into sugar-nonspecific nucleases in host defense. *Curr Opin Struct Biol* 15:126-134.

Hsu, C., Singh, P., Ochoa, W., Manayani, D. J., Manchester, M., Schneemann, A. and Reddy, V. S. (2006). Characterization of polymorphism displayed by the coat protein mutants of tomato bushy stunt virus. *Virology* 349:222-229.

Hsu, W. L., Oldfield, C. J., Xue, B., Meng, J., Huang, F., Romero, P., Uversky, V. N. and Dunker, A. K. (2013). Exploring the binding diversity of intrinsically disordered proteins involved in one-to-many binding. *Protein Sci* 22:258-273.

http://3.bp.blogspot.com/_me39fAf7ZBY/TQnk8JmMJRI/AAAAAAAAAYI/Csg-EwfIlsQ/s1600/tejidos+transporte.png)

http://www.zmbp.uni-tuebingen.de/dev-genetics/pimpl.html (PIMPS group)

Huang, Z., Andrianov, V.M., Han, Y. and Howell, S.H. (2001). Identification of arabidopsis proteins that interact with the cauliflower mosaic virus (CaMV) movement protein. *Plant Mol Biol* 47:663-675.

Huang, S., Xiang, Y. and Ren, H. (2011). Actin-binding proteins and actin dynamics in plant cells. In The plant cytoskeleton. Advances in Plant Biology Volume 2 (Liu, B. ed), New York: Springer Science+Business Media, pp 57-80.

Huh, S. U., Choi, L. M., Lee, G. J., Kim, Y. J. and Paek, K. H. (2012). Capsicum annuum WRKY transcription factor d (CaWRKYd) regulates hypersensitive response and defense response upon Tobacco mosaic virus infection. *Plant Sci* 197:50-58.

Huh, S. U., Lee, G. J., Jung, J. H., Kim, Y., Kim, Y. J. and Paek, K. H. (2015). Capsicum annuum transcription factor WRKYa positively regulates defense response upon TMV infection and is a substrate of CaMK1 and CaMK2. *Sci Rep* 5:7981.

Hui, E. and Rochon, D. (2006). Evaluation of the roles of specific regions of the Cucumber necrosis virus coat protein arm in particle accumulation and fungus transmission. *J Virol* 80:5968-5975.

Hui, E., Xiang, Y. and Rochon, D. (2010). Distinct regions at the N-terminus of the Cucumber necrosis virus coat protein target chloroplasts and mitochondria. *Virus Res* 153:8-19.

Hull, R. (2002). Chapter 9 - Induction of Disease 1: Virus Movement through the Plant and Effects on Plant Metabolism. Pages 373-436 in: Matthews' Plant Virology (Fourth Edition), R. Hull, ed. Academic Press, London.

Hutchinson, E. G. and Thornton, J. M. (1994). A revised set of potentials for beta-turn formation in proteins. *Protein Sci*. 3:2207-2216.

Hwang, Y. T., McCartney, A. W., Gidda, S. K. and Mullen, R. T. (2008). Localization of the Carnation Italian ringspot virus replication protein p36 to the mitochondrial outer membrane is mediated by an internal targeting signal and the TOM complex. *BMC Cell Biol* 9*:* 54.

Iglesias, V. A. and Meins, F. (2000). Movement of plant viruses is delayed in a β-1, 3-glucanase-deficient mutant showing a reduced plasmodesmatal size exclusion limit and enhanced callose deposition. *Plant J* 21:157-166.

Incarbone, M. and Dunoyer, P. (2013). RNA silencing and its suppression: novel insights from in planta analyses. *Trends Plant Sci* 18:382-392.

Iwakawa, H. O., Tajima, Y., Taniguchi, T., Kaido, M., Mise, K., Tomari, Y., Taniguchi, H and Okuno, T. (2012). Poly(A)-binding protein facilitates translation of an uncapped/nonpolyadenylated viral RNA by binding to the 3' untranslated region. *J Virol* 86:7836-7849.

Jackson, A. O., Lim, H. S., Bragg, J., Ganesan, U. and Lee, M. Y. (2009). Hordeivirus replication, movement, and pathogenesis. *Annu Rev Phytopathol* 47:385-422.

Jackson, R. J., Hellen, C. U. and Pestova, T. V. (2010). The mechanism of eukaryotic translation initiation and principles of its regulation. *Nat Rev Mol Cell Biol* 11:113-127.

Jamalkandi, S. A. and Masoudi-Nejad, A. (2009). Reconstruction of *Arabidopsis thaliana* fully integrated small RNA pathway.*Funct Integr Genomics* 9:419-432.

Jansen, K. A., Wolfs, C. J., Lohuis, H., Goldbach, R. W. and Verduin, B. J. (1998). Characterization of the brome mosaic virus movement protein expressed in E. coli. *Virology* 242:387-394.

Jaspers, E. M. J. (1985). Interaction of alfalfa mosaic virus nucleic acid and protein. J.W. Davies (Ed.), Molecular Plant Virology, CPC Press, Boca Raton (1985)

Jiménez, I., López, L., Alamillo, J. M., Valli, A. and García, J. A. (2006). Identification of a plum pox virus CI-interacting protein from chloroplast that has a negative effect in virus infection. *Mol Plant Microbe Interac* 19:350-358.

Jones, J. D. and Dangl, J. L. (2006). The plant immune system. *Nature* 444:323-329.

Jones, L., Hamilton, A. J., Voinnet, O., Thomas, C. L., Maule, A. J. and Baulcombe, D. C. (1999). RNA-DNA interactions and DNA methylation in post-transcriptional gene silencing. *Plant Cell* 11:2291-2301.

Jorrín, J. V., Maldonado, A. M. and Castillejo, M. A. (2007). Plant proteome analysis: a 2006 update. *Proteomics* 7: 2947–2962.

Jung, C. J., Lee, M. H., Min, M. K. and Hwang, I. (2011). Localization and trafficking of an isoform of the AtPRA1 family to the Golgi apparatus depend on both N- and C-terminal sequence motifs. *Traffic* 12:185-200.

Jurgens, G. (2004). Membrane trafficking in plants. *Annu Rev Cell Dev Bi* 20:481-504.

Kakani, K., Reade, R., Katpally, U., Smith, T. and Rochon, D. (2008). Induction of particle polymorphism by cucumber necrosis virus coat protein mutants in vivo. *J Virol* 82:1547-1557.

Kakani, K., Reade, R. and Rochon, D. A. (2004). Evidence that vector transmission of a plant virus requires conformational change in virus particles. *J Mol Biol* 338:507-517.

Kakani, K., Sgro, J. Y. and Rochon, D. A. (2001). Identification of specific cucumber necrosis virus coat protein amino acids affecting fungus transmission and zoospore attachment. *J Virol* 75:5576-5583.

Kang, B. H. and Staehelin, L. A. (2008). ER-to-Golgi transport by COPII vesicles in Arabidopsis involves a ribosome-excluding scaffold that is transferred with the vesicles to the Golgi matrix. *Protoplasma* 234:51-64.

Kapp, L. D. and Lorsch, J. R. (2004). The molecular mechanics of eukaryotic translation. *Annu Rev Biochem* 73:657-704.

Katpally, U., Kakani, K., Reade, R., Dryden, K., Rochon, D. and Smith, T. J. (2007). Structures of T=1 and T=3 particles of cucumber necrosis virus: evidence of internal scaffolding. *J Mol Biol* 365:502-512.

Kaur, H. and Raghava, G. P. (2004). A neural network method for prediction of beta-turn types in proteins using evolutionary information. *Bioinformatics* 20:2751-2758.

Kawakami, S., Watanabe, Y. and Beachy, R. N. (2004). Tobacco mosaic virus infection spreads cell to cell as intact replication complexes. *Proc Natl Acad Sci U S A* 101:6291-6296.

Ke, J., Schmidt, T., Chase, E., Bozarth, R. F. and Smith, T. J. (2004). Structure of Cowpea mottle virus: a consensus in the genus Carmovirus. *Virology* 321:349-358.

Kehr, J. (2006). Phloem sap proteins: their identities and potential roles in the interaction between plants and phloem-feeding insects. *J Exp Bot* 57:767-774.

Kenrick, K. G., and Margolis, J. (1970). Isoelectric focusing and gradient gel electrophoresis: a two-dimensional technique. Analytical biochemistry, 33(1), 204-207.

Kim, J. T., Kim, K. D., Song, E. Y., Lee, H. G., Kim, J. W., Chae, S. K., Kim, E., Lee, M. S., Yang, Y. and Lim, J. S. (2006). Apoptosis-inducing factor (AIF) inhibits protein synthesis by interacting with the eukaryotic translation initiation factor 3 subunit p44 (eIF3g). *FEBS Lett* 580:6375-6383.

Kim, J. H., Lee, S. R., Li, L. H., Park, H. J., Park, J. H., Lee, K. Y., Kim, M. K., Shin, B. A. and Choi, S. Y. (2011) High cleavage efficiency of a 2A peptide derived from porcine teschovirus-1 in human cell lines, zebrafish and mice. *PLoS One* 6:e18556.

Kim, J. T., Lee, S. J., Kim, B. Y., Lee, C. H., Yeom, Y. I., Choe, Y. K., Yoon, D. Y., Chae, S. K., Kim, J. W., Yang, Y., Lim, J. S. and Lee, H. G. (2013). Caspase-mediated cleavage and DNase activity of the translation initiation factor 3, subunit G (eIF3g). *FEBS Lett* 587:3668-3674.

Kim, S. H., Kalinina, N. O., Andreev, I., Ryabov, E. V., Fitzgerald, A. G., Taliansky, M. E. and Palukaitis, P. (2004). The C-terminal 33 amino acids of the cucumber mosaic virus 3a protein affect virus movement, RNA binding and inhibition of infection and translation. *J Gen Virol* 85:221-230.

Kim, S. H., Ryabov, E. V., Kalinina, N. O., Rakitina, D. V., Gillespie, T., MacFarlane, S., Haupt, S., Brown, J. W. S. and Taliansky, M. (2007) Cajal bodies and the nucleolus are required for a plant virus systemic infection. *EMBO J*. 26:2169-2179.

Kim, V. N. (2003). RNA interference in functional genomics and medicine. *J Korean Med Sci* 18:309.

Kim, Y. H., Cho, K., Yun, S. H., Kim, J. Y., Kwon, K. H., Yoo, J. S. and Kim, S. I. (2006). Analysis of aromatic catabolic pathways in Pseudomonas putida KT 2440 using a combined proteomic approach: 2-DE/MS and cleavable isotope-coded affinity tag analysis. *Proteomics 6*:1301-1318.

Klose, J. (1975). Protein mapping by combined isoelectric focusing and electrophoresis of mouse tissues. *Humangenetik* 26:231-243.

Knoester, M., van Loon, L.C., van den Heuvel, J., Hennig, J., Bol, J. F. and Linthorst, H. J. M. (1998). Ethylene-insensitive tobacco lacks nonhost resistance against soil-borne fungi. *Proc Natl Acad Sci USA* 95:1933-1937.

Kormelink, R., García, M. L., Goodin, M., Sasaya, T. and Haenni, A. L. (2011). Negative-strand RNA viruses: the plant-infecting counterparts. *Virus Res* 162:184-202.

Kottapalli, K. R., Satoh, K., Rakwal, R., Shibato, J., Doi, K., Nagata, T. and Kikuchi, S. (2007). Combining in silico mapping and arraying: an approach to identifying common candidate genes for submergence tolerance and resistance to bacterial leaf blight in rice. *Mol Cells* 24:394-408.

Krab, I. M., Caldwell, C., Gallie, D. R. and Bol, J. F. (2005). Coat protein enhances translational efficiency of Alfalfa mosaic virus RNAs and interacts with the eIF4G component of initiation factor eIF4F. *J Gen Virol* 86: 1841-1849.

Krenz, B., Windeisen, V., Wege, C., Jeske, H. and Kleinow, T. (2010). A plastid-targeted heat shock cognate 70kDa protein interacts with the Abutilon mosaic virus movement protein. *Virology* 401:6-17.

Kubota, K., Wakabayashi, K. and Matsuoka, T. (2003). Proteome analysis of secreted proteins during osteoclast differentiation using two different methods: Two-dimensional electrophoresis and isotope-coded affinity tags analysis with two-dimensional chromatography. *Proteomics* 3:616-626.

Kumar, A., Reddy, V. S., Yusibov, V., Chipman, P. R., Hata, Y., Fita, I., Fukuyama, K., Rossmann, M. G., Loesch-Fries, L. S., Baker, T. S. and Johnson, J. E. (1997). The structure of alfalfa mosaic virus capsid protein assembled as a T=1 icosahedral particle at 4.0-A resolution. *J Virol* 71:7911-7916.

Lacomme, C. and Chapman, S. (2008). Use of potato virus X (PVX)-based vectors for gene expression and virus-induced gene silencing (VIGS). *Curr Protoc Microbiol* Chapter 16:Unit 16I 11.

Lampl, N., Budai-Hadrian, O., Davydov, O., Joss, T. V., Harrop, S. J., Curmi, P. M., Roberts, T. H. and Fluhr, R. (2010). Arabidopsis AtSerpin1, crystal structure and in vivo interaction with its target protease RESPONSIVE TO DESICCATION-21 (RD21). *J Biol Chem* 285:13550-13560.

Langhans, M., Meckel, T., Kress, A., Lerich, A. and Robinson, D. G. (2012). ERES (ER exit sites) and the "secretory unit concept". *J Microsc* 247:48-59.

Lakatos, L., Csorba, T., Pantaleo, V., Chapman, E. J., Carrington, J. C., Liu, Y. P., Dolja, V. V., Calvino, L. F., Lopez-Moya, J. J. and Burgyán, J. (2006). Small RNA binding is a common strategy to suppress RNA silencing by several viral suppressors. *EMBO J* 25:2768-2780.

Lalonde, S., Francesch, V. R. and Frommer, W. B. (2001). Commpanion cells. In: eLS. John Wiley & Sons Ltd, Chichester. http://www.els.net [doi: 10.1038/npg.els.0002087].

Laporte, C., Vetter, G., Loudes, A. M., Robinson, D. G., Hillmer, S., Stussi-Garaud, C. and Ritzenthaler, C. (2003). Involvement of the secretory pathway and the cytoskeleton in intracellular targeting and tubule assembly of Grapevine fanleaf virus movement protein in tobacco BY-2 cells. *Plant Cell* 15:2058-2075.

Larbi, N. B. and Jefferies, C. (2009). 2D-DIGE: comparative proteomics of cellular signalling pathways. *Methods Mol Biol* 517:105-132.

Larson, S. B., Lucas, R. W. and McPherson, A. (2005). Crystallographic structure of the T=1 particle of brome mosaic virus. *J Mol Biol* 346:815-831.

Law, R. H., Zhang, Q., McGowan, S., Buckle, A. M., Silverman, G. A., Wong, W., Rosado, C. J., Langendorf, C. G., Pike, R. N., Bird, P. I. and Whisstock, J. C. (2006). An overview of the serpin superfamily. *Genome Biol* 7:216.

Lechner, E., Achard, P., Vansiri, A., Potuschak, T. and Genschik, P. (2006). F-box proteins everywhere. *Curr Opin Plant Biol* 9:631-638.

Lee, B. J., Kwon, S. J., Kim, S. K., Kim, K. J., Park, C. J., Kim, Y. J., Park, O. K. and Paek, K. H. (2006). Functional study of hot pepper 26S proteasome subunit RPN7 induced by tobacco mosaic virus from nuclear proteome analysis. *Biochem Biophys Res Commun* 351:405-411.

Lee, C. C., Ho, Y. N., Hu, R. H., Yen, Y. T., Wang, Z. C., Lee, Y. C., Hsu, Y, H. and Meng, M. (2011). The interaction between bamboo mosaic virus replication protein and coat protein is critical for virus movement in plant hosts. *J Virol* 85:12022-12031.

Lee, J. Y., Taoka, K., Yoo, B. C., Ben-Nissan, G., Kim, D. J. and Lucas, W.J. (2005). Plasmodesmal-associated protein kinase in tobacco and Arabidopsis recognizes a subset of non-cell-autonomous proteins. *Plant Cell* 17:2817-2831.

Lee, K., Bae, D. W., Kim, S. H., Han, H. J., Liu, X., Park, H. C., Lim, C. O., Lee, S. Y. and Chung, W. S. (2010). Comparative proteomic analysis of the short-term responses of rice roots and leaves to cadmium. *J Plant Physiol* 167:161-168.

Lee, M. C. and Miller, E. A. (2007). Molecular mechanisms of COPII vesicle formation. *Semin Cell Dev Biol* 18:424-434.

Lee, M. C. S., Miller, E. A., Goldberg, J., Orci, L. and Schekman, R. (2004). Bi-directional protein transport between the ER and Golgi. *Annu Rev Cell Dev Biol* 20:87-123.

Leisner, S.M., Turgeon, R., and Howell, S.H. (1993). Effects of host plant development and genetic determinants on the long-distance movement of cauliflower mosaic virus in Arabidopsis. Plant Cell. 5, 191–202.

Lerich, A., Hillmer, S., Langhans, M., Scheuring, D., van Bentum, P. and Robinson, D. G. (2012). ER import sites and their relationship to ER exit sites: a new model for bidirectional ER-Golgi transport in higher plants. *Front Plant Sci* 3:143.

Li, K., Xu, C. and Zhang, J. (2011). Proteome profile of maize (Zea Mays L.) leaf tissue at the flowering stage after long-term adjustment to rice black-streaked dwarf virus infection. *Gene* 485:106-113.

Li, S., Ma, J. and Liu, P. (2013). OPR3 is expressed in phloem cells and is vital for lateral root development in Arabidopsis. *Can J Plant Sci* 93:165-170.

Li, V. Z., Qu, F. and Morris, T. J. (1998). Cell-to-cell movement of turnip crinkle virus is controlled by two small open reading frames that function in trans. *Virology* 244:405-416.

Li, W., Zhao, Y., Liu, C., Yao, G., Wu, S., Hou, C., Zhang, M. and Wang, D. (2012). Callose deposition at plasmodesmata is a critical factor in restricting the cell-to-cell movement of Soybean mosaic virus. *Plant Cell Rep* 31:905-916.

Lin, B. and Heaton, L. A. (1999). Mutational analysis of the putative calcium binding site and hinge of the Turnip crinkle virus coat protein. *Virology* 259:34-42

Lin, M. K., Lee, Y. J., Lough, T. J., Phinney, B. S. and Lucas, W. J. (2009). Analysis of the pumpkin phloem proteome provides insights into angiosperm sieve tube function. *Mol Cell Proteomics* 8:343-356.

Lippincott-Schwartz, J., Roberts, T. H. and Hirschberg, K. (2000). Secretory protein trafficking and organelle dynamics in living cells. *Annu Rev Cell Dev Biol* 16:557-589.

Liu, C. and Nelson, R. S. (2013). The cell biology of Tobacco mosaic virus replication and movement. Front. *Plant Sci* 4:12.

Liu, Y., Schiff, M., Czymmek, K., Tallóczy, Z., Levine, B. and Dinesh-Kumar, S. P. (2005). Autophagy regulates programmed cell death during the plant innate immune response. *Cell* 121:567-577.

Liu, Y., Schiff, M., Serino, G., Deng, X. W. and Dinesh-Kumar, S. P. (2002). Role of SCF ubiquitin-ligase and the COP9 signalosome in the N gene–mediated resistance response to Tobacco mosaic virus. *Plant Cell* 14:1483-1496.

Lommel, S. A., Martelli, G. P. and Russo, M. (2000). Family Tombusviridae. In: Van Regenmortel MHV, Fauquet, C. M., Bishop, D. H. L. *et al.,* eds. Virus Taxonomy. Seventh Report of the International Committee on Taxonomy of Viruses. San Diego, CA, USA: Academic Press, 791–825.

Lough, T. J. and Lucas W. J. (2006). Integrative plant biology: role of phloem long-distance macromolecular trafficking. *Annu Rev Plant Biol* 57:203-232.

Lough, T. J., Netzler, N. E., Emerson, S. J., Sutherland, P., Carr, F., Beck, D. L., Lucas, W. J. and Forster, R. L. (2000). Cell-to-cell movement of Potexviruses: evidence for a ribonucleoprotein complex involving the coat protein and first triple gene block protein. *Mol Plant Microbe Interact* 13:962-974.

Lucas, W. J. (2006). Plant viral movement proteins: agents for cell-to-cell trafficking of viral genomes. *Virology* 344:169-184.

Ma, B., Elkayam, T., Wolfson, H. and Nussinov, R. (2003). Protein-protein interactions: structurally conserved residues distinguish between binding sites and exposed protein surfaces. *Proc Natl Acad Sci U S A* 100:5772-5777.

Mahalingam, R., Gómez-Buitrago, A., Eckardt, N., Shah, N., Guevara-García, A., Day, P., Raina, R. and Fedoroff, N. V. (2003). Characterizing the stress/defense transcriptome of Arabidopsis. *Genome Biol* 4:R20.

Manabayeva, S. A., Shamekova, M., Park, J. W., Ding, X. S., Nelson, R. S., Hsieh, Y. C., Omarov, R. T. and Scholthof, H. B. (2013). Differential requirements for Tombusvirus coat protein and P19 in plants following leaf versus root inoculation. *Virology 439*:89-96.

Malter, D. and Wolf, S. (2011). Melon phloem-sap proteome: developmental control and response to viral infection. *Protoplasma* 248:217-224.

Mandadi, K. K. and Scholthof K.-B. G. (2013). Plant immune responses against viruses: how does a virus cause disease?. *Plant Cell* 25:1489-1505.

Mandahar, C.L. (2006). Multiplication of RNA plant viruses. Springer Netherlands.

Marcos, J. F., Vilar, M., Perez-Payá, E. and Pallás, V. (1999). In vivo detection, RNA-binding properties and characterization of the RNA-binding domain of the p7 putative movement protein from carnation mottle carmovirus (CarMV). *Virology* 255:354-365.

Marouga, R., David, S. and Hawkins, E. (2005). The development of the DIGE system: 2D fluorescence difference gel analysis technology. *Anal Bioanal Chem* 382:669-678.

Marsh, M. and Helenius, A. (2006). Virus entry: open sesame. *Cell* 124:729-740.

Martin, G. B., Bogdanove, A. J. and Sessa, G. (2003). Understanding the functions of plant disease resistance proteins. *Annu Rev Plant Biol* 54:23-61.

Martínez-Gil, L., Sánchez-Navarro, J. A., Cruz, A., Pallás, V., Pérez-Gil, J. and Mingarro, I. (2009). Plant virus cell-to-cell movement is not dependent on the transmembrane disposition of its movement protein. *J Virol* 83:5535-5543.

Martínez-Gil, L., Saurí, A., Vilar, M., Pallás, V. and Mingarro, I. (2007) Membrane insertion and topology of the p7B movement protein of Melon necrotic spot virus (MNSV). *Virology* 367:348-357.

Martínez-Turiño, S. and Hernández, C. (2009). Inhibition of RNA silencing by the coat protein of Pelargonium flower break virus: distinctions from closely related suppressors. *J Gen Virol* 90:519-525.

Martínez-Turiño, S. and Hernández, C. (2011). A membrane-associated movement protein of Pelargonium flower break virus shows RNA-binding activity and contains a biologically relevant leucine zipper-like motif. *Virology* 413:310-319.

Mas, P. and Pallás, V. (1996) Long distance movement of cherry leaf roll virus in infected tobacco plants. Journal of General Virology. 77, 531-540.

Matthews, R. E. F. (1991). Plant Virology. 3rd ed. SanDiego: Academic Press New York

Matheson, L. A., Hanton, S. L. and Brandizzi, F. (2006). Traffic between the plant endoplasmic reticulum and Golgi apparatus: to the Golgi and beyond. *Curr Opin Plant Biol* 9:601-609.

Matsushita, Y., Miyakawa, O., Deguchi, M., Nishiguchi, M., and Nyunoya, H. (2002). Cloning of a tobacco cDNA coding for a putative transcriptional coactivator MBF1 that interacts with the tomato mosaic virus movement protein. *J Exp Bot* 53:1531-1532.

Maule, A. J. (2008). Plasmodesmata: structure, function and biogenesis. *Curr Opin Plant Biol* 11:680-686.

McCartney, A. W., Greenwood, J. S., Fabian, M. R., White, K. A. and Mullen, R. T. (2005). Localization of the tomato bushy stunt virus replication protein p33 reveals a peroxisome-to-endoplasmic reticulum sorting pathway. *Plant Cell* 17:3513-3531.

McGaughey, G. B., Gagne, M. and Rappe, A. K. (1998). pi-Stacking interactions. Alive and well in proteins. *J Biol Chem* 273:15458-15463.

Melcher, U. (1990). Similarities between putative transport proteins of plant viruses. *J Gen Virol* 71:1009-1018.

Melcher, U. (2000). The 30K superfamily of viral movement proteins. *J Gen Virol* 81:257-266.

Melnyk, C. W., Molnar, A. and Baulcombe, D.C. (2011). Intercellular and systemic movement of RNA silencing signals. *EMBO J* 30:3553-3563.

Meng, C., Chen, J., Peng, J. and Wong, S. M. (2006). Host-induced avirulence of hibiscus chlorotic ringspot virus mutants correlates with reduced gene-silencing suppression activity. *J Gen Virol* 87:451-459.

Menke, F. L., Kang, H. G., Chen, Z., Park, J. M., Kumar, D. and Klessig, D. F. (2005). Tobacco transcription factor WRKY1 is phosphorylated by the MAP kinase SIPK and mediates HR-like cell death in tobacco. *Mol Plant Microbe Interact* 18:1027-1034.

Merai, Z., Kerenyi, Z., Kertesz, S., Magna, M., Lakatos, L. and Silhavy, D. (2006). Double-stranded RNA binding may be a general plant RNA viral strategy to suppress RNA silencing. *J Virol* 80:5747-5756.

Meshi, T., Ishikawa, M., Motoyoshi, F., Semba, K. and Okada, Y. (1986). In vitro transcription of infectious RNAs from full-length cDNAs of tobacco mosaic virus. *Proc Natl Acad Sci U S A* 83:5043-5047.

Meshi, T., Motoyoshi, F., Maeda, T., Yoshiwoka, S., Watanabe, H. and Okada, Y. (1989). Mutations in the Tobacco mosaic virus 30-kD protein gene overcome Tm-2 resistance in tomato. *Plant Cell* 1:515-522.

Meyer, E. A., Castellano, R. K. and Diederich, F. (2003). Interactions with aromatic rings in chemical and biological recognition. *Angew Chem Int Ed Engl* 42:1210-1250.

Miller, S. and Krijnse-Locker, J. (2008). Modification of intracellular membrane structures for virus replication. *Nat Rev Microbiol* 6:363-374.

Minois, N., Sykacek, P., Godse, B. and Kreil, D. P. (2010). RNA interference in ageing research - a mini-review. *Gerontology* 56:496-506

Miras, M., Sempere, R. N., Kraft, J. J., Miller, W. A., Aranda, M. A. and Truniger, V. (2014). Interfamilial recombination between viruses led to acquisition of a novel translation-enhancing RNA element that allows resistance breaking. *New Phytol* 202:233-246.

Mochizuki, T., Hirai, K., Kanda, A., Ohnishi, J., Ohki, T. and Tsuda, S. (2009). Induction of necrosis via mitochondrial targeting of Melon necrotic spot virus replication protein p29 by its second transmembrane domain. *Virology* 390:239-249.

Mochizuki, T., Ohnishi, J., Ohki, T., Kanda, A. and Tsuda, S. (2008). Amino acid substitution in the coat protein of Melon necrotic spot virus causes loss of binding to the surface of Olpidium bornovanus zoospores. *J Gen Plant Pathol* 74:176-181.

Módena, N. A., Zelada, A. M., Conte, F. and Mentaberry, A. (2008). Phosphorylation of the TGBp1 movement protein of Potato virus X by a Nicotiana tabacum CK2-like activity. *Virus Res* 137:16-23.

Moffett, P. (2009). Mechanisms of recognition in dominant R gene mediated resistance. *Adv Virus Res* 75:1-229.

Molnar, A., Melnyk, C. W., Bassett, A., Hardcastle, T. J., Dunn, R. and Baulcombe, D. C. (2010). Small silencing RNAs in plants are mobile and direct epigenetic modification in recipient cells. *Science* 328:872-875.

Moreira, I. S., Martins, J. M., Ramos, R. M., Fernandes, P. A. and Ramos, M. J. (2013). Understanding the importance of the aromatic amino-acid residues as hot-spots. *Biochim Biophys Acta* 1834:404-414.

Moreno, J. I., Martin, R. and Castresana, C. (2005). Arabidopsis SHMT1, a serine hydroxymethyltransferase that functions in the photorespiratory pathway influences resistance to biotic and abiotic stress. *Plant J* 41:451-63.

Moreno, I. M., Thompson, J. R. and García-Arenal, F. (2004). Analysis of the systemic colonization of cucumber plants by Cucumber green mottle mosaic virus. *J Gen Virol* 85:749-759.

Morgunova, E., Dauter, Z., Fry, E., Stuart, D. I., Stel'mashchuk, V., Mikhailov, A. M., Wilson, K. S. and Vainshtein, B. K. (1994). The atomic structure of Carnation Mottle Virus capsid protein. *FEBS Lett* 338:267-271.

Morozov, S. Y. and Solovyev, A. G. (2003). Triple gene block: modular design of a multifunctional machine for plant virus movement. *J Gen Virol* 84:1351-1366.

Morozov, S. Y., and Solovyev, A. G. (2012). Did Silencing Suppression Counter-Defensive Strategy Contribute to Origin and Evolution of the Triple Gene Block Coding for Plant Virus Movement Proteins?. *Front Plant Sci* 3:136.

Muthukrishnan, S., Liang, G. H., Trick, H. N. and Gill, B. S. (2001). Pathogenesis-related proteins and their genes in cereals. *Plant Cell Tissue Organ Cult* 64:93-114.

Nagy, P. D. and Pogany, J. (2000). Partial purification and characterization of Cucumber necrosis virus and Tomato bushy stunt virus RNA-dependent RNA polymerases: similarities and differences in template usage between tombusvirus and carmovirus RNA-dependent RNA polymerases. *Virology* 276:279-288.

Nagy, P. D. (2008). Yeast as a model host to explore plant virus-host interactions. *Annu Rev Phytopathol* 46:217-242.

Nakamura, S. I., Hayashi, H., Mori, S. and Chino, M. (1995). Detection and Characterization of Protein Kinases in Rice Phloem Sap. *Plant Cell Physiol* 36:19-27.

Navarro, B., Rubino, L. and Russo, M. (2004). Expression of the Cymbidium ringspot virus 33-kilodalton protein in Saccharomyces cerevisiae and molecular dissection of the peroxisomal targeting signal. *J Virol* 78:4744-4752

Navarro, J. A., Genovés, A., Climent, J., Saurí, A., Martínez-Gil, L., Mingarro, I. and Pallás, V. (2006). RNA-binding properties and membrane insertion of Melon necrotic spot virus (MNSV) double gene block movement proteins. *Virology* 356:57-67.

Navarro, J. A., Serra-Soriano, M.and Pallás, V. (2014). A protocol to measure the extent of cell-to-cell movement of RNA viruses in planta. Bio-protocol 4:e1269.

Navrot, N., Collin, V., Gualberto, J., Gelhaye, E., Hirasawa, M., Rey, P., Knaff, D. B., Issakidis, E., Jacquot, J. P. and Rouhier, N. (2006). Plant glutathione peroxidases are functional peroxiredoxins distributed in several subcellular compartments and regulated during biotic and abiotic stresses. *Plant Physiol* 142:1364-1379.

Nebenführ, A., Gallagher, L. A., Dunahay, T. G., Frohlick, J. A., Mazurkiewicz, A. M., Meehl, J. B. and Staehelin, L. A. (1999). Stop-and-go movements of plant Golgi stacks are mediated by the acto-myosin system. *Plant Physiol* 121:1127-1142.

Neeleman, L., Olsthoorn, R. C., Linthorst, H. J. and Bol, J. F. (2001). Translation of a nonpolyadenylated viral RNA is enhanced by binding of viral coat protein or polyadenylation of the RNA. *Proc Natl Acad Sci U S A* 98:14286-14291.

Neilson, K. A., Mariani, M. and Haynes, P. A. (2011). Quantitative proteomic analysis of cold-responsive proteins in rice. *Proteomics* 11:1696-1706.

Nelson, R.S., and van Bel, A.J.E. (1998). The mystery of virus trafficking into, through and out of vascular tissue. Prog. Bot. 59, 476–533.

Nemeth, K., Salchert, K., Putnoky, P., Bhalerao, R., Koncz-Kalman, Z., Stankovic-Stangeland, B., Bako, L., Mathur, J., Okresz, L., Stabel, S., Geigenberger, P., Stitt, M., Redei, G. P., Schell, J. and Koncz, C. (1998). Pleiotropic control of glucose and hormone responses by PRL1, a nuclear WD protein, in Arabidopsis. *Genes Dev* 12:3059-3073.

Netherton, C., Moffat, K., Brooks, E. and Wileman, T. (2007). A guide to viral inclusions, membrane rearrangements, factories, and viroplasm produced during virus replication. *Adv Virus Res* 70:101-182.

Neumann, U., Brandizzi, F. and Hawes, C. (2003). Protein transport in plant cells: In and out of the Golgi. *Ann Botany* 92:167-180.

Ng, J. C. and Perry, K. L. (2004). Transmission of plant viruses by aphid vectors. *Mol Plant Pathol* 5:505-511.

Niehl, A. and Heinlein, M. (2011). Cellular pathways for viral transport through plasmodesmata. *Protoplasma* 248:75-99.

Niehl, A., Pasquier, A., Ferriol, I., Mély, Y. and Heinlein, M. (2014). Comparison of the Oilseed rape mosaic virus and Tobacco mosaic virus movement proteins (MP) reveals common and dissimilar MP functions for tobamovirus spread.*Virology* 456:43-54.

Nieto, C., Morales, M., Orjeda, G., Clepet, C., Monfort, A., Sturbois, B., Puigdomènech, P., Pitrat, M., Caboche, M., Dogimont, C., Garcia-Mas, J., Aranda, M. A. and Bendahmane, A. (2006). An eIF4E allele confers resistance to an uncapped and non-polyadenylated RNA virus in melon. *Plant J* 48:452-462.

Nieto, C., Rodríguez-Moreno, L., Rodríguez-Hernández, A. M., Aranda, M. A. and Truniger, V. (2011). *Nicotiana benthamiana* resistance to non-adapted Melon necrotic spot virus results from an incompatible interaction between virus RNA and translation initiation factor 4E. *Plant J* 66:492-501.

Ni, P. and Cheng Kao, C. (2013). Non-encapsidation activities of the capsid proteins of positive-strand RNA viruses. *Virology* 446:123-132.

Noueiry, A. O., Lucas, W. J. and Gilbertson, R. L. (1994). Two proteins of a plant DNA virus coordinate nuclear and plasmodesmal transport. *Cell* 76:925-932.

Novikov, V. K., Belenovich, E. V., Dobrov, E. N. and Zavriev, S. K. (2000). Kazakh strains of tobacco mosaic virus: two strains with potentially destabilizing amino acid substitutions in the coat protein. *Physiol Mol Plant Pathol* 56:71-77.

Nürnberger, T., Nennstiel, D., Jabs, T., Sacks, W. R., Hahlbrock, K. and Scheel, D. (1994). High affinity binding of a fungal oligopeptide elicitor to parsley plasma membranes triggers multiple defense responses. *Cell* 78:449-460.

O'Farrell, P. H. (1975). High resolution two-dimensional electrophoresis of proteins. *J Biol Chem* 250:4007-4021.

Oh, J. W., Kong, Q., Song, C., Carpenter, C. D. and Simon, A. E. (1995). Open reading frames of turnip crinkle virus involved in satellite symptom expression and incompatibility with *Arabidopsis thaliana* ecotype Dijon. *Mol Plant Microbe Interact* 8:979-987.

Ohki, T., Akita, F., Mochizuki, T., Kanda, A., Sasaya, T., Tsuda, S. (2010). The protruding domain of the coat protein of Melon necrotic spot virus is involved in compatibility with and transmission by the fungal vector Olpidium bornovanus. *Virology* 402:129-134.

Omid, A., Keilin, T., Glass, A., Leshkowitz, D. and Wolf, S. (2007). Characterization of phloem-sap transcription profile in melon plants. *J Exp Bot* 58:3645-3656.

Opalka, N., Brugidou, C., Bonneau, C., Nicole, M., Beachy, R. N., Yeager, M. and Fauquet, C. (1998). Movement of rice yellow mottle virus between xylem cells through pit membranes. *Proc Natl Acad Sci USA* 95:3323-3328.

Oparka, K. J., Prior, D. A. M., Cruz, S. S., Padgett, H. S. and Beachy, R. N. (1997). Gating of epidermal plasmodesmata is restricted to the leading edge of expanding infection sites of tobacco mosaic virus (TMV). *Plant J* 12:781-789.

Oparka, K. J. and Turgeon, R. (1999). Sieve elements and companion cells-traffic control centers of the phloem. *Plant Cel* 11:739-750.

Owens, R. A., Blackburn, M. and Ding, B. (2001). Possible involvement of the phloem lectin in long-distance viroid movement. *Mol Plant Microbe Interact* 14:905-909.

Pallás, V. (2007). En el límite de la vida: un siglo de virus. Universidad Politécnica de Valencia. Servicio de Publicaciones.

Pallás, V. (2013). Una breve historia del fenómeno del silenciamiento del RNA. Contribuciones de la Virología a su descubrimiento. *Virología* 16:14-21

Pallás, V., Aparicio, F., Herranz, M. C., Sánchez-Navarro, J. A. and Scott, S. W. (2012). The molecular biology of ilarviruses. *Adv Virus Res* 87:139-181.

Pallás, V. and García, J. A. (2011). How do plant viruses induce disease? Interactions and interference with host components. *J Gen Virol* 92:2691-2705.

Pallás, V., Genovés, A., Sánchez-Pina, M. A., and Navarro, J. A. (2011). Systemic movement of viruses via the plant phloem. In: Recent Advances in Plant Virology, Edited by Carole Caranta, Miguel A. Aranda, Mark Tepfer and Juan Jose López-Moya. Caister Academic Press.

Pallás, V and Gómez, G. (2013). Phloem RNA-binding proteins as potential components of the long-distance RNA transport system. *Front Plant Sci*. 4:130.

Pallás, V., Mas, P. and Sánchez-Navarro, J. A. (1998). Detection of plant RNA viruses by nonisotopic dot-blot hybridization. *Methods Mol Biol* 81:461-468.

Pallas, V., Navarro, JA, Serra-Soriano, M., Peiro, A. and Sanchez-Navarro, J.A. (2015). El movimiento de los virus en las plantas. En: Enfermedades de las plantas causadas por virus. Ed. Phytoma-SEF. (en prensa).

Panavas, T., Pogany, J. and Nagy, P. D. (2002). Analysis of minimal promoter sequences for plus-strand synthesis by the Cucumber necrosis virus RNA-dependent RNA polymerase. *Virology* 296:263-274.

Panaviene, Z., Panavas, T., Serva, S. and Nagy, P. D. (2004). Purification of the cucumber necrosis virus replicase from yeast cells: role of co-expressed viral RNA in stimulation of replicase activity. *J Virol* 78:8254-8263.

Pandey, S. P. and Somssich, I. E. (2009). The role of WRKY transcription factors in plant immunity. *Plant Physiol* 150:1648-1655.

Pappachan, A., Subashchandrabose, C., Satheshkumar, P. S., Savithri, H. S. and Murthy, M. R. (2008). Structure of recombinant capsids formed by the beta-annulus deletion mutant -- rCP (Delta48-59) of Sesbania mosaic virus. *Virology* 375:190-196.

Park, H. S. and Kim, K. H. (2012). Virus-induced silencing of the WRKY1 transcription factor that interacts with the SL1 structure of Potato virus X leads to higher viral RNA accumulation and severe necrotic symptoms. *Plant Pathol J* 28:40-48.

Park, H. S., Himmelbach, A., Browning, K. S., Hohn, T. and Ryabova, L. A. (2001). A plant viral "reinitiation" factor interacts with the host translational machinery. *Cell* 106:723-733.

Patton, E. E., Willems, A. R., Sa, D., Kuras, L., Thomas, D., Craig, K. L., & Tyers, M. (1998). Cdc53 is a scaffold protein for multiple Cdc34/Skp1/F-box protein complexes that regulate cell division and methionine biosynthesis in yeast. *Genes Dev* 12:692-705.

Pavelka, M. and Robinson, D. G. (2003). The Golgi apparatus in mammalian and higher plant cells: a comparison. In The Golgi apparatus and the plant secretory pathway (Robinson, D.G. ed). Oxford: Blackwell Publishing, pp. 16-35.

Pazhouhandeh, M., Dieterle, M., Marrocco, K., Lechner, E., Berry, B., Brault, V., Hemmer, O., Kretsch, T., Richards, K. E., Genschik, P. and Ziegler-Graff, V. (2006). F-box-like domain in the polerovirus protein P0 is required for silencing suppressor function. *Proc Natl Acad Sci USA* 103:1994-1999.

Peiró, A., Martínez-Gil, L., Tamborero, S., Pallás, V., Sánchez-Navarro, J. A. and Mingarro, I. (2014). The Tobacco mosaic virus movement protein associates with but does not integrate into biological membranes. *J Virol* 88:3016-3026.

Pereira, S., de Andrade, E. M., Matos, E., Oliveira, A., Silva, B., Santos, L., Peres, K., da Silva, A., Pirovani C. P. and Micheli, F. (2014). The pathogenesis-related protein PR-4b from Theobroma cacao presents RNase activity, Ca(2+) and Mg(2+) dependent-DNase activity and antifungal action on Moniliophthora perniciosa. *BMC Plant Biol* 14:161.

Peremyslov, V. V., Pan, Y. W. and Dolja, V. V. (2004). Movement protein of a closterovirus is a type III integral transmembrane protein localized to the endoplasmic reticulum. *J Virol* 78:3704-3709.

Pérez-Cañamás M, Hernández C. (2015). Key importance of small RNA binding for the activity of a glycine-tryptophan (GW) motif-containing viral suppressor of RNA silencing. *J Biol Chem* 290:3106-3120.

Phair, R. D., Gorski, S. A. and Misteli, T. (2004). Measurement of dynamic protein binding to chromatin in vivo, using photobleaching microscopy. *Methods Enzymol* 375:393-414.

Phillipson, B. A., Pimpl, P., daSilva, L. L., Crofts, A. J., Taylor, J. P., Movafeghi, A., Robinson, D. G. and Denecke, J. (2001). Secretory bulk flow of soluble proteins is efficient and COPII dependent. *Plant Cell* 13:2005-2020.

Pineda, M., Sajnani, C. and Barón, M. (2010). Changes induced by the Pepper mild mottle tobamovirus on the chloroplast proteome of *Nicotiana benthamiana*. *Photosynth Res* 103:31-45.

Piro, G., Leucci, M. R., Waldron, K. and Dalessandro, G. (2003). Exposure to water stress causes changes in the biosynthesis of cell wall polysaccharides in roots of wheat cultivars varying in drought tolerance. *Plant Sci* 165:559-569.

Pontier, D., Godiard, L., Marco, Y. and Roby, D. (1994). hsr203J, a tobacco gene whose activation is rapid, highly localized and specific for incompatible plant/pathogen interactions. *Plant J* 5:507-521.

Pouwels, J., Van Der Krogt, G. N. M., Van Lent, J., Bisseling, T. and Wellink, J. (2002) The cytoskeleton and the secretory pathway are not involved in targeting the cowpea mosaic virus movement protein to the cell periphery. *Virology* 297:48-56.

Powers, J. G., Sit, T. L., Heinsohn, C., George, C. G., Kim, K. H. and Lommel, S. A. (2008). The Red clover necrotic mosaic virus RNA-2 encoded movement protein is a second suppressor of RNA silencing. *Virology* 381:277-286.

Profit, A. A., Felsen, V., Chinwong, J., Mojica, E. R. and Desamero, R. Z. (2013). Evidence of pi-stacking interactions in the self-assembly of hIAPP(22-29). *Proteins* 81:690-703.

Prokhnevsky, A. I., Peremyslov, V. V. and Dolja, V. V. (2005). Actin cytoskeleton is involved in targeting of a viral Hsp70 homolog to the cell periphery. *J Virol* 79:14421-14428.

Prokhnevsky, A. I., Peremyslov, V. V., Napuli, A. J. and Dolja, V. V. (2002). Interaction between long-distance transport factor and Hsp70-related movement protein of beet yellows virus. *J Virol* 76:11003-11011.

Prosser, D. C., Tran, D., Gougeon, P. Y., Verly, C. and Ngsee, J. K. (2008). FFAT rescues VAPA-mediated inhibition of ER-to-Golgi transport and VAPB-mediated ER aggregation. *J Cell Sci* 121:3052-3061.

Pumplin, N. and Voinnet, O. (2013). RNA silencing suppression by plant pathogens: defence, counter-defence and counter-counter-defence. *Nat Rev Microbiol* 11:745-760.

Qiu, W. and Scholthof, K. B. G. (2004). Satellite panicum mosaic virus capsid protein elicits symptoms on a nonhost plant and interferes with a suppressor of virus-induced gene silencing. *Mol Plant Microb Interact* 17:263-271.

Qu, F. and Morris, T. J. (1997). Encapsidation of turnip crinkle virus is defined by a specific packaging signal and RNA size. *J Virol* 71:1428-1435.

Qu, F., Ren, T. and Morris, T. J. (2003). The coat protein of turnip crinkle virus suppresses posttranscriptional gene silencing at an early initiation step. *J Virol* 77:511-522.

Quintero, C. A., Giraudo, C. G., Villarreal, M., Montich, G. and Maccioni, H. J. (2010). Identification of a site in Sar1 involved in the interaction with the cytoplasmic tail of glycolipid glycosyltransferases. *J Biol Chem* 285:30340-30346.

Rajendran, K. S. and Nagy, P. D. (2003). Characterization of the RNA-binding domains in the replicase proteins of tomato bushy stunt virus. *J Virol* 77:9244-9258.

Rajendran, K. S., Pogany, J. and Nagy, P. D. (2002). Comparison of turnip crinkle virus RNA-dependent RNA polymerase preparations expressed in Escherichia coli or derived from infected plants. *J Virol* 76:1707-1717.

Rao, A. L. (2006). Genome packaging by spherical plant RNA viruses. *Annu Rev Phytopathol* 44:61-87.

Reade, R., Kakani, K. and Rochon, D. (2010). A highly basic KGKKGK sequence in the RNA-binding domain of the Cucumber necrosis virus coat protein is associated with encapsidation of full-length CNV RNA during infection. *Virology* 403:181-188.

Ren, T., Qu, F. and Morris, T. J. (2005). The nuclear localization of the Arabidopsis transcription factor TIP is blocked by its interaction with the coat protein of Turnip crinkle virus. *Virology* 331:316-324.

Reichel, C. and Beachy, R. N. (2000). Degradation of tobacco mosaic virus movement protein by the 26S proteasome. *J Virol* 74:3330-3337.

Reichert, V. L., Choi, M., Petrillo, J. E. and Gehrke, L. (2007). Alfalfa mosaic virus coat protein bridges RNA and RNA-dependent RNA polymerase in vitro. *Virology* 364:214-226.

Requena, A., Simon-Buela, L., Salcedo, G. and García-Arenal, F. (2006). Potential involvement of a cucumber homolog of phloem protein 1 in the long-distance movement of Cucumber mosaic virus particles. *Mol Plant Microbe Interact* 19:734-746.

Ribeiro, D., Jung, M., Moling, S., Borst, J. W., Goldbach, R. and Kormelink, R. (2013). The cytosolic nucleoprotein of the plant-Infecting bunyavirus Tomato spotted wilt recruits endoplasmic reticulum-resident proteins to endoplasmic reticulum export sites. *Plant Cell* 25:3602-3614.

Rinne, P. L., van den Boogaard, R., Mensink, M. G., Kopperud, C., Kormelink, R., Goldbach, R. and van der Schoot, C. (2005). Tobacco plants respond to the constitutive expression of the Tospovirus movement protein NS(M) with a heat-reversible sealing of plasmodesmata that impairs development. *Plant J* 43:688-707.

Ritzenthaler, C. and Hofmann, C. (2007). Tubule-guided movement of plant viruses. In: viral transport in plants. Edited by E. Waigmann and M. Heinlein. Springer, Berlin/Heidelberg. pp. 63-84.

Riviere, C. J., Pot, J., Tremaine, J.H. and Rochon, D.M. (1989). Coat protein of melon necrotic spot carmovirus is more similar to those of tombusviruses than those of carmoviruses. *J Gen Virol* 70:3033-3042.

Riviere, C. J., Pot, J., Tremaine, J. H. and Rochon, D. M. (1989). Coat protein of melon necrotic spot carmovirus is more similar to those of tombusviruses than those of carmoviruses. *J Gen Virol* 70:3033-3042.

Riviere, C. J. and Rochon, D. M. (1990). Nucleotide sequence and genomic organization of melon necrotic spot virus. *J Gen Virol* 71:1887-1896.

Robaglia, C., and Caranta, C. (2006). Translation initiation factors: a weak link in plant RNA virus infection. *Trends Plant Sci* 11:40-45.

Roberts, K., and McCann, M. C. (2000). Xylogenesis: the birth of a corpse. *Curr Opin Plant Biol* 3:517-522.

Robinson, D. G., Herranz, M. C., Bubeck, J., Pepperkok, R. and Ritzenthaler, C. (2007). Membrane dynamics in the early secretory pathway. *CRC Crit Rev Plant Sci* 26:199-225.

Rodrigo, G., Carrera, J., Ruiz-Ferrer, V., del Toro, F. J., Llave, C., Voinnet, O. and Elena, S. F. (2012). A meta-analysis reveals the commonalities and differences in *Arabidopsis thaliana* response to different viral pathogens. *Plos One* 7: e40526

Rodrigues, S. P., Ventura, J. A., Aguilar, C., Nakayasu, E. S., Choi, H., Sobreira, T. J., Nohara, L. L., Wermelinger, L. S., Almeida, I. C., Zingali, R. B. and Fernandes, P. M. (2012). Label-free quantitative proteomics reveals differentially regulated proteins in the latex of sticky diseased Carica paPayá L. plants. *J Proteomics* 75:3191-3198.

Rodríguez-Medina, C., Atkins, C. A., Mann, A. J., Jordan, M. E. and Smith, P. M. C. (2011). Macromolecular composition of phloem exudate from white lupin (Lupinus albus L.). *BMC Plant Biol* 11:36.

Rose, G. D., Gierasch, L. M. and Smith, J. A. (1985). Turns in peptides and proteins. *Adv Protein Chem* 37:1-109.

Roth, B. M., Pruss, G. J. and Vance, V. B. (2004). Plant viral suppressors of RNA silencing. *Virus Res* 102:97-108.

Rushton, P. J., Somssich, I. E., Ringler, P. and Shen, Q. J. (2010). WRKY transcription factors. *Trends Plant Sci* 15:247-258.

Ruiz-Ferrer, V. and Voinnet, O. (2009). Roles of plant small RNAs in biotic stress responses. *Annu Rev Plant Biol* 60:485-510.

Ruiz-Medrano, R., Xoconostle-Cazares, B., Lucas, W. J. (1999). Phloem long-distance transport of CmNACP mRNA: implications for supracellular regulation in plants. *Development* 126:4405-4419.

Runions, J., Brach, T., Kuhner, S. and Hawes, C. (2006). Photoactivation of GFP reveals protein dynamics within the endoplasmic reticulum membrane. *J Exp Bot* 57:43-50.

Rushton, P. J., Somssich, I. E., Ringler, P. and Shen, Q. J. (2010). WRKY transcription factors. *Trends Plant Sci* 15:247-258.

Ryabova, L. A., Pooggin, M. M., and Hohn, T. (2006). Translation reinitiation and leaky scanning in plant viruses. *Virus Res* 119:52-62.

Ryder, S. P., Recht, M. I. and Williamson, J. R. (2008). Quantitative analysis of protein-RNA interactions by gel mobility shift. *Methods Mol Biol* 488:99-115.

Saint-Jore, C. M., Evins, J., Batoko, H., Brandizzi, F., Moore, I. and Hawes, C. (2002). Redistribution of membrane proteins between the Golgi apparatus and endoplasmic reticulum in plants is reversible and not dependent on cytoskeletal networks. *Plant J* 29:661-678.

Sambade, A., Brandner, K., Hofmann, C., Seemanpillai, M., Mutterer, J. and Heinlein, M. (2008). Transport of TMV movement protein particles associated with the targeting of RNA to plasmodesmata. *Traffic* 9:2073-2088.

Sánchez-Madrid, F., Vidales, F. J., and Ballesta, J. P. (1981). Effect of phosphorylation on the affinity of acidic proteins from Saccharomyces cerevisiae for the ribosomes. *Eur J Biochem* 114:609-613.

Sánchez-Navarro, J. A., Fajardo, T., Zicca, S., Pallás, V. and Stavolone, L. (2010). Caulimoviridae tubule-guided transport is dictated by movement protein properties. *J Virol* 84:4109-4112.

Sánchez-Navarro, J. A., Herranz, M. C. and Pallás, V. (2006). Cell-to-cell movement of Alfalfa mosaic virus can be mediated by the movement proteins of Ilar-, bromo-, cucumo-, tobamo- and comoviruses and does not require virion formation. *Virology* 346:66-73.

Sánchez-Navarro, J. A., Herranz, M. C. and Pallás, V. (2006). Cell-to-cell movement of Alfalfa mosaic virus can be mediated by the movement proteins of Ilar-, bromo-, cucumo-, tobamo-and comoviruses and does not require virion formation. *Virology* 346:66-73.

Sangita, V., Lokesh, G. L., Satheshkumar, P. S., Vijay, C. S., Saravanan, V., Savithri, H. S. and Murthy, M. R. (2004). T=1 capsid structures of Sesbania mosaic virus coat protein mutants: determinants of T=3 and T=1 capsid assembly. *J Mol Biol* 342:987-999.

Sanfaçon, H. (2005). Replication of positive-strand RNA viruses in plants: contact points between plant and virus components. *Botany* 83:1529-1549.

Satheshkumar, P. S., Lokesh, G. L., Murthy, M. R. and Savithri, H. S. (2005). The role of arginine-rich motif and beta-annulus in the assembly and stability of Sesbania mosaic virus capsids. *J Mol Biol* 353:447-458.

Sato, H., Masuda, M., Kanai, M., Tsukiyama-Kohara, K., Yoneda, M. and Kai, C. (2007). Measles virus N protein inhibits host translation by binding to eIF3-p40. *J Virol* 81:11569-11576.

Saurí, A., Saksena, S., Salgado, J., Johnson, A. E. and Mingarro, I. (2005). Double-spanning plant viral movement protein integration into the endoplasmic reticulum membrane is signal recognition particle-dependent, translocon-mediated, and concerted. *J Biol Chem* 280:25907-25912.

Scheets, K., Jordan, R., White, K. A. and Hernández, C. (2015). Pelarspovirus, a proposed new genus in the family Tombusviridae.*Arch Virol* 160:2385-2393.

Scheiffele, P. and Fullekrug, J. (2000). Glycosylation and protein transport. *Essays Biochem* 36:27-35.

Schenk, P. M., Kazan, K., Wilson, I., Anderson, J. P., Richmond, T., Somerville, S. C. and Manners, J. M. (2000). Coordinated plant defense responses in Arabidopsis revealed by microarray analysis. *Proc Natl Acad Sci USA* 97:11655-11660.

Schilmiller, A. L. and Howe, G. A. (2005). Systemic signaling in the wound response. *Curr Opin Plant Biol* 8:369-377.

Schoberer, J., Vavra, U., Stadlmann, J., Hawes, C., Mach, L., Steinkellner, H. and Strasser, R. (2009). Arginine/Lysine residues in the cytoplasmic tail promote ER export of plant glycosylation enzymes. *Traffic* 10:101-115.

Schoelz, J. E., Harries, P. A. and Nelson, R. S. (2011). Intracellular transport of plant viruses: finding the door out of the cell. *Mol Plant* 4:813-831.

Scholthof, H. B. (2005). Plant virus transport: motions of functional equivalence. *Trends Plant Sci* 10:376-382.

Seemanpillai, M., Elamawi, R., Ritzenthaler, C. and Heinlein, M. (2006). Challenging the role of microtubules in *Tobacco mosaic virus* movement by drug treatments is disputable. *J. Virol* 80:6712–6715.

Sen, G. L. and Blau, H. M. (2006). A brief history of RNAi: the silence of the genes. *FASEB J* 20:1293-1299.

Serra-Soriano, M., Pallás, V. and Navarro, J. A. (2014). A model for transport of a viral membrane protein through the early secretory pathway: minimal sequence and endoplasmic reticulum lateral mobility requirements. *Plant J* 77:863-879.

Serra-Soriano, M., Navarro, J. A., Genovés, A. and Pallás, V. (2015). Comparative proteomic analysis of melon phloem exudates in response to viral infection. *J Proteomics* 124:11-24.

Selth, L. A., Dogra, S. C., Rasheed, M. S., Randles, J. W. and Rezaian, M. A. (2006). Identification and characterization of a host reversibly glycosylated peptide that interacts with the Tomato leaf curl virus V1 protein. *Plant Mol Biol* 61:297-310.

Sherman, M. B., Guenther, R. H., Tama, F., Sit, T. L., Brooks, C. L., Mikhailov, A. M., Orlova, E. V., Baker, T. S. and Lommel, S. A. (2006). Removal of divalent cations induces structural transitions in red clover necrotic mosaic virus, revealing a potential mechanism for RNA release. *J Virol* 80:10395-10406.

Shevchenko, A., Wilm, M., Vorm, O. and Mann, M. (1996). Mass spectrometric sequencing of proteins silver-stained polyacrylamide gels. *Anal Chem* 68:850-858.

Shimizu, T., Yoshii, A., Sakurai, K., Hamada, K., Yamaji, Y., Suzuki, M., Namba, S. and Hibi, T. (2009). Identification of a novel tobacco DnaJ-like protein that interacts with the movement protein of tobacco mosaic virus. *Arch Virol* 154:959-967.

Shimura, H. and Pantaleo, V. (2011). Viral induction and suppression of RNA silencing in plants. *BBA. Gene Regulatory Mechanisms* 1809:601-612.

Skuzeski, J. M. and Morris, T. J. (1995). Quantitative analysis of the binding of turnip crinkle virus coat protein to RNA fails to demonstrate binding specificity but reveals a highly cooperative assembly interaction. *Virology* 210:82-90.

Solovyev, A. G., Kalinina, N. O. and Morozov, S. Y. (2012). Recent advances in research of plant virus movement mediated by triple gene block. *Front Plant Sci* 3:276.

Somssich, I. E. and Hahlbrock, K. (1998). Pathogen defence in plants-a paradigm of biological complexity. *Trends Plant Sci* 3:86-90.

Soosaar, J. L., Burch-Smith, T. M. and Dinesh-Kumar, S. P. (2005). Mechanisms of plant resistance to viruses.*Nat Rev Microbiol* 3:789-798.

Sparkes, I., Runions, J., Hawes, C. and Griffing, L. (2009a). Movement and remodeling of the endoplasmic reticulum in nondividing cells of tobacco leaves. *Plant Cell* 21:3937-3949.

Sparkes, I. A., Ketelaar, T., de Ruijter, N. C. and Hawes, C. (2009b). Grab a Golgi: laser trapping of Golgi bodies reveals in vivo interactions with the endoplasmic reticulum. *Traffic* 10:567-571.

Spicer R. (2014). Symplastic network in secondary vascular tissues: parenchyma distribution and activity supporting long-distant transport. *J Exp Bot* 65:1829-1848.

Staehelin, L. A. and Moore, I. (1995). The plant golgi apparatus: structure, functional organization and trafficking mechanisms. *Annu Rev Plant Physiol Plant Mol Biol* 46:261-288.

Stavolone, L., Villani, M. E., Leclerc, D. and Hohn, T. (2005). A coiled-coil interaction mediates Cauliflower mosaic virus cell-to-cell movement. *Proc Natl Acad Sci USA* 102:6219-6224.

Sugiyama, M., Sato, H., Karasawa, A., Hase, S., Takahashi, H. and Ehara, Y. (2000). Characterization of symptom determinants in two mutants of cucumber mosaic virus Y strain, causing distinct mild green mosaic symptoms in tobacco. *Physiol Mol Plant Pathol* 56:85-90.

Sun, A. Q., Salkar, R., Sachchidanand, Xu, S., Zeng, L., Zhou, M. M. and Suchy, F. J. (2003). A 14-amino acid sequence with a beta-turn structure is required for apical membrane sorting of the rat ileal bile acid transporter. *J Biol Chem* 278:4000-4009.

Su, S., Liu, Z., Chen, C., Zhang, Y., Wang, X., Zhu, L., Miao, L., Wang, X.C., and Yuan, M. (2010). Cucumber mosaic virus movement protein severs actin filaments to increase the plasmodesmal size exclusion limit in tobacco. *Plant cell* 22:1373-1387.

Szick, K., Springer, M. and Bailey-Serres, J. (1998). Evolutionary analyses of the 12-kDa acidic ribosomal P-proteins reveal a distinct protein of higher plant ribosomes. *Proc Natl Acad Sci USA* 95:2378-2383.

Takamatsu, N., Ishikawa, M., Meshi, T. and Okada, Y. (1987). Expression of bacterial chloramphenicol acetyltransferase gene in tobacco plants mediated by TMV-RNA. *EMBO J* 6:307-311.

Tamai, A. and Meshi, T. (2001). Cell-to-cell movement of Potato virus X: the role of p12 and p8 encoded by the second and third open reading frames of the triple gene block. *Mol Plant Microbe Interact* 14:1158-1167.

Thiébeauld, O., Pooggin, M. M. and Ryabova, L. A. (2007). Alternative translation strategies in plant viruses. Plant Viruses. pp. 1–20. The Global Science Books.

Thomas, C. L., Bayer, E. M., Ritzenthaler, C., Fernandez-Calvino, L. and Maule, A. J. (2008). Specific targeting of a plasmodesmal protein affecting cell-to-cell communication. *PLoS Biol* 6:e7.

Thomas, C. L., Leh, V., Lederer, C. and Maule, A. J. (2003). Turnip crinkle virus coat protein mediates suppression of RNA silencing in *Nicotiana benthamiana. Virology.* 306:33-41.

Thomma, B.P ., Nurnberger, T. and Joosten, M. H. (2011). Of PAMPs and effectors: the blurred PTI-ETI dichotomy. *Plant Cell* 23:4-15.

Tilsner, J., Linnik, O., Wright, K. M., Bell, K., Roberts, A. G., Lacomme, C., Cruz, S. S. and Oparka, K. J. (2012). The TGB1 movement protein of Potato virus X reorganizes actin and endomembranes into the X-body, a viral replication factory. *Plant Physiol* 158:1359-1370.

Tilsner, J., Linnik, O., Louveaux, M., Roberts, I. M., Chapman, S. N. and Oparka, K. J. (2013). Replication and trafficking of a plant virus are coupled at the entrances of plasmodesmata. *J Cell Biol* 201:981-995.

Timmins, P. A., Wild, D. and Witz, J. (1994). The three-dimensional distribution of RNA and protein in the interior of tomato bushy stunt virus: a neutron low-resolution single-crystal diffraction study. *Structure* 2:1191-1201.

Tomenius, K., Clapham, D. and Meshi, T. (1987). Localization by immunogold cytochemistry of the virus-coded 30K protein in plasmodesmata of leaves infected with Tobacco mosaic virus. *Virology* 160:363-371.

Trapphoff, T., Beutner, C., Niehaus, K. and Colditz, F. (2009). Induction of distinct defense-associated protein patterns in Aphanomyces euteiches (Oomycota)-elicited and -inoculated Medicago truncatula cell-suspension cultures: a proteome and phosphoproteome approach. *Mol Plant Microbe Interact* 22:421-436.

Truniger, V., Nieto, C., González-Ibeas, D. and Aranda, M. A. (2008). Mechanism of plant eIF4E-mediated resistance against a Carmovirus (Tombusviridae): cap-independent translation of a viral RNA controlled in cis by an (a) virulence determinant. *Plant J* 56:716-727.

Tsukumo, Y., Tsukahara, S., Saito, S., Tsuruo, T. and Tomida, A. (2009). A novel endoplasmic reticulum export signal: proline at the +2-position from the signal peptide cleavage site. *J Biol Chem* 284:27500-27510.

Tsurugi, K., and Ogata, K. (1985). Evidence for the exchangeability of acidic ribosomal proteins on cytoplasmic ribosomes in regenerating rat liver. *J Biochem* 98:1427-1431.

Turgeon, R. and Wolf, S. (2009). Phloem transport: cellular pathways and molecular trafficking. *Annu Rev Plant Biol* 60:207-221.

Turnbull, C. G. and Lopez-Cobollo, R. M. (2013). Heavy traffic in the fast lane: long-distance signalling by macromolecules. *New Phytol* 198:33-51.

Turner, K. A., Sit, T. L., Callaway, A. S., Allen, N. S. and Lommel, S. A. (2004). Red clover necrotic mosaic virus replication proteins accumulate at the endoplasmic reticulum. *Virology* 320:276-290.

Ueda, H., Yokota, E., Kutsuna, N., Shimada, T., Tamura, K., Shimmen, T., Hasezawa, S., Dolja, V. V. and Hara-Nishimura, I. (2010). Myosin-dependent endoplasmic reticulum motility and F-actin organization in plant cells. *Proc Natl Acad Sci USA* 107:6894-6899.

Ueki, S. and Citovsky, V. (2002). The systemic movement of a tobamovirus is inhibited by a cadmium-ion-induced glycine-rich protein. *Nat Cell Biol* 4:478-486.

Ueki, S., and Citovsky, V. (2007). Spread throughout the plant: systemic transport of viruses. In Viral Transport in Plants, Plant Cell Monographs; Heinlein, M. and Waigmann, E., eds. Springer-Verlag), pp. 86–117.

van Bel, A. J., Helariutta, Y., Thompson, G. A., Ton, J., Dinant, S., Ding, B. and Patrick, J. W. (2013). Phloem: the integrative avenue for resource distribution, signaling, and defense. *Front Plant Sci* 4:471.

van der Scheer, C. and Groenewegen, J. (1971). Structure in cells of Vigna unguiculata infected with Cowpea mosaic virus. *Virology* 46:493-497.

Van Loon, L. C. (1987). Disease induction by plant viruses. *Adv Virus Res* 33:205-256.

Van Loon, L. C. and Van Strien, E. A. (1999). The families of pathogenesis-related proteins, their activities, and comparative analysis of PR-1 type proteins. *Physiol Mol Plant Pathol* 55:85-97.

Vaucheret, H. (2006). Post-transcriptional small RNA pathways in plants: mechanisms and regulations. *Gene Dev* 20:759-771.

Vazquez, F., Legrand, S. and Windels, D. (2010). The biosynthetic pathways and biological scopes of plant small RNAs.*Trends Plant Sci* 15:337-345.

Ventelon-Debout, M., Delalande, F., Brizard, J. P., Diemer, H., Van Dorsselaer, A. and Brugidou, C. (2004). Proteome analysis of cultivar-specific deregulations of Oryza sativa indica and O. sativa japonica cellular suspensions undergoing Rice yellow mottle virus infection. *Proteomics* 4:216-225.

Vercammen, D., Belenghi, B., van de Cotte, B., Beunens, T., Gavigan, J. A., De Rycke, R., Brackenier, A., Inzé, D., Harris, J. L. and Van Breusegem, F. (2006). Serpin1 of *Arabidopsis thaliana* is a Suicide Inhibitor for Metacaspase 9. *J Mol Biol* 364:625-636.

Verchot, J., Driskel, B. A., Zhu, Y., Hunger, R. M. and Littlefield, L. J. (2001). Evidence that soilborne wheat mosaic virus moves long distance through the xylem in wheat. *Protoplasma* 218:57-66.

Verchot-Lubicz, J. (2005). A new cell-to-cell transport model for potexviruses. *Mol Plant Microbe Interact* 18:283-290.

Verchot-Lubicz, J., Torrance, L., Solovyev, A. G., Morozov, S. Y., Jackson, A. O. and Gilmer, D. (2010). Varied movement strategies employed by triple gene block-encoding viruses. *Mol Plant-Microbe Interact* 23:1231-1247.

Verchot-Lubicz, J., Ye, C. M. and Bamunusinghe, D. (2007). Molecular biology of Potexviruses: recent advances. *J Gen Virol* 88:1643-1655.

Vijayapalani, P., Maeshima, M., Nagasaki-Takekuchi, N. and Miller, W. A. (2012). Interaction of the trans-frame potyvirus protein P3N-PIPO with host protein PCaP1 facilitates potyvirus movement. *PLoS Pathog* 8:e1002639.

Vilar, M., Esteve, V., Pallás, V., Marcos, J. F., and Pérez-Payá, E. (2001). Structural properties of carnation mottle virus p7 movement protein and its RNA-binding domain. *J Biol Chem* 276:18122-18129.

Vilar, M., Saurí, A., Monne, M., Marcos, J. F., von Heijne, G., Perez-Payá, E. and Mingarro, I. (2002). Insertion and topology of a plant viral movement protein in the endoplasmic reticulum membrane. *J Biol Chem* 277:23447-23452.

Vilar, M., Saurí, A., Marcos, J. F., Mingarro, I. and Pérez-Payá, E. (2005). Transient structural ordering of the RNA-binding domain of Carnation mottle virus p7 movement protein modulates nucleic acid binding. *Chembiochem* 6:1391-1396.

Vlot, A. C., Klessig, D. F. and Park, S.W. (2008). Systemic acquired resistance: the elusive signal(s). *Curr Opin Plant Biol* 11:436-442.

Vogel, F., Hofius, D. and Sonnewald, U. (2007). Intracellular trafficking of Potato leafroll virus movement protein in transgenic Arabidopsis. *Traffic* 8:1205-1214.

Voinnet, O., Pinto, Y. M. and Baulcombe, D. C. (1999). Suppression of gene silencing: a general strategy used by diverse DNA and RNA viruses of plants. *Proc Natl Acad Sci U S A* 96:14147-14152.

Voinnet, O., Vain, P., Angell, S. and Baulcombe, D. C. (1998). Systemic spread of sequence-specific transgene RNA degradation in plants is initiated by localized introduction of ectopic promoterless DNA. *Cell* 95:177-187.

Vuorinen, A. L., Kelloniemi, J. and Valkonen, J. P. (2011). Why do viruses need phloem for systemic invasion of plants? *Plant Sci* 181:355-363.

Wada, Y., Tanaka, H., Yamashita, E., Kubo, C., Ichiki-Uehara, T., Nakazono-Nagaoka, E., Omura, T. and Tsukihara, T. (2008). The structure of melon necrotic spot virus determined at 2.8 A resolution. *Acta Crystallogr Sect F Struct Biol Cryst Commun* 64:8-13.

Waigmann, E., Curin, M. and Heinlein, M. (2007). Tobacco mosaic virus-a model for macromolecular cell-to-cell spread. In: Viral Transport in Plants (Waigmann, E. and Heinlein, M., eds.). Springer-Verlag Berlin Heidelberg, pp. 29-62.

Waigmann, E., Ueki, S., Trutnyeva, K. and Citovsky, V. (2004). The ins and outs of non-destructive cell-to-cell and systemic movement of plant viruses. *Crit Rev Plant Sci* 23:195-250.

Walsh, D. and Mohr, I. (2011). Viral subversion of the host protein synthesis machinery. *Nat Rev Microbiol* 9:860-875.

Walz, C., Giavalisco, P., Schad, M., Juenger, M., Klose, J. and Kehr, J. (2004). Proteomics of curcurbit phloem exudate reveals a network of defence proteins. *Phytochemistry* 65:1795-1804.

Walz, C., Juenger, M., Schad, M. and Kehr, J. (2002). Evidence for the presence and activity of a complete antioxidant defence system in mature sieve tubes. *Plant J* 31:189-197.

Wan, J., Cabanillas, D. G., Zheng, H. and Laliberte, J. F. (2015). Turnip mosaic virus moves systemically through both phloem and xylem as membrane-associated complexes. *Plant Physiol* 167:1374-1388.

Wang, H., Fan, W., Li, H., Yang, J., Huang, J. and Zhang, P. (2013) Functional characterization of Dihydroflavonol-4-reductase in anthocyanin biosynthesis of purple sweet potato underlies the direct evidence of anthocyanins function against abiotic stresses. *PloS One* 8:e78484.

Wang, M. B., Masuta, C., Smith, N. A. and Shimura, H. (2012). RNA silencing and plant viral diseases. *Mol Plant Microbe Interact* 25:1275-1285.

Wang, X., Ma, Y., Huang, C., Li, J., Wan, Q. and Bi, Y. (2008). Involvement of glucose-6-phosphate dehydrogenase in reduced glutathione maintenance and hydrogen peroxide signal under salt stress. *Plant Signal Behav* 3:394-395.

Washburn, M. P., Wolters, D. and Yates, J. R. (2001). Large-scale analysis of the yeast proteome by multidimensional protein identification technology. *Nat Biotechnol* 19:242-247.

Weber-Lotfi, F., Dietrich, A., Russo, M. and Rubino, L. (2002). Mitochondrial targeting and membrane anchoring of a viral replicase in plant and yeast cells. *J Virol* 76:10485-10496.

Weber, P. H. and Bujarski, J. J. (2015). Multiple functions of capsid proteins in (+) stranded RNA viruses during plant-virus interactions. *Virus Res* 196:140-149.

Wei, T. Y., Zhang, C. W., Hong, J. A., Xiong, R. Y., Kasschau, K. D., Zhou, X. P., Carrington, J. C. and Wang, A. M. (2010). Formation of complexes at plasmodesmata for potyvirus intercellular movement is mediated by the viral protein P3N-PIPO. *PLoS Pathog* 6:e1000962.

Wenk, M., Ba, Q., Erichsen, V., MacInnes, K., Wiese, H., Warscheid, B. and Koch, H. G. (2012). A universally conserved ATPase regulates the oxidative stress response in Escherichia coli. *J Biol Chem* 287:43585-43598.

Whitham, S., McCormick, S. and Baker, B. (1996). The N gene of tobacco confers resistance to tobacco mosaic virus in transgenic tomato. *Proc Natl Acad Sci USA* 93:8776-8781.

Whitham, S. A., Yang, C. and Goodin, M. M. (2006). Global impact: elucidating plant responses to viral infection. *Mol Plant Microbe Interact* 19:1207-1215.

Willmann, M. R., Endres, M. W., Cook, R. T. and Gregory, B. D. (2011). The functions of RNA-dependent RNA polymerases in Arabidopsis. *Arabidopsis Book 9:e0146*

Wolf, S., Lucas, W. J., Deom, C. M., and Beachy, R. N. (1989). Movement protein of tobacco mosaic virus modifies plasmodesmatal size exclusion limit. *Science* 246:377-379.

Wool, I. G., Chan, Y. L., Gluck, A., and Suzuki, K. (1991). The primary structure of rat ribosomal proteins P0, P1, and P2 and a proposal for a uniform nomenclature for mammalian and yeast ribosomal proteins. *Biochimie* 73:861-870.

Xie, Z. and Qi, X. (2008). Diverse small RNA-directed silencing pathways in plants. *BBA. Gene Regulatory Mechanisms* 1779:720-724.

Xoconostle-Cazares, B., Xiang, Y., Ruiz-Medrano, R., Wang, H. L., Monzer, J., Yoo, B. C., McFarland, K. C., Franceschi, V. R. and Lucas, W. J. (1999). Plant paralog to viral movement protein that potentiates transport of mRNA into the phloem. *Science* 283:94-98.

Xu, P., Chen, F., Mannas, J. P., Feldman, T., Sumner, L. W. and Roossinck, M. J. (2008). Virus infection improves drought tolerance. *New Phytol* 180:911-921.

Xu, Q., Ni, H., Chen, Q., Sun, F., Zhou, T., Lan, Y. and Zhou, Y. (2013). Comparative proteomic analysis reveals the cross-talk between the responses induced by H_2O_2 and by long-term rice black-streaked dwarf virus infection in rice. *PloS One* 8:e81640.

Yaegashi, H., Isogai, M. and Yoshikawa, N. (2012). Characterization of plant virus-encoded gene silencing suppressors. *Methods Mol Biol* 894:113-122.

Yang, H., Liu, C., Jamsen, J., Wu, Z., Wang, Y., Chen, J., Zheng, L. and Shen, B. (2012). The DNase domain-containing protein TATDN1 plays an important role in chromosomal segregation and cell cycle progression during zebrafish eye development. *Cell Cycle* 11:4626-4632.

Yang, Y. D., Elamawi, R., Bubeck, J., Pepperkok, R., Ritzenthaler, C. and Robinson, D. G. (2005). Dynamics of COPII vesicles and the Golgi apparatus in cultured Nicotiana tabacum BY-2 cells provides evidence for transient association of Golgi stacks with endoplasmic reticulum exit sites. *Plant Cell* 17:1513-1531.

Yang, Y., Qiang, X., Owsiany, K., Zhang, S., Thannhauser, T. W. and Li, L. (2011). Evaluation of different multidimensional LC–MS/MS pipelines for isobaric tags for relative and absolute quantitation (iTRAQ)-based proteomic analysis of potato tubers in response to cold storage. *J Proteome Res* 10:4647-4660.

Yi, G., Vaughan, R. C., Yarbrough, I., Dharmaiah, S. and Kao, C. C. (2009). RNA binding by the brome mosaic virus capsid protein and the regulation of viral RNA accumulation. *J Mol Biol* 391:314-326.

Yoo, B. C., Aoki, K., Xiang, Y., Campbell, L. R., Hull, R. J., Xoconostle-Cazares, B., Monzer. J., Lee, J. Y., Ullman, D. E. and Lucas, W. J. (2000). Characterization of cucurbita maxima phloem serpin-1 (CmPS-1). A developmentally regulated elastase inhibitor. *J Biol Chem* 275:35122-35128.

Yoshioka, K., Matsushita, Y., Kasahara, M., Konagaya, K. and Nyunoya, H. (2004). Interaction of Tomato mosaic virus movement protein with tobacco RIO kinase. *Mol Cells* 17:223-229.

Yuan, Z. J., Chen, H. Y., Chen, Q., Omura, T., Xie, L. H., Wu, Z. J. and Wei, T. Y. (2011). The early secretory pathway and an actin-myosin VIII motility system are required for plasmodesmatal localization of the NSvc4 protein of Rice stripe virus. *Virus Res* 159:62-68.

Zamyatnin, A. A. Jr., Solovyev, A. G., Bozhkov, P. V., Valkonen, J. P., Morozov, S. Y. and Savenkov, E. I. (2006). Assessment of the integral membrane protein topology in living cells. *Plant J* 46:145-154.

Zanetti, G., Pahuja, K.B., Studer, S., Shim, S. and Schekman, R. (2012). COPII and the regulation of protein sorting in mammals. *Nat Cell Biol* 14:20-28.

Zavaliev, R., Ueki, S., Epel, B. L. and Citovsky, V. (2011). Biology of callose (β-1, 3-glucan) turnover at plasmodesmata. *Protoplasma* 248:117-130.

Zeevaart, J. A. (2008). Leaf-produced floral signals. *Curr Opin Plant Biol* 11:541-547.

Zhang, C., Kotchoni, S. O., Samuels, A. L. and Szymanski, D. B. (2010). SPIKE1 signals originate from and assemble specialized domains of the endoplasmic reticulum. *Curr Biol* 20:2144-2149.

Zhang F, and Simon AE. (2003). Enhanced viral pathogenesis associated with a virulent mutant virus or a virulent satellite RNA correlates with reduced virion accumulation and abundance of free coat protein. Virology 312:8-13.

Zhang, J., Rubio, V., Lieberman, M. W. and Shi, Z. Z. (2009). OLA1, an Obg-like ATPase, suppresses antioxidant response via nontranscriptional mechanisms. *Proc Natl Acad Sci U S A* 106:15356-15361.

Zhang, L., Handa, K. and Palukaitis, P. (1994). Mapping local and systemic symptom determinants of cucumber mosaic cucumovirus in tobacco. *J Gen Virol* 75:3185-3191.

Zhang, Y., Zhao, J., Xiang, Y., Bian, X., Zuo, Q., Shen, Q., Gai, J. and Xing, H. (2011). Proteomics study of changes in soybean lines resistant and sensitive to Phytophthora sojae. *Proteome Sci* 9:52.

Zinker, S. and Warner, J. R. (1976). The ribosomal proteins of Saccharomyces cerevisiae. Phosphorylated and exchangeable proteins. *J Biol Chem* 251:1799-1807.

Zurbriggen, M. D., Carrillo, N. and Hajirezaei, M. R. (2010). ROS signaling in the hypersensitive response: when, where and what for?. *Plant Signal Behav* 5:393-396.

AGRAÏMENTS

En aquesta pàgina m'agradaria recordar a tota la gent que m'ha ajudat a arribar ací, fins i tot sense saber-ho.

Al meu director, el Dr. Vicente Pallás, moltes gràcies per confiar amb mi, sense ell tot aquest projecte no hauria sigut possible.

També vull agrair al meu altre director el Dr. José Antonio Navarro per tota la paciència que ha tingut amb mi, totes les hores dedicades a ensenyar-me el treball pulcre i ben organitzat, a que les coses ben fetes sempre al final t'estalvien temps, a eixes "master class" de confocal per trobar la cèl·lula perfecta i representativa. En fi, per tota la ajuda ja que sense ell aquesta tesi no seria igual.

A tots els meus companys de laboratori Toni, MC, Ana, Lorena C., Germán, Techu, Fede, Lorena L., Gustavo per no perdre la paciència amb les preguntes indiscriminades, tots els moments compartits, cafès i dinars en els que no han faltat les rialles i les vesprades al final d'un dia llarg cantant "Sweet Caroline".

A la meva família, als meus pares i germans que a pesar de la distància m'han recolzat incondicionalment.

A les bioquímiques Valencianes: Pilar, Bea i Ana, gràcies per eixes discussions de biblioteca i dinars sobre el què fer, al final hem assolit l'objectiu (per fi!).

A tota la "RE" per estar sempre que els he necessitat, incondicionalment.

A les noves amistats rubinenques, ja que gràcies als dinars, sopars i jornades de jugar a les pel·lícules fan que tot l'esforç sigui més fàcil de portar.

Als "IUCTeros" Rafa, Víctor, Marta, Laura, Carles, Sergi, Marcos, Andrea, Ana, Alba i Danis per la seva acollida i comprensió, que ha facilitat que pugui tirar aquest projecte endavant, i pel "fer rises", que m'han fet sentir-me com una més.

Finalment a la meva filla Júlia, per haver-la deixat un poc de costat i per no poder jugar amb ella perquè estava "treballant", i a Santi per donar-me el temps que necessitava, per no retreure les absències i per totes les paraules d'alè i suport, en definitiva per estar simplement amb mi.

Moltes gràcies a tots!!!!